

**NANOFLUID MEDIATED GAS- LIQUID
MASS TRANSFER ENHANCEMENT IN
PULSED PLATE COLUMN**

Thesis

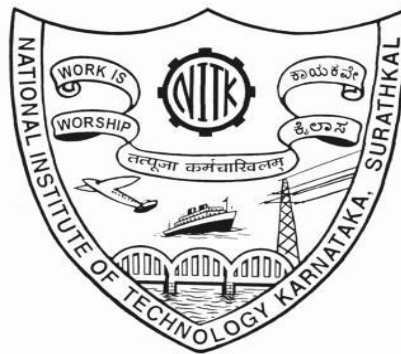
Submitted in partial fulfillment of the requirements for the degree of

DOCTOR OF PHILOSOPHY

by

AMRUTA S SHET

Registration No. 155004CH15F01



DEPARTMENT OF CHEMICAL ENGINEERING
NATIONAL INSTITUTE OF TECHNOLOGY KARNATAKA
SURATHKAL, MANGALORE -575025

October, 2023

DECLARATION

I hereby *declare* that the Research Thesis entitled “**Nanofluid mediated gas-liquid mass transfer enhancement in pulsed plate column**” which is being submitted to the **National Institute of Technology Karnataka, Surathkal** in partial fulfillment of the requirements for the award of the Degree of **Doctor of Philosophy** in the Department of Chemical Engineering, *is a bonafide report of the research work carried out by me.* The material contained in this Research Thesis has not been submitted to any University or Institution for the award of any degree.

Amruta S. Shet

AMRUTA S SHET

Register No. 155004CH15F01

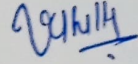
Department of Chemical Engineering

Place: NITK, Surathkal

Date: *19/10/2023*

CERTIFICATE

This is to *certify* that the Research Thesis entitled “**Nanofluid mediated gas-liquid mass transfer enhancement in pulsed plate column**” submitted by **AMRUTA S SHET** (Register Number: 155004CH15F01) as the record of the research work carried out by her, *is accepted as the Research Thesis submission* in partial fulfillment of the requirements for the award of degree of **Doctor of Philosophy**.



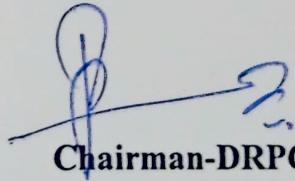
Research Guide

Dr. Vidya Shetty K

Professor,

Department of Chemical Engineering

NITK, Surathkal



Chairman-DRPC

Department of Chemical Engineering

NITK, Surathkal

Department of Chemical Engineering

रासायनिक अभियांत्रिकी विभाग

National Institute of Technology Karnataka - Surathkal

राष्ट्रीय प्रौद्योगिकी संस्थान कर्नाटक, हयत्कल

PO Srinivasnagar, Mangalore - 575025 Karnataka

पी.ओ. श्रीनिवासनगर, मंगलौर - ५७५०२५, कर्नाटक

DEDICATED TO MY FATHER

Prof. S. M. Shet

(Rtd. Prinicpal)
Department of Chemistry
RES, Kanakapura.

ACKNOWLEDGEMENT

The route I took to complete this doctoral research has been a highly illuminating stage in my life's journey. I will always be grateful to the many people who helped me to complete this and left behind the beautiful experience.

First and foremost, with great respect and love, I wish to thank my supervisor Professor **Vidya Shetty K.**, for her guidance throughout the years of my PhD research pursuit, as well as her significant contributions in shaping the thesis. She has been and always will be a role model for me in NITK and my Life. I thank her from the bottom of my heart for giving me the courage and the knowledge I needed to alter both my career and personal lives.

I am very much thankful to my RPAC members **Dr. Hariprasasd Dasari**, Assistant Professor, Department of Chemical Engineering, and **Dr. Arun M Isloor**, Professor, Department of Chemistry, NITK, Surathkal for their valuable advice and suggestions that enabled me to identify gaps in my research and make necessary improvements based on their insights and comments.

I humbly express my sincere gratitude to The Director, NITK Surathkal, the former and present Academic Dean. I wish to thank our former H.O.D.s Dr. Vidya Shetty K., Professor, Dr. Rajmohan B., Professor, Dr. Hari Mahalingam, Associate professor, and, Dr. Prasanna B.D., Associate Professor, present H.O.D Dr. Jagdeesh Babu, Department of Chemical Engineering, NITK Surathkal for providing me necessary facilities, funding, and support during the phase of this research work. I would also like to thank all the faculty members of the Department of Chemical Engineering, NITK Surathkal for their valuable support and encouragement. I would also like to express my sincere thanks to Mr. Harish Mr. Suresh, Mr. Ramesh, Mr. Mahadev, Mr. Sukesh, Mrs. Shashikala S, Mrs. Shashikala Mohan, Mr. Sadashiva, Mr. Jnaneshwar, Mrs. Thrithila Shetty, Mrs. Bhavyashree, Mrs. Sandhya and Mrs. Vijetha and all other non-teaching staffs for their helpful suggestions and timely maintenance of the laboratory equipment and all the official documentation required.

I gratefully acknowledge my friends Dr. Manjula P Sunil, Dr. Shankamma S. Dr. Aishwarya D. Ms. Deekshitha. K, Mrs. Minimol M, Mrs. Sreelakshmi, Ms. Sedevino

Sophia, Ms. Deeksha Mathew, Dr. Smruthi Prabhu, Dr. Archana, Dr. Rohit P Kalnake, Dr. Lister H. Fallerio, and Mr. Girish I Hangal for their care, support, and encouragement.

There aren't enough words to express my gratitude to my strength my two besties my Mother **Mrs. Shashikala S Shet** and my Grandmother **Mrs. Sumitra Ramachandra Samasgikar** for their inspirational remarks that got me through the difficult and trying times I encountered on this journey. I owe my gratefulness to my understanding and helpful in-law's family for their help and support.

The best is saved for last, and I am truly appreciative of my spouse, **Mr. Manjunath N Raikar**, and My Son **Master. Amarnath M Raikar** for their unwavering support, encouragement, and patience throughout all the stages of my life. They have consistently encouraged me in all of my academic activities, which has helped me get through the last few years and finish my research project.

Above all, I am indebted to Almighty God for bestowing upon me the intelligence, health, and stamina necessary to complete this research work.

Amruta S Shet

ABSTRACT

Oxygen transfer limitations result in poor performance in bioreactors and reduced efficiency in catalytic and photocatalytic reaction systems where oxygen transfer is involved. Adequate oxygen transfer can be achieved by increasing the volumetric oxygen transfer coefficient ($k_{L}a$). Several investigations have shown that the enhancement of $k_{L}a$ can be achieved in the presence of nanofluid which is a colloidal suspension of nanoparticles in any base fluid. Nanoparticles may be intentionally added to the reactor fluid or may be inherently present in the reactor to form a nanofluid. Pulsed plate column (PPC) is widely used as an aerobic bioreactor and gas-liquid contactor for various applications. In the present study, the influence of TiO_2 , SiO_2 , and $\alpha\text{-Fe}_2\text{O}_3$ nanofluids with water as the base fluid on $k_{L}a$ was studied in PPC. The effect of nanofluid parameters such as nanofluid type in terms of nanoparticles used, their size and loading along with the column parameters such as frequency (f) and amplitude (A) of pulsation, pulsing velocity ($A \times f$) and gas velocity (U_g) was studied. The use of nanofluids led to $k_{L}a$ enhancement. It was found that $k_{L}a$ increased as the nanoparticle loading increased, attained a maximum at the critical loading, and then reduced as the loading was further increased. The critical loading depended on the nanofluid. $k_{L}a$ was found to increase with the increase in A , f , and U_g . The nanoparticle loading and $A \times f$ showed an interacting effect on $k_{L}a$ resulting in one or more hydrodynamic regimes depending upon the type of nanofluids, size, and loading of the nanoparticles. Nanofluids with lower-size nanoparticles showed higher $k_{L}a$ compared to those with larger sizes. TiO_2 nanofluid provided a better $k_{L}a$ enhancement than SiO_2 and $\alpha\text{-Fe}_2\text{O}_3$ nanofluid. The maximum enhancement factors were obtained with TiO_2 , SiO_2 , and $\alpha\text{-Fe}_2\text{O}_3$ nanofluids at the critical loading conditions. The order of magnitude analysis implied that the convective currents caused by the Brownian movement of the nanoparticles in the fluid can be the possible reason for mass transfer enhancement in PPC. Pseudo-homogeneous model was tested and it was found to accurately predict the enhancement only till the critical loading conditions. The developed dimensionless correlations and artificial neural network models could accurately predict $k_{L}a$ and thus may find potential applications in the design of pulsed plate column when used as gas-liquid mass transfer contactors, bioreactors, or photocatalytic reactors. The results of this study indicate that the pulsing conditions required to achieve the desired mass transfer characteristics can be reduced by using a nanofluid instead of the base fluid, thus potentially leading to tremendous saving of energy.

Keywords: Artificial neural network, Nanofluids, Oxygen mass transfer coefficient Pulsed Plate Column, Pulsing velocity.

Table of Contents

Section No.	Contents	Page No.
	Abstract	i
	Table of Contents	ii
	List of Tables	vi
	List of Figures	viii
	List of Abbreviations	xiv
Chapter 1.	Introduction	1
Chapter 2	Literature review	8
2.1	Volumetric gas-liquid mass transfer coefficient ($k_L a$)	8
2.2	Factors affecting gas-liquid mass transfer rates	11
2.3	Nanofluids	12
2.3.1	Preparation of Nanofluids	13
2.3.2	Applications of Nanofluids	14
2.4	Heat transfer in Nanofluids	16
2.4.1	Thermal conductivity	16
2.4.2	Convective heat transfer	17
2.5	Mass transfer in Nanofluids	17
2.5.1	Studies on mass diffusion in Nanofluids	17
2.5.2	Studies on convective mass transfer coefficients in Nanofluids	19
2.5.3	Influence of Nanofluids on gas-liquid mass transfer coefficient	25
2.5.4	Mechanism of mass transfer enhancement in nanofluids	27
2.6	Pulsed Plate Column	29
2.6.1	Studies on gas-liquid mass transfer coefficient in PPC	32
2.7	Dimensionless correlations, theoretical models, and Artificial Neural Network (ANN) models for mass transfer in nanofluids.	34

2.8	Scope of the research work	37
2.9	Objectives of the research work	40
Chapter 3	Materials and Methods	41
3.1	Chemicals used	41
3.2	Nanomaterials used	41
3.2.1	Morphology and the average size of Nanoparticles	41
3.3	Preparation of Nanofluid	43
3.4	Properties of Nanofluid	44
3.5	Experimental setup	45
3.5.1	Experimental procedure for the determination of k_{LA} in PPC	47
3.6	Analysis of sodium sulphite concentration by iodometric method	49
3.6.1	Preparation of sodium thiosulphate	49
3.6.2	Standardization of sodium thiosulphate	49
3.6.3	Preparation of iodine solution	49
3.6.4	Preparation of starch indicator	49
3.6.5	Chemical reactions	50
Chapter 4	Results and Discussion	51
4.1	Determination of properties of Nanofluids	51
4.2	Effect of nanoparticles loading in the nanofluid on k_{LA}	62
4.3	Effect of frequency of pulsation on k_{LA} with nanofluids	75
4.4	Effect of the amplitude of pulsation on k_{LA} in the presence of Nanofluids.	77
4.5	Effect of superficial air velocity (U_g) on k_{LA} in a PPC	82
4.6	Effect of pulsing velocity on k_{LA} in the presence of Nanofluids	89
4.7	Effect of size of nanoparticles on k_{LA} in PPC	98
4.8	Comparison of the effect of TiO_2 , SiO_2 , and $\alpha-Fe_2O_3$ nanofluids on volumetric oxygen mass transfer coefficient (k_{LA}) in a PPC	101
Chapter 5	Theoretical analysis and modeling studies	107
5.1	Order of magnitude analysis for mass transfer enhancement mechanism	107
5.2	Pseudo-homogeneous model	109

5.3	Development of dimensional correlations for k_{LA} : Multiple Regression Analysis (MRA) model	115
5.4	Artificial Neural Network	120
Chapter 6	Summary and Conclusions	125
	Future Scope of the work	128
	References	129
	Appendix	169
	Work presented in the conference, Paper Published	172

List of Tables

Table No.	Title of the Table	Page No.
2.1	Studies on mass diffusion in nanofluids	18
2.2	Studies on convective mass transfer coefficients in nanofluids	20
2.3	Application of Pulsed plate column as a bioreactor, chemical reactors, or for gas absorption which involves the g-l transfer.	30
3.1	Average particle size of TiO ₂ , SiO ₂ , and α -Fe ₂ O ₃ nanoparticles	43
3.2	Amount of nanoparticles used to prepare nanofluids of varying nanoparticle loading	43
4.1	Surface tension of TiO ₂ , SiO ₂ and α -Fe ₂ O ₃ nanofluids	52
4.2	Nanoparticle loading in volume fraction	60
4.3	Values of Diffusivity of oxygen in Nanofluids, D_{nf}	61
4.4	Enhancement factor obtained at critical loading of TiO ₂ , SiO ₂ , and α -Fe ₂ O ₃ nanofluids with varying amplitude of pulsation, at the lowest (0.25 s ⁻¹) and Highest (1 s ⁻¹) frequency at an airflow rate of 1.8 LPM.	72
4.5	Maximum Enhancement factor obtained at critical loading of TiO ₂ , SiO ₂ , and α -Fe ₂ O ₃ nanoparticles with different superficial air velocities at an amplitude of pulsation of 3.2 cm and the lowest frequency of 0.25 s ⁻¹ .	89
4.6	Maximum Enhancement factor obtained at critical loading of TiO ₂ , SiO ₂ , and α -Fe ₂ O ₃ nanoparticles with amplitude of pulsation of 3.2 cm at the lowest frequency of 0.25 s ⁻¹ , at an airflow rate of 1.8 LPM.	101
4.7	Enhancement factor obtained at critical loading of TiO ₂ , SiO ₂ , and α -Fe ₂ O ₃ nanoparticles with amplitude of pulsation of 6.3 cm at the highest frequency of 1 s ⁻¹ , at an airflow rate of 1.8 LPM.	103
4.8	Maximum k_{LA} and k_{LA} enhancement factors along with the optimum conditions for the operation of PPC	104
4.9	Comparison of Maximum k_{LA} enhancement factors at the optimum conditions of operation of various reactors with this study	105
5.1	The values of t_m , t_b , and t_c for TiO ₂ , SiO ₂ and α -Fe ₂ O ₃ nanofluid	108

5.2	Calculated surface renewal rate values using experimental flux with base fluid and nanofluids under critical loading of nanoparticles and varying pulsing velocities and superficial gas velocity.	114
5.3	Statistical parameters for different nanofluids of the Pseudo homogenous model	115
5.4	Range of validity of dimensionless numbers and statistical parameters for different nanofluids.	118
5.5	Statistical parameters for different nanofluids of the ANN model	122

List of Figures

Figure No.	Title of the Figure	Page No.
2.1	Concentration gradients near the gas-liquid interface	9
2.2	Application of nanofluids in various sectors	16
2.3	Schematic diagrams of various gas-liquid contactors	19
3.1	SEM image of TiO ₂ nanoparticle of the size range (a) 25 nm and (b) less than 100 nm	42
3.2	SEM image of SiO ₂ nanoparticle of the size range (a) 20-30 nm and (b) 5-15 nm	42
3.3	SEM image of α -Fe ₂ O ₃ nanoparticle of the size range (a) less than 50 nm and (b) less than 80 nm	42
3.4	Prepared Nanofluids (a) TiO ₂ -25, (b) TiO ₂ -72, (c) SiO ₂ -24, (d) SiO ₂ - 12, (e) α -Fe ₂ O ₃ - 76 and (f) α -Fe ₂ O ₃ - 43	44
3.5	Schematic diagram of an experimental setup	46
3.6	Experimental conditions under which the k _{La} values were determined in PPC	48
4.1	Effect of nanoparticle loading on the Surface tension of (a) TiO ₂ , (b) SiO ₂ , and (c) α -Fe ₂ O ₃ nanofluids.	53
4.2	Effect of nanoparticle loading on the Dynamic viscosity of (a) TiO ₂ , (b) SiO ₂ and (c) α -Fe ₂ O ₃ nanofluids	56
4.3	Effect of nanoparticle loading on the Density of (a) TiO ₂ , (b) SiO ₂ and (c) α -Fe ₂ O ₃ nanofluids	59
4.4	Diffusivity of oxygen in TiO ₂ , SiO ₂ and α -Fe ₂ O ₃ nanofluids	61
4.5	Effect of TiO ₂ nanoparticle Loading on k _{La} at different frequency of pulsation and an airflow rate of 1.8 LPM for (a) TiO ₂ -25 at A= 3.2 cm (b) TiO ₂ -72 at A = 3.2 cm (c) TiO ₂ -25 at A= 4.7 cm (d) TiO ₂ -72 at A = 4.7 cm (e) TiO ₂ -25 at A= 6.3 cm (f) TiO ₂ -72 at A = 6.3 cm	63
4.6	Effect of TiO ₂ nanoparticle Loading on k _{La} at different frequency of pulsation and an airflow rate of 3.2 LPM for (a) TiO ₂ -25 at A= 3.2 cm (b) TiO ₂ -72 at A= 3.2 cm (c) TiO ₂ -25 at A= 4.7 cm (d) TiO ₂ -72 at A= 4.7 cm (e) TiO ₂ -25 at A= 6.3 cm (f) TiO ₂ -72 at A= 6.3 cm	64

4.7	Effect of TiO ₂ nanoparticle Loading on k _L a at different frequency of pulsation and at an air flow rate of 4.8 LPM for (a) TiO ₂ -25 at A= 3.2 cm (b) TiO ₂ -72 at A= 3.2 cm (c) TiO ₂ -25 at A= 4.7 cm (d) TiO ₂ -72 at A= 4.7 cm (e) TiO ₂ -25 at A= 6.3 cm (f) TiO ₂ -72 at A= 6.3 cm	64
4.8	Effect of SiO ₂ nanoparticle Loading on k _L a at different frequency of pulsation and at an air flow rate of 1.8 LPM for (a) SiO ₂ -12 at A= 3.2 cm (b) SiO ₂ -24 at A= 3.2 cm (c) SiO ₂ - 12 at A= 4.7 cm (d) SiO ₂ -24 at A= 4.7 cm (e) SiO ₂ - 12 at A= 6.3 cm (f) SiO ₂ -24 at A= 6.3 cm	67
4.9	Effect of SiO ₂ nanoparticle Loading on k _L a at different frequency of pulsation and at an air flow rate of 3.2 LPM for (a) SiO ₂ -12 at A= 3.2 cm (b) SiO ₂ -24 at A= 3.2 cm (c) SiO ₂ - 12 at A= 4.7 cm (d) SiO ₂ -24 at A= 4.7 cm (e) SiO ₂ - 12 at A= 6.3 cm (f) SiO ₂ -24 at A= 6.3 cm	67
4.10	Effect of SiO ₂ nanoparticle Loading on k _L a at different frequency of pulsation and at an air flow rate of 4.8 LPM for (a) SiO ₂ -12 at A= 3.2 cm (b) SiO ₂ -24 at A= 3.2 cm (c) SiO ₂ - 12 at A= 4.7 cm (d) SiO ₂ -24 at A= 4.7 cm (e) SiO ₂ - 12 at A= 6.3 cm (f) SiO ₂ -24 at A= 6.3 cm	68
4.11	Effect of α-Fe ₂ O ₃ nanoparticle loading on k _L a at different frequency of pulsation and at an air flow rate of 1.8 LPM for (a) α-Fe ₂ O ₃ – 43 at A= 3.2 cm (b) α-Fe ₂ O ₃ – 76 at A = 3.2 cm (c) α-Fe ₂ O ₃ – 43 at A= 4.7 cm (d) α-Fe ₂ O ₃ – 76 at A = 4.7 cm (e) α-Fe ₂ O ₃ – 43 at A= 6.3 cm (f) α-Fe ₂ O ₃ – 76 at A = 6.3 cm	69
4.12	Effect of α-Fe ₂ O ₃ nanoparticle loading on k _L a at different frequency of pulsation and at an air flow rate of 3.2 LPM for (a) α-Fe ₂ O ₃ – 43 at A= 3.2 cm (b) α-Fe ₂ O ₃ – 76 at A = 3.2 cm (c) α-Fe ₂ O ₃ – 43 at A= 4.7 cm (d) α-Fe ₂ O ₃ – 76 at A = 4.7 cm (e) α-Fe ₂ O ₃ – 43 at A= 6.3 cm (f) α-Fe ₂ O ₃ – 76 at A = 6.3 cm	70
4.13	Effect of α-Fe ₂ O ₃ nanoparticle loading on k _L a at different frequency of pulsation and at an air flow rate of 4.8 LPM for (a) α-Fe ₂ O ₃ – 43 at A= 3.2 cm (b) α-Fe ₂ O ₃ – 76 at A = 3.2 cm (c) α-Fe ₂ O ₃ – 43 at A= 4.7 cm (d) α-Fe ₂ O ₃ – 76 at A = 4.7 cm (e) α-Fe ₂ O ₃ – 43 at A= 6.3 cm (f) α-Fe ₂ O ₃ – 76 at A = 6.3 cm	71

4.14	Effect of amplitude of pulsation on k_{LA} at different TiO_2 -25 nanoparticle loading at varying frequency of pulsation of (a) 0.25 s^{-1} (b) 0.5 s^{-1} , (c) 0.75 s^{-1} and (d) 1 s^{-1}	78
4.15	Effect of amplitude of pulsation on k_{LA} at different TiO_2 -72 nanoparticle loading at varying frequency of pulsation of (a) 0.25 s^{-1} (b) 0.5 s^{-1} , (c) 0.75 s^{-1} and (d) 1 s^{-1}	79
4.16	Effect of amplitude of pulsation on k_{LA} at different SiO_2 – 12 nanoparticle loading at varying frequency of pulsation of (a) 0.25 s^{-1} (b) 0.5 s^{-1} , (c) 0.75 s^{-1} and (d) 1 s^{-1}	79
4.17	Effect of amplitude of pulsation on k_{LA} at different SiO_2 - 24 nanoparticle loading at varying frequency of pulsation of (a) 0.25 s^{-1} (b) 0.5 s^{-1} , (c) 0.75 s^{-1} and (d) 1 s^{-1}	80
4.18	Effect of amplitude of pulsation on k_{LA} at different α - Fe_2O_3 – 43 nanoparticle loading at varying frequency of pulsation of (a) 0.25 s^{-1} (b) 0.5 s^{-1} , (c) 0.75 s^{-1} and (d) 1 s^{-1}	80
4.19	Effect of amplitude of pulsation on k_{LA} at different α - Fe_2O_3 – 76 nanoparticle loading at varying frequency of pulsation of (a) 0.25 s^{-1} (b) 0.5 s^{-1} , (c) 0.75 s^{-1} and (d) 1 s^{-1}	81
4.20	Effect of U_g on k_{LA} with TiO_2 – 25 nanofluid at varying (a) TiO_2 – 25 nm nanoparticle loading, at $A=6.3$ cm; $f = 1 s^{-1}$ (b) amplitude of pulsation at $f = 1s^{-1}$ and critical loading = 0.068 % w/v (c) frequency of pulsation at $A = 6.3$ cm and critical loading = 0.068 % w/v	83
4.21	Effect of U_g on k_{LA} with TiO_2 – 72 nanofluid at varying (a) TiO_2 – 72 nm nanoparticle loading, at $A=6.3$ cm ; $f = 1 s^{-1}$ (b) amplitude of pulsation at $f = 1 s^{-1}$ and critical loading = 0.051 % w/v (c) frequency of pulsation at $A = 6.3$ cm and critical loading = 0.051 % w/v	83
4.22	Effect of U_g on k_{LA} with SiO_2 – 12 nanofluid at varying (a) SiO_2 – 12 nm nanoparticle loading, at $A=6.3$ cm; $f = 1 s^{-1}$ (b) amplitude of pulsation at $f = 1 s^{-1}$ and critical loading = 0.051 % w/v	84

	(c) frequency of pulsation at $A = 6.3$ cm and critical loading = 0.051 %w/v	
4.23	Effect of U_g on k_{La} with $SiO_2 - 24$ nanofluid at varying (a) $SiO_2 - 24$ nm nanoparticle loading, at $A=6.3$ cm; $f = 1s^{-1}$ (b) amplitude of pulsation at $f = 1 s^{-1}$ and critical loading = 0.051 % w/v (c) frequency of pulsation at $A = 6.3$ cm and critical loading = 0.051 %w/v	84
4.24	Effect of U_g on k_{La} with $\alpha- Fe_2O_3 - 43$ nanofluid at varying (a) $\alpha- Fe_2O_3 - 43$ nm nanoparticle loading, at $A=6.3$ cm; $f = 1s^{-1}$ (b) amplitude of pulsation at $f = 1 s^{-1}$ and critical loading = 0.034 %w/v (c) frequency of pulsation at $A = 6.3$ cm and critical loading = 0.034 %w/v	85
4.25	Effect of U_g on k_{La} with $\alpha- Fe_2O_3 - 76$ nanofluid at varying (a) $\alpha- Fe_2O_3 - 76$ nm nanoparticle loading, at $A=6.3$ cm; $f = 1 s^{-1}$ (b) amplitude of pulsation at $f = 1 s^{-1}$ and critical loading = 0.034 %w/v (c) frequency of pulsation at $A = 6.3$ cm and critical loading = 0.034 %w/v	85
4.26	Effect of $(A \times f)$ on k_{La} as a function of $TiO_2 - 25$ nanoparticle loadings at an airflow rate of 1.8 LPM. (a) $\Phi \leq \Phi_L$ (b) $\Phi > \Phi_L$	90
4.27	Effect of $(A \times f)$ on k_{La} as a function of $TiO_2 - 72$ nanoparticle loadings at an airflow rate of 1.8 LPM.	94
4.28	Effect of $(A \times f)$ on k_{La} as a function of $SiO_2 - 12$ nanoparticle loadings at an airflow rate of 1.8 LPM.	95
4.29	Effect of $(A \times f)$ on k_{La} as a function of $SiO_2 - 24$ nanoparticle loadings at an airflow rate of 1.8 LPM.	95
4.30	Effect of $(A \times f)$ on k_{La} as a function of $\alpha-Fe_2O_3 - 43$ nanoparticle loadings at an airflow rate of 1.8 LPM.	96
4.31	Effect of $(A \times f)$ on k_{La} as a function of $\alpha-Fe_2O_3 - 76$ nanoparticle loadings at an airflow rate of 1.8 LPM.	97
4.32	Effect of nanoparticle size on k_{La} at different TiO_2 nanoparticle loading and at $A = 6.3$ cm at different frequency of pulsation (a) $0.25 s^{-1}$ (b) $0.5 s^{-1}$ (c) $0.75 s^{-1}$ and (d) $1 s^{-1}$	98

4.33	Effect of nanoparticle size on $k_{L,a}$ at different SiO_2 nanoparticle loading and at $A = 6.3$ cm at different frequency of pulsation (a) 0.25 s^{-1} (b) 0.5 s^{-1} (c) 0.75 s^{-1} and (d) 1 s^{-1}	99
4.34	Effect of nanoparticle size on $k_{L,a}$ at different $\alpha\text{-Fe}_2\text{O}_3$ nanoparticle loading and at $A = 6.3$ cm at different frequency of pulsation (a) 0.25 s^{-1} (b) 0.5 s^{-1} (c) 0.75 s^{-1} and (d) 1 s^{-1}	99
4.35	Effect of TiO_2 and SiO_2 nanofluids on $k_{L,a}$ at different nanoparticle loadings with similar average particle size (25 nm and 24 nm respectively) at $A = 6.3$ cm, $f = 1 \text{ s}^{-1}$	102
4.36	Effect of TiO_2 and $\alpha\text{-Fe}_2\text{O}_3$ nanofluids on $k_{L,a}$ at different nanoparticle loadings with similar average particle size (72 nm and 76 nm respectively) at $A = 6.3$ cm, $f = 1 \text{ s}^{-1}$.	102
5.1	Predicted and experimental Enhancement in mass transfer rate in the presence of TiO_2 nanofluids.	110
5.2	Predicted and experimental Enhancement in mass transfer rate in the presence of SiO_2 nanofluids.	111
5.3	Predicted and experimental Enhancement in mass transfer rate in the presence of $\alpha\text{-Fe}_2\text{O}_3$ nanofluids.	111
5.4	The variation in Surface renewal rate (s), at critical nanoparticle loading for TiO_2 , SiO_2 and $\alpha\text{-Fe}_2\text{O}_3$ nanofluid at varying pulsing velocity at an air flow rate of 0.011 m/s.	113
5.5	The variation in Surface renewal rate (s), at critical nanoparticle loading for TiO_2 , SiO_2 and $\alpha\text{-Fe}_2\text{O}_3$ nanofluid at varying pulsing velocity at an air flow rate of 0.019 m/s.	113
5.6	The variation in Surface renewal rate (s), at critical nanoparticle loading for TiO_2 , SiO_2 and $\alpha\text{-Fe}_2\text{O}_3$ nanofluid at varying pulsing velocity at an air flow rate of 0.029 m/s.	114
5.7	Predicted and experimental Sherwood number for (a) TiO_2 nanofluid (b) SiO_2 nanofluid (c) $\alpha\text{-Fe}_2\text{O}_3$ nanofluid	119
5.8	Structure of feed-forward neural network with input, hidden, and output layer	122
5.9	Mean Squared Error versus Number of Neurons hidden in the layer	123

5.10	Predicted ANN output vs. the experimental value of k_{LA} in the presence of TiO_2 nanofluid for the (a) training, (b) testing, and (c) validation data points (d) overall data points.	123
5.11	Predicted ANN output vs. the experimental value of k_{LA} in the presence of SiO_2 nanofluids for the (a) training, (b) testing and (c) validation data points (d) overall data points.	124
5.12	Predicted ANN output vs. the experimental value of k_{LA} in the presence of $\alpha-Fe_2O_3$ nanofluids for the (a) training, (b) testing and (c) validation data points (d) overall data points.	124

List of Abbreviations

ANN	Artificial Neural Network
ASTM	American Society for Testing and Materials
A	Amplitude of pulsation, cm
A_a	Interfacial area
$A \times f$	Pulsing velocity, cm/s
bf	Base fluid
C_L	Bulk concentration of oxygen in the reactor
C^*	Saturation solubility of oxygen in sodium sulphite solution
CNT	Carbon Nanotube
cP	centipoise
D_{nf}	Diffusivity of Nanofluid
D_L	Diffusivity of a solution without nanoparticles
E	Enhancement factor
f	Frequency of pulsation, s^{-1}
$\alpha\text{-Fe}_2\text{O}_3\text{-43}$	Iron oxide nanofluid with an average nanoparticle size of 43nm
$\alpha\text{-Fe}_2\text{O}_3\text{-76}$	Iron oxide nanofluid with an average nanoparticle size of 76nm
g-l	Gas-liquid
J_{nf}	overall mass transfer rate with nanofluids
J_{bf}	overall mass transfer rate with base fluid
k_{La}	Volumetric oxygen mass transfer coefficient, m/s
k_G	Gas phase mass transfer coefficient, m/s
k_L	Liquid phase mass transfer coefficient, m/s
LPM	Liters Per Minute
MSE	Mean Squared Error
MAE	Mean Absolute Error
MRA	Multiple Regression Analysis
min	minutes
nf	Nanofluids
np	Nanoparticles
nm	Nanometer
PPC	Pulsed Plate Column

RPC	Reciprocating Plate Column
rpm	Revolutions Per Minute
s^{-1}	Per second
s	Surface renewal rate
SiO ₂ -12	Silicon dioxide nanofluid with average nanoparticle size of 12 nm
SiO ₂ -24	Silicon dioxide nanofluid with average nanoparticle size of 24 nm
TiO ₂ -25	Titanium dioxide nanofluid with average nanoparticle size of 25 nm
TiO ₂ -72	Titanium dioxide nanofluid with average nanoparticle size of 72 nm
t	Experimental time
t_m	time required for the oxygen to diffuse through a distance equal to the diameter of nanoparticle
t_b	time required for a Brownian particle to travel a distance equal to its diameter
t_c	the time required for convection currents to travel a particle diameter
U_g	Superficial air velocity
V	Volume of the working liquid
X_A	bulk liquid concentration in the liquid phase
X_{Ai}	Liquid interphase concentration
Y_A	bulk gas concentration in the gas phase
Y_{Ai}	gas interface concentration
ψ	Nanoparticle Loading in volume fraction
Φ	Nanoparticle loading, w/v%
α	alpha

CHAPTER 1 INTRODUCTION

The operations involving the contact between the gas-liquid (g-l) phases are common in a variety of chemical process industries. Chemical reactions may include hydrogenation, chlorination, oxidation, polymerization of alkenes, etc., comprised of the g-l contacting. The globalization of industries has increased the special interests in the design and operation of process equipment that achieves lower operating costs, energy conservation, effective transfer of gas molecules to a liquid medium, higher efficiency, better performance, environmental protection, and enhancement in energy efficiency. The major problem in reactions consisting of more than one phase is the transfer of gases into aqueous phases. Most frequently, the diffusion of a low or moderately soluble gaseous entity across the g-l interface limits the reaction rate due to mass transfer (Olle et al. 2006). The g-l mass transfer plays a significant role in various fields related to chemical and biochemical industries and environmental pollution control, such as wastewater treatment, absorption of pollutants from air or flue gas, and others. Efficient gas transfer from gas bubbles to the liquid medium is the primary step in such operations. It determines the overall reaction rate in the g-l reactions (Dhanasekaran and Karunanithi 2010). Absorption of gases into a liquid phase becomes a crucial step in many multiphase processes because the rate of reactions is often constrained by the diffusion of sparingly soluble gas across the g-l interface (Olle et al. 2006). Reactors or columns are used as multiphase contacting for various bioprocess, separation processes involving mass transfer, chemical processes (Dhanasekaran and Karunanithi 2010; Rahmanian et al. 2015; Shetty et al. 2013; Zhang et al. 2022).

Transferring oxygen (aerobic) or CO₂ (like in bioprocesses involving algal development) from the gas to the liquid phase is necessary for biotechnological processes involving microorganisms (Moo-Young and Chisti 1994). In most aerobic biochemical processes, oxygen is a critical substrate. The performance may be affected due to the improper oxygen supply (Garcia-Ochoa and Gomez 2009).

The efficacy of any aerobic processes is hampered due to the lack of oxygen because microorganism metabolic rates drastically decrease (Gomaa and Al Taweel 2005), and the culture may react negatively to the accompanying stress (Suresh et al. 2009). The inadequacy of the transfer of oxygen results in less efficient bioreactors. Similarly,

catalytic and photocatalytic reaction systems may also encounter reduced efficiency because of the insufficient oxygen transfer rate. Adequate oxygen transfer is vital, as with photocatalytic reactions, where oxygen is used as an electron acceptor to produce superoxide radicals (Khanna and Shetty 2014; Saravanan et al. 2017; Shet and Shetty 2016). So, enhancing the oxygen transfer rate into the aqueous medium is imperative to perform these types of processes effectively. Generally, oxygen transfer into the liquid is carried out by sparging air or supplying oxygen. However, these reactions proceed in aqueous media wherein oxygen has low solubility. Under these circumstances, an inadequate supply of oxygen and low fluid turbulence lead to oxygen mass transfer limitations in the system.

Suitable g-l contactors must be selected to enhance the performance and achieve effective g-l mass transfer in multiphase systems (Lounes and Thibault 1994). Dhanasekaran and Karunanithi (2010) used columns with moving parts to improve the g-l mass transfer rate. To achieve high mass transfer rate, different contactors such as packed bed columns (Rahmanian et al. 2015), bubble columns (Gómez-Díaz et al. 2009), stirred tank reactors (Zokaei-Kadijani et al. 2013), fluidized bed reactors (Yang et al. 2001), airlift reactors (Moraveji et al. 2012), rotating disk reactors (Yang 1982), oscillatory baffled columns (Hewgill et al. 1993), reciprocating plate columns or pulsed plate columns (Brauer 1990; Daniel and Brauer 1994; Rangappa et al. 2016; Shetty et al. 2013; Shetty and Srinikethan 2010) and liquid pulsating column (Torab-Mostaedi et al. 2010) have been used by several researchers.

The packed bed columns reduce the back mixing in comparison to the spray column. However, channeling and clogging are the common disadvantages involved in packed columns. It cannot handle the liquid with higher viscosities. Though plate columns can be designed to handle a wider range of liquid and gas flow rates than packed columns, they are prone to flooding and may not be suitable to be operated with particulate systems involving the use of catalyst, photocatalyst, or biomass. Bubble columns provide a uniform distribution due to the high circulation of liquid. However, back mixing and low contact efficiency reduce the mass transfer rate. Stirred tank reactors and rotating disc reactors provide higher interfacial area, however, high power consumption is required and the top-to-bottom mixing is poor. Airlift reactors and fluidized bed reactors are simple designs with no moving parts or agitators for less

maintenance and less risk of defects. The disadvantage is that inefficient in avoiding the foaming and greater air throughput and higher pressures are needed.

Either oscillating a stack of plates as in a pulsed plate column (also known as a reciprocating plate column) or oscillating the liquid phase as in a pulsing liquid column can be utilized as a gas-liquid contactor to apply the oscillatory motion that creates an oscillation velocity vector between the plates and the phases (Dhanasekaran and Karunanithi 2010) to enhance mass transfer.

Karr (1959) developed a Reciprocating plate column (RPC) or pulsed plate column (PPC), which was predominantly used for industrial-scale liquid-liquid extraction processes. As an advancement of the bubble column, PPC has been found to provide an increased interfacial area for g-l mass transfer and has received much attention (Stella et al. 2008) as a g-l contactor. However, unlike bubble columns, in the PPC, the mixing between the phases is facilitated by gas flow through the column and more predominantly by the reciprocating motion of the axially mounted stack of perforated plates (Skala and Veljković 1988). PPC is a multiphase contactor. It combines aeration and agitation and ensures favorable hydrodynamics and mass transfer characteristics. The pulsing effect provides good mixing, more extensive turbulence, an improved interfacial area, and a greater dispersed phase holdup. Hence, it helps to enhance the g-l mass transfer efficiency (Jiao et al. 2013; Kodialbail and Srinikethan 2011; Lounes and Thibault 1994; Panahinia et al. 2017; Shetty et al. 2007) and the excellent g-l mass transfer characteristics of PPC (Gomaa and Al Taweel 2005; Lounes and Thibault 1994; Shetty and Srinikethan 2010; Skala and Veljković 1988).

PPCs have been used as biological reactors for several applications, including aerobic wastewater treatment (Brauer 1985, 1990; Prabhu et al. 2020; Shetty et al. 2007, 2013). The superior g-l mass transfer characteristics of this contactor may lead to it finding applications in many other processes such as CO₂ absorption, NH₃ absorption, and catalytic or photocatalytic reactions apart from its use in biochemical reactions, involving the transfer of oxygen or other gases from the gas to the liquid phase. It is noticed from the literature that g-l mass transfer in this type of contactor may be enhanced by increasing the amplitude and frequency of pulsation (Gomaa and Al Taweel 2005; Lounes and Thibault 1994; Shetty and Srinikethan 2010).

Several investigations have shown that the enhancement of g-l mass transfer can also be achieved by the addition of solid particles in the reactor fluid. This improves the rate of transfer compared to that in the conventional aqueous medium (Komati and Suresh 2010; Linek et al. 2008; Manikandan et al. 2012; Nagy et al. 2007; Nagy and Hadik 2003; Olle et al. 2006). The progressive effect of nanosized particles is utilized to overcome the scarcity of oxygen supply to the aqueous medium by enhancing the mass transfer coefficient and interfacial area for mass transfer (Jiang et al. 2015; Labbeiki et al. 2014; Wenmakers et al. 2016).

Regarding PPC, if the mass transfer enhancement can be achieved by dispersing the nanoparticles in the reactor liquid to form a nanofluid, the column may be operated at lower frequencies of pulsation to achieve a similar mass transfer rate. This would result in lower operating costs and improved performance with higher energy efficiency. In other words, desired mass transfer efficiency can be achieved at lower pulsing conditions if a nanofluid replaces the conventional base fluid. The nanoparticles may be added into the system fluid to form nanofluids as in biochemical reactors or absorption systems to enhance gas-liquid mass transfer. There may be a natural presence of nanofluids in the contactors, such as reactors used for catalytic and photocatalytic applications, wherein nanosized catalysts may be present in dispersed form in the process fluid. In the photocatalytic reactors, oxygen acts as an oxidant, thus supplying oxygen. The photocatalytic reactors employed with TiO₂ nanoparticles as photocatalysts are generally equipped with an air supply to provide oxygen as the oxidant (Armaković et al. 2023). Dissolved oxygen plays a vital role in these reactors and thus oxygen mass transfer becomes essential.

Further, nanoparticles may be added to enhance g-l mass transfer (Ghasem 2019; Jiang et al. 2015; Olle et al. 2006). In either case of the inherent presence or intentional inclusion of nanoparticles, the presence of these nanoparticles as nanofluids may influence the oxygen mass transfer characteristics of the column. Thus, there arises a need to study the g-l mass transfer in pulsed plate columns in the presence of nanofluids.

Nanofluids (NFs) are the engineered colloidal suspensions prepared by dispersing nano-sized particles (size lesser than 100 nm) into conventional liquids which act as base fluids (Das et al. 2007). During the last decade, nanostructured materials have received increasing enthusiastic interest in various disciplines such as engineering

sciences, chemistry, physics, medical science, and biology (Chang et al. 2005). Choi (1995), coined the term nanofluid and proposed that the engineered conventional fluids showed better thermal conductivities compared to conventional fluids and enhanced the heat transfer characteristics. The particles could be metal nanoparticles such as Cu, and Ni; oxides such as TiO₂, SiO₂, Fe₂O₃, CuO, Fe₃O₄, and other materials such as AlN, SiC, and graphene (Mahbulul et al. 2012; Pang et al. 2015; Uddin et al. 2016; Yılmaz Aydın and Gürü 2022) and composite materials such as core-shell nanoparticles, nanocomposites that are well suspended in a base fluid to obtain nanofluid (Nithiyantham et al. 2019). Though different base fluids such as oil, ethylene glycol, toluene, kerosene, etc., are used effectively as a carrier in many industrial processes due to their unique thermodynamic and transport properties, water is used extensively as a base fluid because of its availability, low cost, and friendliness to the environment (Saidur et al. 2011). Moreover, the choice of base fluid targeted at nanofluid-mediated mass transfer enhancement also depends on the liquid phase being used in the reactors, bioreactors, or gas-liquid, liquid-liquid contactors. As, most of the catalytic, photocatalytic reactor, or bioreactor systems used for wastewater treatment applications or other bioprocesses are operated with the aqueous phase, the base fluid may be generally water.

The use of nanofluids plays a major role in the development of energy-efficient equipment. These NFs are said to be superior compared to base fluid, because of enhanced thermal and physical properties like thermal conductivity, density, viscosity, and diffusivity (Ali et al. 2018) that result in enhancement of heat and mass transfer rates. Several researchers have studied the enhancement of heat transfer performance using nanofluids (Jiang et al. 2019c; Keblinski et al. 2005; Pang et al. 2015; Prasher et al. 2006; Vakilinejad et al. 2018) with improved thermal conductivity, and convective and boiling heat transfer properties in various heat exchangers. To understand the enhancement (Buongiorno 2006; Krishnamurthy et al. 2006; Serna 2016) investigations on various mechanisms are the Brownian movement of the nanoparticles following the micro-convection (Keblinski et al. 2005b), thermal diffusion (Rudyak 2015), increased conduction through aggregates, or particle-to-particle coupling through the interparticle potentials, liquid layering on the nanoparticle-liquid interface and reduction in thermal boundary layer thickness (Xue et al. 2004) have been reported.

Investigations on possible applications of nanofluids in mass transfer were sparked by the success of using nanoparticles to improve heat transfer (Fang et al. 2009). As the mass transfer processes are analogous to most of the heat transfer processes in various aspects, the tremendous achievement in the usage of nanofluids for improving heat transfer performance has robustly motivated the researchers to study their potential application in the field of mass transfer for enhancing the g-l mass transfer process (Ashrafmansouri and Esfahany 2014; Krishnamurthy et al. 2006; Pang et al. 2015; Veilleux and Coulombe 2011). Since some researchers believed that one of the main reasons for the intensification of heat transfer was the Brownian movement of nanoparticles, exploration of mass transfer enhancement in nanofluids with a similar mechanism has been reported. (Jang and Choi 2004; Krishnamurthy et al. 2006; Rahbar et al. 2011).

Several researchers have investigated the effect of nanofluids on mass transfer, mainly focused on the absorption of gases such as O₂, CO₂, NH₃, H₂S, etc., in various nanofluids in different reactors or contractors (Beiki et al. 2013; Darvanjooghi et al. 2018; Esmaeili-Faraj and Nasr Esfahany 2016; Esmaeili Faraj et al. 2014; Irani et al. 2019; Kim et al. 2006; Komati and Suresh 2010; Li et al. 2014; Nagy et al. 2007; Olle et al. 2006; Su et al. 2015; Torres Pineda and Kang 2016). Various studies have shown the mass transfer enhancement in the presence of nanofluids such as the enhancement in k_{La} in the colloidal dispersions of magnetite (Fe₃O₄) nanoparticles coated with oleic acid in an agitated sparged reactor (Olle et al. 2006), by silica nanofluids in Taylor flow regime in the microchannel (Huang et al. 2021), mass transfer enhancement of NH₃/H₂O in absorber with distributor using Al₂O₃ and CNT nanoparticles (Lee et al. 2010), enhancement in rate of absorption of CO₂ in packed bed column with Al₂O₃ and SiO₂ nanofluids (Salimi et al. 2015), enhancement in absorption of CO₂ by Al₂O₃ - methanol and SiO₂ - methanol nanofluids in a tray column absorber (Torres Pineda et al. 2012), improvement of absorption of CO₂ using Al₂O₃ nanofluids in a stirred thermostatic reactor (Lu et al. 2015), enhancement in CO₂ absorption using Al₂O₃/water and Fe₃O₄/water nanofluids in a wetted-wall column with external magnetic field (Samadi et al. 2014), k_{La} enhancement with TiO₂, Al₂O₃, and SiO₂ NFs in water in rotating packed bed column (Ghadyanlou et al. 2022), enhancement in dye diffusion rate in liquids containing Al₂O₃ nanoparticles (Krishnamurthy et al. 2006), enhancement in k_{La} using oxygen -sensitive dye in a helically coiled tube reactor

(Jokiel et al. 2017), enhancement of CO₂ absorption in Fe₂O₃, CNT SiO₂ and Al₂O₃ nanofluid in hollow fiber membrane contactor (Peyravi et al. 2015), mass transfer enhancement by Fe₂O₄ nanoparticles for CO₂ absorption in bubbling reactor (Zhang et al. 2020a), enhancement in mass transfer coefficient for carbon dioxide and oxygen absorption in wetted wall column and in a capillary tube with magnetic iron oxide nanoparticles (Komati and Suresh 2010), k_{LA} enhancement with Fe₂O₃ - water nanofluids in an agitated bioreactor (Manikandan et al. 2012), enhancement in oxygen absorption rate with TiO₂ and SiO₂ nanofluids in a thermostatic stirred tank (Jiang et al. 2015) and enhancement of g-l mass transfer in the presence of TiO₂ nanoparticles in the process of droplet evaporation (Jiang et al. 2020).

In the present work, the influence of the nanofluids on the g-l mass transfer coefficient in terms of volumetric oxygen mass transfer coefficient (k_{LA}) in PPC is studied with water-based TiO₂, SiO₂ and, α -Fe₂O₃ Nanofluids. The studies on the effect of nanoparticle loading in the nanofluid, pulsing parameters of the column, superficial air velocity, size of nanoparticles, and type of nanofluid are reported. Further, order of magnitude analysis to understand the basic mechanism responsible for k_{LA} enhancement, evaluation, and assessment of the validity of Pseudo homogeneous model along with the development of Multiple regression models in terms of dimensionless numbers and Artificial neural network models to predict the k_{LA} in PPC are presented.

CHAPTER 2 LITERATURE REVIEW

This chapter focuses on the review of literature on the subject of this research work. The importance of volumetric gas-liquid mass transfer coefficient (k_{LA}), factors affecting k_{LA} , nanofluids, and their applications, the influence of nanofluids on mass diffusion and convective mass transfer coefficient with special focus on gas-liquid mass transfer and oxygen mass transfer in various types of contactors. This chapter also discusses the review of literature on PPC, its application, and the effect of various operating conditions on k_{LA} in PPC. The literature review on various types of models for the prediction of k_{LA} is presented along with the methods for finding the possible mechanism behind the enhancement of k_{LA} in the presence of nanofluids.

2.1. Volumetric gas-liquid mass transfer coefficient (k_{LA})

The gas-liquid mass transfer has significant importance in various fields such as chemical biochemical industries, environmental pollution control such as wastewater treatment, absorption of pollutants from air or flue gas, and others (Ho et al. 2020). Transfer of oxygen or gas transfer is essential in wastewater treatment plants to uphold the aerobic degradation, dissolve the chlorine gas or ozone, and also to separate or remove undesirable volatile chemicals such as carbon tetrachloride, tetrachloroethylene, trichloroethylene, chloroform, bromodichloromethane, and bromoform from water (Zander et al. 1989). k_{LA} is the primary parameter utilized to ensure adequate oxygen transfer and also the key parameter for the design and scale-up of the biochemical reactors (Mestre et al. 2019). Oxygen is considered to be the most efficient and favored electron acceptor for most microorganisms (Gupta and Ibaraki 2006; Liu et al. 2022). Oxygen mass transfer is an essential process in aerobic bioreactors or other chemical reactors involving the transfer of oxygen to the liquid phase from the gas phase. The transport of oxygen from a gaseous phase to a liquid phase becomes a rate-limiting step in various bioreactor systems because of the lower oxygen solubility in water. Therefore, the oxygen transfer is of greater importance and it is essential to achieve higher value of k_{LA} in all the systems where oxygen transfer to liquid phase is involved. k_{LA} is an important design parameter which is required in designing reactor systems or contactors in chemical, pharmaceutical, food, bio-fuel and other bio-chemical process industries.

In an aeration system, a gaseous species is transferred through the g-l interface followed by the liquid phase diffusion from the air bubble. Whitman's two-film theory states that equilibrium at the interface is assumed and that the resistances to mass transfer in the two phases are summed to determine the overall resistance. An overall coefficient is the overall resistance's reciprocal (Lewis and Whitman 1924). Concentration gradients near a gas-liquid interface are shown in Fig.2.1

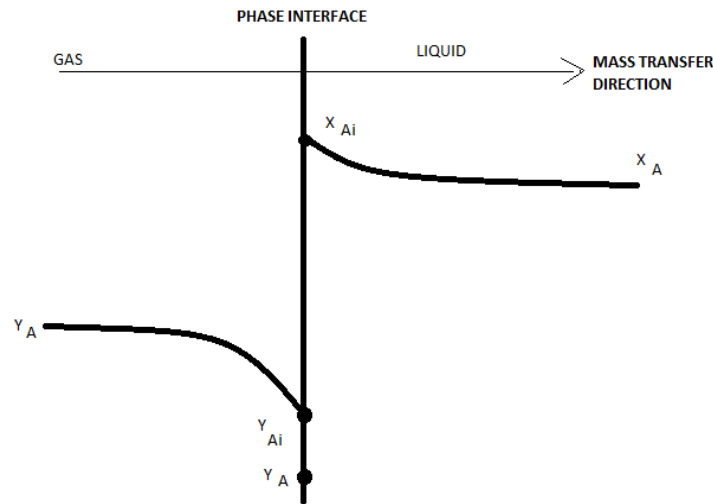


Fig 2.1: Concentration Gradients near Gas-Liquid Interface.

Considering the transfer rate to the interface is equal to the transfer rate from the interface. They can be expressed as shown below.

Rate of mass transfer on the gas side,

$$r_G = k_G A_a (Y_A - Y_{Ai}) \dots\dots\dots (2.1)$$

Rate of mass transfer on the liquid side,

$$r_L = k_L A_a (X_{Ai} - X_A) \dots\dots\dots (2.2)$$

At a steady state, because there can be no accumulation of A at the interface or anywhere else in the system, any A transported through gas must also be transported through liquid. This means the following:

$$r = r_G = r_L \dots\dots\dots (2.3)$$

At the interface, between the g-l phase, an equilibrium is attained. For dilute concentrations of most gases and a wide range of concentration for some gases, the equilibrium concentration in the gas phase is a linear function of liquid concentration. Therefore, we can write:

$$Y_{A_i} = mX_{A_i} \dots\dots\dots (2.4)$$

Where m is the distribution factor.

Since $k_G \gg k_L$, i.e. which means all the resistance is in the liquid film, which is generally true if the gas is sparingly soluble in the liquid as in the case of reduced oxygen solubility in water.

Then $Y_A = Y_{A_i}$;

k_G = mass transfer coefficient at gas phase m/s

k_L = mass transfer coefficient at liquid phase m/s

X_A = bulk liquid phase concentration

X_{A_i} = Liquid interphase concentration

Y_A = bulk gas phase concentration

Y_{A_i} = interface concentration in the gas phase

A_a = interfacial area

Therefore, equation (2.1) can be written as

$$r = k_L A_a \left(\frac{Y_A}{m} - X_A \right) \dots\dots\dots (2.5)$$

The driving force is the difference between the concentration of gas species A in the liquid and it is in equilibrium with the bulk gas and liquid phase concentration.

While the transfer of gas is considered for complete reactor volume, then, A_a is the total interfacial area and k_L is the average mass transfer coefficient. Hence the concentrations

in Equation. (2.5) are bulk gas and liquid phase species concentrations. When the equation is divided by liquid phase volume V, the resulting term is the amount of gas species transferred per unit volume per unit time. The rate of transfer is expressed per unit volume of reactor (R) in Equation. (2.6).

$$R = k_L \frac{A_a}{V} \left(\frac{Y_A}{m} - X_A \right) \dots\dots\dots (2.6)$$

Furthermore, it is convenient to use interfacial area per unit volume, ‘a’ as in Equation. (2.7) rather than total area A_a, because the rate of transfer is expressed per unit volume of the reactor.

$$R = k_L a \left(\frac{Y_A}{m} - X_A \right) \dots\dots\dots (2.7)$$

The term, k_La represents the product of the mass transfer coefficient and ‘a’, the interfacial area available for mass transfer per unit volume of the reactor. To maintain a high interfacial area and increase the rate of transfer, gas is sparged into a reactor while the liquid is stirred to break up bubbles. The area "a" in such systems is difficult to measure or estimate. However, the term k_La formed by the product of the mass transfer coefficient and the interfacial area is easier to quantify. Therefore, the term "k_La" is created by adding the terms "interfacial area per unit volume" (a) and "mass transfer coefficient" (k_L). In Equation (2.7) the term, Y_A/m can be replaced by component gas solubility at the reactor conditions, X_A^{*}.

$$R = k_L a (X_A^* - X_A) \dots\dots\dots (2.8)$$

Equation 2.8 is used for describing the transfer of gaseous species from a gas phase to a liquid phase.

2.2 Factors affecting g-l mass transfer rates

Many factors affect mass transfer in g-l dispersions, including (Akita and Yoshida 1973; Amaral et al. 2019; Garcia-Ochoa and Gomez 2005; Littlejohns and Daugulis 2007; Sideman et al. 1966) gas and liquid properties, different types of gas diffusers, column dimensions such as number of plates or baffles, spacing, perforation diameter, energy required for the oscillatory motions, flow rates of the gas and liquid, presence of third phase as solid catalysts, occurrence of reactions.

The most dependent parameters are as follows:

- (i) **Bubble size:** The bubble size is a very essential factor in designing the g-l reactors as it has a direct influence on the gas holdup and the interfacial area (Bouaifi et al. 2001; Manjrekar et al. 2017). Wang et al. (2020), have experimentally found that decreasing the bubble size can efficiently increase the k_{La} . Ham et al. (2021), studied that a decrease in the bubble size results in higher interfacial area and gas holdup values.
- (ii) **Gas holdup:** Gas holdup is the ratio of occupied volume by the bubbles to the total volume, it's the volume fraction of the dispersed gas in the gas-liquid system. To enhance the mass transfer rate, higher gas holdup is preferred along with the reduced bubble size (Barros et al. 2022).

Recently, there have been reports on enhancing gas-liquid mass transfer by using nanofluids (Ding et al. 2023; Jiang et al. 2019; Ramprasad et al. 2019; Zhang et al. 2018a). The ability of nanofluids to improve mass and heat transfer processes has been demonstrated. (Ashrafmansouri and Esfahany 2014; Dong et al. 2022; Qureshi et al. 2017; Uddin et al. 2016; Zhang et al. 2022)

2.3 Nanofluids

Advancement in nanotechnology has developed a perception of researchers towards nanosized materials. The detailed exploration of small materials ranging from 1 to 100nm has grabbed the attention of developing research areas. This has empowered many researchers to construct different unique and improved nanomaterials, nanodevices, and, nanotools that are used in various fields such as electronics, pharmaceutical, medicine, photography, and energy, etc., (Khalil et al. 2017). Nanomaterials are manufactured using a large variety of chemical components for example metals, metal oxides, carbon, semiconductors, and, polymers. They can be obtained in different forms such as fibers, spheres, wires, tubes, rods, needles, shells, plates, coatings, rings, etc., Specific functionalities can be incorporated into the nanomaterials by treating or coating a surface. Generally, nanomaterials are preferred over bulk-sized materials due to their exceptional adjustable size-dependent physical and chemical properties which are not found in their original bulk-sized materials (Liu Yang, Jian-nan Huang, Weikai Ji 2020; Souza et al. 2022).

The term “Nanofluid” was coined by Choi et al. (1996) at Argonne National Laboratory to refer to a new class of fluids consisting of colloidal suspensions of nanoparticles into a base fluid. Maxwell in 1881, was the first person to report from his research that the usage of colloidal particles that have higher thermal conductivity might show improvement in the thermal properties of conventional base fluids. Therefore, this suspension of nanoparticle liquid is termed Nanofluids (Gupta et al. 2020). As discussed in the introduction part, nanofluids possess improved properties compared to conventional base fluids. Researchers have done numerous experiments on nanofluids due to their anomalous enhancement of heat transfer (Masuda et al. 1993; Pang et al. 2015; Souza et al. 2022), and mass transfer (Imran et al. 2022; Krishnamurthy et al. 2006; Pahlevaninezhad et al. 2021). Different superior properties of nanofluids have initiated many researchers to perform experiments on nanofluids for various applications such as solar systems, refrigeration systems with enhanced thermal and physical properties, and transfer of heat of various systems, nanomedicines, and absorption (Deshmukh et al. 2019; Wang et al. 2023).

2.3.1 Preparation of Nanofluids

Nanofluids are prepared to obtain a uniformly dispersed colloidal suspension of nanoparticles in the base fluid (Kumar and Subudhi 2019). They are produced by two different methods (i) One-step or single-step method and (ii) two-step method and are as follows:

(i) One-step / Single-step Method:

This method consists of simultaneous production and suspending the particles in the base fluid. The agglomeration of nanoparticles is reduced, and the stability of nanofluids is increased here by avoiding the drying, storage, transportation, and dispersion of nanoparticles. (Bairwa et al. 2015; Mamat and Ramadan 2022). The major disadvantage is that as a consequence of incomplete reactions a residual may remain in the suspension and large-scale synthesis of nanofluids is difficult (Dhinesh Kumar and Valan Arasu 2018).

(ii) Two-Step Method:

This method is the most widely used method for the preparation of nanofluids. Initially, nanoparticles are produced as dry powders by chemical or

physical methods or any other methods. Secondly, the nanosized powder will be suspended in a base fluid using either intensive magnetic force agitation, ultrasonic agitation, high-shear mixing, or homogenizing (Deshmukh et al. 2019). The two-step method has proved to be the most economical and advantageous method to produce nanofluids, especially for large-scale requirements. The only difficulty with this method is the preservation of the long-term stability of nanofluids (Aglawe et al. 2020; Ranjbarzadeh et al. 2019).

According to the literature, the nanoparticles may be purposefully added into the system fluid to form nanofluids as in biochemical reactors or in absorption systems to enhance gas-liquid mass transfer or there may be an inherent presence of nanofluids in the contactors such as reactors used for catalytic and photocatalytic applications (Yılmaz Aydın and Gürü 2022), wherein nanosized catalyst may be present in dispersed form in the process fluid. In the present study, a two-step method for the preparation of nanofluids was adopted.

2.3.2 Applications of Nanofluids

The concept of nanofluids has originated more than a decade ago. The unique properties of nanofluids have attracted the attention of researchers from various fields. For this reason, nanofluids are utilized for various purposes. The various applications of nanofluid are depicted in Fig. 2.2 and are as follows:

- ✓ **Nanofluids in cooling application:** Nanofluids provide improved thermal properties compared to pure water and other coolants (Bairwa et al. 2015). They can be used as automotive oil, coolant, lubricant, gear oil, and, transmission fluid, brake fluid (Sarafraz and Peyghambarzadeh 2012).
- ✓ **Nanofluids in solar devices:** Nanofluid-based collector has better absorption capacity compared to other working fluids (Mahian et al. 2013). Due to their higher thermal conductivity and radiative properties nanoparticles, they are being utilized in water heaters, solar cooling systems, solar cells, solar stills, and solar absorption refrigeration systems, (Okonkwo et al. 2021; Raghav and Dinesh 2016).

- ✓ **Nanofluids in biomedical applications:** Nanofluids have been used for, cancer therapeutics, sensing, imaging, and Nano-cryosurgery (Agnihotri et al. 2019; Deodhar et al. 2014). Magnetic nanofluids for hyperthermia (Ghazanfari et al. 2016), magnetic cell separations, and magnetic resonance imaging (Imran et al. 2022; Sheikhpour et al. 2020).
- ✓ **Nanofluids as media for chemical reactions:** Photocatalytic nanofluids have been used for the conversion of CO₂ into methane, methanol, ethylene, and formaldehyde (Tan et al. 2017). Nanofluid-based – fuel (namely biodiesel and biofuels) helps to enhance engine efficiency by controlling particulate emissions (Chamsa-ard et al. 2017).
- ✓ **Other electromagnetic applications:** Nanofluids can be potentially utilized to produce optical fibers (Khan et al. 2019) or to produce lasers (Lu et al. 2021).
- ✓ **Applications of nanofluids in domestic refrigerators:** Nowadays in refrigeration equipment the usage of nanofluids has improved the thermodynamic, mechanical performance, and energy efficiency of the refrigerating systems associated with the reduction in CO₂ emissions. Haque et al. (2016), found that by the addition of the TiO₂ and Al₂O₃ nanoparticles into the polyester oil energy consumption was less compared to the pure POE oil system and it enhanced the performance of the refrigerator.
- ✓ **Nanofluids in other applications:** The usage of nanofluids helps in decreasing the consumption of energy along with the emissions from domestic and industrial air conditioning applications. Due to nanofluids' high critical heat flux capacity, they have been utilized in defense systems like submarines, high-power diode lasers, etc. Nanofluids are potentially used in these fields due to the lighter weight components and greater power density. Magnetic nanofluids are more cost-effective, environmentally friendly, and hazard-proof sealing compared to mechanical sealing to the larger number of rotational equipment in the industry (Jama et al. 2016; Munyalo and Zhang 2018; Yılmaz Aydın and Gürü 2022).

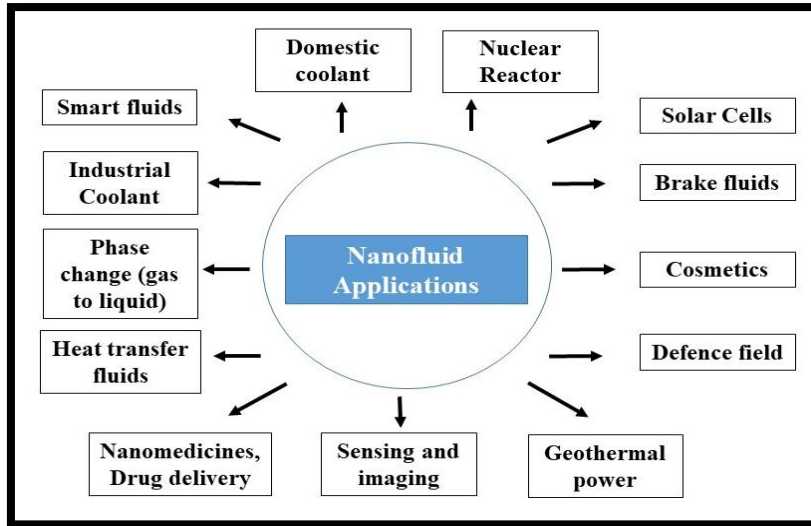


Fig. 2.2: Application of nanofluids in various sectors.

2.4 Heat transfer in Nanofluids

From the review of literature, in comparison to base fluids like oil or water, nanofluids have been found to have improved thermo-physical properties like thermal conductivity, thermal diffusivity, viscosity, and convective heat transfer (Choi 1995; Dong et al. 2022; K R et al. 2014; Murshed et al. 2020; Park et al. 2006). The research on the heat transport in nanofluids mainly focuses on Thermal conductivity and convective heat transfer (Kebllinski et al. 2005).

2.4.1 Thermal conductivity

Enhancement in thermal conductivity concerning base fluid has been observed in the Nanofluids of various nanoparticles such as Al_2O_3 (Purbia et al. 2019), CuO (Boukerma and Kadja 2017), Cu (Ali et al. 2021), SiC (Wang et al. 2020), TiO_2 (Purbia et al. 2019), SiO_2 (Jeelani et al. 2020), Au (Li et al. 2015), Ag (Jafarimoghaddam and Aberoumand 2017), ZnO (He et al. 2016), etc. prepared with base fluids such as water (Hamid et al. 2018), oil (Said et al. 2022) or ethylene glycol (Traciak and Żyła 2022).

Kebllinski et al. (2002) have explained the possible reasons for the significant enhancement in the thermal conductivity of nanofluids. The increased collision because of the Brownian movement of the nanoparticles through the liquid results in direct heat transfer between the particles and hence the thermal conductivity increases. At the solid

interface, molecular-level liquid layering provides the more ordered arrangement of the atomic structure of the liquid compared to the bulk liquid. Thus this helps in improved conduction and enhances the thermal conductivity.

2.4.2 Convective heat transfer

The investigations on convective and boiling heat transfer are still few compared to the studies on thermal conductivity. Pak and Cho (1998), first experimentally found the convective heat transfer coefficient of submicron metal oxide particles under turbulent flow conditions. Later enhancement in convective heat transfer coefficient has been observed in nanofluids with various base fluids and nanoparticles (Dong et al. 2022; Eastman et al. 2004; Murshed et al. 2020; Purbia et al. 2019; Wen et al. 2009; Xuan and Li 2000).

2.5 Mass transfer in Nanofluids

In many aspects, researchers have shown that there is a close resemblance between heat and mass transfer. The correlations in mass transfer are analogous to heat transfer equations. The interesting investigations on the enhancement of heat transfer in the presence of nanofluids created a natural curiosity to explore the rates of mass transfer or the enhancement of mass transfer in the presence of nanofluids. The investigations on mass transfer in nanofluids were mainly divided into two groups (Ashrafmansouri and Esfahany 2014; Cheng et al. 2019; Pang et al. 2015).

- ✓ Studies on diffusion coefficients in nanofluids and
- ✓ Studies on convective mass transfer coefficients in nanofluids.

2.5.1 Studies on mass diffusion coefficients in nanofluids

Mass diffusion in nanofluids has not been studied as extensively as heat diffusion. A few studies related to mass diffusion in nanofluids are listed in Table 2.1. The enhancement factor shown in Table 2.1 is the ratio of molecular diffusivity of the nanofluid to that of the base fluid. Table 2.1 shows that the mass diffusivity in nanofluids is higher than that with the base fluid and the presence of nanoparticles tends to enhance the diffusivity of components.

Table 2.1 Studies on mass diffusion in nanofluids

Experimental approach	Type of Nanofluid	Enhancement factor	Reference
Diffusion of Fluorescent dye by optical method	Al ₂ O ₃ – Water	14 at 0.5% Al ₂ O ₃	Krishnamurthy et al. 2006
Diffusion of Fluorescent Rhodamine B dye by Taylor dispersion method	Cu- Water	26 at 0.5% Cu	Fang et al. 2009
Diffusion of Fluorescein di-sodium dye by diffusiophoretic	Alumina -water	6-15%	Dhuriya et al. 2018
CO ₂ absorption in nanofluids by equilibrium cell	Graphene-Oxide (GO)/MDEA	10.4%	Irani et al. 2019
Mass diffusivity of CO ₂ by pressure decay method	TiO ₂ – water SiO ₂ – water Al ₂ O ₃ - water	Maximum enhancement with TiO ₂ nanofluid	Dehghan et al. 2020
Diffusion of CO ₂ in nanofluids using Shadow graph method	SiO ₂ - methanol	23.04% for 0.05 vol%	Lee et al. 2021

2.5.2 Studies on convective mass transfer coefficients in nanofluids

Convective mass transfer coefficients play an important role in various gas-liquid contactors such as stirred tank contactors, wetted wall columns, bubble columns, airlift reactors, fluidized bed columns, packed columns, trickle bed columns, and rotating drum reactors. Fig 2.3 presents the schematic representation of the commonly used gas-liquid contactors. Investigations on convective mass transfer in nanofluids have been carried out by various researchers in different systems such as agitated absorption reactors, three-phase airlift reactors, bubble-type absorption systems, falling film absorption systems, tray column absorption systems, gas-liquid hollow fiber membrane systems, packed columns, direct measurements of mass transfer coefficients in the nanofluid system and liquid-liquid extraction system. The studies related to these systems are listed in Table 2.2. Most of the studies on convective mass transfer in nanofluids are related to enhancing the liquid side mass transfer coefficients for oxygen mass transfer, CO₂ absorption, and NH₃ absorption. Nanofluids have also been found to enhance the mass transfer in liquid-liquid extraction systems. It has been found that in most cases, the enhancement factor which is a ratio of the mass transfer coefficient in nanofluid to that in base fluid is greater than 1, indicating that nanofluids intensify mass transfer and lead to enhancement in mass flux or mass transfer coefficient.

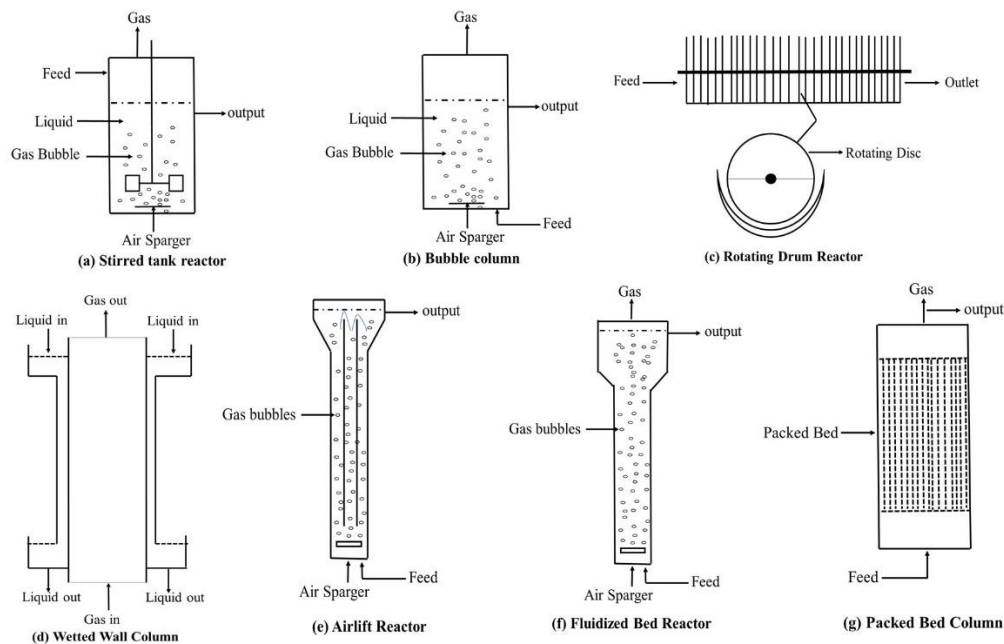


Fig 2.3 Schematic diagrams of various gas-liquid contactors

Table 2.2: Studies on convective mass transfer coefficients in nanofluids

Gas absorption in an agitated vessel			
Studies	Nanofluid	Enhancement factor	Reference
Oxygen mass transfer in an agitated sparged reactor	Fe ₃ O ₄ -Oleic acid	6 at 4% Fe ₃ O ₄	Olle et al. 2006
Oxygen transfer in a laboratory-scale stirred reactor	Nanometer n-hexadecane droplets - Water	2 at 10% vol or more droplets	Nagy et al. 2007
CO ₂ absorption in an agitated microreactor	SiO ₂ - Water	1.55 and 1.9 without and with mercaptan group surfactants at 4% SiO ₂	Zhu et al. 2008
Oxygen absorption in an agitated, aerated bioreactor	Fe ₂ O ₃ - Water	1.63 at 0.065% Fe ₂ O ₃	Manikandan et al. 2012
CO ₂ absorption in stirred thermostatic reactor	Al ₂ O ₃ – Water CNT- Water	1.15 for Al ₂ O ₃ and 1.83 for CNT	Lu et al. 2013
CO ₂ annular contactor absorption	Al ₂ O ₃ -methanol SiO ₂ -methanol TiO ₂ - methanol	1.012(at 56rpm), 1.011(at 90rpm), and 1.046 (at 112rpm)	Pineda et al. 2014
CO ₂ absorption in an isothermal stirred high-pressure cell	SiO ₂ – Water ZnO - Water	14% for ZnO and 7% for SiO ₂	Haghtalab et al. 2015
Oxygen absorption in thermostatic stirred tank	TiO ₂ -Na ₂ SO ₃ and SiO ₂ -Na ₂ SO ₃	1.82 – TiO ₂ 1.70 – SiO ₂	Jiang et al. 2015
CO ₂ absorption in a stirred self-designed cell	TiO ₂ – Propylene carbonate	1.6	Zhang et al. 2016

CO ₂ absorption in stirred thermostatic reactor	CNT - Water	4.5	Lu et al. 2017
CH ₄ hydrate formation in a stirred tank reactor	Graphite - Distilled water	3% increase compared to liquid water	Lu et al. 2021
Bubble-type absorption systems			
Studies	Nanofluid	Enhancement factor	Reference
Ammonia Absorption	Cu-NH ₃ /H ₂ O	3.21	Kim et al. 2006
	CuO-NH ₃ /H ₂ O	3.11	
	Al ₂ O ₃ -NH ₃ /H ₂ O	3.04	
Ammonia absorption	Cu-NH ₃ /H ₂ O	5.32	Kim et al. 2007
Ammonia absorption	CNTs-NH ₃ /H ₂ O	1.162	Ma et al. 2007
CO ₂ absorption	SiO ₂ -water	1.76	Kim et al. 2008
	SiO ₂ -	1.12	
	Piperazine/K ₂ CO ₃		
CO ₂ bubble absorption column	Al ₂ O ₃ -methanol	1.045	Lee et al. 2011
	SiO ₂ -methanol	1.056	
Ammonia bubble absorption column	Ag-NH ₃ /H ₂ O	1.55	Pang et al. 2012
CO ₂ absorption	Al ₂ O ₃ - NaCl/H ₂ O	1.125	Lee and Kang 2013
CO ₂ bubble absorption column	Al ₂ O ₃ -methanol	1.26	Kim et al. 2014
Ammonia tubular bubble absorption column	MWCNTs- NH ₃ /LiNO ₃	1.64	Amaris et al. 2014
CO ₂ bubble absorption column	CNT – Water TiO ₂ – Water SiO ₂ - Water	1.78	Saeednia et al. 2015

CO ₂ bubble column absorber	Fe ₂ O ₃ - Water	Enhanced CO ₂ solubility and average molar flux	Karimi Darvanjooghi et al. 2017
CO ₂ absorption in ammonia	TiO ₂ , SiO ₂ , CuO in ammonia	For TiO ₂ and SiO ₂ >1	Fang et al. 2017
CO ₂ capture in a bubble reaction system	TiO ₂ , Al ₂ O ₃ and SiO ₂ -TETA based nanofluids	1.29	Jiang et al. 2019
CO ₂ absorption in high-pressure column absorber	Fe ₂ O ₃ @ glutamine - N-methyl-2-pyrrolidone (NMP) nanofluid	Absorption of CO ₂ increased up to 19.41%	Elhambakhsh et al. 2021
H ₂ S and CO ₂ absorption in bubble absorber	NH ₂ functionalized MWCNTs -water	2.66 for CO ₂ and 4.04 for H ₂ S	Jafari Farsaani and Ameri 2022
Falling film flow absorption systems			
Studies	Nanofluid	Enhancement factor	Reference
CO ₂ absorption in a wetted wall column	Fe ₃ O ₄ -CO ₂ /MDEA	1.928 -	Komati and Suresh 2008
H ₂ O/LiBr falling film absorption	Al ₂ O ₃ -H ₂ O/LiBr	1.77	Lee et al. 2009
O ₂ and CO ₂ mass transfer in a wetted wall column and a capillary tube	Fe ₃ O ₄ -water	2.74 1.93	Komati and Suresh 2010
NH ₃ absorption in falling film flow	ZnFe ₂ O ₄ , Fe ₂ O ₃ , or Al ₂ O ₃ – NH ₃ /H ₂ O solution	1.7, 1.5, and 1.3 for Fe ₂ O ₃ , ZnFe ₂ O ₄ and	Yang et al. 2011

		Al ₂ O ₃ respectively	
CO ₂ column tray absorption	Al ₂ O ₃ -methanol SiO ₂ -methanol	1.094 1.097	Torres Pineda et al. 2012
CO ₂ membrane absorption	MWCNT-water SiO ₂ - water	1.4 1.2	Golkhar et al. 2013
CO ₂ Wetted wall column absorption with the magnetic field	Fe ₃ O ₄ -water	1.2235	Samadi et al. 2014
H ₂ O/LiBr falling film absorption	Ag - H ₂ O/LiBr	Mass transfer enhanced by 60% at solid volume fraction 10% of Ag nanoparticles	Armou et al. 2017
NH ₃ absorption in falling film flow	Al ₂ O ₃ , ZnO, and ZrO ₂ – H ₂ O	Al ₂ O ₃ - 1.122, ZnO -1.132, ZrO ₂ - 1.105,	Wu et al. 2017
Falling film absorption of LiBr/H ₂ O system	Cu, Al ₂ O ₃ and CNT -water	Absorption ration found to be above 1	Zhang et al. 2018
CO ₂ absorption in membrane contactor	CNT, SiO ₂ - water	Absorption rate increased upto 16% with SiO ₂ and 34% with CNT nanofluid	Rezakazemi et al. 2019
CO ₂ absorption in falling liquid film absorber system	Fe ₃ O ₄ – water	Mass transfer enhanced by 29% at loading of 0.05 vol%	Pahlevaninezhad et al. 2021
CO ₂ absorption in laboratory scale wetted wall column	Al ₂ O ₃ - water	67% increase in mass transfer coefficient with	Rashidi and Mamivand 2022

		0.025 % v/v nanoparticle.	
Liquid-Liquid Extraction Systems			
Studies	Nanofluid	Enhancement factor	Reference
Liquid – liquid extraction of kerosene-acetic acid	SiO ₂ –Kerosene + Acetic acid	mass transfer for the nanofluids enhances 4 – 60%.	Bahmanyar et al. 2011
Liquid–liquid extraction of toluene – acetic acid-water.	Fe ₃ O ₄ or Al ₂ O ₃ /toluene	Fe ₃ O ₄ :1.157, Al ₂ O ₃ :1.121	Saien and Bamdadi 2012
Liquid–liquid extraction of n-butanol–succinic acid–water	ZnO, CNT, and TiO ₂ -water	2.2, 1.8 and 1.6	Mirzazadeh Ghanadi et al. 2015
Liquid-liquid extraction of toluene - water	SiO ₂ -water	The mass transfer enhanced with liquid hold up by 4%	Nematbakhsh and Rahbar Kelishami 2016
Liquid-liquid extraction of toluene-acetic acid and water	Modified TiO ₂ - water	Overall enhancement of 70% with 3 wt% of solute.	Hatami et al. 2017
Liquid–liquid extraction of n-butanol-water - succinic acid	SiO ₂ -water	0.943	Azimi et al. 2019
Liquid–liquid extraction of toluene-Aston-water.	SiO ₂ -water	23%	Ghazvehi et al. 2021
Liquid–liquid extraction of kerosene-acetic acid-water	Carbon quantum dot nanofluid	263.5%	Jafari et al. 2022

2.5.3 Influence of nanofluids on gas-liquid mass transfer coefficient

The influence of Nanofluids on g-l mass transfer is summarized in Table 2.2.

Olle et al. (2006), have observed enhancement of oxygen transfer in an agitated sparged reactor using the nanofluid of magnetite nanoparticles coated with oleic acid and surfactant. They found the improved g-l oxygen mass transfer up to 6-fold (600%) for the volume fraction of nanoparticles below 1%. k_{LA} was determined by the physical method (Stirred beaker as experimental system) and chemical method (sodium sulfite oxidation). Enhancement in k_L measured by these methods was found to be almost similar and ranged from 20 to 60% approximately. The results showed that the enhancement in the k_{LA} is strongly temperature-dependent. The presence of nanoparticles enhanced the k_{LA} with a total enhancement of 80% or more. The results are applied to a wide range of activities, including fermentation, waste management, and hydrogenation reactions, which are restricted by the mass transfer of a solute between a gas phase and a liquid phase.

Nagy et al. (2007) also found the enhancement of oxygen mass transfer in the presence of organic material nanoparticles, namely 65nm n-hexadecane droplets, in a laboratory-scale stirred reactor. The enhancement measured reached over 200% for a relatively large loading of 10 vol%. Olle et al. (2006) and Nagy et al. (2007) proposed homogeneous as well as heterogeneous models of mass transfer enhancement in nanofluids considering Brownian motion.

Komati and Suresh (2010), synthesized the ferrofluids and examined its effect on g-l mass transfer rates and investigated the absorption of Carbon dioxide and Oxygen gases in various reactive and non-reactive liquids. The authors used wetted wall column and capillary tube connected to a gas balloon as model g-l contactors. The increase in kLa is mainly attributed to the increase in diffusivities of nanoparticles. The enhancement due to nanoparticles was correlated with holdup and modified Sherwood number as shown below

$$E_p = 1.519\varepsilon^{0.169} Sh'_m{}^{-0.157}$$

$$Sh'_m = \frac{d_p}{\lambda} = \frac{k_L d_p E}{D_A}$$

Where, E_p = enhancement in k_{LA} (E_p is defined as the ratio of k_{LA} with particles to k_{LA} without particles), d_p = diameter of the particle, nm; λ = penetration depth according to film theory, μm ; k_L = mass transfer coefficient m/s; D_A = diffusivity of A in the liquid phase m^2/s ; E = Chemical enhancement factor (defined as the difference between an interface's average concentration gradient with and without a chemical reaction).

Manikandan et al. (2012), experimentally found the enhancement in k_{LA} in an agitated, aerated bioreactor. Nanofluids were prepared by dispersing the Fe_2O_3 , iron oxide nanoparticles in water at a pH of 8.5. Results showed that the k_{LA} increased with an increase in nanoparticle concentration. An enhancement in k_{LA} was obtained to be 1.63 fold for 0.065% Fe_2O_3 – water nanofluids. At operating conditions of 200 rpm and 0.75 LPM air flow, 63% enhancement in oxygen transfer from gas to liquid was achieved.

Krishnamurthy et al. (2006) and **Olle et al. (2006)** have attributed the enhancement in mass transfer using nanofluids to nanoscale stirring of the liquid by Brownian motion. But in agitated aerated reactor, the role of nanoscale stirring was found negligible due to highly turbulent environment. Hence under this situation the responsible mechanism for enhancement was attributed to either ‘grazing effect’ or reduction in film thickness by shearing action.

Saeednia et al. (2015), investigated the effect of nanoparticles (CNT, TiO_2 , and SiO_2) on the mass transfer enhancement in absorption of CO_2 in a bubble column system. The absorption rate was found by determining the CO_2 concentration of the nanofluids using titration method. The nanofluid prepared with TiO_2 and SiO_2 in weight percentages of 0.01, 0.05, 0.1 and 0.5 Wt % and CNT in weight percentages of 0.01, 0.05, 0.07 and 0.1 Wt % were used. From the results it was found that absorption of CO_2 increased with the increase in the weight percentage of nanoparticles. Maximum absorption was obtained for CNT nanofluid at 0.07 wt % CNT and for TiO_2 nanofluid at 0.05% of TiO_2 and SiO_2 nanofluid 0.1% of SiO_2 nanoparticles. CNT was considered as the most effective nanomaterial among others. It was found that gas holdup increases with increasing nanomaterials concentration and gas superficial velocity and is higher in nanofluids than in water.

Jiang et al. (2015) studied the influence of $\text{TiO}_2\text{-Na}_2\text{SO}_3$ and $\text{SiO}_2\text{-Na}_2\text{SO}_3$ nanofluids in a thermostatic stirred tank. Various working conditions such as the influence of nanoparticles (TiO_2 and SiO_2), nanoparticle solids loading, stirring speed, temperature, and particle size on the average oxygen absorption rate were experimentally investigated during forced sulphite oxidation. The TiO_2 and SiO_2 nanoparticles improved the g-l mass transfer. The enhancement factor obtained was 1.95 and 1.82 for the TiO_2 nanoparticle of particle size 10 nm and 20 nm respectively, while for the SiO_2 nanoparticle the enhancement factor was 1.70 with the same loading and with particle size of 20 nm. The oxygen absorption enhancement factor was found to increase by increasing the stirring speed.

Fang et al. (2017) investigated the effect of nanoparticles (TiO_2 , CuO and SiO_2) on the CO_2 absorption in ammonia. Nanofluids were prepared with different concentrations of ammonia and different nanoparticles loading. The nanoparticle solid loading was varied from 1.0 – 8.0 g/L. They compared the effects of nanoparticle loading, types, ammonia concentration on the removal efficiency and removal rate with blank absorption experiment. Experimental results showed that the removal rate was enhanced in the presence of nanoparticles. They found that initial the enhancement factor increased, then decreased with increase in nanoparticle loading. With SiO_2 nanofluid the enhancement factor was marginally more than 1 for 1.0 g/L, 2.0 g/L and less than 1 for other loadings. With CuO nanofluid the enhancement factor was around 1, it was observed that CuO nanofluid showed no obvious enhancement or inhibition effect. With TiO_2 nanofluid the enhancement factor was greater than 1.

2.5.4 Mechanism of mass transfer enhancement in nanofluids

Knowledge of the mass transfer mechanism plays a crucial role in understanding the behavior of the nanoparticles in enhancing the mass transfer rate by nanoparticles in two-phase or multiphase systems. For g-l mass transfer, Kluytmans et al. (2003) have explained the possible mechanisms for the mass transfer enhancement.

- a) The particles are expected to increase the mass transfer coefficient by adding more gas to the liquid bulk through adsorption in the gas-liquid diffusion layer and desorption in the liquid bulk. This effect as a shuttle or grazing has been

described by Alper et al. (1980); Ashrafmansouri and Nasr Esfahany (2014); Quicker et al. (1987).

- b) The collision of nanoparticles and interaction with the g-l interface may cause turbulence at the g-l interface, this results in a reduction in the boundary layer thickness (Zhang et al. 2022). Therefore, the mass transfer coefficient could be increased in the existence of nanoparticles.
- c) The presence of nanoparticles helps in preventing the bubble coalescence as the movement of nanoparticles collides with each other and the bubbles. This results in the reduction of bubble size from bigger to smaller and thus the interfacial area becomes larger leading to the increase in mass transfer coefficient (Jiang et al. 2019).

As discussed by Keblinski et al. (2005), the possibility of enhancement of thermal conductivity evolves from different mechanisms. They are the Brownian motion of the particles, the molecular level of liquid layering of the liquid at the liquid/particle interface, and examined the nature of heat transport in nanoparticles. Therefore, to study the possibility of enhancement in mass transport, order-of-magnitude analysis was performed to predict the phenomenon clearly (Krishnamurthy et al. 2006).

Keblinski et al. (2001), studied the Brownian motion time and the time for conduction in liquid using an order-of-magnitude analysis. They found that Brownian diffusion time is two orders smaller compared to the time for conduction in liquid. However, the energy transport due to convection produced by the Brownian movement of nanoparticles was not considered. Hence, Prasher et al. (2006) implemented an analysis considering the time scale of the Brownian movement of particles and the time scale of the convection due to the movement of the particles. They found that the convection effects are instantaneous compared to the Brownian diffusion of the particle.

Krishnamurthy et al. (2006), investigated the effect of the presence of nanoparticles in a fluid on mass diffusion by visualizing the mass transport of dye in water and nanofluids. they conducted an order-of-magnitude analysis to investigate the reason for the observed enhancement in mass transport. They calculated the time (t_m) for the dye to diffuse through a distance equal to the diameter of the nanoparticles, the time required for a Brownian particle to travel its diameter (t_b), and further the time required for convection currents to travel a particle diameter (t_c). From the analysis, they found

that $t_b > t_m$, clearly indicated that there is no direct contribution of Brownian movement of nanoparticles in mass transfer enhancement. Also, t_c was smaller compared to both t_b and t_m . Thus, both the rise in the rate of mass transfer and the increases in thermal conductivity in nanofluids might be attributed to the disturbance field formed by the mobility of the nanoparticles in the fluid. This demonstrates how mass diffusion and other convection currents move through space considerably more quickly than individual particles.

2.6 Pulsed Plate Column

Pulsed plate columns (PPC) or Reciprocating plate columns (RPC) were originally developed for liquid-liquid extraction applications. The foremost characteristic of a Pulsed Plate Column is the arrangement of the reciprocating perforated plates mounted on a central rod inside a column. Initially, it was used for the liquid-liquid extraction process to generate a higher degree of turbulence, increase interfacial area, and obtain higher retentions of the dispersed phase. PPC provides higher energy to break down the droplets that contribute to attaining a large interfacial area to enhance mass transfer efficiency (Jiao et al. 2013a). The general principles of reciprocating plate columns were established by Van Dijk in 1935, who developed several systems to improve the efficiency of the solid-liquid extraction process. Later it was developed by Karr (1959) and has been used increasingly as a g-l contactor. Reciprocating plate columns have been extensively studied in recent years for their application in the contact of liquid-liquid and g-l phases. They were found effective for g-l contacting by offering much higher interfacial areas than a conventional tray or bubble columns and at a lower power consumption than those estimated for mechanically agitated tanks (H.G. Gomma 1991; Rama Rao and Baird 1988; Sundaresan and Varma 1990; Al Taweel 1984; VeljkoviC and Skala 1986; Yang et al. 1986). The size of the air bubbles reduces as they come in contact with the reciprocating motion of the plate stack, resulting in the enhancement of oxygen mass transfer. The reciprocating motion of the plate stack reduces the size of the air bubbles enhancing the oxygen mass transfer. In general, slightly higher k_{LA} values were obtained in a reciprocating plate column compared to other reactors (Gagnon et al. 1998). Thus, the Reciprocating Plate Column has been ranked as the bioreactor of the new generation due to the efficient mass transfer from the gas to the liquid phase (Stamenković et al. 2005).

Pulsed Plate column has been extensively studied for their application in the contact of liquid-liquid and g-l phases. Table 2.6 shows some of the applications of pulsed plate column as a bioreactor, chemical reactors, or gas absorption which involves the g-l transfer. The efficiency of the column depends on the geometry of the plates, the amplitude and the moving speed of the plates, and the flow velocity of each phase, factors that also control the velocity of axial mixing. Pulsed plate column has several advantages

- Large mass transfer coefficient due to periodical renewal of the interfacial area.
- the intensity of turbulence is uniform and prevents the dead spaces.
- The scaling up of the reactor is easier because the medium is open to identical conditions regardless of the diameter of the column.
- High utilization of oxygen contained in the air.
- High volume-based purification efficiency, at least ten times that of conventional bioreactors.
- A higher level of mixing enhances extended mass transfer from a liquid to a solid phase.
- The mixing of two phases is uniform
- It reduces the resistance to mass transfer

The applications cited in Table 2.3, show that pulsed plate column is widely used for applications that involve a g-l transfer.

Table 2.3 Summarizes the application of Pulsed plate column as a bioreactor, chemical reactor, or gas absorption which involves the g-l transfer.

Equipment used	Process type	References
Reciprocating jet bioreactor	Wastewater treatment	Brauer 1985
Reciprocating plate column	Air and different aqueous solutions (Dextran- Sucrose Fermentation broth)	Skala and Veljković 1988
Reciprocating plate column	Absorption of CO ₂	Sundaresan and Varma 1990

Reciprocating jet bioreactor	Growth of fungi and bacteria	Brauer 1990
Reciprocating jet bioreactor	Continuous production of citric acid	Daniel and Brauer 1994
Reciprocating plate bioreactor	Pullulan fermentation	Audet et al. 1996
Reciprocating plate bioreactor	<i>Vitis vinifera</i> culture	Gagnon et al. 1998
Pulsed Plate bioreactor	Biodegradation of phenol	Shetty et al. 2007a
Pulsed Plate bioreactor	Removal of phenol using immobilized cells	Shetty et al. 2007
Reciprocating plate column	The reaction system of $\text{Na}_2\text{CO}_3 - \text{CO}_2 - \text{H}_2\text{O}$ (absorption of CO_2)	An et al. 2010
Pulsed Plate bioreactor	Phenol degradation using immobilized <i>Nocardiahydrocarbonoxydans</i>	Shetty et al. 2011
Reciprocating plate bioreactor	fungal fermentation of <i>Trichoderma reesei</i> RUT-C30	Choy et al. 2011
Pulsed Sieve Plate Column	Arsenic removal from natural gas condensate	Chaturabul et al. 2012
Pulsed Plate bioreactor	Biodegradation of Phenol using immobilized <i>Nocardia hydrocarbonoxydans</i>	Shetty et al. 2013
Pulsed Plate bioreactor	Production of Exopolymeric Substances and Biofilm Characteristics during Phenol Biodegradation by Immobilized	Veena et al. 2016

	<i>Pseudomonas desmolyticum</i> (NCIM2112) Cells	
Pulsed Plate bioreactor	phenol biodegradation using immobilized <i>Pseudomonas desmolyticum</i> cells	Rangappa et al. 2016
Pulsed plate column	Bioleaching of copper from electronic waste using <i>Acinetobacter</i> sp. Cr B2	Jagannath et al. 2017
Reciprocating plate reactor	Production of biodiesel production from a waste pig-roasting lard, methanol and KOH	Miladinović et al. 2019
Pulsed Plate Column	Biosorption of Pb(II) on <i>Pteris vittata L.</i>	Prabhu et al. 2020
Pulsed Sieve Plate Column	Recovery of essential oils from wastewater	Najafipour et al. 2021

2.6.1 Studies on Gas-Liquid Mass Transfer Coefficient in Pulsed Plate Column

The most important feature of a Pulsed Plate Column is the provision of homogeneous g-l dispersion. The main benefit of the column is it can be used as a bioreactor since it provides the maximum oxygen transfer to fulfill the demand of microorganisms for oxygen. Also reduces the back mixing and energy dissipation.

Skala and Veljković (1988), conducted experiments to study the mass transfer characteristics of g-l reciprocating plate columns of the Karr type by different methods. The investigation was divided into two parts (1) determination of liquid phase volumetric mass transfer coefficient, k_{LA} (2) determination of interfacial area. k_{LA} was investigated using the sulfite oxidation method, the pure physical absorption of oxygen, and a dynamic method under culture conditions. The physical absorption method appeared to be the most favorable. The k_{LA} values determined by different methods under similar operating conditions were approximately the same. They found that k_{LA} increased with increasing vibration intensity (Axf), superficial gas velocity, and the

number of perforated plates. Liquid phase properties appeared to affect k_{LA} only slightly.

Rama Rao and Baird (1988), measured k_{LA} in a RPC under semi-batch and counter-current conditions. they reported that k_{LA} increased with the agitation rate and flow rates of continuous and dispersed phases. The correlation was developed to relate k_{LA} with flowrates of air and water, specific input power.

Sundaresan and Varma (1990), found k_{LA} and the interfacial area for carbon dioxide absorption into water. They found that k_{LA} is strongly influenced by the free area available in the plate and the perforation affects the interfacial area of the bubbles.

Lounes and Thibault (1993), used RPC as a bioreactor and studied the hydrodynamics, axial dispersion coefficient, and k_{LA} . Results indicated that the axial dispersion coefficient is dependent on the reciprocation motion and it is independent of the airflow rate. They determined k_{LA} by two separate methods. (a) sulphite oxidation method (b) gassing out method. They also found higher values of k_{LA} than in other types of mixing devices like helical ribbon screw mixers and Rushton turbines for identical volumetric power input.

(Vasić et al. (2007)), measured the volumetric mass transfer coefficient in 16.6cm i.d. multiphase reciprocating plate column by using the sulphite oxidation method and studied the effects of vibrational intensity, superficial gas velocity and content of solid particles (0 to 10%) on volumetric oxygen mass transfer coefficient. The authors reported that k_{LA} increased with increasing vibration intensity and superficial gas velocity with decreasing content of solid particles and increased with increasing diameter of reciprocating plate column.

(Shetty and Srinikethan (2010)), evaluated volumetric oxygen mass transfer coefficients in a three-phase pulsed plate column with a fixed bed of glass particles by using the sulphite oxidation methods and found that volumetric oxygen mass transfer increased (0.067 to 0.1495 s^{-1}) with an increase in superficial air velocity (0.011 to 0.047m/s) and vibrational velocity (0.825 to 6cm/s). The authors developed an empirical correlation relating k_{LA} with variables such as superficial air velocity and vibrational velocity.

The literature review suggests that there are no studies on gas-liquid mass in pulsed plate column with nanofluids.

2.7 Dimensionless correlations, theoretical models, and Artificial Neural Network (ANN) models for mass transfer in nanofluids.

Dimensionless correlations are commonly used in engineering to predict the behavior of complex systems and enable an improvement of the systems (Ramos et al. 2022). They are developed with dimensionless numbers, combining a group of variables in such a way that they have no units. It is represented as a ratio between the measurement of two different phenomena. The correlations for the mass transfer coefficient include the dimensionless groups such as Reynolds (Re), Sherwood (Sh), and Schmidt (Sc) numbers. These dimensionless groups were created for process scale-up, thus dimensionless analysis can be used to compare several reactors. (Chiang and Pan 2015). There is not much literature on g-l mass transfer in a pulsed plate column, and there are limited correlations for estimating it in the presence of nanoparticles.

Komati and Suresh (2010), have proposed correlations in terms of modified Sherwood number and particle volumetric holdup, that support the prediction of mass transfer enhancements. In particular, they have investigated the nanoparticle volumetric holdup and the size of the nanoparticles to the depth of the penetration of the diffusing solute as the important factor that helps in determining the enhancement in the mass transfer.

Feng and Johnson (2012), investigated that solution viscosity was influenced by the presence of nanoparticles and they found that the liquid mass transfer coefficients were found to decrease with an increase in viscosity. Hence a dimensionless correlation was developed to predict the liquid film mass transfer coefficient and to estimate the viscosity effects.

Bahmanyar et al. (2014), suggested an approach and proposed a correlation to predict the effective diffusivity and mass transfer coefficient. The dimensionless numbers involved are Reynolds number and Schmidt number. These were related to nanoparticle volume fraction in a pulsed liquid-liquid extraction column. The results indicated a good fit with the comparison of predicted and experimental results.

Khanolkar and Suresh (2015), have studied the effect of TiO₂ and SiO₂ nanoparticles on the rate of g-l mass transfer in capillary tube apparatus and proposed the convective diffusion model to explain the observed effects of particle size, holdup, and density of the material. The convective motion caused by the Brownian movement of the nanoparticles was considered to be the reason for the enhancement. Hence an effective convective velocity was suggested and determined by the experimental findings. The effective convective velocity was correlated with the modified Sherwood number, volume fraction of nanoparticles, and solid Reynolds number. The suggested model provided a good fit for the data from the wetted wall column (Komati and Suresh 2010) and capillary tube experiment for TiO₂, SiO₂, and Fe₃O₄ nanoparticles.

Nagy and Hadik (2003) and Nagy and Moser (1995), developed theoretical models that helped in understanding the ways to improve the mass transfer in the presence of nanosized particles. They constructed the two models, a pseudo-homogeneous and heterogeneous model. The development of the pseudo-homogeneous model was applied; the mass transfer is considered to be instantaneous inside the nanoparticles. The other heterogeneous model was applied when the solubility of the component in the dispersed phase is much higher than in the liquid phase, similarly as reported by Nagy (2007), an organic phase was used to enhance the oxygen mass transfer.

Hence there is a need to develop a correlation to predict the volumetric gas-liquid mass transfer coefficient in the Pulsed plate column with respect to the effect of nanoparticles and the experimental operating conditions.

ANN is a robust tool for modeling and is inspired by the human nervous system. For extremely complex simulation models, the ANN may be an effective substitute for parametric modeling. Therefore, it can be used for estimation and prediction. ANN can be of greater interest in chemical engineering, and it has been used for many purposes such as process control (Ungar et al. 1990), prediction of variables, optimization, and modeling of bioreactors (Tholudur and Ramirez 1996; Thompson and Kramer 1994) and has been applied for k_{La} estimation in water (Baawain et al. 2007; Kojić and Omorjan 2017; Reuss 1995).

ANN is composed of multiple interrelated processing elements called neurons. It has a network structure wherein neurons are arranged in different layers such as, initially an

input layer that receives the input variable data, a hidden layer in which the data is processed, and finally, an output layer that sends the processed information. Each neuron of the hidden layer is interconnected to input and output layers using weights and biases. (Janghorban Esfahani et al. 2012). The main advantage of an ANN is that a precise output or target can be obtained by training and regulating the determined input (Kahani and Vatankhah 2019). From the literature findings, it is reported that ANN is used in many applications such as to predict the k_{LA} , gas hold-up, and the average bubble diameter in bubble columns using column geometry and operating conditions as input parameters (Baawain et al. 2007). Lemoine et al. (2003) have developed dimensional and dimensionless back propagation neural networks (BPNNs), correlating the volumetric mass transfer coefficient for various gas-liquid systems both in surface-aeration reactors and gas-inducing reactors that are operated under different industrial conditions. The ANN-based model was also developed for the prediction of the biodegradation of phenol in a pulsed plate bioreactor (Shetty et al. 2008). Valera et al. (2021) have also developed an ANN model for the prediction of SO_2 removal efficiency and volumetric mass transfer coefficient at the gas side (k_{ga}) for Gas Desulfurization in the Spray Tower as a function of the operating conditions and configuration of the spray nozzles. Liu et al. (2019) have developed ANN model by employing dimensionless variables like the Reynolds number of gas, liquid, Froude number, and Weber number used to estimate the mass transfer coefficient of the ozone absorption process in a rotating packed bed. Saha (2009), employed ANN to predict mass transfer coefficient in a rotating packed bed. ANN model has been developed by García-Ochoa and Castro (2001) to estimate the oxygen mass transfer coefficient in stirred tank reactors. A dimensional and dimensionless back-propagation neural network has been developed to correlate k_{LA} for surface-aeration reactors and gas-inducing reactors operating under wide ranges of industrial conditions (Erzin et al. 2009; Lemoine et al. 2003; Shetty et al. 2008). Several researchers have reported that the ANN models exhibit higher prediction performance than the MRA models (Kim and Oh 2021; Miloš Madić 2012).

Based on the literature review, it was proposed to test the existing theoretical model to test their validity for the pulse plate column. Further, to account for the inaccurate predictions by theoretical models and wider and easier applicability dimensionless correlations and ANN models were proposed to be developed.

2.8 Scope of the research work

With pulsed plate column is used for several g-l contacting operations such as for aerobic biological reactions (Brauer 1985; Jagannath et al. 2017; Shetty et al. 2007) or gas absorption (Sundaresan and Varma 1990) or chemical reactions involving g-l transfer (An et al. 2010), there is a need to study if the gas-liquid mass transfer can be enhanced by using different nanofluids so that energy requirement of pulsation is reduced.

Oxygen mass transfer characteristics in the presence of nanofluids have been studied in various reactors such as agitated sparged reactors (Olle et al. 2006), stirred laboratory-scale reactors (Nagy et al. 2007), in an agitated aerobic bioreactor (Manikandan et al. 2012), bubble column (Darvanjooghi et al. 2018), hydrophobic polypropylene hollow fibre membrane contactor (Han et al. 2021) and Stirred tank bioreactor (Ding et al. 2023). There is no study reported on the influence of nanofluids on gas-liquid mass transfer enhancement in pulsed plate column.

In either case of the inherent presence of nanoparticles as in catalytic or photocatalytic reactors or the addition of nanoparticles intentionally to enhance mass transfer characteristics, the presence of these nanoparticles as nanofluids may influence the oxygen mass transfer characteristics of the column. Thus, there arises a need to study the g-l mass transfer in pulsed plate columns in the presence of nanofluids.

TiO₂ nanoparticles may be used as a photocatalyst in several photochemical reactions. The photocatalytic reactors are generally equipped with an air supply to provide oxygen as the oxidant. Dissolved oxygen plays a vital role in these reactors. The presence of TiO₂ nanoparticles may influence the oxygen mass transfer characteristics of the column. TiO₂ nanofluids have excellent stability without any stabilizers and the TiO₂ nanoparticles are chemically more stable compared to other metal oxides. It is also less hazardous to humans and living organisms.

Silicon dioxide (SiO₂), is usually known as silica. Silica nanoparticles are widely used in nanotechnology since they are easy to prepare on a large scale and inexpensive to produce, hydrophilic in nature, good biocompatibility, (Bitar et al. 2012). Silica nanoparticles are used for environmental remediation of pollutants such as the removal of heavy metals, radioactive elements, metals, non-metals, and the purification of water

(Jeelani et al. 2020). They are widely studied as catalysts (Lai 2013; Farzaneh and Fourouzone 2014). If they are used as catalysts in reactors involving the transfer of oxygen or other gases from a gas phase to a liquid phase, their presence may influence the oxygen mass transfer characteristics of the column.

α -Fe₂O₃ (hematite) iron oxide nanoparticles are abundantly used as biomaterials due to their good biocompatibility and minimum toxicity level. More importantly, these nanoparticles are available in large quantities, at low cost, show a greater extent of solar activity, and have good sustainability towards the environment with smaller bandgap energy. The nanoparticle separation from the reaction mixture is also easy with the help of an external magnetic field (Basavegowda et al. 2017). Therefore α -Fe₂O₃ nanoparticles are significantly used in different areas such as photocatalysis for the degradation of organic pollutants (Kusior et al. 2019; Liu et al. 2019a; Mishra and Chun 2015), photoelectrochemical water splitting (Rufus et al. 2017; Xu et al. 2012), in bioreactors to prevent membrane fouling (Sabalanvand et al. 2019) in aerobic bioreactors (Hesni et al. 2020), as catalysts (Zheng et al. 2006; Ahmad et al. 2019) and as an effective adsorbent for the removal of pollutants. Apart from these, it was also found that these nanoparticles have a higher tendency for the adsorption of trace metals and metalloids onto their surface (Chen and Li 2010; Fouad et al. 2019). These nanoparticles are added to bioreactors to enhance gas-liquid mass transfer (Labbeiki et al. 2014; Ahmad et al. 2019). Generally, TiO₂, SiO₂, and Fe₂O₃ are regarded as safe materials for human beings as well as for animals. The photocatalytic reactors employed with TiO₂, SiO₂, and α -Fe₂O₃ nanoparticles as photocatalysts, are generally equipped with an air supply to provide oxygen as the oxidant. Dissolved oxygen plays a vital role in these reactors and thus oxygen mass transfer becomes important. The presence of these nanoparticles may influence the oxygen mass transfer characteristics of the column. Further, these nanoparticles may be added to enhance gas-liquid mass transfer (Olle et al. 2007; Jiang et al. 2014; Ghasem 2019).

The scope of this work is to study the effect of TiO₂, SiO₂, and α -Fe₂O₃ nanofluids with water as the base fluid on k_{LA} in pulsed plate column operated with liquid phase in batch mode and with continuous flow of air along with the effect of nanofluids on k_{LA} enhancement with reference to the base fluid. The study focuses on the effect of nanofluid parameters such as nanofluid type in terms of nanoparticles used, their size,

and loading along with the effect of column operating conditions like frequency and amplitude of pulsation, pulsing velocity, and gas velocity. Further, the scope involves the order of magnitude analysis to determine the prime mechanism causing the oxygen mass transfer enhancement in the pulsed plate column. The assessment of the validity of a theoretical model and the development of Blackbox models in the form of dimensionless correlations and artificial neural network models using the experimental data to predict k_{La} are included in the scope.

2.9 Objectives of the research work

The main objective of the present work is to study the gas-liquid mass transfer enhancement in Pulsed plate column operated in batch mode by using nanofluids of TiO_2 , SiO_2 , and $\alpha\text{-Fe}_2\text{O}_3$ nanoparticles in terms of oxygen transfer.

Specific objectives are

- To determine the volumetric oxygen mass transfer coefficients in a pulsed plate column in the presence of TiO_2 , SiO_2 , and $\alpha\text{-Fe}_2\text{O}_3$ nanofluids.
- To study the effect of the type of nanoparticles, nanoparticles loading, size of nanoparticles, frequency, and amplitude of pulsation of the plates, and gas flow rate on volumetric oxygen mass transfer coefficients in pulsed plate column.
- To study the effect of aforesaid factors on the mass transfer enhancement by nanofluids
- To investigate and determine the mechanism responsible for the enhanced oxygen mass transport in nanofluids through Order of Magnitude Analysis.
- To apply the theoretical model based on first principles such as the Pseudo-homogenous model to predict Mass transfer enhancement by nanofluids and to test its validity.
- To develop dimensionless correlations based on Multiple Regression Analysis using the experimental data to predict the volumetric oxygen mass transfer coefficients in pulsed plate columns in the presence of nanofluids.
- To develop Artificial Neural Network based models to predict the volumetric oxygen mass transfer coefficients in pulsed plate columns in the presence of nanofluids.

CHAPTER 3 Materials and Methodology

This chapter presents the details of the materials used in the present work along with the methodologies adopted to fulfil the objectives.

3.1 Chemicals used:

Sodium sulfite (Na_2SO_3) (96% Purity) and Sodium thiosulphate Pentahydrate ($\text{Na}_2\text{S}_2\text{O}_3 \cdot 5\text{H}_2\text{O}$) (99% Purity) were purchased from Nice Chemicals, Kochi, Kerala. Cobalt (II) sulfate heptahydrate ($\text{CoSO}_4 \cdot 7\text{H}_2\text{O}$) (98% Purity) was purchased from CDH Analytical Reagent, New Delhi. Resublimed iodine (I_2) (99.8% Purity) was purchased from Fine Chemicals, Bangalore. Iodate-free potassium iodide (KI) (98% Purity) was purchased from Hi-Pure Rankem, New Delhi. Potassium dichromate ($\text{K}_2\text{Cr}_2\text{O}_7$) (99.9% Purity), hydrochloric acid (99.9% Purity), and starch were purchased from Nice Chemicals, Cochin.

3.2 Nanomaterials used:

TiO_2 (average diameter of 25 nm), SiO_2 nanoparticles (20-30 nm size range), and Iron oxide nanoparticles ($\alpha\text{-Fe}_2\text{O}_3$) (< 80 nm) were purchased from Intelligent Materials Pvt. Ltd. Punjab, India with 99.9% Purity. TiO_2 (less than 100 nm), SiO_2 nanoparticles of 5-15 nm and Iron oxide nanoparticles ($\alpha\text{-Fe}_2\text{O}_3$) of less than 50 nm were purchased from Sigma – Aldrich Chemicals Pvt. Ltd., Bangalore with 99.9% Purity.

3.2.1 Morphology and the average size of nanoparticles

Scanning Electron Microscopy (SEM) was used to study the morphology and average size of the nanoparticles. A high-resolution Scanning Electron Microscopic (SEM) analysis of the nanoparticles was performed by JSM-6380A operated at 20kV. The resulting images of the nanoparticles with two different sizes of TiO_2 (25 nm and less than 100 nm); SiO_2 (20-30 nm and 5-15 nm) and $\alpha\text{-Fe}_2\text{O}_3$ (less than 50 nm and less than 80 nm) are shown in Fig. 3.1 (a) and (b); Fig 3.2 (a) and (b) and Fig.3.3 (a) and (b) respectively.

As observed in Fig 3.1 (a) and (b) to 3.3 (a) and (b), the particles are nearly spherical. The average size of the nanoparticles was obtained from the SEM images using Image J analyser. The average particle size of the procured nanoparticles were found using ImageJ analysis and are shown in Table 3.1.

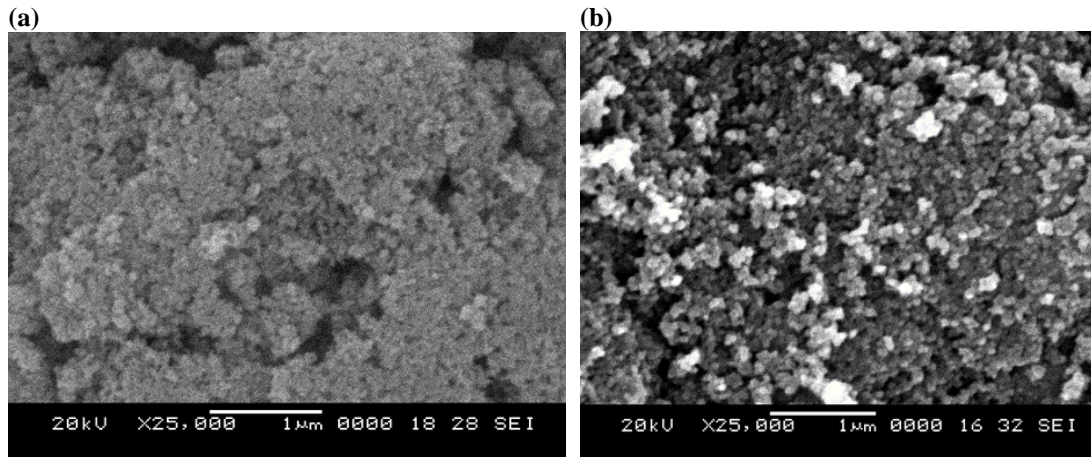


Fig 3.1 SEM image of TiO_2 nanoparticle of size range (a) 25 nm and (b) less than 100 nm

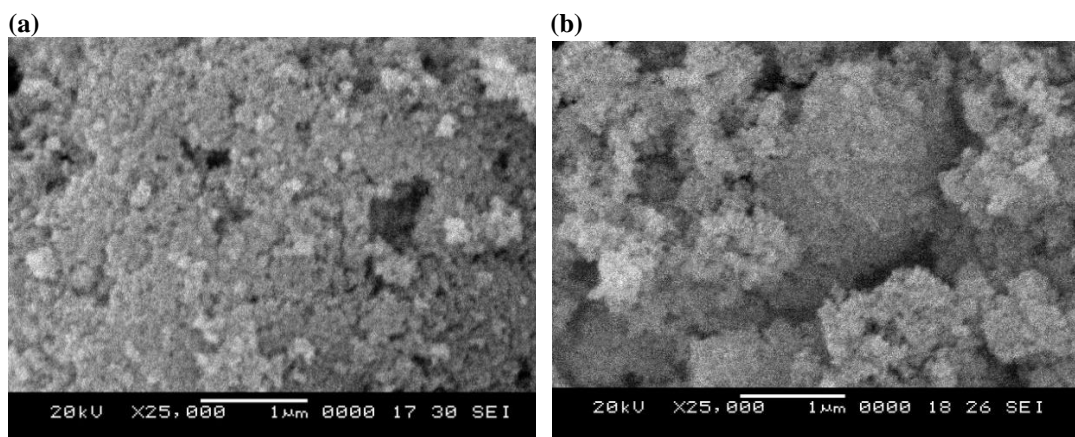


Fig 3.2 SEM image of SiO_2 nanoparticle of size range (a) 20-30 nm and (b) 5-15 nm

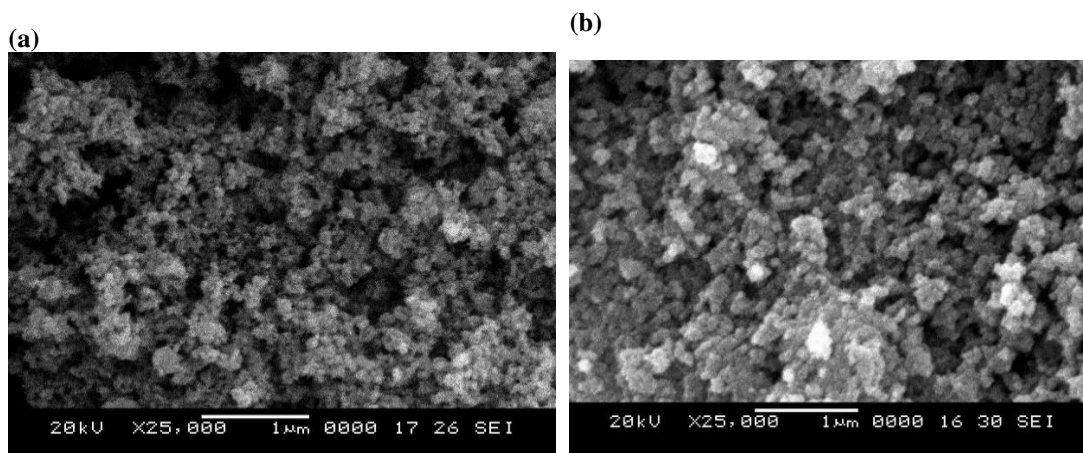


Fig 3.3 SEM image of $\alpha\text{-Fe}_2\text{O}_3$ nanoparticle of size range (a) less than 50 nm and (b) less than 80 nm

Table 3.1 Average particle size of TiO₂, SiO₂, and α-Fe₂O₃ nanoparticles

Nanoparticle type	Procured size range of nanoparticles, nm	Average particle size using ImageJ analysis, nm
TiO ₂	25	25
	< 100	72
SiO ₂	5-15	12
	20-30	24
α-Fe ₂ O ₃	< 50	43
	< 80	76

3.3 Preparation of Nanofluid

To prepare the nanofluid, “two-step method” has been followed in the present work. Initially required quantity of nanoparticles was weighed and dispersed into 0.08M aqueous solution of sodium sulphite. This solution was ultrasonicated for 30 minutes at (Elmasonic P ultrasonicator with 35 khz frequency). The prepared nanofluid sample are presented in Fig.3.4. The nanofluid thus prepared was used for further experiments.

TiO₂, SiO₂ and α-Fe₂O₃ nanofluids with varying nanoparticle loadings were prepared with an aqueous solution of sodium sulphite as the base fluid. The amount of nanoparticles dispersed in 1.5L of sodium sulphite solution to prepare nanofluids with various nanoparticle loading are presented in Table 3.2.

Table 3.2. Amount of nanoparticles used to prepare nanofluids of varying nanoparticle loading

Nanoparticle loading (% w/v)	Amount of nanoparticles used to prepare 1.5 L nanofluid (g)
0.017	0.25
0.034	0.5
0.051	0.75
0.068	1
0.085	1.25
0.102	1.5

TiO₂ nanofluid prepared with the TiO₂ nanoparticles with average particle size of 25 nm and 72 nm are here in after referred as TiO₂-25 and TiO₂-72 nanofluid respectively. Similarly, SiO₂ nanofluid prepared with the SiO₂ nanoparticles with average particle size of 12 nm and 24 nm are here in after referred as SiO₂-12 and SiO₂-24 nanofluid respectively. α -Fe₂O₃ nanofluid prepared with the α -Fe₂O₃ nanoparticles with average particle size of 43 nm and 76 nm are here in after referred as α -Fe₂O₃-43 and α -Fe₂O₃-76 nanofluid.

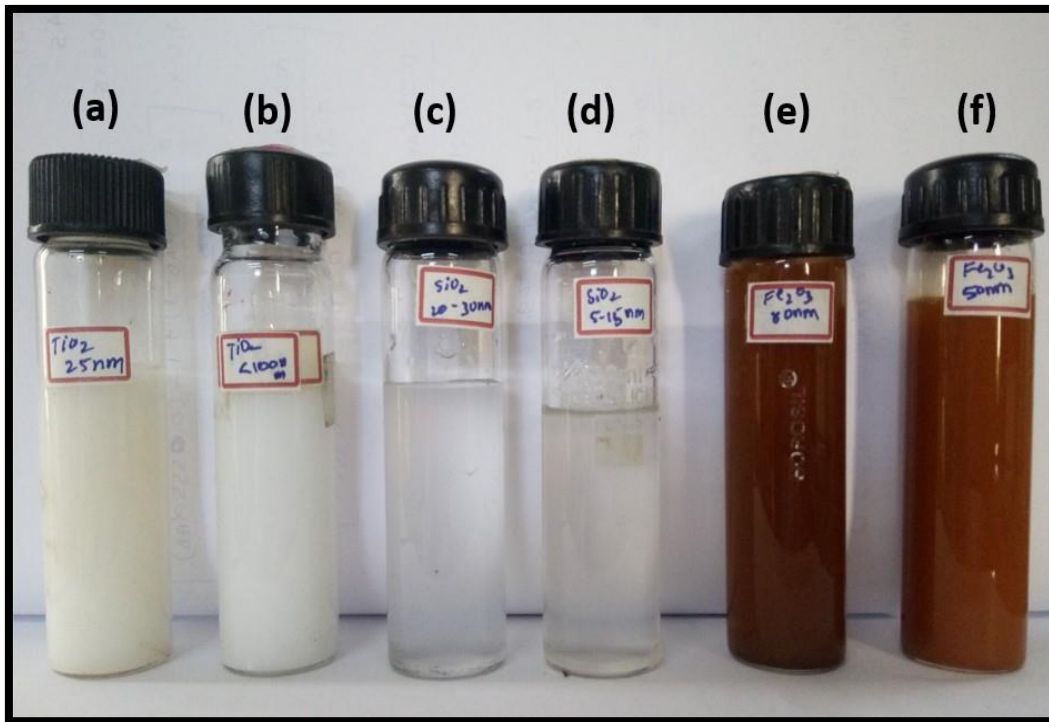


Fig 3.4. Prepared Nanofluids (a) TiO₂ -25, (b) TiO₂ -72, (c) SiO₂ -24, (d) SiO₂ - 12, (e) α -Fe₂O₃ - 76 and (f) α -Fe₂O₃ - 43

3.4 Properties of Nanofluid

- (i) The surface tension of TiO₂, SiO₂ and α -Fe₂O₃ nanofluid was measured using a surface tensiometer (Surface & Electro -Optics; SEO-DST30M). The platinum Du-Nouy ring method was used with ASTM D1331. The measurement ranges from 1-1000 mNm.
- (ii) The dynamic viscosity of nanofluids at room temperature was measured using Rolling ball viscometer (Lovis 2000M Microviscometer) under shear rate conditions imparted with a capillary size of 1.59 mm inclined at 45° angle and

a ball of dimension 2.5 mm. The measuring accuracy is up to 0.5% and the measuring range is 0.3 mPas – 10000 mPas.

- (iii) The density of nanofluids at room temperature was measured using DDM 2911 automatic Density meter from Rudolph research analytical with high precision using mechanical oscillator method. The measuring accuracy up to 0.00005g/cm³ and the measuring range is 0 to 3 g/cm³.

3.5 Experimental setup

The volumetric oxygen mass transfer coefficients (k_{1a}) in the pulsed plate column were determined in the presence and absence of nanofluids. The schematic diagram of the experimental pulsed plate column (PPC) used for the study is shown in Fig 3.5 (a & b). It consisted of a vertical Perspex column of 6.8 cm inner diameter, 7.5 cm outer diameter, and 62 cm height. The plate stack consisted of five perforated plates with 3.5 cm plate spacing, a plate diameter of 6.3 cm, and a 0.1 cm thickness mounted over a central shaft. The plate consisted of 104 perforations of 2mm diameter placed in square pitch. The fractional free area was 0.961%. The pulsation of the plate stack is generated by a variable speed motor with a frequency controller, through a slider/crank arrangement. The entire stack of plates can be pulsated at the required frequency and amplitude through this arrangement (Shetty et al. 2007). The working volume of the column was 1.5 liter. Compressed air was fed continuously through an air inlet port provided at the bottom of the column. Airflow was regulated using an air pressure regulator and a calibrated rotameter. Using the variable voltage speed regulator, the frequency of pulsation could be controlled and by changing the position of the crankshaft the amplitude of pulsation could be varied.

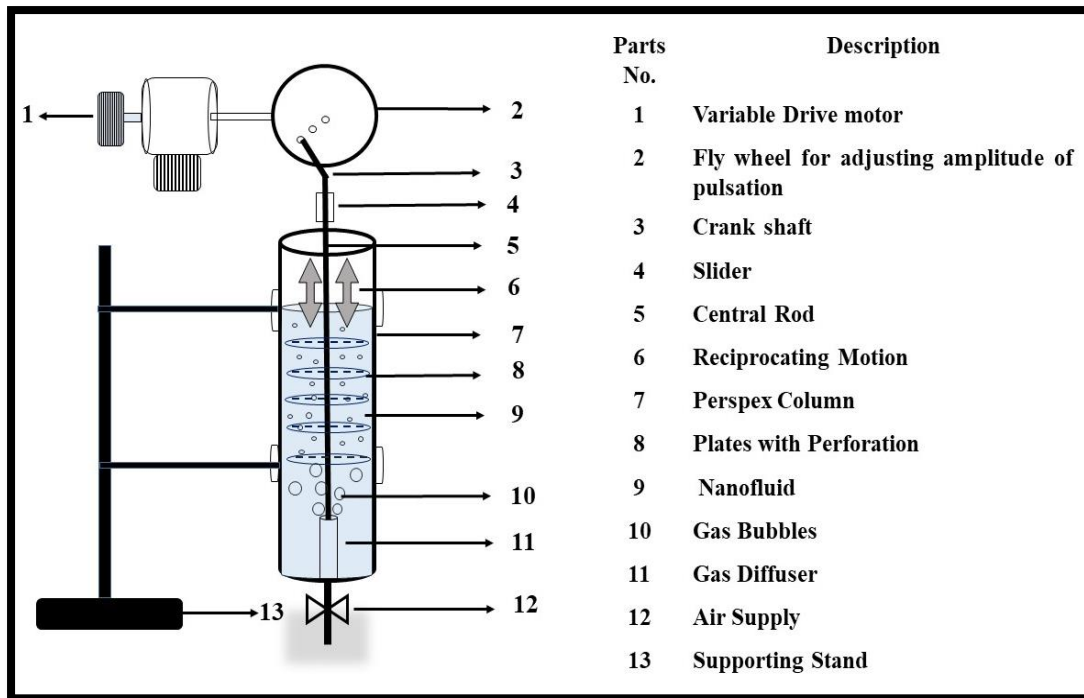


Fig 3.5 (a) Schematic diagram of an experimental setup

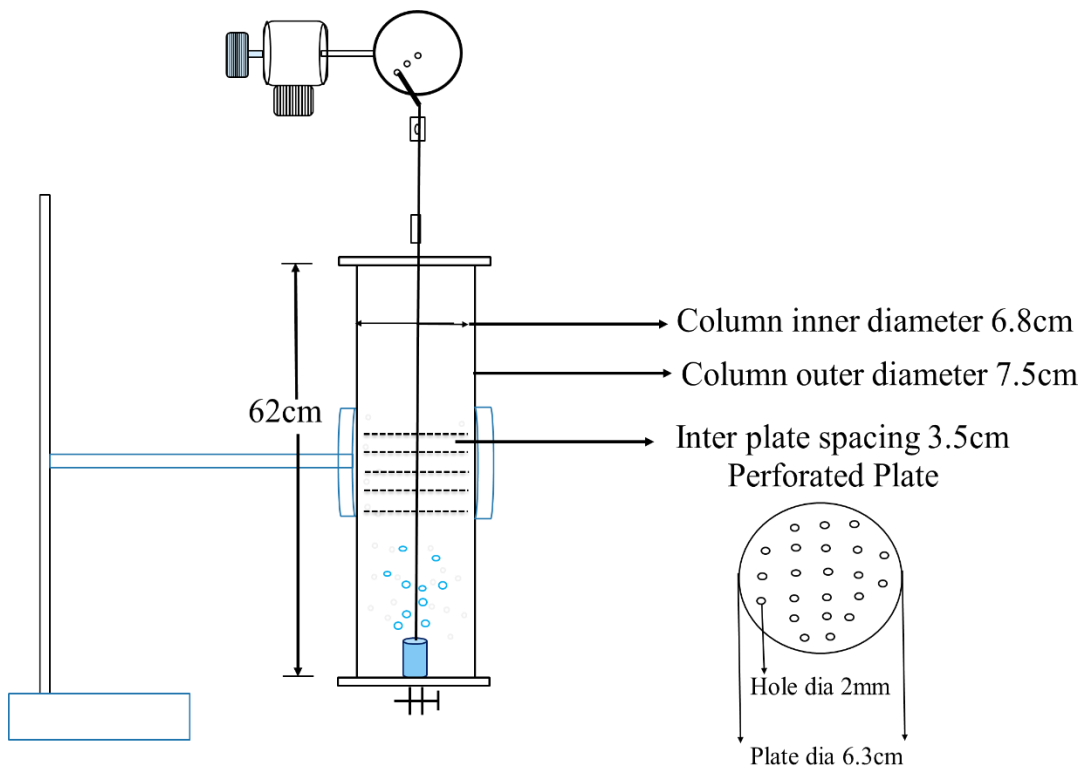


Fig 3.5 (b) Schematic diagram of an experimental setup with dimensions

3.5.1 Experimental Procedure for the Determination of k_{La} in PPC

The Pulsed plate column was cleaned thoroughly with water. After drying, the central rod with the plate stack assembly was inserted into the column and fitted properly. The central shaft was then connected to the slider of the slider-crank arrangement with the bottom portion of the central rod positioned in the guiding tube. After assembling the plate stack and checking for its axial symmetry in the column, the active section of the column up to a height of 45cm was filled with the nanofluid. The prepared nanofluid (1.5 liters) was then fed into the column. To determine k_{La} , the sulfite oxidation method (Maier et al. 2001) has been adopted. The value of k_{La} was calculated from the maximum oxygen absorption rate and the oxygen solubility in the sodium sulfite solution. The oxygen absorption rate was experimentally measured utilizing sodium sulfite oxidation in the presence of cobalt sulfate as a catalyst. An aqueous solution of sodium sulfite (0.08M) was prepared in a separate vessel by dissolving the predetermined amount of sodium sulfite salt in water. Accurately weighed cobalt sulfate crystals were added into this sulfite solution and properly mixed so that the final catalyst concentration was 10^{-6} M. A desired quantity of nanoparticles as required for the experiment was dispersed in the sodium sulphite solution and the solution was ultrasonicated for 30 min. Then this solution was fed into the column. The sulfite concentration in the initial stock sulfite solution was determined iodometrically. Compressed air was sent from the bottom of the column for aeration at a constant rate. The required frequency and amplitude of pulsing motion were set.

The samples were collected from the bottom of the column at a particular time interval of 30 minutes and the collected sample was immediately centrifuged at 10,000 rpm for 10 minutes. The supernatant was analyzed for final sodium sulfite concentration at the end of 30 min of experimental time. It was measured by iodometric titration against sodium thiosulphate as described in section 3.6. The initial and final moles of sodium sulphite in the reactor volume was determined. The value of the k_{La} was calculated using the Equation 3.4.

$$k_{La} = \frac{((\text{initial-final})\text{moles of } SO_3^{2-}) \frac{1 \text{ moles of } O_2}{2 \text{ moles of } SO_3^{2-}}}{t V (C^* - C_L)} \dots\dots\dots (3.4)$$

Where, t = time for which reaction is allowed to carry out (30 min).

V = volume of the working liquid, L; C_L is the bulk concentration of oxygen in the reactor, mg/L; C^* is the saturation solubility of oxygen in sodium sulphite solution, mg/L.

The reaction between oxygen and sulphite ($2Na_2SO_3 + O_2 \rightarrow 2Na_2SO_4$) is assumed to be instantaneous because it is a fast reaction catalyzed by cobalt ions because of the low solubility of oxygen in the liquid phase. This assumption allows to use $C_L = 0$. C^* was determined using Henry's Law and was calculated as 7.6 mg/L at 30°C (Room temperature at which the experiment was conducted). All the experiments were conducted in duplicates. Fig. 3.6 shows the schematic diagram of the different experimental conditions at which the k_{La} in PPC was determined.

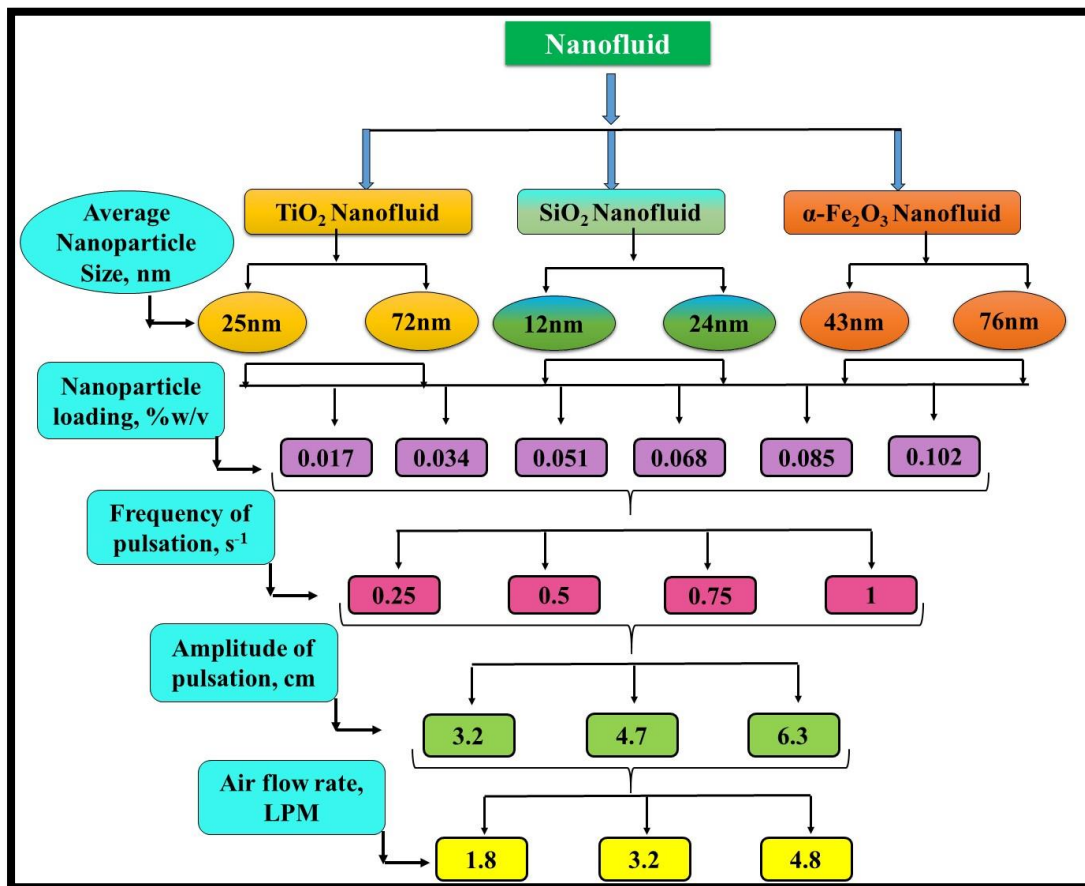


Fig 3.6. Experimental conditions under which the k_{La} values were determined in PPC

3.6 Analysis of sodium sulfite concentration by iodometric method

3.6.1 Preparation of sodium thiosulphate

Sodium thiosulphate solution (0.01N) was prepared by dissolving 0.625g of sodium thiosulphate crystals in 250 ml of distilled water in a graduated flask. If the solution is to be kept for more than a few days, 0.1g of sodium carbonate or 3 drops of chloroform was added.

3.6.2 Standardization of sodium thiosulphate

A standard solution of potassium dichromate was prepared by dissolving 0.49g in 100 ml of distilled water. 25ml of this solution was taken in a conical flask. 10ml of 10% KI solution and 5ml of concentrated HCl were added to it and titrated against sodium thiosulphate in the burette. The starch solution was added when pale yellowish green colour was obtained to get a dark blue colour which on further titration gives a green colour solution.

3.6.3 Preparation of iodine solution

Iodine solution (0.05M) was prepared by dissolving 20g of iodate-free KI in 30 to 40ml distilled water in a glass stoppered 1000ml standard flask and 12.7g of resublimed iodine was added to this KI solution. The glass stopper was inserted into the flask and the flask was shaken in the cold until all the iodine had dissolved. The solution was allowed to acquire the room temperature and then made up to the mark with distilled water. The solution was preserved in a glass stoppered bottle in a cool, dark place.

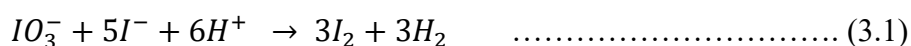
3.6.4 Preparation of starch indicator

A paste of 0.1g of soluble starch was made with little water and the paste was poured into 100ml boiling water and boiled for 1 min. the solution was kept in a stoppered bottle.

3.6.5 Chemical Reactions

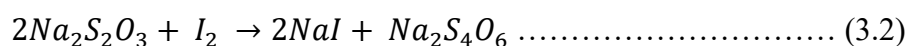
(a) Liberation of free iodine from salt:

Addition of HCl liberates free iodine from the iodate in the salt sample. Excess KI was added to help solubilize the free iodine, which was quite insoluble in pure water under normal conditions.



(b) Titration of free iodine with sodium thiosulphate:

Free iodine was consumed by sodium thiosulphate in the titration step. The amount of sodium thiosulphate used was proportional to the amount of free iodine liberated from the salt. Starch was added as an external (indirect) indicator of this reaction and reacts with free iodine to produce a blue colour. When added towards the end point of the titration (that was, when only a trace amount of free iodine was left) the loss of blue colour or endpoint, which occurs with further titration, indicated that all remaining free iodine was been consumed by sodium thiosulphate.



25ml of the sodium sulphite solution was taken in a conical flask and iodine solution was added from the burette till a slight orange colour was added. 5ml iodine solution was added in excess. Volume of iodine as V_1 ml was noted and to this solution, 5ml HCl was added and titrated against the Standardised sodium thiosulphate using a starch solution as indicator near endpoint (A ml). the procedure was repeated to get V_2 ml iodine solution and B ml of sodium thiosulphate solution.

Concentration of sodium sulphite (Na_2SO_3) was calculated using the following formula (3.3):

$$\text{Conc. of } Na_2SO_3 = \left(\frac{\{[B \times (V_1/V_2) - A] \times (N_{Na_2S_2O_3}) \times (\text{eq. wt of } Na_2S_2O_3) \times 1500\}}{25 \times 1000} \right) \dots\dots (3.3)$$

Where,

B= ml of $Na_2S_2O_3$ required for blank titration

A = ml of $Na_2S_2O_3$ required for estimation

$N_{Na_2S_2O_3}$ = Normality of $Na_2S_2O_3$

Eq. wt of $Na_2S_2O_3$ = Equivalent wt of $Na_2S_2O_3$ = 63.02

V_1 = ml of iodine required for estimation

V_2 = ml of iodine required for blank titration

CHAPTER 4 Results and Discussion

In the present work, the influence of the nanofluids on the g-l mass transfer in terms of volumetric oxygen mass transfer coefficient (k_{La}) in PPC operated with liquid phase in batch mode and continuous airflow is studied.

This chapter presents the characterization of TiO_2 , SiO_2 , and $\alpha-Fe_2O_3$ nanofluids and the results on the effect of these nanofluids on k_{La} and its enhancement in PPC. The effect of nanoparticle loading (Φ) in the nanofluid, pulsing parameters such as frequency (f), amplitude (A), and pulsing velocity ($A \times f$) along with the superficial air velocity (U_g) effect on k_{La} are presented and discussed. The results and discussions on the effect of the size of nanoparticles in the nanofluid and the comparison of different nanofluids in terms of enhancement in k_{La} in PPC are also presented.

The k_{La} was experimentally determined at different operating conditions with varying amplitudes (3.2 cm, 4.7 cm, 6.3 cm), frequencies of pulsation (0.25, 0.5, 0.75, and 1 s⁻¹), and superficial air velocities (0.011 m/s, 0.019 m/s, and 0.029 m/s). Experiments were conducted under these conditions with TiO_2 -25, TiO_2 -72, SiO_2 -12, SiO_2 -24, $\alpha-Fe_2O_3$ -43 and $\alpha-Fe_2O_3$ -76 nanofluids containing varying concentrations of nanoparticles such as 0.017 % w/v, 0.034 % w/v, 0.051 % w/v, 0.068 % w/v, 0.085 % w/v, and 0.102 % w/v.

4.1 Properties of nanofluids

The properties such as surface tension, dynamic viscosity and density of TiO_2 , SiO_2 and $\alpha-Fe_2O_3$ nanofluids with varying nanoparticle loading were determined and are presented in Fig.4.1 (a), (b) and (c); Fig.4.2 (a), (b) and (c) and Fig 4.3 (a), (b) and (c) respectively.

As observed in Table 4.1 and Fig.4.1 (a) to (c), the surface tension of nanofluid is lesser compared to that of the base fluid at lower loadings, though it increased with the increase in the loading. However, beyond a certain loading value the surface tension becomes higher compared to that of the base fluid. The loading values at and above which the surface tension becomes equal to or greater with respect to the base fluid are 0.102 % w/v for TiO_2 -25 and TiO_2 -72 nanofluids, 0.085 % w/v and 0.051 % w/v for

SiO₂-12 and SiO₂-24 nanofluids respectively, 0.051 % w/v and 0.017 % w/v for α-Fe₂O₃ – 43 and α-Fe₂O₃ – 76 nanofluids respectively.

Table 4.1. Surface tension of TiO₂, SiO₂ and α-Fe₂O₃ nanofluids.

Surface tension of nanofluids, mN/m						
Nanoparticle type	TiO₂ nanofluid		SiO₂ nanofluid		α-Fe₂O₃ nanofluid	
Nanoparticle Loading, (%w/v)	Nanoparticle Size, nm					
	25 nm	72 nm	12 nm	24 nm	43 nm	76 nm
base fluid	72.6	72.6	72.6	72.6	72.6	72.6
0.017	48.0	61.0	55.2	63.0	63.3	76.4
0.034	52.3	65.6	61.1	68.6	69.0	78.6
0.051	58.1	66.8	66.8	73.4	75.0	82.3
0.068	63.5	70.8	69.2	76.3	78.0	82.5
0.085	65.7	72.2	72.6	79.0	79.1	83.1
0.102	75.2	79.0	76.2	81.3	81.6	84.9

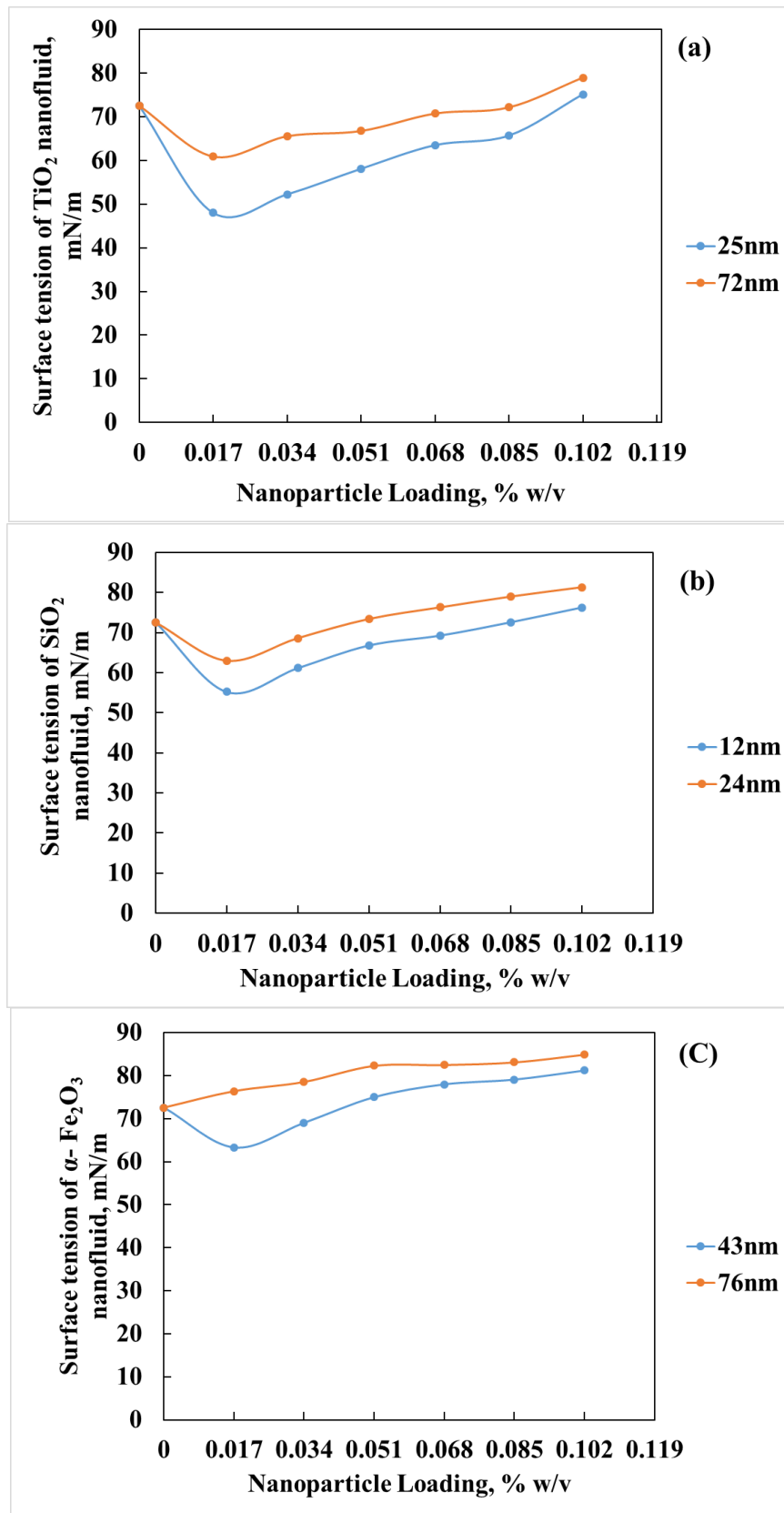


Fig.4.1 Effect of nanoparticle loading on the Surface tension of (a) TiO₂ ,(b) SiO₂ and (c) α -Fe₂O₃ nanofluids.

The lowered values of surface tension in the dilute nanofluids than the base fluid, is because at the g-l interface, the cohesive energy reduces as the nanosized particles are added to the base fluid (Becher 1972; Schonhorn 1965; Vavruca 1978). The Brownian motion of nanoparticles within the liquid can scatter the nanoparticles present at the g-l interface to other directions with the reduced free energy of the interface, thus reducing the surface tension (Murshed et al. 2005; 2008). Murshed et al. (2008), also attributed the reduction to the adsorption of nanoparticles at the interfaces. Such a decrease in the surface tension by adding the nanoparticles has been found by Radiom et al. (2009), (Murshed et al. 2005, 2008) in TiO₂-water nanofluid and by Vafaei et al. (2009) with Bi₂Te₃/water nanofluids. Tanvir and Qiao (2012), have studied the effect of nanoparticle loading on the surface tension of nanofluids and have reported that the surface tension decreased at lower particle concentrations than the pure base fluid. They attributed it to the reduction of surface free energy due to the repulsive electrostatic force among the particles leads to the decrease in surface tension.

As observed in Fig 4.1 (a) – (c), the surface tension of the TiO₂, SiO₂ and α -Fe₂O₃ nanofluid increased with an increase in the nanoparticle loading. The presence of nanoparticles may alter the surface tension based on its nature (Sinha and Singh 2017). Tanvir and Qiao (2012) have found that the surface tension of water, ethanol and n-decane increased with increase in weight percentage of alumina nanoparticles. Bhuiyan et al. (2015), have experimentally shown the increase surface tension of Al₂O₃, TiO₂, and SiO₂ nanoparticles in distilled water with nanoparticle concentration and size. Żyła et al. (2017), experimentally investigated that the increase in surface tension of ethylene glycol (EG) nanofluid with increase in volume fraction of titanium nitride (TiN) nanoparticles.

At low particle concentrations, addition of particles was generally found to have little influence on the surface tension because the distance between the particles is large enough even at the liquid/gas interface. Such observations have been made by Tanvir and Qiao (2012) and Traciak and Żyła (2022). Tanvir and Qiao (2012) have also found that at high particle concentrations, increase in the nanoparticle loading increases the nanofluids surface tension and goes above the base fluid.

As the nanoparticle loading increases, the number of nanoparticles increase in the nanofluid resulting in the particles getting closer to each other decreasing the

interparticle spacing at the g-l interface. An increased nanoparticle concentration may result in nanoparticles exerting large attractive pull at the interfacial water molecules, the accumulation of particles at the g-l interface exerts an increased Van der Waals force among them and leads to the rigid interface that results in high surface free energy causing the increased surface tension (Vafaei et al. 2009, Sinha and Singh 2017). Meanwhile the forces of attraction between the particles at the g-l interface increases and agglomeration of particles increases due to the exertion of cohesive force between the particles. this results in the higher value of surface tension (Bhuiyan et al. 2015; Tanvir and Qiao 2012).

Surface tension was also found to increase with the increase in the size of nanoparticles as observed in Fig 4.1 (a) - (c). Similar trend of increase in surface tension with increase in nanoparticle size has been observed by Bhuiyan et al. (2015) in their studies with Al_2O_3 (13 nm and 50 nm) and SiO_2 (5~15 nm and 10~20 nm) nanoparticles; Monji and Jabbareh (2017) with Ag-Au alloy nanoparticles (1, 2, 5 and 10 nm) ; Vafaei et al. (2009) with Bi_2Te_3 - water (2.5 and 10.4 nm); Zhang et al. (2021) with Cadmium sulphide nanoparticles (>10 nm and <10 nm). The surface charge density is found to be higher in the smaller size nanoparticles compared to that of the larger size nanoparticles (Abbas et al. 2008), which results in an increase in the electrostatic repulsion force between the liquid molecules and the nanoparticles, which promotes the surface adsorption and hence reduces the surface tension of nanoparticles with the smaller size (Brown et al. 2013). With the increase in the nanoparticle size, the surface area decreases along with the surface free energy thus the surface tension of nanofluids increases (Bhuiyan et al. 2015).

Similarly, the viscosity of TiO_2 , SiO_2 , and $\alpha\text{-Fe}_2\text{O}_3$ nanofluid increased with the increase in the nanoparticle loading and is shown in Fig. 4.2 (a) – (c) respectively. The plot shows that the increase in nanoparticle loading increases the viscosity of nanofluid.

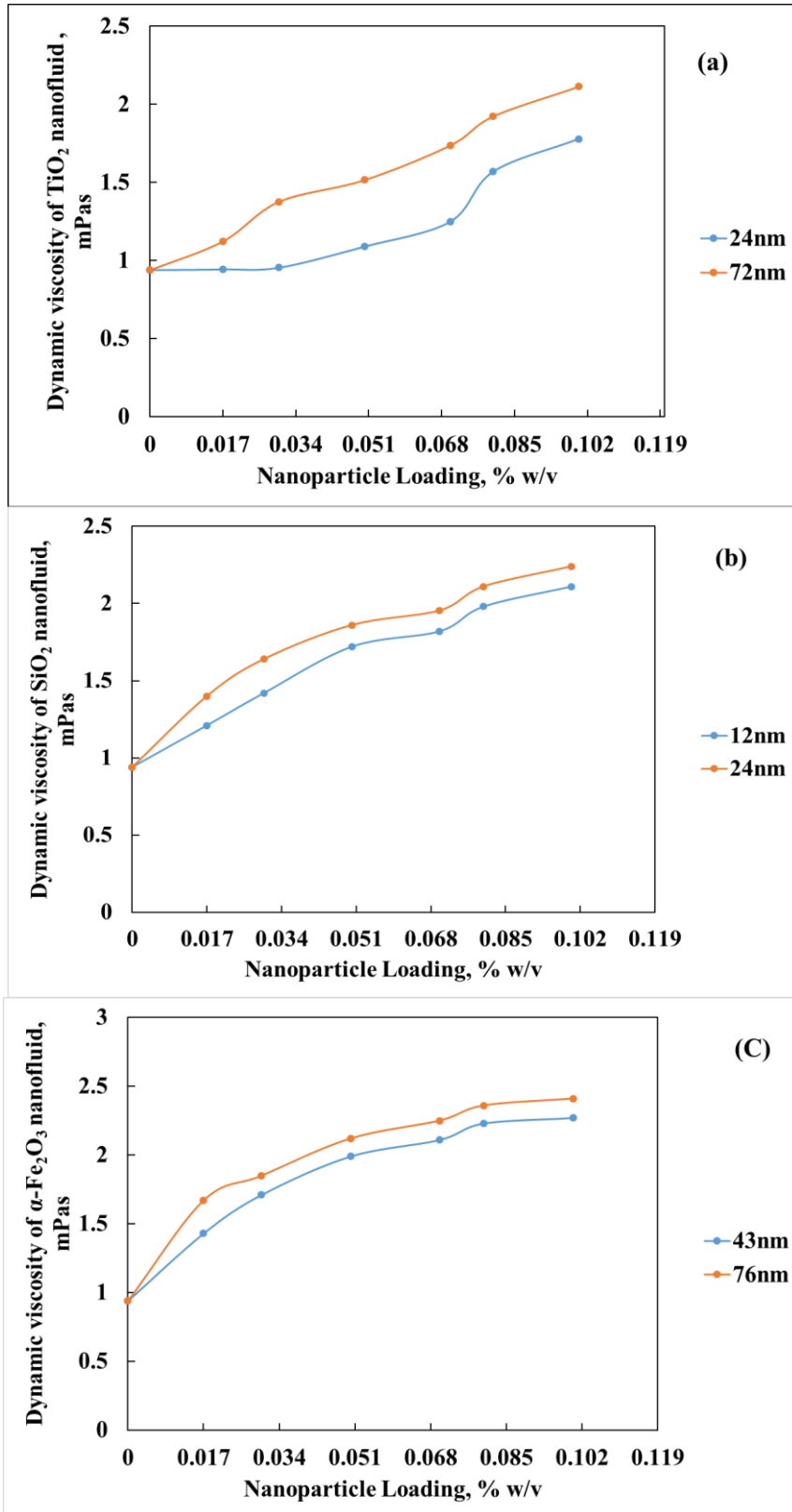


Fig.4.2 Effect of nanoparticle loading on the Dynamic viscosity of (a) TiO₂ ,(b) SiO₂ and (c) α -Fe₂O₃ nanofluids.

It is found that when the nanoparticle loading increased from 0.017 % w/v to 0.102 % w/v the viscosity has increased from 0.90 cP to 1.78 cP for TiO₂ -25 nanofluid and 1.12

cP to 2.11 cP for TiO₂-72 nanofluid as observed in Fig.4.2 (a). Similarly, the increase in nanoparticle loading from 0.017 % w/v to 0.102 % w/v has resulted in an increase in viscosity from 0.94 cP to 2.14 cP and 1.40 cP to 2.24 cP for SiO₂-12 and SiO₂-24 nanofluid, as observed in Fig.4.2 (b). The viscosity increased from 1.43 cP to 2.27 cP and from 1.67 cP to 2.41 cP when the nanoparticle loading increased from 0.017 % w/v to 0.102 % w/v for α -Fe₂O₃-43 and α -Fe₂O₃-76 nanofluids respectively as observed in Fig. 4.2 (c).

Phuoc and Massoudi (2009) in their studies on Fe₂O₃-Distilled water (Fe₂O₃-DW) nanofluids have experimentally found that viscosity is dependent on the nanoparticle concentration. Duangthongsuk and Wongwises (2009), have reported that the measured viscosity of TiO₂-water nanofluids increased with the increased particle concentrations and experimental results showed that the measured nanofluid viscosity is higher than the base fluid. Yapici et al. (2018), observed that the increase in nanoparticle mass concentration increased the nanofluid viscosity. Minakov et al. (2021) have also observed an increase in viscosity with the increase in nanoparticle loading for Al₂O₃, TiO₂, ZrO₂, CuO, Fe₂O₃ nanofluids. They found that the viscosity of nanofluids depends on the type of nanoparticles and the loading of nanoparticles. Similar results were observed by many researchers wherein they have found that the increase in nanoparticle loadings increases the nanofluid viscosity (Abareshi et al. 2011; Hasani Goodarzi and Nasr Esfahany 2016; Hatami et al. 2017; Nematbakhsh and Rahbar-Kelishami 2015; Rahbar et al. 2011; Zhang and Han 2018, Hassan et al. 2022).

The increase in the viscosity is attributed mainly to the collective effects of Brownian motion, Vander Waals force and electric charge repulsive force (Cabaleiro et al. 2018; Hu et al. 2020; Nguyen et al. 2007; Phuoc and Massoudi 2009; Said et al. 2022). Chen et al. (2009) explained that a well-dispersed nanofluid suspension exhibits lower viscosity as compared to the agglomerated suspension. The tendency of aggregation of nanoparticles is enhanced due to the increase in the volume of the nanoparticle loading exceeding the dilute regime, particularly when the Van der Waals force of attraction is significant. The clustering of nanoparticles leads to the formation of porous particles with the liquid of the base fluid packing the space. This hinders the movement of additional liquid in the space increasing the effective volume fraction of nanoparticles, which influences the enhancement of the viscosity of nanofluid (Gaganpreet and

Srivastava 2015; Meyer et al. 2016). The increase in the number of nanoparticles dispersed in the base fluid causes the explicit drag effect on each nanoparticle due to the Brownian motion, which in turn increases the overall drag effect existing in the base fluid. Likewise, the increase in viscosity is explained by the mechanism of the surface charge of particles relating to the suspension base fluid. The attraction of counter ion onto the surface of the nanoparticles takes place due to the dispersion of charged nanoparticles into the polar base fluid. This process leads to the formation of an electrical double layer (EDL). The distance between the EDLs is extended and the interparticle distance will be reduced by increasing the nanoparticle loading. Hence an electroviscous force develops and leads to a further increase in viscosity. Electroviscous force is the force of interaction between the EDLs (Anoop et al. 2009). Further, the interparticle distances are reduced by the increase in the volume of nanoparticles (Larson 1999; Phuoc and Massoudi 2009). Kandelousi (2017) have observed that the variations in the viscosity of nanofluids are mainly dependent on the concentration of nanoparticles, properties of base fluid and nanofluids such as density and surface tension, and nanoparticle properties such as size and density.

The viscosity of nanofluids increases with the size of the nanoparticles as observed in Fig 4.2 (a) to (c). Similar observations have been reported by He et al. (2007), with TiO₂/water (95 nm, 145 nm, and 210 nm); Hemmat Esfe et al. (2015) with Fe-water nanofluid (with three different sizes 37 nm, 71 nm, and 98 nm); Lee et al. (2016) with ZnO nanofluid (average sizes of 40 nm, 70 nm, and 90 nm; Hu et al. (2020) with Al₂O₃ (20 nm, 50 nm, and 100 nm) and ZnO (20 nm, 40 nm, 60 nm, 80 nm and 100 nm) nanofluids. Hu et al (2020) have found that the dependency of viscosity on particle size varied with nanoparticle type and concentrations. At lower concentrations, the viscosity was found to be either unaltered or decreased with an increase in particle size depending on the type of the nanoparticles, whereas at higher concentrations it increased with the increase in size. This is mainly due to the interparticle spacing and the extent of the aggregation of the nanoparticles to be the key factors determining the viscosity of nanofluid and these are greatly affected by the variation in the size, type and concentration of the nanoparticles.

Further, the density of TiO₂, SiO₂, and α -Fe₂O₃ nanofluid was found to increase with the increase in nanoparticle loading as seen in Fig.4.3. Several studies in the literature

signifies that the addition of nanoparticles into the base fluid enhances the density of the nanofluids linearly (Naddaf and Zeinali Heris 2019; Said et al. 2022). As the nanoparticle concentration increases the density of nanofluid increases due to an increased influence of solid mass in the base fluid (Yadav et al. 2020).

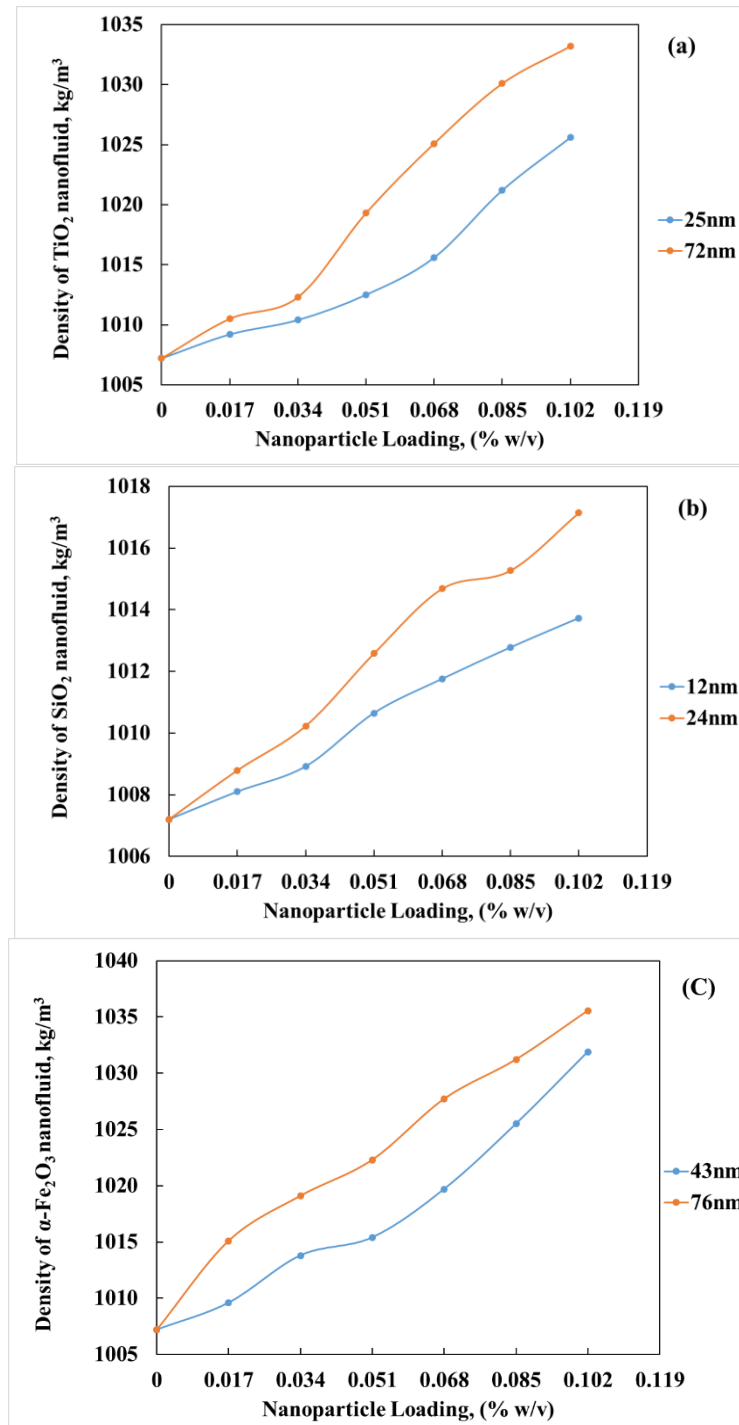


Fig.4.3 Effect of nanoparticle loading on the Density of (a) TiO₂ ,(b) SiO₂ and (c) α -Fe₂O₃ nanofluids.

Diffusivity of oxygen in TiO₂, SiO₂ and α-Fe₂O₃ nanofluid (D_{nf}), was calculated using Equation (4.1) (Feng and Johnson 2012),

$$D_{nf} = D_L \left(\frac{1 + \Psi}{1 - \frac{\Psi}{2}} \right) \quad (4.1)$$

where D_L is the diffusivity of a solution without nanoparticles which was found by using Wilke - Chang correlation (Wilke & Chang 1955) and ψ is nanoparticle loading in volume fraction.

The volume fraction of nanoparticles in the nanofluids (Nurdin and Satriananda 2017) is calculated using the Equation (4.2) and the values are given in the Table 4.2

$$(\Psi) = \frac{\frac{M_{np}}{\rho_{np}}}{\frac{M_{np}}{\rho_{np}} + \frac{M_{bf}}{\rho_{bf}}} \quad (4.2)$$

Where, M_{np} is the mass of the nanoparticles, ρ_{np} is the density of the nanoparticles, M_{bf} is the mass of the base fluid, ρ_{bf} is the density of the base fluid. The values of density of procured TiO₂, SiO₂ and α-Fe₂O₃ nanoparticles from Intelligent Materials Pvt. Ltd were 4.26 g/cm³, 2.4 g/cm³ and 5.242 g/cm³ respectively.

The values of D_{nf} are given in Table 4.3. The variation of D_{nf} with the increase in nanoparticle loading for TiO₂, SiO₂ and α-Fe₂O₃ nanofluids are shown in Fig.4.4.

Table 4.2. Nanoparticle loading in volume fraction.

Nanoparticle Loading in % w/v	Volume fraction of TiO ₂ nanoparticles	Volume fraction of SiO ₂ nanoparticles	Volume fraction of α-Fe ₂ O ₃ nanoparticles
0.017	3.91E-05	6.94E-05	3.18E-05
0.034	7.82E-05	1.39E-04	6.36E-05
0.051	1.17E-04	2.08E-04	9.54E-05
0.068	1.56E-04	2.78E-04	1.27E-04
0.085	1.96E-04	3.47E-04	1.59E-04
0.102	2.35E-04	4.16E-04	1.91E-04

Table 4.3. Values of Diffusivity of oxygen in nanofluids, D_{nf}

Diffusivity of oxygen in nanofluids, $\times 10^{-9} \text{ m}^2/\text{s}$			
Nanoparticle Loading, (%w/v)	TiO ₂ nanofluid	SiO ₂ nanofluid	α -Fe ₂ O ₃ nanofluid
base fluid	1.030	1.030	1.030
0.017	1.034	1.040	1.033
0.034	1.041	1.050	1.038
0.051	1.047	1.061	1.043
0.068	1.052	1.072	1.048
0.085	1.058	1.083	1.053
0.102	1.065	1.094	1.058

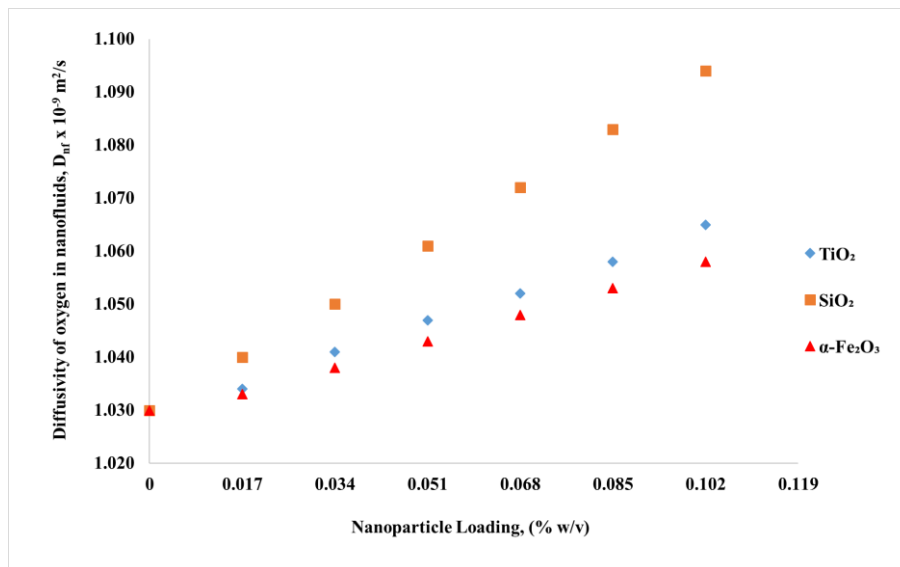


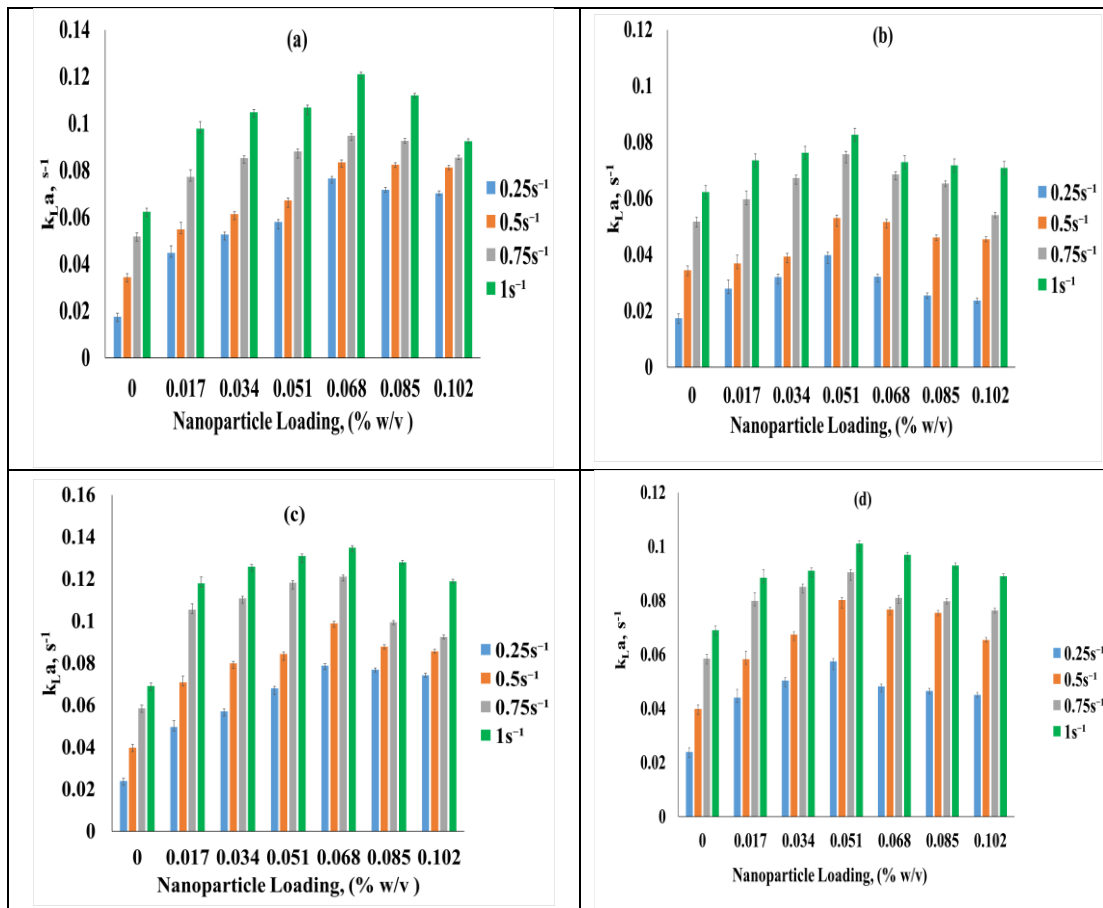
Fig.4.4 Diffusivity of oxygen in TiO₂, SiO₂, and α -Fe₂O₃ nanofluids.

The plot shows that the increase in nanoparticle loading increases the diffusivity of oxygen in nanofluid. It is observed that the diffusivity of SiO₂ nanofluid is greater compared to TiO₂ and α -Fe₂O₃ nanofluids which is due to the variation in the density of nanoparticles.

4.2 Effect of nanoparticles loading in the nanofluid on $k_{L,a}$.

To study the effect of TiO_2 , SiO_2 , and $\alpha\text{-Fe}_2\text{O}_3$ nanoparticle loading (Φ) on $k_{L,a}$, batch experiments were conducted with different nanoparticle loadings of 0.017 % w/v, 0.034 % w/v, 0.051 % w/v, 0.068 % w/v, 0.085 % w/v, and 0.102 % w/v with TiO_2 - 25, TiO_2 - 72, SiO_2 -12, SiO_2 -24, $\alpha\text{-Fe}_2\text{O}_3$ – 43 and $\alpha\text{-Fe}_2\text{O}_3$ – 76 nanofluids at different frequencies and amplitudes of pulsation at airflow rates of 1.8 LPM, 3.2 LPM, and 4.8 LPM and the results are presented in Fig. 4.5 to 4.7, Fig. 4.8 to 4.10 and Fig. 4.11 to 4.13 for TiO_2 , SiO_2 and $\alpha\text{-Fe}_2\text{O}_3$ nanofluids respectively.

The effect of nanoparticle loadings as a function of frequencies on $k_{L,a}$ in TiO_2 nanofluid at various amplitudes of pulsation of 3.2 cm, 4.7 cm, and 6.3 cm at varying air flow rates of 1.8 LPM, 3.2 LPM and 4.8 LPM are shown respectively in Fig. 4.5 (a) to (f); Fig.4.6 (a) to (f) and Fig.4.7 (a) to (f) TiO_2 -25 and TiO_2 - 72 respectively.



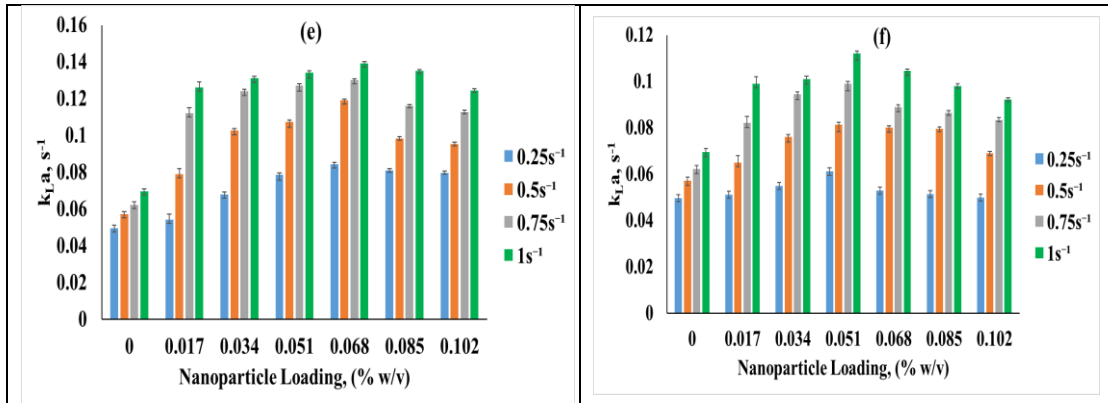
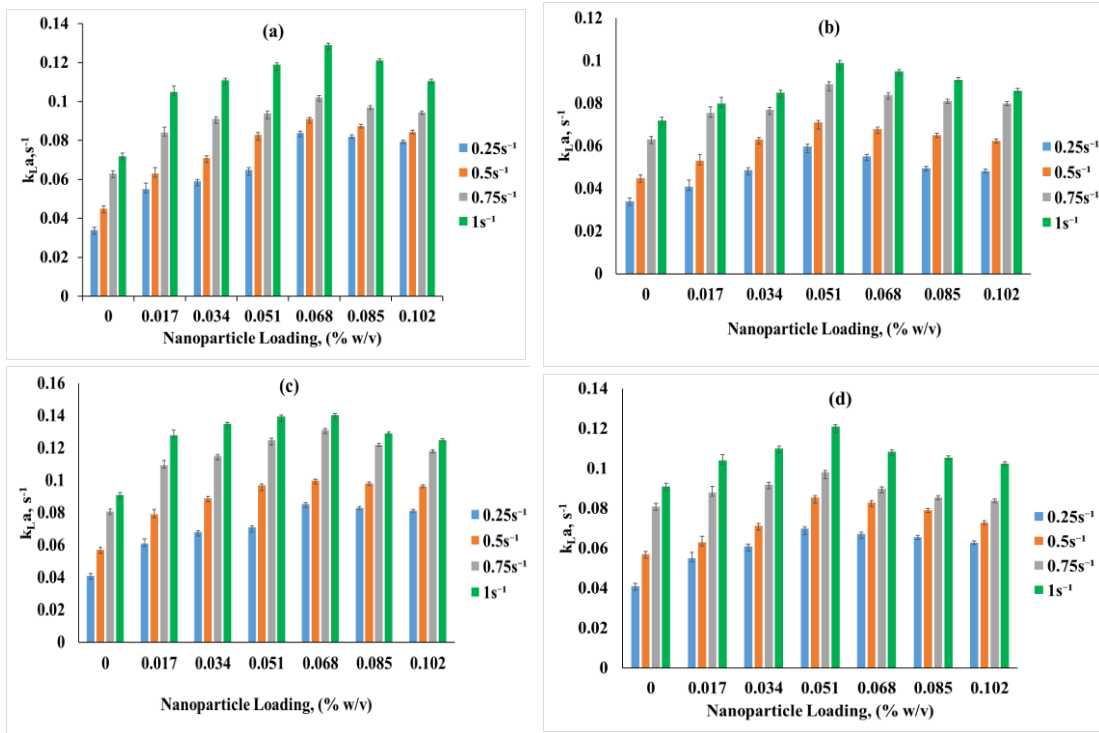


Fig 4.5. Effect of TiO₂ nanoparticle Loading on $k_{L,a}$ at different frequency of pulsation and at an air flow rate of 1.8 LPM for
 (a) TiO₂-25 at A= 3.2 cm (b) TiO₂-72 at A = 3.2 cm
 (c) TiO₂-25 at A= 4.7 cm (d) TiO₂-72 at A = 4.7 cm
 (e) TiO₂-25 at A= 6.3 cm (f) TiO₂-72 at A = 6.3 cm



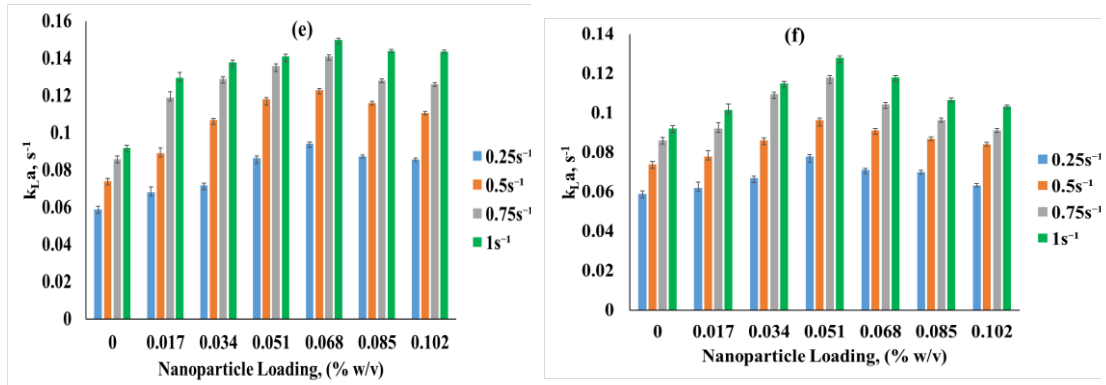


Fig.4.6 Effect of TiO₂ nanoparticle Loading on $k_{L,a}$ at different frequency of pulsation and at an air flow rate of 3.2 LPM for

- (a) TiO₂-25 at A= 3.2 cm (b) TiO₂-72 at A= 3.2 cm
 (c) TiO₂-25 at A= 4.7 cm (d) TiO₂-72 at A= 4.7 cm
 (e) TiO₂-25 at A= 6.3 cm (f) TiO₂-72 at A= 6.3 cm

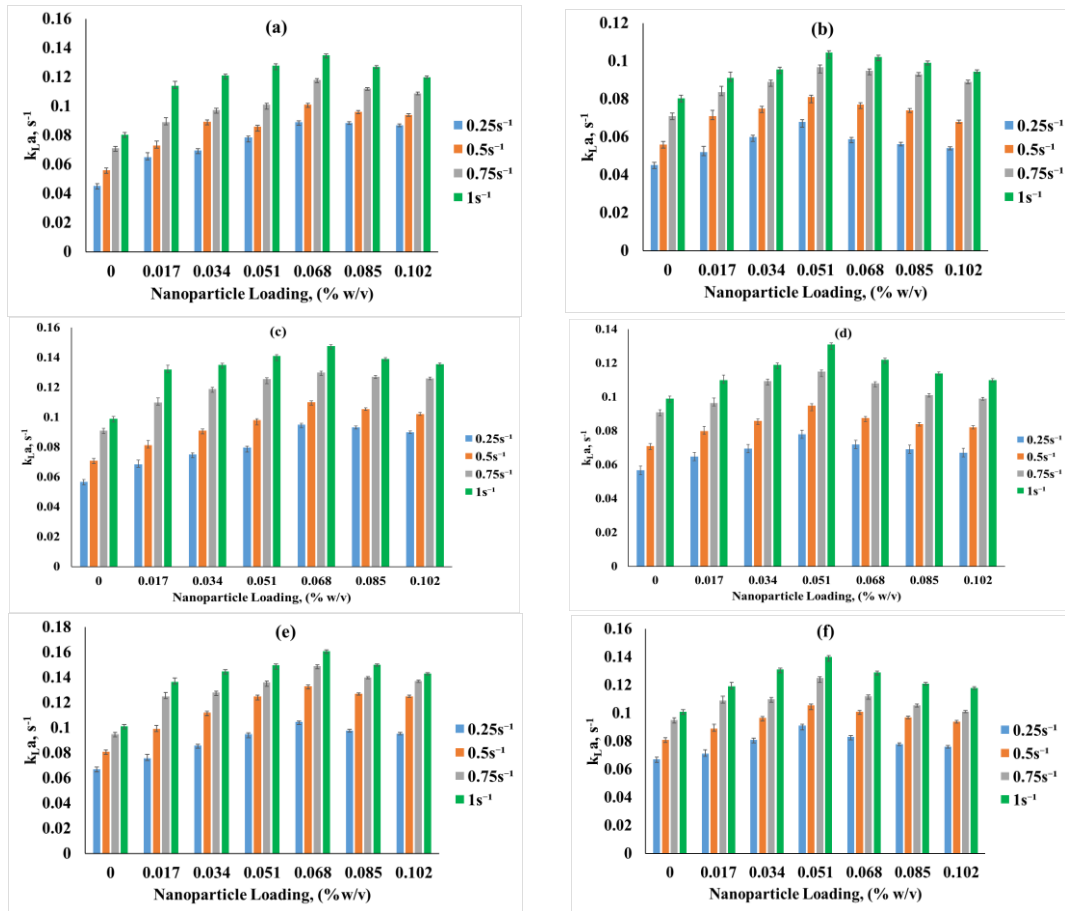


Fig.4.7 Effect of TiO₂ nanoparticle Loading on $k_{L,a}$ at different frequency of pulsation and at an air flow rate of 4.8 LPM for

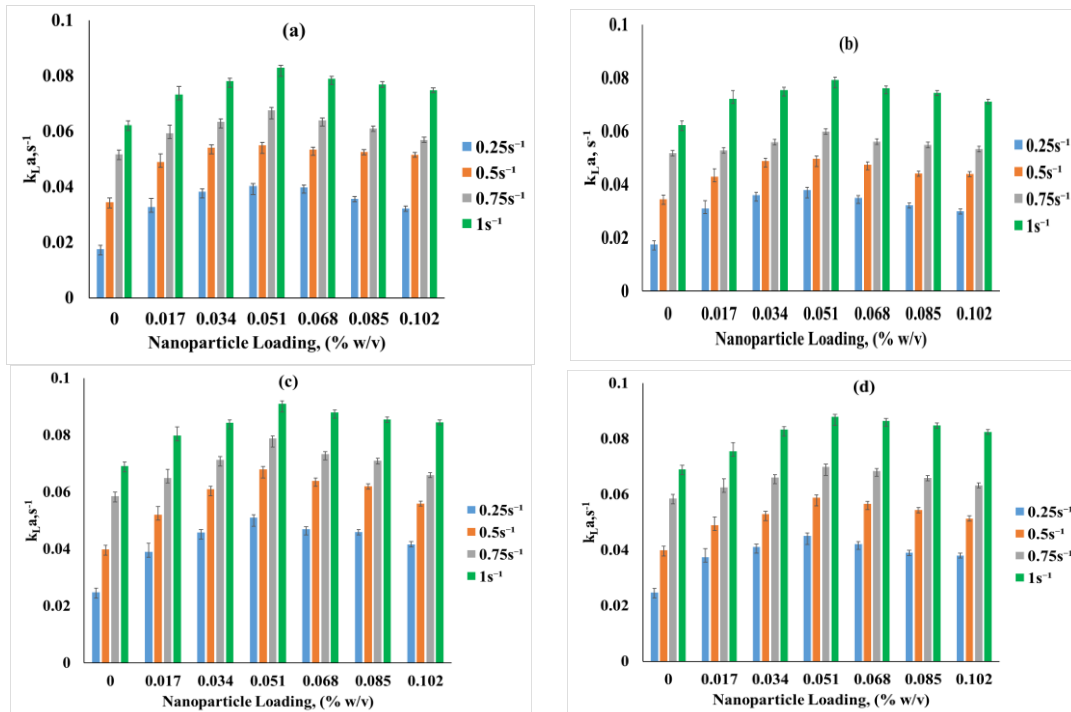
- (a) TiO₂-25 at A= 3.2 cm (b) TiO₂-72 at A= 3.2 cm
 (c) TiO₂-25 at A= 4.7 cm (d) TiO₂-72 at A= 4.7 cm
 (e) TiO₂-25 at A= 6.3 cm (f) TiO₂-72 at A= 6.3 cm

The k_{LA} was found to be enhanced in the presence of nanofluids as compared to that in the base fluid. The k_{LA} was found to increase with the increase in nanoparticle loading from 0.017 % w/v to 0.068 % w/v in TiO₂ -25 nanofluid as evidenced in Fig 4.5 (a), (c) and (e); Fig 4.6 (a), (c) and (e) and Fig 4.7 (a), (c) and (e) at all the frequencies, amplitude of pulsation and airflow rates for TiO₂ nanoparticles. However, a further increase in the loading has led to a decrease in the k_{LA} values. The maximum value of k_{LA} with TiO₂ -25 nanofluid is obtained with nanoparticles loading of 0.068 % w/v at highest frequency of 1s⁻¹ and at all the amplitudes of pulsation and air flow rates. Similar trend has been observed with TiO₂ -72 nanofluid, with maximum k_{LA} values being observed at loading of 0.051 % w/v. The increase in k_{LA} is observed when nanoparticle loading was increased from 0.017 % w/v to 0.051% w/v with TiO₂ -72 nanofluid as shown in the Fig. 4.5 (b), (d) and (f); Fig 4.6 (b), (d) and (f) and Fig 4.7 (b), (d) and (f) at all the frequencies, amplitude of pulsation and air flow rates. Further, as observed in Fig. 4.5 to 4.7, there is a decrease in volumetric mass transfer coefficient with increase in TiO₂ loading above the critical loading of 0.068 % w/v and 0.051 % w/v for nanofluids with TiO₂ -25, TiO₂- 72 nanofluids respectively. Jiang et al (2015) have also reported similar trend of the increase in k_{LA} with increasing solid loading in a thermostatic stirred tank reactor using TiO₂ nanoparticles in aqueous solution by determining k_{LA} using sodium sulphite method. They have found an optimum loading of 0.4 kg/m³ (equivalent to 0.04 wt%) of TiO₂ nanoparticles for the maximum enhancement, beyond which loading a decrease in k_{LA} was noticed.

The effect of SiO₂ nanoparticle loadings as a function of frequencies on k_{LA} at various amplitudes of pulsation of 3.2 cm, 4.7 cm and 6.3 cm at varying air flow rate of 1.8 LPM, 3.2 LPM and 4.8 LPM are shown respectively in Fig. 4.8 (a) to (f); Fig.4.9 (a) to (f) and Fig.4.10 (a) to (f) with SiO₂ -12, SiO₂ -24 nanofluids. The k_{LA} values in PPC are higher in SiO₂ nanofluid than in the base fluid.

The k_{LA} was found to be increased with the increase in nanoparticles loading from 0.017 % w/v to 0.051% w/v, as evidenced in Figure 4.8 to 4.10 with SiO₂ -12, SiO₂ -24 nanofluids at all the frequencies, amplitude of pulsation and air flow rates. However, further increase in the loading has led to decrease in the k_{LA} values. Maximum value of k_{LA} is obtained with 0.051% w/v at highest frequency of 1s⁻¹ and all the amplitudes of pulsation with SiO₂ -12, SiO₂ -24 nanofluids. Jiang et al (2015) in

their studies on k_{La} in a thermostatic stirred tank reactor have found that k_{La} increased with increase in solid loading in SiO_2 nanofluid in aqueous solution by sodium sulphite with largest enhancement for an optimum loading of 0.6kg/m^3 (equivalent to 0.06 wt%) of SiO_2 nanoparticles. Nematbaksh and Ahmad (2015) reported that SiO_2 nanoparticles near the interface forms a resistant layer and when the concentration of nanoparticles increased the thickness of solid like layer around the air bubbles and the interface resistance (a hindrance to mass transfer) increases which results in the reduced mass transfer coefficient. Feng and Johnson (2012) reported that liquid film mass transfer coefficients of silica nanofluids reduced with increasing viscosity. Goodarzi and Esfahany (2016) observed the decreasing trend in mass transfer coefficient with increasing concentration of silica nanoparticles in their investigation of influence of hydrophilic silica nanoparticles on mass transfer in liquid-liquid extraction process. They attributed their observation of decreasing trend as reduction of the effective fraction of gas-liquid contact area due to the presence of higher concentration of suspended nanoparticles and also increase in solution viscosity.



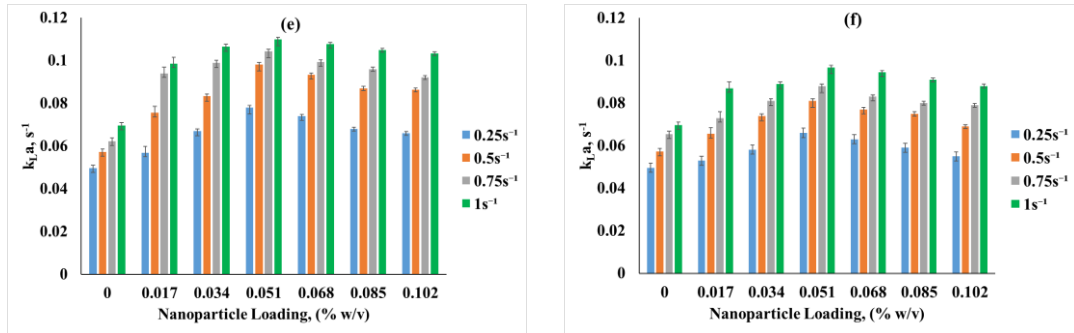


Fig.4.8 Effect of SiO₂ nanoparticle Loading on $k_{L,a}$ at different frequency of pulsation and at an air flow rate of 1.8 LPM for

- (a) SiO₂-12 at A= 3.2 cm (b) SiO₂-24 at A= 3.2 cm
- (c) SiO₂- 12 at A= 4.7 cm (d) SiO₂-24 at A= 4.7 cm
- (e) SiO₂- 12 at A= 6.3 cm (f) SiO₂ -24 at A= 6.3 cm

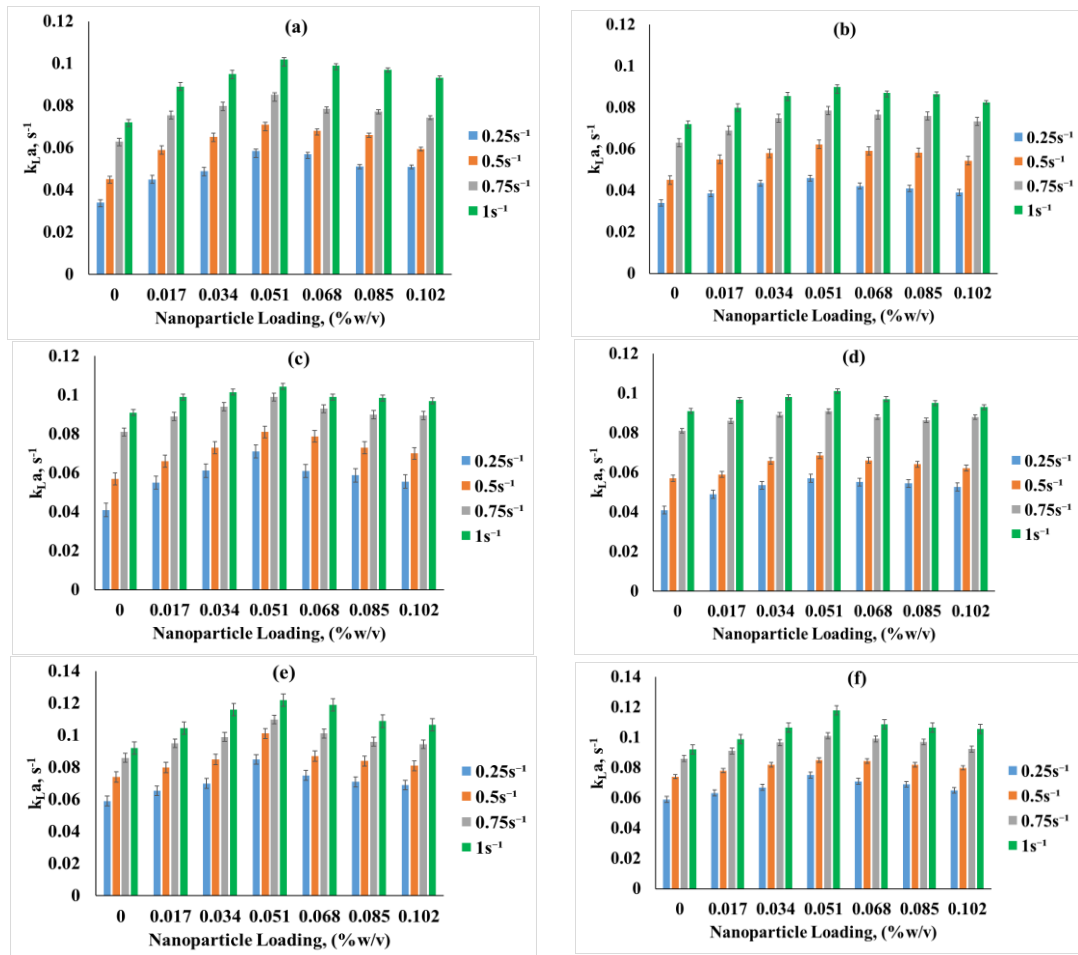


Fig.4.9 Effect of SiO₂ nanoparticle Loading on $k_{L,a}$ at different frequency of pulsation and at an air flow rate of 3.2 LPM for

- (a) SiO₂-12 at A= 3.2 cm (b) SiO₂-24 at A= 3.2 cm
- (c) SiO₂- 12 at A= 4.7 cm (d) SiO₂-24 at A= 4.7 cm
- (e) SiO₂- 12 at A= 6.3 cm (f) SiO₂ -24 at A= 6.3 cm

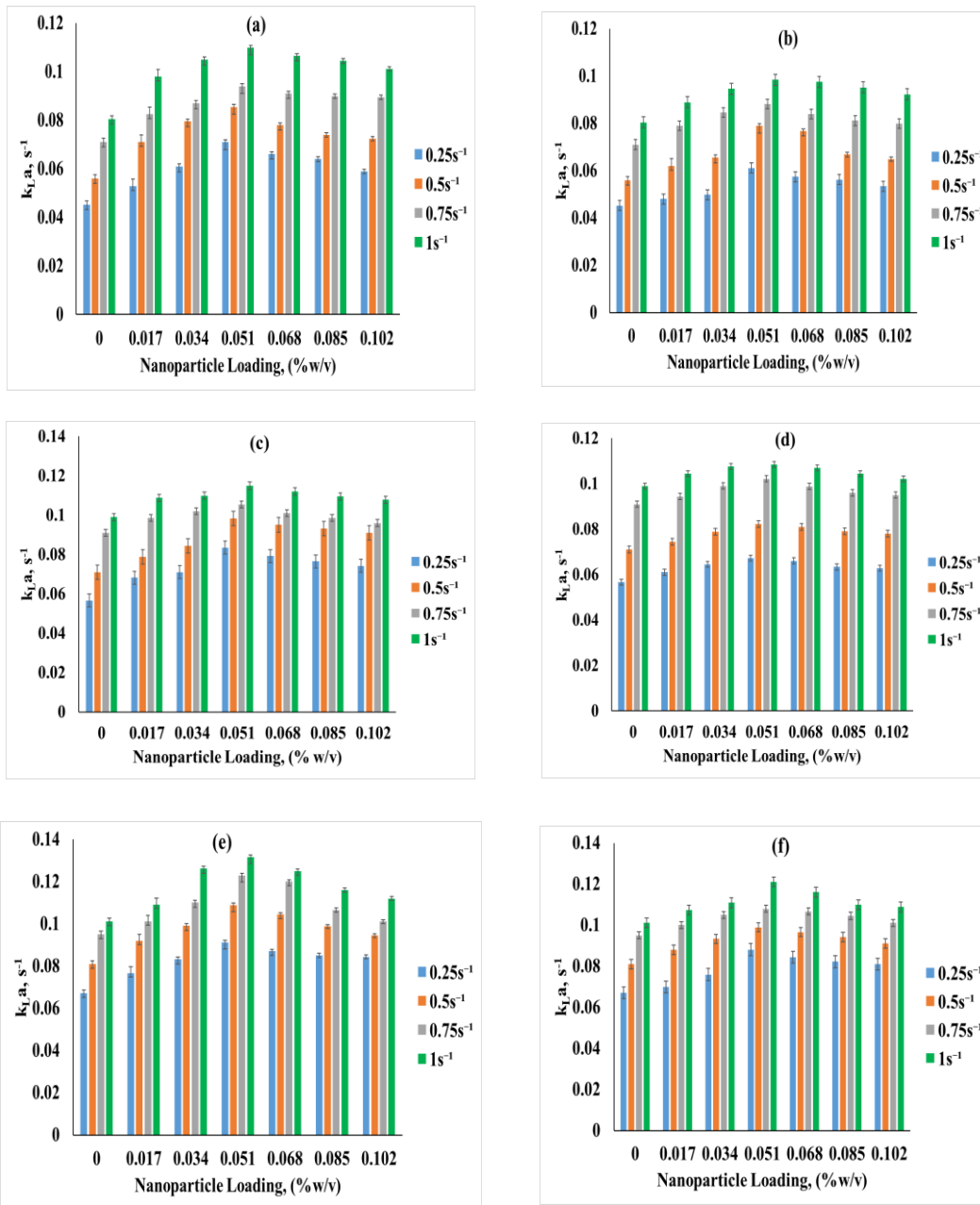


Fig.4.10 Effect of SiO₂ nanoparticle Loading on k_{La} at different frequency of pulsation and at an air flow rate of 4.8 LPM for

- (a) SiO₂-12 at A= 3.2 cm
- (b) SiO₂-24 at A= 3.2 cm
- (c) SiO₂- 12 at A= 4.7 cm
- (d) SiO₂-24 at A= 4.7 cm
- (e) SiO₂- 12 at A= 6.3 cm
- (f) SiO₂-24 at A= 6.3 cm

The effect of $\alpha\text{-Fe}_2\text{O}_3$ nanoparticle loadings as a function of frequencies on $k_{L,A}$ at various amplitudes of pulsation of 3.2 cm, 4.7 cm and 6.3 cm at varying air flow rate of 1.8 LPM, 3.2 LPM and 4.8 LPM are shown respectively in Fig. 4.11(a) to (f); Fig.4.12 (a) to (f) and Fig.4.13 (a) to (f) with $\alpha\text{-Fe}_2\text{O}_3 - 43$ and $\alpha\text{-Fe}_2\text{O}_3 - 76$ nanofluids respectively.

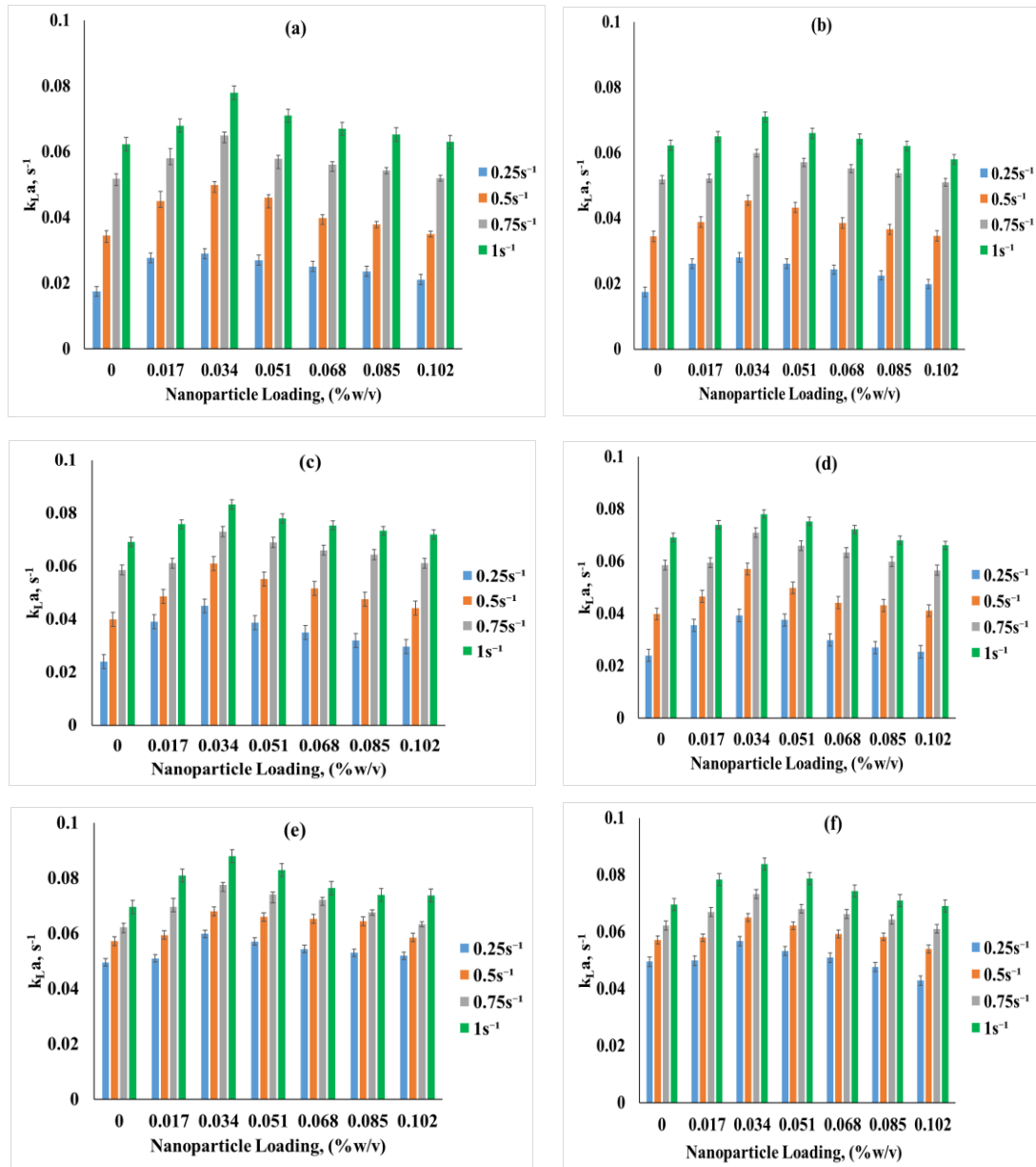


Fig.4.11 Effect of $\alpha\text{-Fe}_2\text{O}_3$ nanoparticle loading on $k_{L,A}$ at different frequency of pulsation and at an air flow rate of 1.8 LPM for

- (a) $\alpha\text{-Fe}_2\text{O}_3 - 43$ at $A = 3.2$ cm
- (b) $\alpha\text{-Fe}_2\text{O}_3 - 76$ at $A = 3.2$ cm
- (c) $\alpha\text{-Fe}_2\text{O}_3 - 43$ at $A = 4.7$ cm
- (d) $\alpha\text{-Fe}_2\text{O}_3 - 76$ at $A = 4.7$ cm
- (e) $\alpha\text{-Fe}_2\text{O}_3 - 43$ at $A = 6.3$ cm
- (f) $\alpha\text{-Fe}_2\text{O}_3 - 76$ at $A = 6.3$ cm

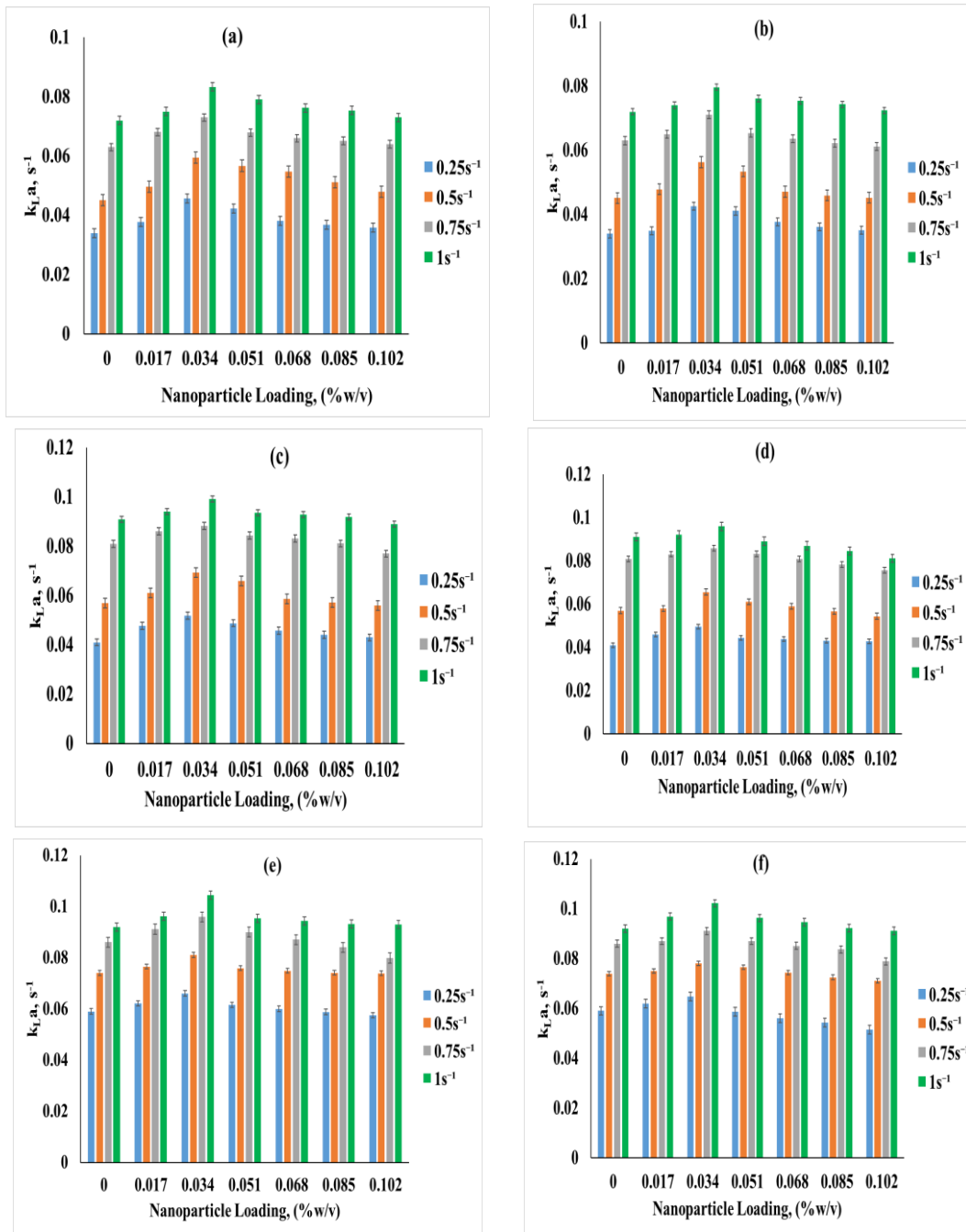


Fig.4.12 Effect of $\alpha\text{-Fe}_2\text{O}_3$ nanoparticle loading on $k_{L,a}$ at different frequency of pulsation and at an air flow rate of 3.2 LPM for

- (a) $\alpha\text{-Fe}_2\text{O}_3$ – 43 at $A = 3.2$ cm
- (b) $\alpha\text{-Fe}_2\text{O}_3$ – 76 at $A = 3.2$ cm
- (c) $\alpha\text{-Fe}_2\text{O}_3$ – 43 at $A = 4.7$ cm
- (d) $\alpha\text{-Fe}_2\text{O}_3$ – 76 at $A = 4.7$ cm
- (e) $\alpha\text{-Fe}_2\text{O}_3$ – 43 at $A = 6.3$ cm
- (f) $\alpha\text{-Fe}_2\text{O}_3$ – 76 at $A = 6.3$ cm

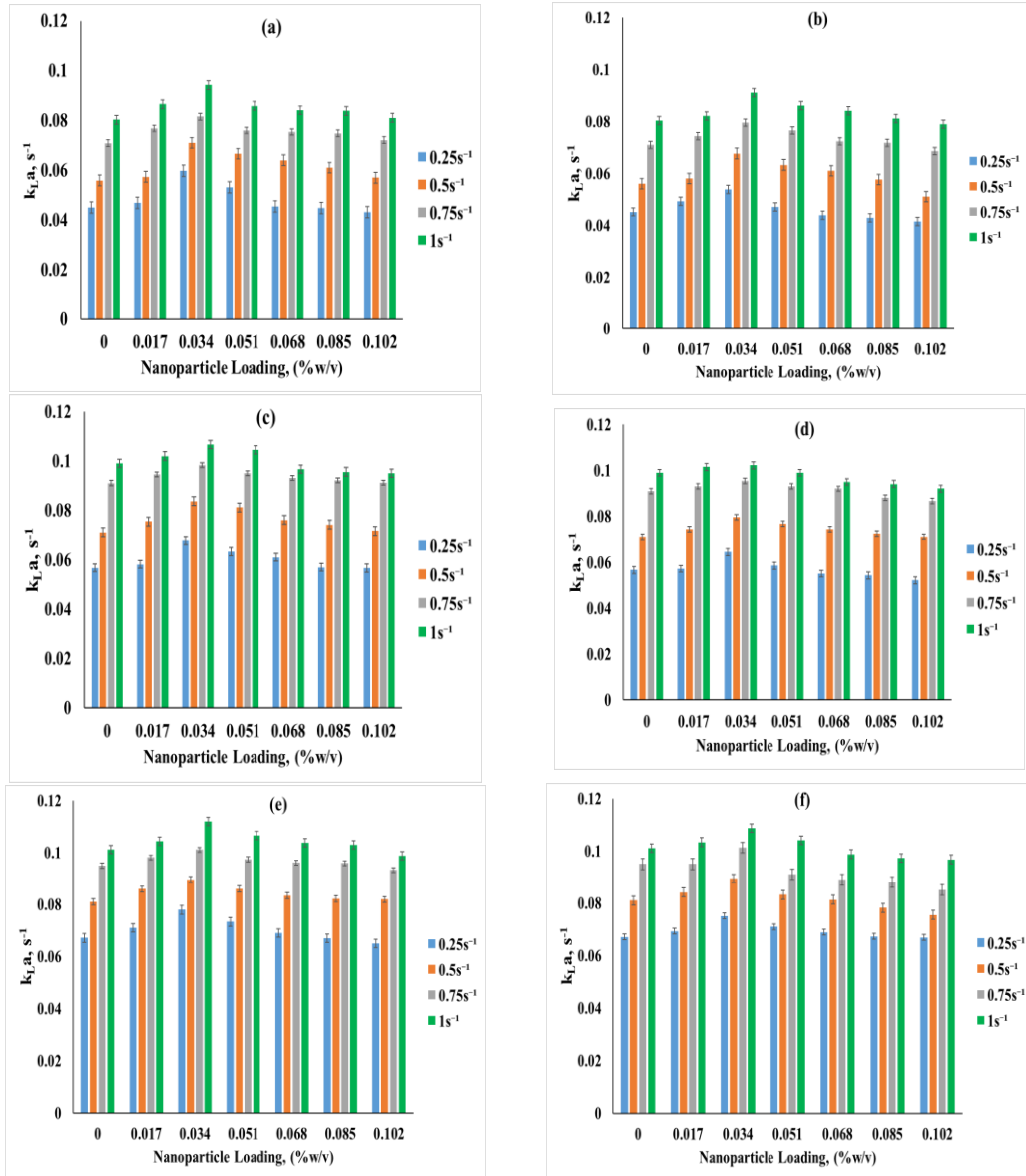


Fig.4.13 Effect of $\alpha\text{-Fe}_2\text{O}_3$ nanoparticle loading on k_{LA} at different frequency of pulsation and at an air flow rate of 4.8 LPM for

- (a) $\alpha\text{-Fe}_2\text{O}_3$ – 43 at $A= 3.2$ cm
- (b) $\alpha\text{-Fe}_2\text{O}_3$ – 76 at $A = 3.2$ cm
- (c) $\alpha\text{-Fe}_2\text{O}_3$ – 43 at $A= 4.7$ cm
- (d) $\alpha\text{-Fe}_2\text{O}_3$ – 76 at $A = 4.7$ cm
- (e) $\alpha\text{-Fe}_2\text{O}_3$ – 43 at $A= 6.3$ cm
- (f) $\alpha\text{-Fe}_2\text{O}_3$ – 76 at $A = 6.3$ cm

The k_{LA} was found to increase with the increase in nanoparticle loading from 0.017 to 0.034 % w/v in $\alpha\text{-Fe}_2\text{O}_3$ nanofluid as evidenced in Fig. 4.11 to Fig.4.13 with $\alpha\text{-Fe}_2\text{O}_3$ – 43 and $\alpha\text{-Fe}_2\text{O}_3$ – 76 nanofluids at all the frequencies, amplitude of pulsation and air flow rates and a further increase in loading has led to a decrease in the k_{LA} values. The maximum value of k_{LA} is obtained with the nanoparticle loading of 0.034 % w/v at the highest frequency of 1s^{-1} and at all the amplitude of pulsation and with $\alpha\text{-Fe}_2\text{O}_3$ – 43 and $\alpha\text{-Fe}_2\text{O}_3$ – 76 nanofluids. (Olle et al. 2006b), have observed an increase in the mass transfer coefficient at a loading below 1 wt % in an agitated sparged reactor with α -

Fe₂O₃ nanofluid. Manikandan et al. (2012), have observed that the increase solid loading has increased the k_{LA} in an agitated aerated bioreactor using Fe₂O₃ – water nanofluid. They have found the decrease in k_{LA} value beyond the optimum loading of 0.065 wt% Fe₂O₃ nanoparticles and for the optimum loading they have achieved the maximum enhancement of k_{LA}.

The results obtained in the present study indicated that the k_{LA} values with TiO₂, SiO₂ and α-Fe₂O₃ nanofluid are higher than that with the base fluid in PPC. Further, maximum k_{LA} was obtained at the critical loading, which were found to be 0.068 % w/v and 0.051 % w/v with TiO₂ -25 and TiO₂- 72 nanofluids; 0.051 % w/v with SiO₂ -12 and SiO₂ -24 nanofluids; 0.034 % w/v with α-Fe₂O₃ – 43 and α-Fe₂O₃ – 76 nanofluids.

The maximum enhancement factors with TiO₂, SiO₂ and α-Fe₂O₃ nanofluids at critical loading conditions are presented in in Table 4.4. As observed in Table 4.4, the enhancement factor values are greater than “ONE” with all three nanofluids at the nanoparticle loadings and size, which signifies the effect of nanofluid in enhancing k_{LA} in PPC.

Table 4.4 Maximum Enhancement factor obtained at critical loading of TiO₂, SiO₂ and α-Fe₂O₃ nanofluids with varying amplitude of pulsation, at the lowest (0.25 s⁻¹) and Highest (1 s⁻¹) frequency at an air flow rate of 1.8 LPM

Nano particle Type	Nano particle critical loading, %w/v	Average Nano particle Size, nm	Enhancement factor					
			A=3.2 cm		A=4.7 cm		A=6.3 cm	
			0.25 s ⁻¹	1s ⁻¹	0.25 s ⁻¹	1s ⁻¹	0.25 s ⁻¹	1s ⁻¹
TiO ₂	0.068	25 nm	4.37	2.02	3.28	1.98	1.92	1.87
	0.051	72 nm	2.39	1.38	2.35	1.35	1.63	1.31
SiO ₂	0.051	12 nm	2.30	1.33	2.05	1.31	1.57	1.25
		24 nm	2.17	1.27	1.81	1.22	1.33	1.20
α-Fe ₂ O ₃	0.034	43 nm	1.65	1.25	1.61	1.21	1.20	1.16
		76 nm	1.61	1.15	1.56	1.13	1.17	1.12

Several studies have indicated that the gas – liquid mass transfer coefficient initially increases with nanoparticle loading and then decreases at higher loading. The increase in volumetric oxygen mass transfer coefficient with increase in nanoparticle loading is because of the following reasons, (i) Brownian motion following micro convection and Marangoni flow (the mass transfer along an interface between two phases due to a gradient of the surface tension) generated by nanoparticles will intercept the accumulation of bubbles and helps in increasing the gas hold up and the effective area of mass transfer, therefore are reported to be responsible for increasing the k_{LA} , thus strengthening the rate of mass transfer (Jiang et al. 2019; Manikandan et al. 2012; Mirzazadeh Ghanadi et al. 2015; Saien and Bamdadi 2012; Zhang et al. 2022), (ii) due to the shearing action by the particles present in the suspension which may decrease the film thickness boosting the mass transfer coefficient (Zhou et al. 2003). (iii) Bubble breaking phenomena: in the gas-liquid systems the nanoparticles collide with the gas- liquid interface and accordingly break the bigger size bubbles into smaller size bubbles and lead to larger interfacial area which actively enhances k_{LA} and leads to faster rate of mass transfer from the gas to the liquid (Kim et al. 2008; Torres Pineda et al. 2012; Zhang et al. 2022). (iv) Shuttle effect or Grazing effect mechanism: According to this mechanism, the nanoparticles suspended in the gas – liquid system may adsorb the solute (oxygen) from the gas phase and immediately desorb or transfer in to the bulk liquid (Ashrafmansouri and Nasr Esfahany 2014; Jiang et al. 2015; Lu et al. 2013; Saeednia et al. 2015), or in other words grazing effect is nothing but the intensity of the fluid movement near the gas-liquid surface and particles pass through the concentration film layer and pick up the adsorbate (Darvanjooghi et al. 2018).

It has also been observed in the present study that beyond a certain nanoparticle loading level, the mass transfer coefficient decreases with increase in nanoparticle loading. According to many researchers (Beiki et al. 2013; Krishnamurthy et al. 2006; Nematbakhsh and Rahbar-Kelishami 2015; Veilleux and Coulombe 2010), the decrease in mass transfer coefficient with increase in nanoparticle loading above a certain level can be attributed to the particle – particle clustering or agglomeration that occurs at higher loading . The higher degree of aggregation of nanoparticles opposes the particle motion and hence Brownian motion and micro-convection are decreased (Saien and Bamdadi 2012; Saien and Zardoshti 2015; Zhang et al. 2021). Due to particle aggregation, larger and more massive particles are produced with reduced capacity of

promoting localized convection (Ashrafmansouri et al. 2016; Nematbakhsh and Rahbar-Kelishami 2015). Keshishian et al. (2013), have observed similar deterioration of mass transfer coefficient due to saturation of host fluid by nanoparticles and hence the prominent positive effects of nanoparticle drops down. Zhang et al. (2020), have reported the decreased mass transfer coefficient with an increase in nanoparticle loading and have attributed the same to the neighboring nanoparticles which oppose the free movement of nanoparticles and increased tendency of precipitation and agglomeration that reduces the k_{LA} enhancement. Furthermore, Esmaeili Faraj et al. (2014), suggested that saturation of the gas bubble surface by nanoparticles can justify the decreasing trend. The higher loading of nanoparticles results in increase in the hydrodynamic diameter of the particles due to agglomeration and decrease in the nanofluid stability obstructing the shuttle effect phenomenon and micro-convection mechanisms in the system leading to the diminishing k_{LA} (Ashrafmansouri et al. 2016; Saien and Bamdadi 2012).

Apart from these, the influence of nanofluid properties such as the surface tension and dynamic viscosity of nanofluids may also contribute to the reduction in the k_{LA} with increase in nanoparticle loading. As discussed in the section 4.1, the surface tension of nanofluid has increased with the increase in the loading. The surface tension favours the bubble coalescence leading to an increase in bubble size, which reduces the interfacial area, decreases the gas hold up, and the mass transfer coefficient (Moraveji et al. 2013). The increase in surface tension affects the surface renewal rate which controls the mass transfer coefficient and also reduces the available surface area for molecular diffusion at the interface, forming a hydration layer at the surface. It further gives rise to the higher surface viscosity and increased surface layer thickness, which resists the transfer of oxygen (Masutani and Stenstrom 1991). The increase in surface tension with increase in nanoparticle loading may have contributed dominantly in decreasing the k_{LA} values along with the agglomeration effect at loadings above the critical loading values. Hence lower surface tension of the nanofluids is favourable in enhancing the mass transfer coefficient. It appears from the present study that one of the reasons for the decrease in k_{LA} at high particle concentrations is the result of unfavourable influence of high surface tension.

Similarly, the viscosity of nanofluids have been found to increase with the increase in nanoparticle loading as shown in Fig.4.2 (a), (b) and (c) for TiO₂, SiO₂ and α -Fe₂O₃ nanofluids. Liquid film mass transfer coefficients are known to decrease with an increase in viscosity (Feng and Johnson 2012; Hasani Goodarzi and Nasr Esfahany 2016; Kim et al. 2014; Saien and Hasani 2017; Samadi et al. 2014). The effect of increased viscosity may be more pronounced above the critical loading value and thus reducing the mass transfer coefficients at higher loading. The reduction in mass transfer coefficients with increase in viscosity may be less pronounced than the other effects of increased nanoparticle loading at loadings below the critical loading. So, the mass transfer coefficient increases at lower loading, despite increase in viscosity. However, the influence of increased viscosity is dominant at higher loading causing the mass transfer coefficients to reduce with increase in loading.

It may be concluded that the properties of nanofluid such as surface tension and viscosity may be playing a dominant role in reducing k_{LA} at loadings above the critical loading values along with the agglomeration effect.

4.3 Effect of frequency of pulsation on k_{LA} with nanofluids

Further, the effect of frequency of pulsation on k_{LA} in the presence of TiO₂ -25, TiO₂-72, SiO₂ -12, SiO₂ -24, α -Fe₂O₃ – 43 and α -Fe₂O₃ – 76 nanofluids with varying nanoparticle loading at different frequencies of pulsation of 0.25, 0.5, 0.75, and 1s⁻¹ by varying the amplitude, and air flow rates. The effect of frequency of pulsation as a function of nanoparticle loadings on k_{LA} at various amplitude of pulsation 3.2, 4.7 and 6.3cm and at varying air flow rate of 1.8 LPM, 3.2 LPM and 4.8 LPM are shown in Fig. 4.5 to 4.7, Fig. 4.8 to 4.10 and Fig. 4.11 to 4.13 for TiO₂, SiO₂ and α -Fe₂O₃ nanofluids respectively.

The k_{LA} was found to increase with the increase in the frequency of pulsation from 0.25 s⁻¹ to 1s⁻¹, as shown in Fig. 4.5 to 4.7 (a) –(f); Fig. 4.8 to 4.10 (a) –(f) and Fig. 4.11 to 4.13 (a) –(f) for TiO₂ -25 and TiO₂- 72; SiO₂ -12 and SiO₂ -24; and α -Fe₂O₃ – 43 and α -Fe₂O₃ – 76 nanofluids respectively. Maximum values of k_{LA} was obtained at the highest frequency of 1s⁻¹ with all the nanoparticle loadings with TiO₂ -25, TiO₂- 72, SiO₂ -12, SiO₂ -24, α -Fe₂O₃ – 43 and α -Fe₂O₃ – 76 nanofluids.

As the frequency of pulsation increases, greater velocity of the reciprocating plate motion and movement of nanoparticles in the nanofluid leads to collision of the particles with the gas bubbles that cause the breaking and deformation of gas bubbles which are dispersed in nanofluids (Haghtalab et al. 2015; Kim et al. 2008). As a result of increased frequency of pulsation, the gas bubbles are broken into smaller bubbles (Amani et al. 2017; Kim et al. 2008). The formation of smaller bubbles having higher mass transfer area leads to the enhancement of interfacial area per unit volume of the reactor and thus enhance the volumetric oxygen mass transfer coefficient. The turbulence-induced by increasing the frequency is very high and thus the aggregation potential of nanoparticles reduces (Pashaei et al. 2018) resulting in enhanced bubble dispersion (El-Naas et al. 2017; Stamenković et al. 2005) and bubble residence time (Abufalgha 2018; Gomaa and Al Taweel 2005; Lounes and Thibault 1994; Shetty and Srinikethan 2010) in the column leading to increase in volumetric oxygen mass transfer coefficient. Shetty Kodialbail and Srinikethan (2011), have reported that the frequency of pulsation periodically renews the surface available for mass transfer and also reduces the liquid film thickness through which mass transfer occurs and hence decreases the mass transfer resistance. This increases the mass transfer coefficient with increasing frequency. Shetty and Srinikethan (2010) have also reported an increase in k_{La} with increasing frequency of pulsation in a pulsed plate column for three-phase gas-liquid-solid systems. According to Panahinia et al. (2017), the buoyancy and interfacial tensions are responsible for the bubble breakage in the absence of pulsation. However, in the presence of pulsation, smaller size bubbles are obtained due to an intensified collision between the bubbles, plates, and the internal wall that helps in increasing the rate of breakage. Gwiazda et al. (2020), have observed that the application of liquid pulsations at resonance frequencies in classical bubble column has affected the shape of the gas bubbles and brought nearly to the spherical shape. It leads to an increase in gas hold up and interfacial area enhancing the mass transfer in comparison to the gas liquid mass transfer without pulsations.

Table 4.4 presents the enhancement factors obtained with TiO_2 , SiO_2 and $\alpha-Fe_2O_3$ nanofluids at the respective critical loading conditions at the lowest ($0.25\ s^{-1}$) and highest ($1\ s^{-1}$) frequency of pulsation at 1.8 LPM and at the amplitudes of pulsation of 3.2 cm, 4.7 cm and 6.3 cm. The maximum enhancement factor with reference to the base fluid is observed at a lowest frequency of $0.25\ s^{-1}$. The maximum enhancement

factors of 4.37, 2.39, 2.30, 2.17, 1.65 and 1.61 could be achieved with TiO_2 - 25, TiO_2 - 72, SiO_2 -12, SiO_2 - 24, $\alpha\text{-Fe}_2\text{O}_3$ - 43 and $\alpha\text{-Fe}_2\text{O}_3$ - 76 nanofluids respectively under the condition at amplitude of 3.2cm and at the lowest frequency of pulsation. This shows that the enhancement effect of nanofluid on k_{LA} is more pronounced at lower frequency as compared to the higher frequencies. It implies that in order to achieve a desired mass transfer characteristic, lower pulsing frequencies may be adequate when a nanofluid is used. Thus the frequency required to achieve a desired mass transfer characteristic can be reduced by using a nanofluid instead of the base fluid. So enhanced oxygen mass transfer characteristics can be achieved with the nanofluids in the pulsed plate column with the tremendous saving of energy.

4.4 Effect of the amplitude of pulsation on k_{LA} in the presence of nanofluids.

To study the effect of amplitude of pulsation on k_{LA} , experiments were conducted at three different amplitudes such as 3.2, 4.7 and 6.3 cm by varying the nanoparticle loading, frequency of pulsation and air flowrates. The effect of amplitude of pulsation as a function of nanoparticle loadings on k_{LA} at varying frequency of 0.25, 0.5, 0.75 and 1 s^{-1} with air flow rate of 1.8 LPM are shown in Fig.4.14 and Fig.4.15 for TiO_2 - 25 and TiO_2 - 72 nanofluids; Fig. 4.16 and Fig.4.17 for SiO_2 -12 and SiO_2 - 24 nanofluids; Fig.4.18 and Fig.4.19 for $\alpha\text{-Fe}_2\text{O}_3$ - 43 and $\alpha\text{-Fe}_2\text{O}_3$ - 76 nanofluids.

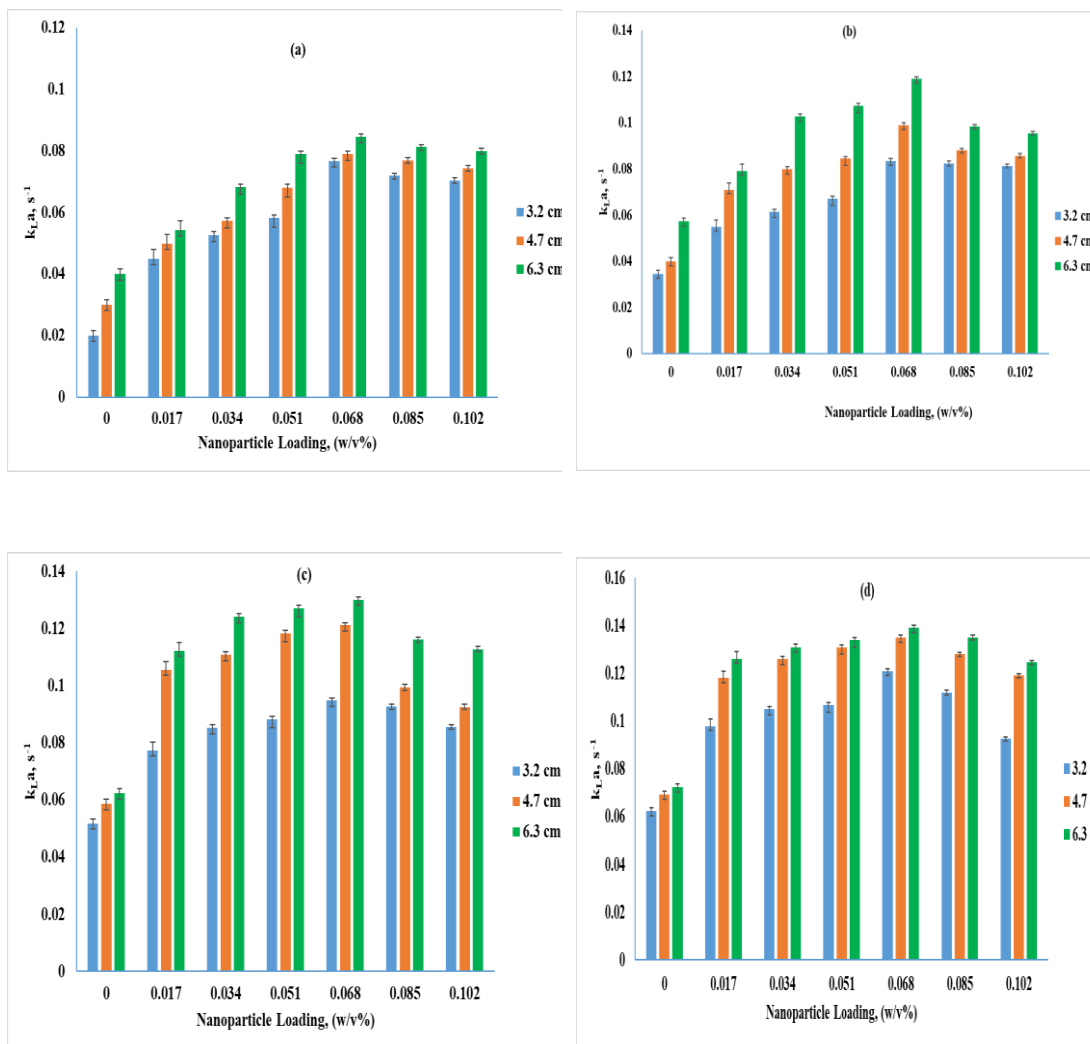


Fig.4.14 Effect of amplitude of pulsation on k_{La} at different $\text{TiO}_2\text{-25}$ nanoparticle loading at varying frequency of pulsation of (a) 0.25 s^{-1} (b) 0.5 s^{-1} , (c) 0.75 s^{-1} and (d) 1 s^{-1}

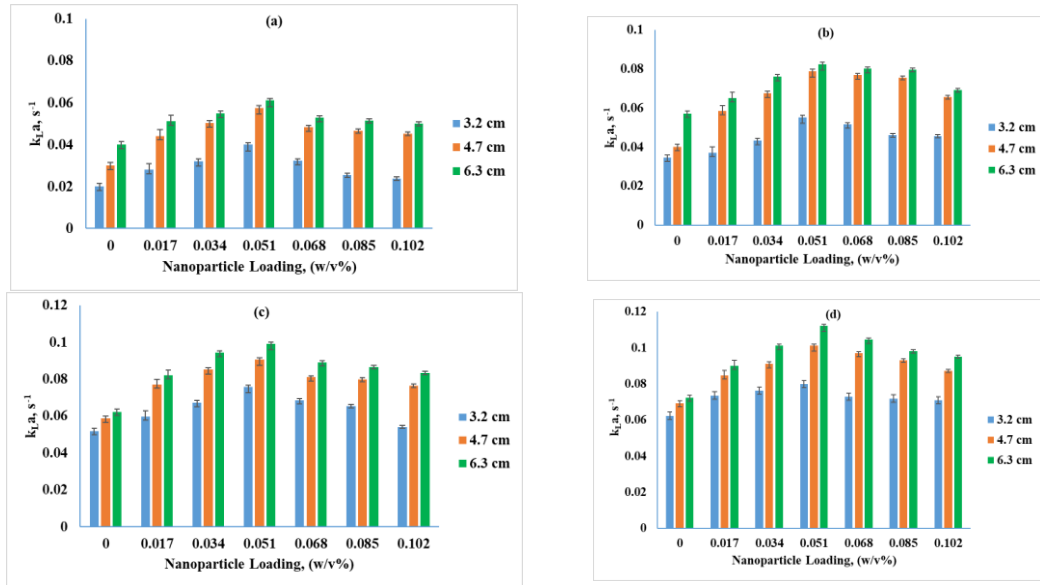


Fig.4.15 Effect of amplitude of pulsation on k_{La} at different TiO_2-72 nanoparticle loading at varying frequency of pulsation of (a) 0.25 s^{-1} (b) 0.5 s^{-1} , (c) 0.75 s^{-1} and (d) 1 s^{-1}

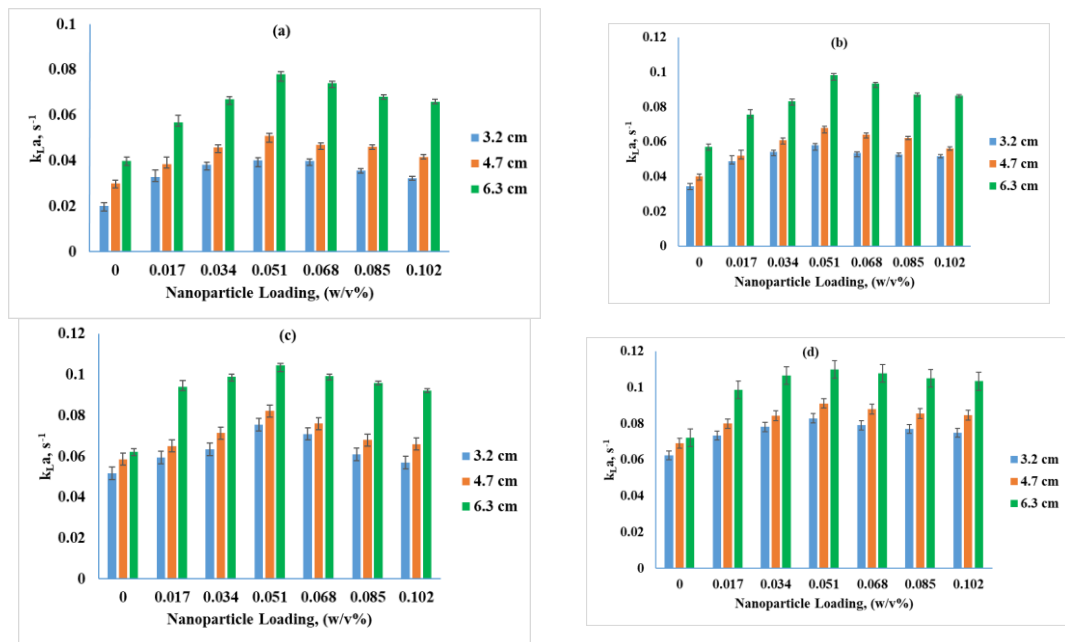


Fig.4.16 Effect of amplitude of pulsation on k_{La} at different SiO_2-12 nanoparticle loading at varying frequency of pulsation of (a) 0.25 s^{-1} (b) 0.5 s^{-1} , (c) 0.75 s^{-1} and (d) 1 s^{-1}

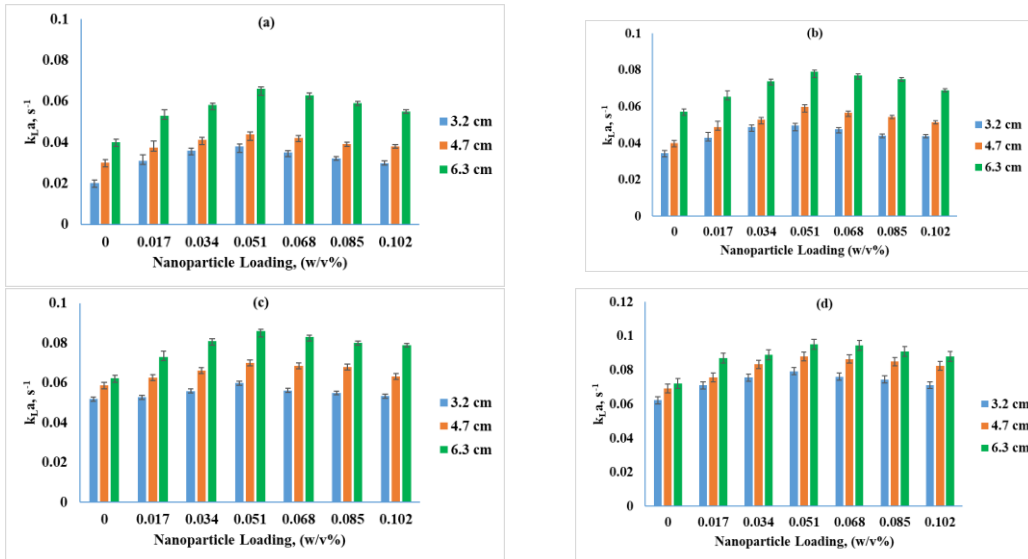


Fig.4.17 Effect of amplitude of pulsation on $k_{L,a}$ at different $\text{SiO}_2 - 24$ nanoparticle loading at varying frequency of pulsation of (a) $0.25 s^{-1}$ (b) $0.5 s^{-1}$, (c) $0.75 s^{-1}$ and (d) $1 s^{-1}$

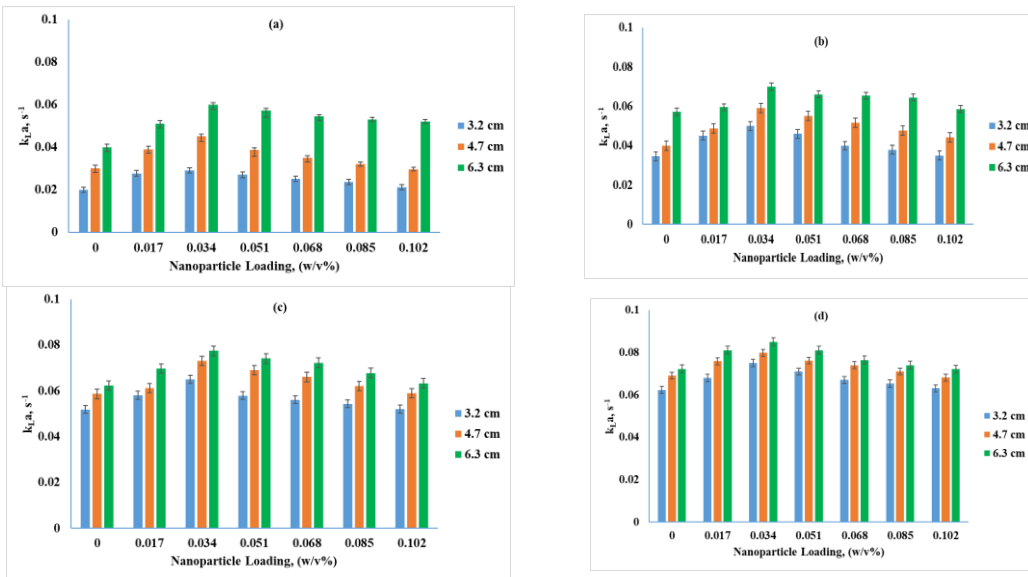


Fig.4.18 Effect of amplitude of pulsation on $k_{L,a}$ at different $\alpha\text{-Fe}_2\text{O}_3 - 43$ nanoparticle loading at varying frequency of pulsation of (a) $0.25 s^{-1}$ (b) $0.5 s^{-1}$, (c) $0.75 s^{-1}$ and (d) $1 s^{-1}$

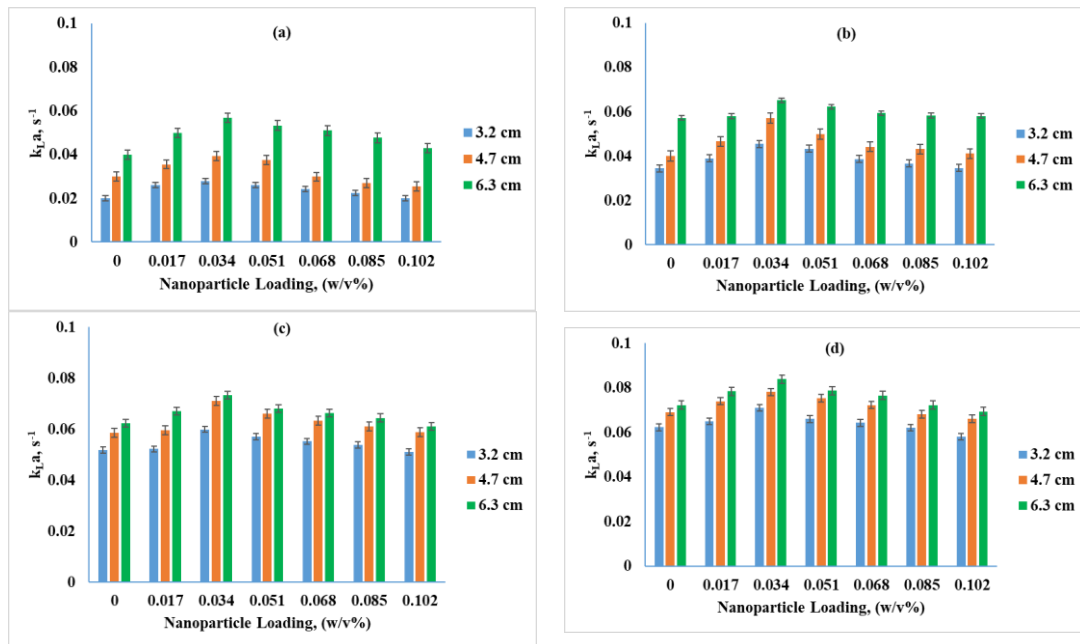


Fig.4.19 Effect of amplitude of pulsation on $k_{L,a}$ at different $\alpha\text{-Fe}_2\text{O}_3 - 76$ nanoparticle loading at varying frequency of pulsation of (a) 0.25 s^{-1} (b) 0.5 s^{-1} , (c) 0.75 s^{-1} and (d) 1 s^{-1}

Fig. 4.14 to 4.19 show that $k_{L,a}$ increases with increase in amplitude from 3.2cm to 6.3cm for TiO_2 , SiO_2 and $\alpha\text{-Fe}_2\text{O}_3$ nanofluids. As the amplitude increases the mixing efficiency increases leading to increased turbulence; the dispersion of gas bubbles becomes more effective, and the gas holdup increases. The volumetric oxygen mass transfer coefficient is influenced by the increased gas hold-up and prolonged residence time of bubbles due to the increased amplitude of pulsation (Oliveira and Ni 2001). The agitation intensity is a function of pulsing velocity ($A \times f$) which increases with the amplitude of pulsation. Supplying the higher energy into the g-l mixture results in smaller size bubbles and a larger portion of volume occupied by the gas in the mixture. Hence to achieve this higher mass transfer, sufficient energy should be provided to the mixture. According to Gagnon et al. (1998), the average power given to the fluid increases with the third power of pulsing velocity ($A \times f$)³. This higher power consumption leads to a higher gas holdup. The rate of bubble breakage will exceed the rate of bubble coalescence and a large number of smaller bubbles will be sustained in the gas-liquid mixture. Ultimately, the interfacial area will begin to increase (Skala and Veljkovic 1988; Dhanasekaran and Karunanithi 2010,) and the turbulence created in the column reduces the liquid film resistance and increases the volumetric oxygen mass transfer coefficient (Lounes and Thibault 1994). Thus, the increase in amplitude leads to enhanced gas-liquid mass transfer. Mohagheghian et al. (2018), reported

intensification of the volumetric oxygen mass transfer coefficient which they attributed to decreased Sauter mean diameter of the bubble which they observed when the amplitude and frequency of pulsation were increased. Table 4.4 shows the enhancement factors obtained at critical loading of TiO_2 , SiO_2 and $\alpha\text{-Fe}_2\text{O}_3$ nanoparticles with different amplitudes and the frequency of 0.25 s^{-1} and 1 s^{-1} , at an airflow rate of 1.8 LPM. As observed in the effect of amplitudes of pulsation on k_{LA} , when the amplitude of pulsation increases the k_{LA} value increases. However as presented in Table 4.4, the enhancement factor is the highest at the lower amplitude (3.2 cm) of pulsation at a critical loading with the lowest frequency of pulsation of 0.25 s^{-1} and an airflow rate of 1.8 LPM. Thus a better enhancement factor is observed at lower amplitude of pulsation, which implies that the effect of presence of nanofluids in enhancement is higher at lower amplitudes and frequency of pulsation. It may be inferred that the frequency and amplitude required to achieve a given mass transfer characteristics is lesser in the presence of nanofluid and thus energy saving is possible with nanofluids in comparison to the base fluid.

4.5 Effect of superficial air velocity (U_g) on k_{LA} in a pulsed plate column

The effect of superficial air velocity (U_g) on volumetric oxygen mass transfer coefficient (k_{LA}) were studied in the presence of TiO_2 -25 and TiO_2 -72; SiO_2 -12, and SiO_2 -24; $\alpha\text{-Fe}_2\text{O}_3$ -43 and $\alpha\text{-Fe}_2\text{O}_3$ -76 nanofluids, by conducting experiments at three different superficial air velocities of 0.011 m/s, 0.019 m/s and 0.029 m/s corresponding to the air flow rates of 1.8, 3.2 and 4.8 LPM respectively with different nanoparticle loading, different amplitude and frequency of pulsation. The effect of superficial air velocity on k_{LA} at different nanoparticle loading, amplitude, and frequency of pulsation are shown in the Fig 4.20 to 4.21; Fig. 4.22 to Fig.4.23; and Fig. 4.24 to Fig.4.25 for TiO_2 -25 and TiO_2 -72; SiO_2 -12, and SiO_2 -24; $\alpha\text{-Fe}_2\text{O}_3$ -43 and $\alpha\text{-Fe}_2\text{O}_3$ -76 nanofluids respectively.

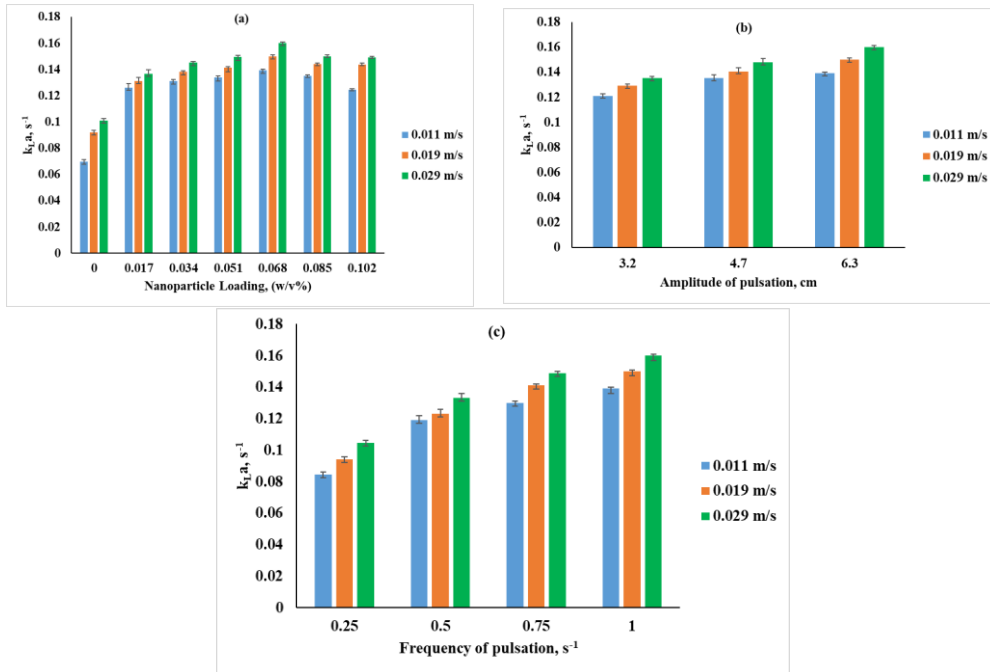


Fig 4.20 Effect of U_g on $k_{L,a}$ with TiO_2 – 25 nm nanofluid at varying
 (a) TiO_2 – 25 nm nanoparticle loading, at $A=6.3$ cm; $f = 1\text{ s}^{-1}$
 (b) amplitude of pulsation at $f = 1\text{ s}^{-1}$ and critical loading = 0.068 % w/v
 (c) frequency of pulsation at $A = 6.3$ cm and critical loading = 0.068 % w/v

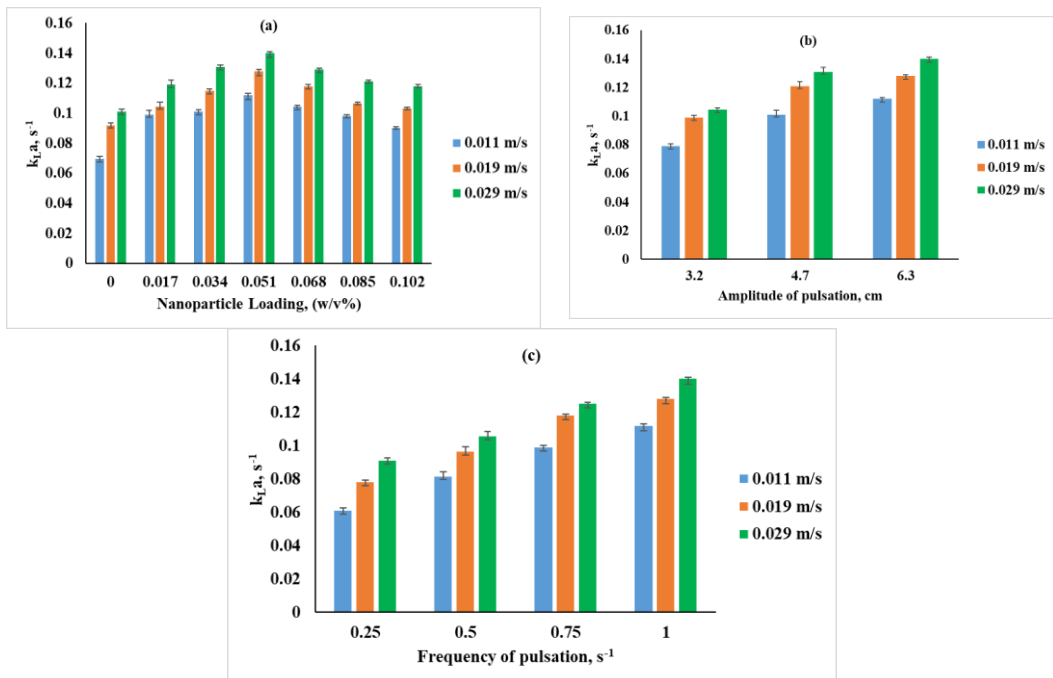


Fig 4.21 Effect of U_g on $k_{L,a}$ with TiO_2 – 72 nm nanofluid at varying
 (a) TiO_2 – 72 nm nanoparticle loading, at $A=6.3$ cm ; $f = 1\text{ s}^{-1}$
 (b) amplitude of pulsation at $f = 1\text{ s}^{-1}$ and critical loading = 0.051 % w/v
 (c) frequency of pulsation at $A = 6.3$ cm and critical loading = 0.051 % w/v

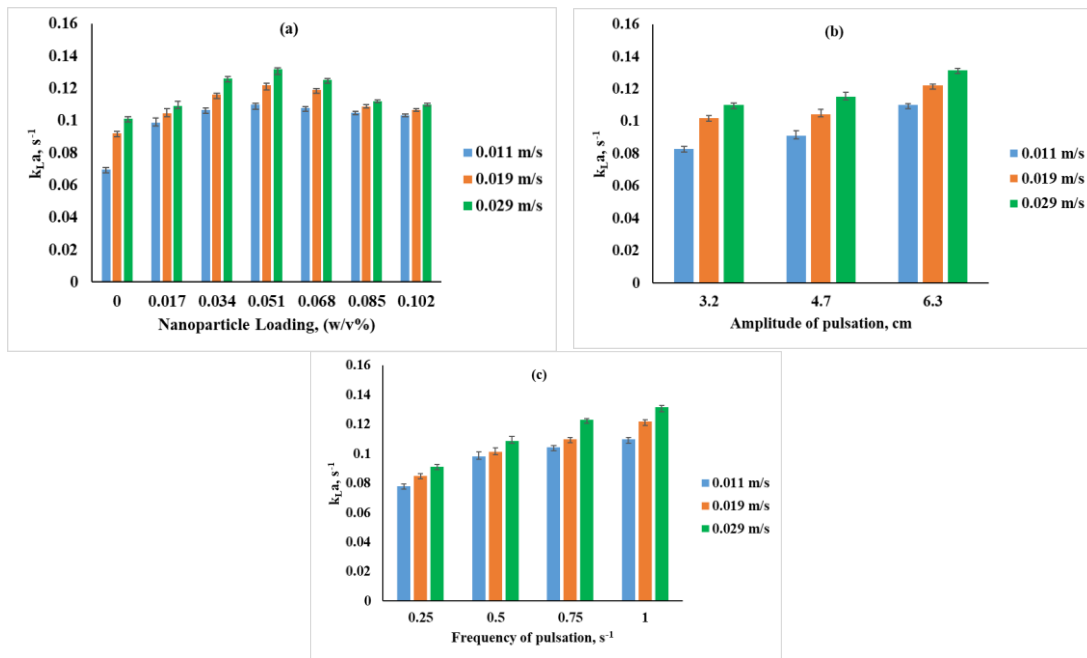


Fig 4.22 Effect of U_g on k_{LA} with $\text{SiO}_2 - 12 \text{ nm}$ nanofluid at varying
 (a) $\text{SiO}_2 - 12 \text{ nm}$ nanoparticle loading, at $A=6.3 \text{ cm}$; $f = 1 \text{ s}^{-1}$
 (b) amplitude of pulsation at $f = 1 \text{ s}^{-1}$ and critical loading = 0.051 \% w/v
 (c) frequency of pulsation at $A = 6.3 \text{ cm}$ and critical loading = 0.051 \% w/v

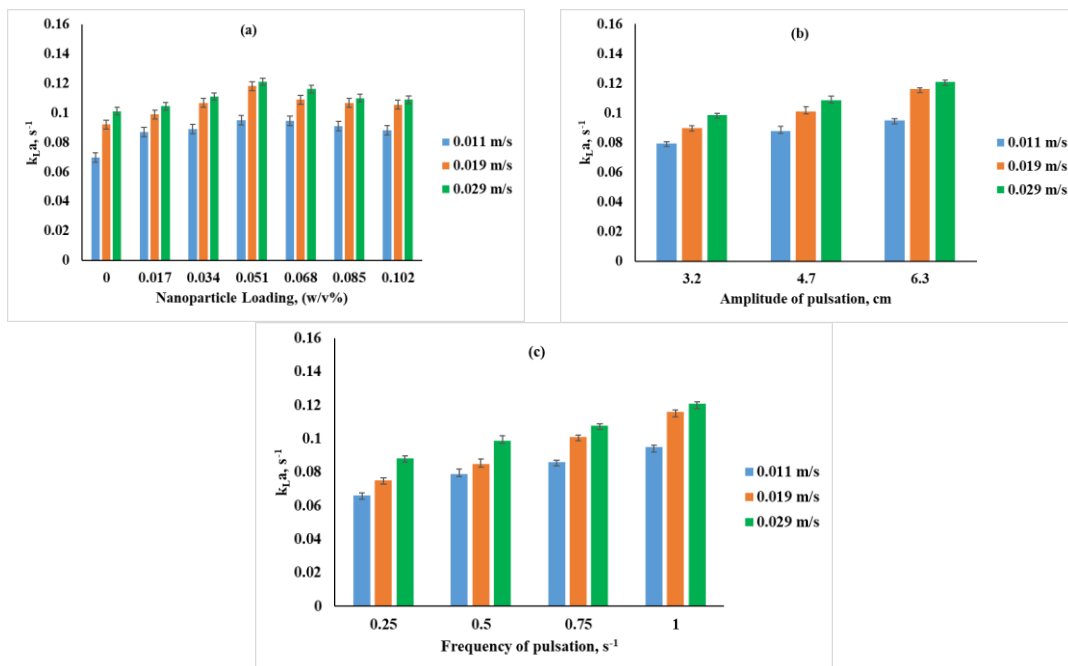


Fig 4.23 Effect of U_g on k_{LA} with $\text{SiO}_2 - 24 \text{ nm}$ nanofluid at varying
 (a) $\text{SiO}_2 - 24 \text{ nm}$ nanoparticle loading, at $A=6.3 \text{ cm}$; $f = 1 \text{ s}^{-1}$
 (b) amplitude of pulsation at $f = 1 \text{ s}^{-1}$ and critical loading = 0.051 \% w/v
 (c) frequency of pulsation at $A = 6.3 \text{ cm}$ and critical loading = 0.051 \% w/v

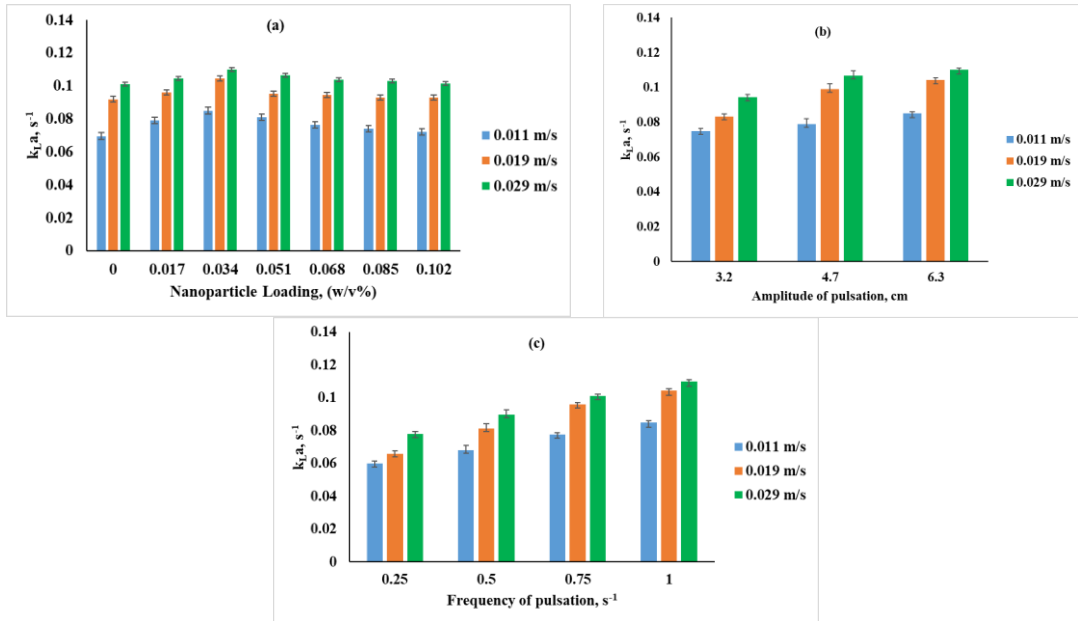


Fig 4.24 Effect of U_g on k_{LA} with α - Fe_2O_3 – 43 nm nanofluid at varying (a) α - Fe_2O_3 – 43 nm nanoparticle loading, at $A=6.3$ cm ; $f = 1$ s^{-1} (b) amplitude of pulsation at $f = 1$ s^{-1} and critical loading = 0.034 % w/v (c) frequency of pulsation at $A = 6.3$ cm and critical loading = 0.034 % w/v

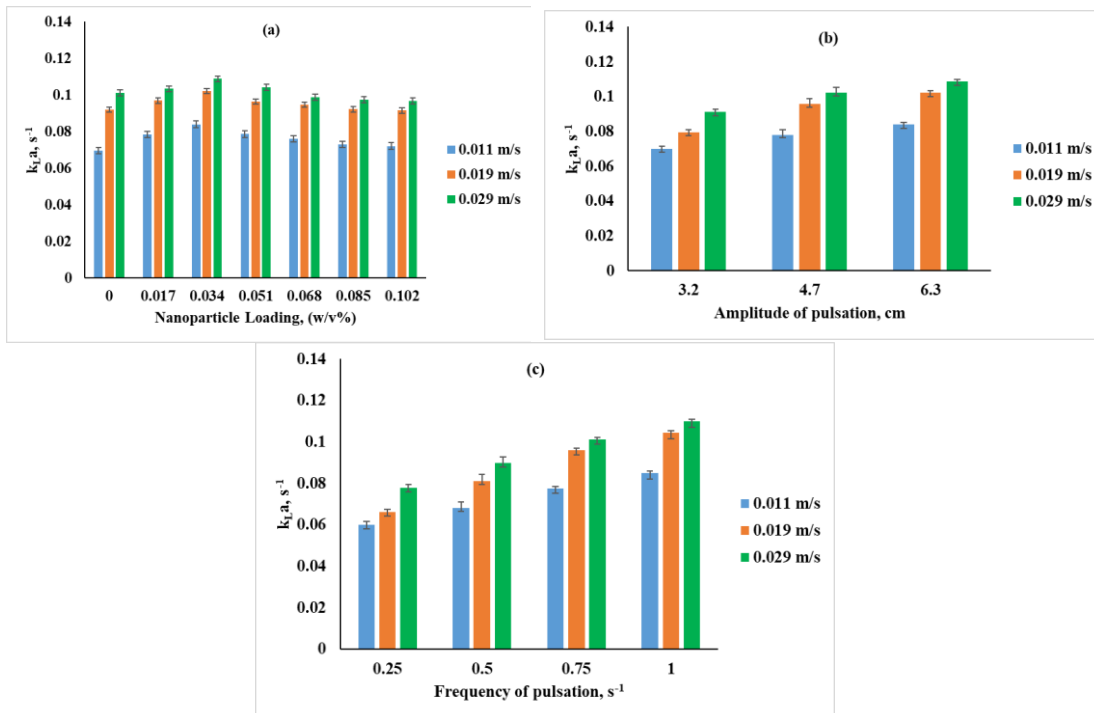


Fig 4.25 Effect of U_g on k_{LA} with α - Fe_2O_3 – 76 nm nanofluid at varying (a) α - Fe_2O_3 – 76 nm nanoparticle loading, at $A=6.3$ cm ; $f = 1$ s^{-1} (b) amplitude of pulsation at $f = 1$ s^{-1} and critical loading = 0.034 % w/v (c) frequency of pulsation at $A = 6.3$ cm and critical loading = 0.034 % w/v

As observed in Fig. 4.20 to 4.25, the volumetric oxygen mass transfer coefficient increased with an increase in U_g under all the operating conditions. The increasing trend is mainly due to the higher mixing and turbulence at higher air velocities to decrease the bubble mean diameter and increase in interfacial area, a (Dhanasekaran and Karunanithi 2010; Jamialahmadi and Müüller-Steinhagen 1993). An increase in superficial air velocity helps to enhance the turbulence. The increased turbulence at higher velocities decreases the stagnant liquid film thickness around the gas bubble (Dhanasekaran and Karunanithi 2012; Sundaresan and Varma 1990) and the liquid side mass transfer resistance is decreased which increases the k_L value. Thus the net effect of increase in k_L and interfacial area 'a' with an increase in superficial air velocities results in higher values of $k_{L,a}$ (Ghani 2012; Manjrekar et al. 2017).

As observed in the plots in Fig. 4.20 to 4.25(a), the influence of U_g is very high in the absence of nanoparticles as compared to that with nanofluids. When the U_g was increased from 0.011 to 0.029 m/s, the $k_{L,a}$ increased by 47% in the absence of nanoparticles, whereas the increase was 20%, 15%, and 42% in presence of nanoparticles under critical loading condition with TiO_2 -25, SiO_2 -12, $\alpha-Fe_2O_3$ -43 nanofluids. Thus, the $k_{L,a}$ increase caused by increasing U_g in the presence of nanofluid, is much lower in comparison with that in base fluid (in the absence of nanoparticles). These results imply that the effect of U_g is very high in the absence of nanoparticles. Though, in the nanofluids, U_g positively influences $k_{L,a}$, the effect is not as high as that in the base fluid. In the absence of nanoparticles, the influence of U_g in bringing about agitation and mixing, leading to bubble breakup and turbulence is very high. When the nanoparticles are present, the effect of nanoparticles may play a dominant role in imparting the agitation and turbulence leading to bubble breakup, as compared to that caused by an increase in U_g . It means that higher $k_{L,a}$ values can be achieved even at lower U_g in the presence of nanoparticles. It is observed that at very high loadings the influence of higher U_g on increasing the $k_{L,a}$ is comparatively lower. A combination of higher gas velocities and high nanoparticle loading leads to an increase in bubble coalescence rate because of the increased probability of bubble-bubble interaction and increased suspension viscosity (Baz-Rodríguez et al. 2014; Mena et al. 2011). It results in a decrease in the interfacial area leading to the reduction of $k_{L,a}$. The effect of increase in the turbulence and agitation due to an increase in U_g causing higher k_L values is countered by a decrease in interfacial area 'a' due to the bubble coalescence at higher

loading. Thus the contribution of superficial velocities on increasing the values of k_{LA} diminishes at higher loadings. Shah et al. (1982) have also mentioned that the effect of solid fractions on k_{LA} depends on the gas velocities. Mena et al. (2011), have observed a negative influence of higher gas velocities on k_{LA} when solid fractions are high.

As observed in the plots in Fig. 4.20 to 4.25 (b), the influence of U_g is high at the lowest amplitude of pulsation. When the U_g was increased from 0.011 to 0.029 m/s, the k_{LA} increased by 17%, 33%, and 26% at the lowest amplitude of pulsation of 3.2 cm with TiO_2 -25, SiO_2 , -12, α - Fe_2O_3 -43 nanofluids respectively, whereas the increase in k_{LA} by 15%, 18% and 22% was achieved when U_g was increased by a similar range at the highest amplitude of pulsation of 6.3 cm. Thus, the k_{LA} increase caused by increasing U_g in the lower amplitude is higher in comparison with that at higher amplitudes. This implies that, at the lower amplitude of pulsation, the effect of U_g in increasing the gas hold up and interfacial area is prominently affecting the increase in k_{LA} , whereas at the higher amplitude of pulsation the increase in k_{LA} caused due to the increased mixing efficiency and prolonged residence time of bubbles which increases the gas hold up becomes more dominant than the effect of U_g on increase in k_{LA} . Thus, the effect of U_g on k_{LA} is seen more prominently at the lower amplitudes as compared to that at higher amplitudes.

Similarly, as observed in the plots in Fig. 4.20 to 4.25 (c), the influence of U_g is higher at lower frequency of pulsation as compared to that with the higher frequency. When the U_g increased from 0.011 to 0.029 m/s at frequency of pulsation of 0.25 s^{-1} , the k_{LA} increased by 23%, 28% and 31% with TiO_2 -25, SiO_2 , -12, α - Fe_2O_3 -43 nanofluids respectively, whereas at frequency of 1 s^{-1} under similar range of increase in U_g the k_{LA} increased by 15%, 19% and 29% with TiO_2 -25, SiO_2 , -12, α - Fe_2O_3 -43 nanofluids respectively. The increase in frequency leads to increase in bubble breakup resulting from higher turbulence along with the increase in gas hold up. This effect outperforms the effect of U_g on k_{LA} at higher frequencies. The contribution of U_g towards increasing the turbulence and increasing k_{LA} becomes lesser at high frequencies, whereas the superficial air velocity has a dominating effect on k_{LA} than the frequency at lower frequencies.

Superficial air velocity and pulsing parameters such as frequency and amplitude of pulsation were found to mutually affect k_{LA} . The extent of rise in k_{LA} with pulsing

parameters in comparison to that with increase in U_g depend on the extent of increase of gas hold up, interfacial area and turbulence. Dhanasekaran and Karunanithi (2012); Sundaresan and Varma (1990) and Yang et al. (2001) have reported that, at low levels of agitation, increase in agitation decreases the hold up of gas in the column and at particular agitation level the gas hold up in the column is the least. This is the minimum gas hold up region or transition region. On increasing the agitation intensity, the gas hold up increases (Rama Rao and Baird 1986; Skala and Veljković 1988). Such trends have been observed in counter-current (Rama Rao and Baird 1988), cocurrent (Yang et al. 1986) and semi batch (Lounes and Thibault 1994) reciprocating columns with gas-liquid systems. The frequency of pulsation along with superficial gas velocity, mutually affect the agitation intensity in the column and the transition region is dependent on both the parameters. As reported in literature at agitation above the transition region, the increase in interfacial area caused due to bubble break up along with increase in gas hold up caused at very high frequencies together lead to enhanced effect of U_g on k_{LA} (Skala and Veljković 1988). Thus in the present study the k_{LA} has increased with the increase in superficial velocities at all the pulsing conditions. So, the effect of higher gas hold-up, higher interfacial area caused by bubble break up due to turbulence along with higher turbulence effect caused by increase in frequency and amplitudes of pulsation has caused an increase in k_{LA} with rise in U_g .

Table 4.5 presents the enhancement factors obtained with TiO_2 -25 and TiO_2 -72; SiO_2 , -12, and SiO_2 , -24; $\alpha-Fe_2O_3$ -43 and $\alpha-Fe_2O_3$ -76 nanofluids at the respective critical loading conditions at the lowest frequency of pulsation (0.25 s^{-1}) at varying superficial air velocities 0.01m/s, 0.019m/s and 0.029m/s, at the amplitude of pulsation of 3.2cm. The maximum enhancement factor with reference to the base fluid is observed at a superficial air velocity 0.011 m/s under these conditions. The maximum enhancement factors of 4.37, 2.30 and 1.65 could be achieved with TiO_2 -25, SiO_2 , -12, $\alpha-Fe_2O_3$ -43 nanofluids respectively at a superficial air velocity of 0.011m/s. This shows that the enhancement effect of nanofluid on k_{LA} is more pronounced at the lowest superficial air velocity. It suggests that if these nanofluids are used in the PPC, lower superficial air velocity may be sufficient to obtain the appropriate enhancement. Therefore, improved oxygen mass transfer properties can be accomplished using nanofluids in the pulsed plate column while also reducing the fluid power.

Table 4.5: Maximum Enhancement factor obtained at critical loading of TiO₂, SiO₂ and α -Fe₂O₃ nanoparticles with different superficial air velocity at amplitude of pulsation of 3.2 cm and at the lowest frequency of 0.25 s⁻¹.

Nanofluid Type	Nanoparticle critical loading, Φ (% w/v)	U_g , m/s			
		Nanoparticle size, nm	0.011	0.019	0.029
TiO ₂	0.068	25	4.37	2.46	1.97
	0.051	72	2.39	1.76	1.50
SiO ₂	0.051	12	2.30	1.72	1.57
		24	2.17	1.35	1.33
α -Fe ₂ O ₃	0.034	43	1.65	1.32	1.24
		76	1.61	1.25	1.14

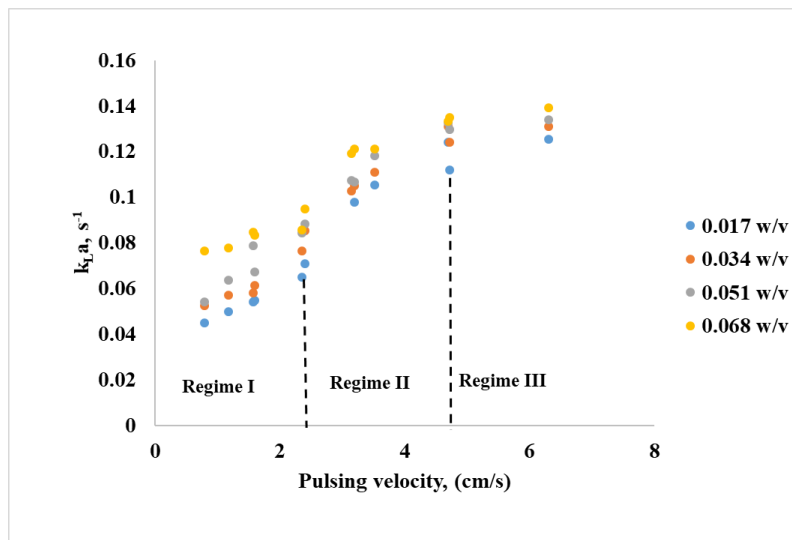
4.6 Effect of the pulsing velocity on k_{LA} in the presence of nanofluids

The effect of pulsing velocity ($A \times f$) on k_{LA} in PPC in association with different nanoparticle loading was experimentally investigated. Pulsing velocity or pulsing intensity ($A \times f$), is the product of amplitude (A) and frequency (f) of pulsation (Akhgar et al. 2017; Lounes and Thibault 1994; Panahinia et al. 2017). The experimental findings have shown that there is a combined effect of ($A \times f$) and nanoparticle loading (Φ) in the enhancement or decrement of the k_{LA} in PPC. The effect of pulsing velocity at different nanoparticle loadings and different nanoparticle sizes at a constant airflow rate of 1.8 LPM is shown in Figure 4.26 to 4.31.

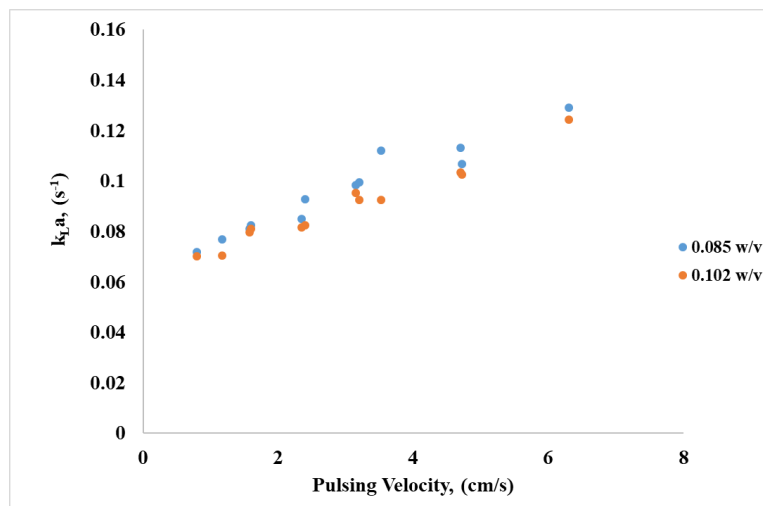
As observed from Figure 4.26 to 4.31, the volumetric oxygen mass transfer coefficient increases with the increase in the pulsing velocity. However, the nature of the increase is regime-dependent.

Many researchers have reported through experimental findings that the mass transfer performance enhances with an increase in the pulsing velocity (Bahmanyar et al. 2014; Khooshechin et al. 2017; Mirmohammadi et al. 2019; Sen et al. 2018). It is found that as the pulsing velocity increases the degree of turbulence effect transmitted in the column is more. The mean bubble diameter is affected by the pulsing velocity, as the

additional rigorous shear forces that are created by the increased pulsing velocity cause the collapse of the bigger bubble into a smaller hence increasing the interfacial area which increases k_{LA} (Ardestani et al. 2021; Dhanasekaran and Karunanithi 2010; Lade et al. 2014; Panahinia et al. 2017; Rahbar et al. 2011; Shetty and Srinikethan 2010; Sincuba et al. 2017; VeljkoviC and Skala 1986).



(a)



(b)

Fig.4.26 Effect of $(A \times f)$ on k_{LA} as a function of $TiO_2 - 25$ nanoparticle loadings at an airflow rate of 1.8 LPM. (a) $\Phi \leq \Phi_L$ (b) $\Phi > \Phi_L$

The effect of pulsing velocity on k_{LA} with TiO_2-25 nanofluid at different nanoparticle loading is shown in Fig 4.26. From Fig 4.26 (a) it is observed that, at $\Phi \leq 0.068$ % w/v (Φ_L), the effect of $(A \times f)$ on k_{LA} falls into three regimes: (i) the first regime (Regime I) of $(A \times f) \leq 2.35$, wherein a smaller increase in k_{LA} with increase in $(A \times f)$ is observed; (ii) the second regime (Regime II) of $2.35 < (A \times f) \leq 4.7$, wherein k_{LA} increases sharply with increase in $(A \times f)$ and (iii) a third regime (Regime III) of $(A \times f) \geq 4.7$ at which the variation in k_{LA} with $(A \times f)$ is negligible. Based on the mixing intensity, three separate flow regimes, namely mixer-settler, dispersion, and emulsion regimes, may exist in the operation of a pulsed column. The mixer-settler regime is a regime of low mixing, and discrete zones are formed in the column. Any one of phases may accumulate in regions above or below each of the plates and discontinuity is produced in the column. The dispersion regime follows the mixer-settler regime and the discontinuity is avoided in this regime. This regime is characterized by a non-uniform bubble size distribution and no bubble coalescence occurs (Khooshechin et al. 2017). At higher pulsing velocities good mixing occurs and the external energy dissipation is even throughout the column (Lounes and Thibault 1994; Vasić et al. 2007). The pulsing velocities in the dispersion regime prevent the accumulation of bubbles either above or below each perforated plate as turbulence stresses dominate over the bubble coalescence tendency (Sundaresan and Varma 1990). As reported by Yadav and Patwardhan (Yadav and Patwardhan 2008) and (Akhgar et al. 2017), dispersion regime is characterized by formation of bubbles with non-uniform size distribution. With increase in pulsing velocity, the bubble size decreases and hold-up starts increasing in this regime favoring gas-liquid mass transfer. With an increase in the pulsing velocity, the bubble size decreases and thus an emulsion is formed. Emulsion regime exists due to operation under highly intense mixing conditions (Dhanasekaran and Karunanithi 2012) and gas bubbles are uniformly distributed in the column. A relatively sharp decrease in bubble diameter with increase in pulsing velocity occurs in the mixer-settler regime than in the dispersion regime. The effect of pulsing velocity on mean bubble diameter is more pronounced in the mixer-settler regime than in the dispersion regime (Usman et al. 2009). The gas hold-up decreases sharply in the mixer settler regime, reaches a minimum where transition occurs from mixer settler to dispersion regime and then increases with further increase in pulsing velocity (Akhgar et al. 2017). The increase in gas holdup with increasing pulsing velocity is smaller for low pulsing velocities, and sharper for higher pulsing velocities (Nikolić et al. 2005). Increase in

gas hold-up increases the residence time of the bubbles in the column (Nikolić et al. 2005) and thus increases k_{La} . In the mixer-settler regime, the oxygen mass transfer depends mainly on aeration rather than pulsation, as the pulsing velocity is lower. In this regime pulsed plate column behaves like a bubble column. At high pulsation intensities, the breakage of gas bubbles is more pronounced and the oxygen transfer becomes intense. Further increase in pulse velocity, increases the inertial and shear forces on bubbles. These forces enhance bubble breakage. Thus, an emulsion is formed (Yadav and Patwardhan 2008). This regime occurs at high pulse velocity. In the homogeneous dispersion regime k_{La} is primarily influenced by pulsation (Skala and Veljković 1988b).

In the emulsion region, due to high pulsing velocities the gas hold up increases tremendously causing the bubbles to coalesce rapidly and the dispersion grows strongly nonhomogeneous with the motion of larger bubbles resembling the mixer-settler regime and that of smaller bubbles resembling the emulsion regime (Rathilal 2010). In Regime III, the increase in k_{La} with the increase in pulsing velocity is marginal. This is the emulsion regime. This zone comes up with the higher turbulent energy that induces the coalescence of bubbles or it may produce many small bubbles that behave as rigid spheres (Torab-Mostaedi et al. 2010), which will hinder the internal circulation of nanoparticles and bubbles through the column. It is also important to be noted that the higher $A \times f$ intensifies the axial mixing which negatively influences the mass transfer efficiency (Jiao et al. 2013). A higher pulsing velocity increases the agitation rate which results in a lower bubble diameter and larger gas holdup which increase the interfacial area. However, the higher pulsation intensity leads to a reduction in the mass transfer coefficient as the bubbles become smaller and more rigid (Torab-Mostaedi et al. 2012). Bahmanyar et al. (2014), explained that the formation of smaller size bubbles at higher pulsing velocities may lead them to behave as rigid spheres and the molecular diffusion governs the mass transfer rate. Towards the higher pulsing velocity in Regime III, the effect of increase in mass transfer coefficient caused due to turbulence may be countered by decrease/ no change in the interfacial area due to the coalescence of bubbles/formation of small rigid bubbles, thus leading to only a marginal variation in k_{La} with increase in pulsing velocity in Regime III.

The first regime in k_{LA} vs $A \times f$ signifies mixer settler regime, wherein the decrease in bubble diameter increases the interfacial area to enhance k_{LA} , but the decrease in gas holdup counters this increase, thus leading to a slow increase in k_{LA} with pulsing velocity in mixer-settler region. In the second regime, which is the dispersion regime, both increases in gas hold-up and decreases in bubble diameter with increasing pulsing velocity favors the sharp increase in k_{LA} . The third regime of the emulsion regime, in which the effect of coalescence of bubbles or the formation of more rigid bubbles may counter the effect of increase in turbulence created by higher pulsing velocity thus leading to only marginal variation in k_{LA} .

However, at $\Phi > 0.068$ % w/v, the plot of k_{LA} vs $(A \times f)$ in Figure 4.26 (b) seems to follow a single trend in the entire range of $(A \times f)$. These results clearly indicate that $A \times f$ and Φ have an interacting effect on k_{LA} . The sharp increase in k_{LA} is observed with increase in pulsing velocity, showing that only dispersion regime exists in the range of operation when the nanoparticle loading is above the critical loading. As the nanoparticle loading increases beyond 0.068 % w/v, mixer settler regime or emulsion regime is not observed in the range of operation of the pulsed plate column. Due to increase in the nanoparticle loading, the shear rate may be higher causing higher turbulence which leads to break up of bubbles into much smaller size and increasing the interfacial area along with increase in mixing and turbulence intensity due to the presence of more number of particles enhancing the mass transfer coefficient. The presence of nanoparticles at higher loading condition, has not only widened the dispersion regime, but also has lowered the $A \times f$ value for the onset of dispersion regime and has increased that for the onset of emulsion regime. Though the nanofluid properties such as dynamic viscosity and surface tension of the nanofluids increase with the increase in nanoparticles loading, which may tend to reduce the gas-liquid mass transfer either due to agglomeration effect or higher viscosity effect, the turbulence effect appears to dominate over the the effect of properties of nanofluids even at higher nanoparticle loading. Thus, only dispersion regime is being observed in the entire range of pulsing velocities at higher loading and k_{LA} increases with increase in pulsing velocities. The emulsion regime is not formed in the range of operation, which may be due to prevention of coalescence of bubbles owing to the presence of large number of nanoparticles enhancing the turbulent circulating effect in the liquid and higher level of mixing.

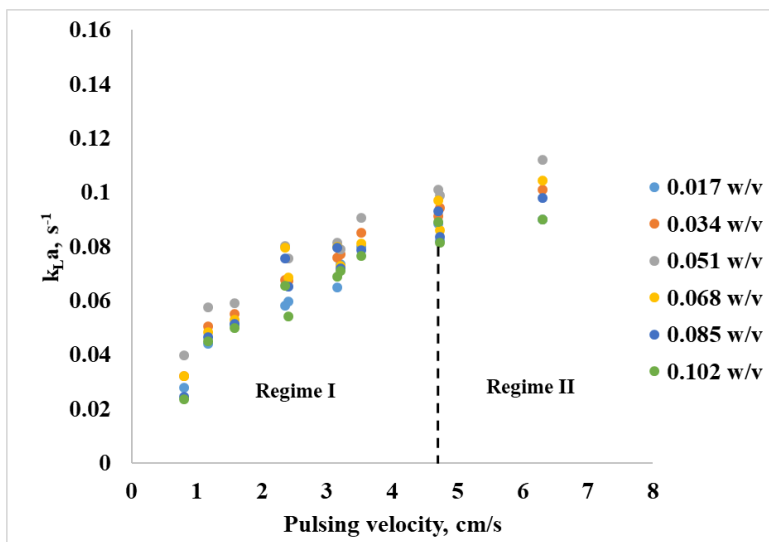


Fig.4.27 Effect of $(A \times f)$ on $k_{L,a}$ as a function of TiO_2-72 nanoparticle loadings at an airflow rate of 1.8 LPM.

The effect of pulsing velocity on $k_{L,a}$ with TiO_2-72 nanofluid at different nanoparticle loading is shown in Fig 4.27. From Fig 4.27 it is observed that the $k_{L,a}$ increased with increase in pulsing velocity at different nanoparticle loading and the effect of $(A \times f)$ on $k_{L,a}$ falls into two regimes: the first regime (Regime I) of $(A \times f) < 4.7$, wherein $k_{L,a}$ increases sharply with increase in pulsing velocity and the second regime (Regime II) of $A \times f \geq 4.7$ at which the variation in $k_{L,a}$ with $(A \times f)$ is negligibly small. In the Regime I, it can be observed that as the pulsing velocity increases, $k_{L,a}$ increases sharply indicating that the dispersion regime occurs till the pulsing velocity is 4.7 cm/s (Roosbahani et al. 2015). This regime may be considered as dispersion regime, where in uniform distribution of nanoparticles takes place gradually and helps in breaking up of bubbles to increase the interfacial area and thus increasing $k_{L,a}$. As the pulsing velocity increases in Regime II, the increase in $k_{L,a}$ with the increase in pulsing velocity is marginal. This is the emulsion regime.

These results show that, both the nanoparticles loading and size may dictate the occurrence of hydrodynamic regimes and the limit of pulsing velocity for transition from one regime to another.

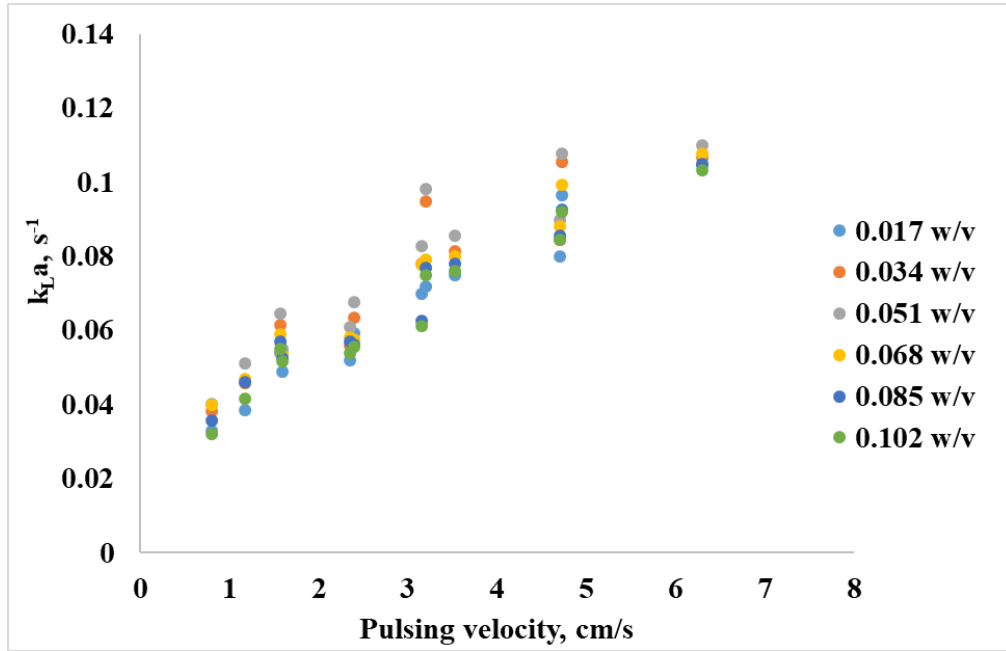


Fig.4.28 Effect of $(A \times f)$ on k_{LA} as a function of SiO_2 -12 nanoparticle loadings at an airflow rate of 1.8 LPM.

The effect of pulsing velocity on k_{LA} with SiO_2 -12 nanofluid at different nanoparticle loading is shown in Fig 4.28. From Fig 4.28 it is observed that the k_{LA} is increasing with increasing pulsing velocity at different nanoparticle loading and the effect of $(A \times f)$ on k_{LA} falls into only one regime in the entire range of operation: In the entire range, k_{LA} increases sharply with increase in $(A \times f)$, indicating the existence of only the dispersion regime with SiO_2 -12 nanofluid.

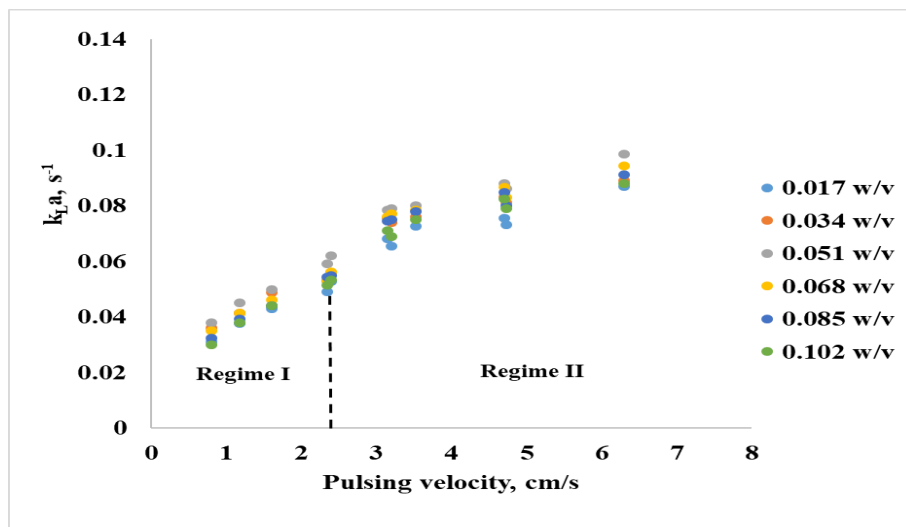


Fig.4.29 Effect of $(A \times f)$ on k_{LA} as a function of SiO_2 -24 nanoparticle loadings at an airflow rate of 1.8 LPM.

The effect of pulsing velocity on k_{LA} with SiO_2 -24 nanofluid at different nanoparticle loading is shown in Fig 4.29. From Fig 4.29 it is observed that the k_{LA} is increasing with increasing pulsing velocity at different nanoparticle loading and the effect of $(A \times f)$ on k_{LA} falls into two regimes: the first regime (Regime I) of lower $(A \times f) < 3.2$, wherein a considerable increase in k_{LA} with increase in $(A \times f)$ is observed showing the presence of dispersion regime; the second regime (Regime II) of $3.2 \leq (A \times f) \leq 6.3$, wherein k_{LA} increases marginally with increase in $(A \times f)$, indicating the existence of emulsion regime at higher pulsing velocities. Roozbahani et al. (2015) demonstrated the effect of pulse strength on static and dynamic holdup for the mass transfer from the continuous phase to the dispersed phase. Their analysis revealed a decrease in a static holdup and an increase in dynamic hold up with the increase in pulsing velocity in the dispersion regimes. The presence of only two regimes, viz. dispersion and emulsion regimes in vertically pulsed packed column have been reported by Khooshechin et al. (2017). The present study reports the presence of two regimes with SiO_2 -24 nanofluid, whereas only one regime with SiO_2 -12 nanofluid. A wider dispersion regime is obtained and emulsion regime formation is prevented with smaller size particles, whereas larger size particles tend to form emulsion regime with SiO_2 nanofluids.

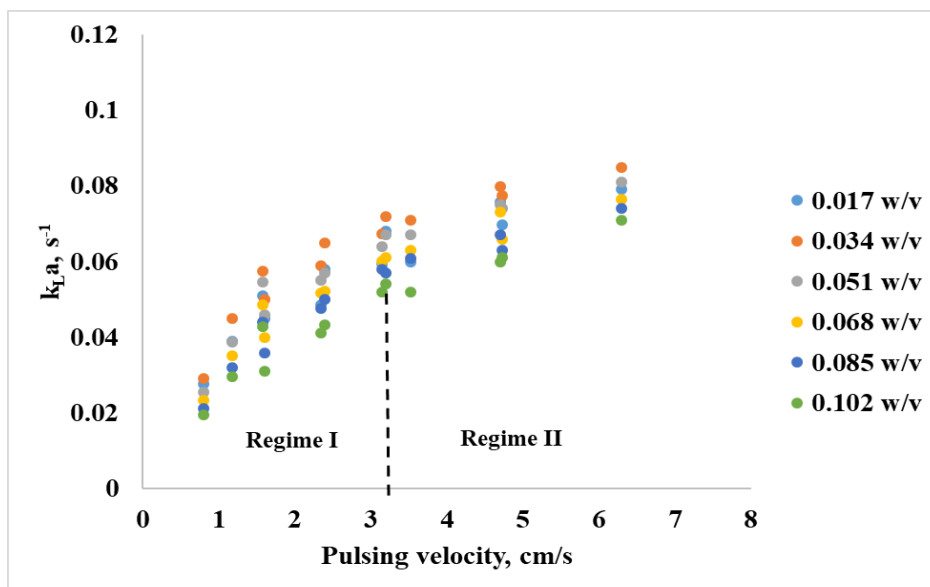


Fig.4.30 Effect of $(A \times f)$ on k_{LA} as a function of $\alpha\text{-Fe}_2\text{O}_3$ – 43 nanoparticle loadings at an airflow rate of 1.8 LPM.

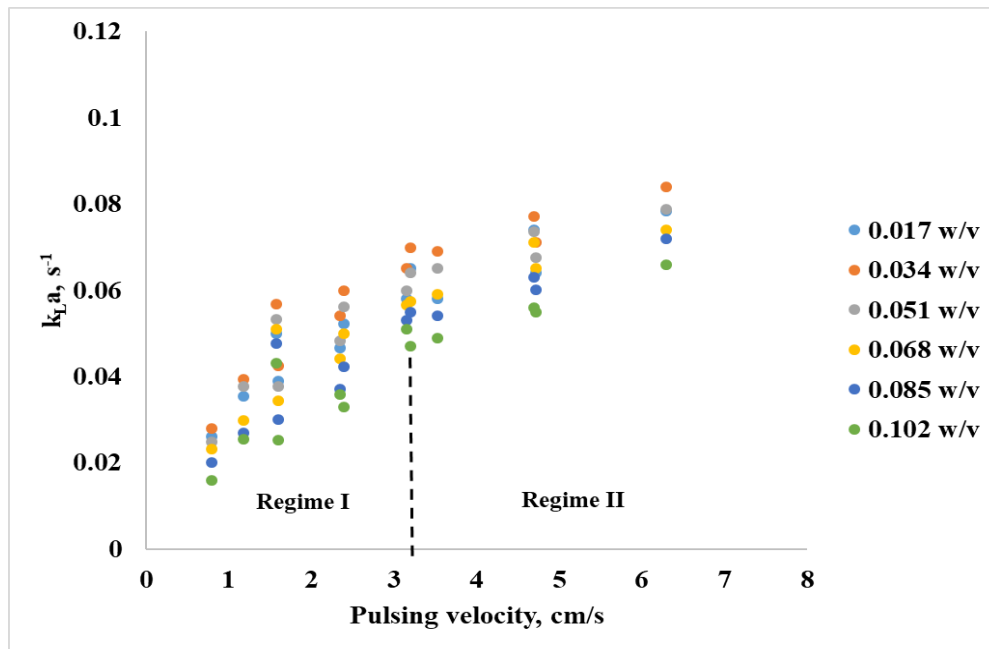


Fig.4.31 Effect of $(A \times f)$ on k_{LA} as a function of $\alpha\text{-Fe}_2\text{O}_3$ -76 nanoparticle loadings at an airflow rate of 1.8 LPM.

The effect of pulsing velocity on k_{LA} with $\alpha\text{-Fe}_2\text{O}_3$ -43 and $\alpha\text{-Fe}_2\text{O}_3$ -76 nanofluid at different nanoparticle loading is shown in Fig 4.30 and 4.31 respectively. From Fig 4.30 and 4.31 it is observed that the k_{LA} is increasing with increasing pulsing velocity at different nanoparticle loading and the effect of $(A \times f)$ on k_{LA} is found to be linear for the entire range of $(A \times f)$. Two regimes are observed with $\alpha\text{-Fe}_2\text{O}_3$ nanofluids irrespective of size of nanoparticles and the nanoparticles loading. The first regime (Regime I) of lower $(A \times f) < 3.2$, is the dispersion regime wherein a k_{LA} increases sharply with increase in $(A \times f)$; the second regime (Regime II) of $3.2 \leq (A \times f) \leq 6.3$, wherein k_{LA} increases marginally with increase in $(A \times f)$, indicating the existence of emulsion regime at higher pulsing velocities.

It is noticed that the mass transfer coefficient increases throughout the entire range of pulsing velocity. An increase in gas hold up and higher interfacial area at high pulsing velocities (Sen et al. 2018; Somkuwar et al. 2014; Torab-Mostaedi et al. 2012) due to bubble breakage leads to dispersion of bubbles and a sharp increase in the k_{LA} in the dispersion regime. The onset of emulsion regime occurs at $A \times f$ of 3.2 cm/s with $\alpha\text{-Fe}_2\text{O}_3$ -43 and $\alpha\text{-Fe}_2\text{O}_3$ -76 nanofluids.

The results on the effect of pulsing velocity on k_{LA} in the presence of nanofluids, show that one or more regimes may occur depending on the type of nanofluid, size of the nanoparticle and the nanoparticle loading. The effect of pulsing velocity on k_{LA} is large

in the dispersion regime and increasing the pulsing velocity in the dispersion regime favours the gas-liquid mass transfer. In the mixer-settler or emulsion regimes the increase in mass transfer coefficient with increasing pulsing velocity is only marginal. So, the operation of pulsed plate column in dispersion regime is recommended with the nanofluids. The pulsing velocity at which regime transition occurs has been found to be dependent on the type of nanofluid, size of the nanoparticles and the nanoparticle loading.

4.7 Effect of size of nanoparticles on k_{LA} in pulsed plate column.

The effect of size of TiO_2 , SiO_2 , and $\alpha-Fe_2O_3$ nanoparticles on k_{LA} in pulsed plate column was studied by conducting experiments with TiO_2 , SiO_2 , and $\alpha-Fe_2O_3$ nanofluids containing nanoparticles of average particle size of 25 nm, 72 nm; 12 nm, 24 nm and 43 nm ,76 nm respectively at different operating conditions. The effect of TiO_2 , SiO_2 , and $\alpha-Fe_2O_3$ nanoparticle size as a function of nanoparticle loadings on k_{LA} at various frequencies of pulsation of 0.25, 0.5, 0.75 and 1 s^{-1} and amplitude of pulsation of 6.3 cm with an air flow rate of 1.8 LPM are shown in Fig. 4.32 to 4.34 respectively.

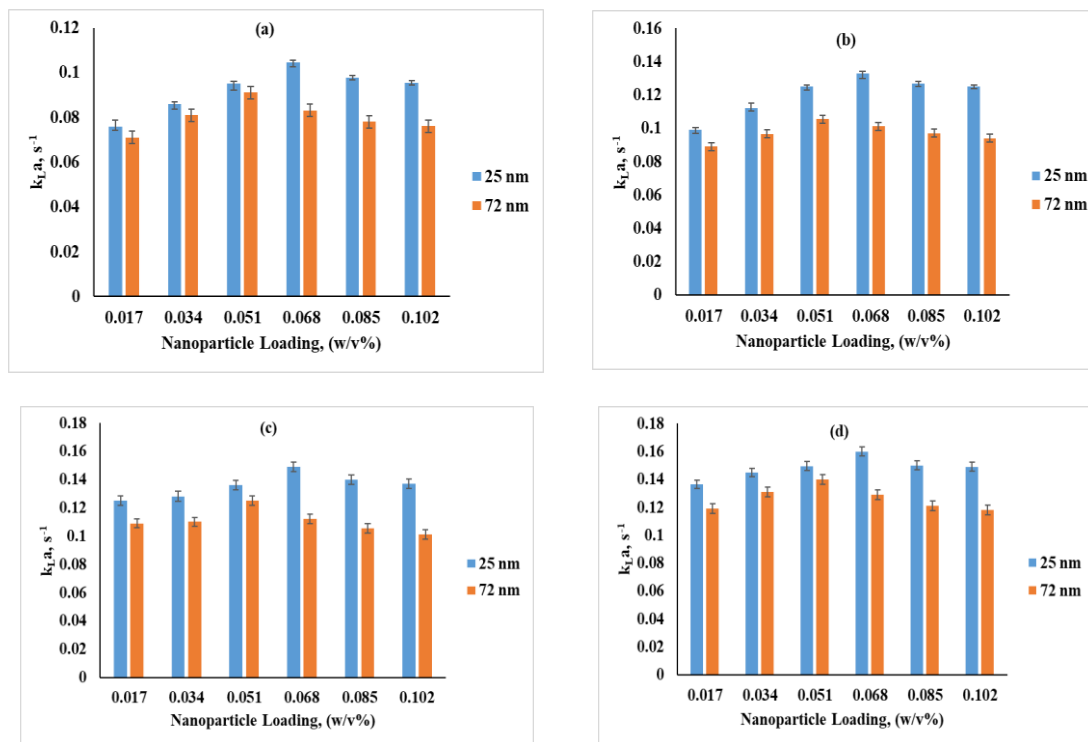


Fig. 4.32 Effect of nanoparticle size on k_{LA} at different TiO_2 nanoparticle loading and at $A = 6.3$ cm at different frequency of pulsation (a) 0.25 s^{-1} (b) 0.5 s^{-1} (c) 0.75 s^{-1} and (d) 1 s^{-1}

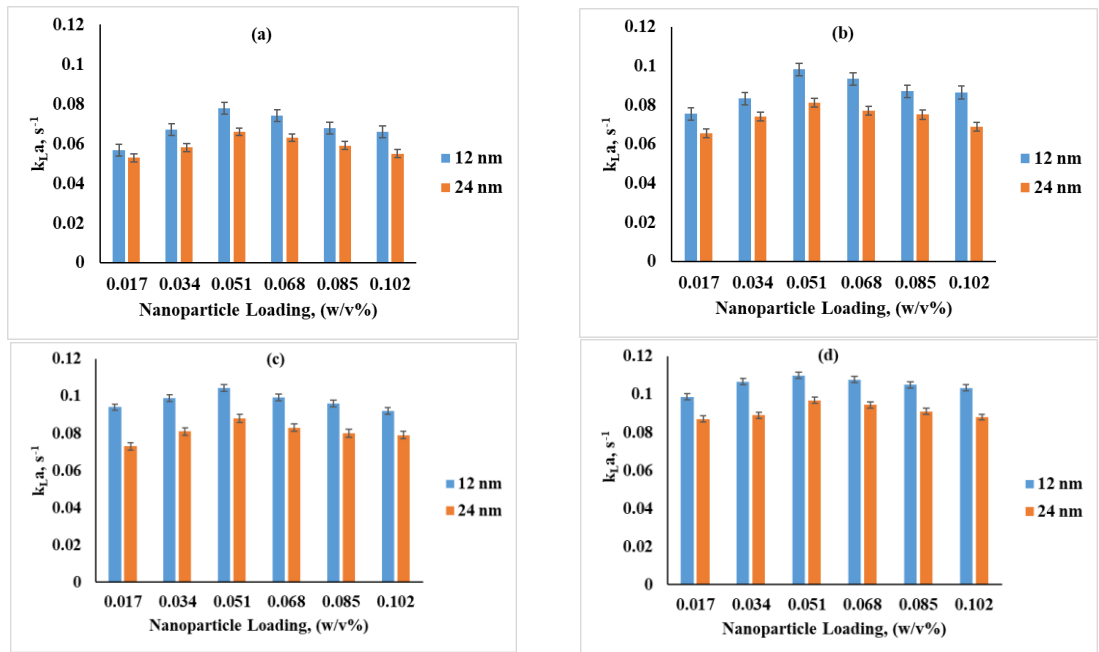


Fig. 4.33 Effect of nanoparticle size on $k_{L,a}$ at different SiO₂ nanoparticle loading and at A=6.3 cm at different frequency of pulsation (a) 0.25 s⁻¹ (b) 0.5 s⁻¹ (c) 0.75 s⁻¹ and (d) 1 s⁻¹

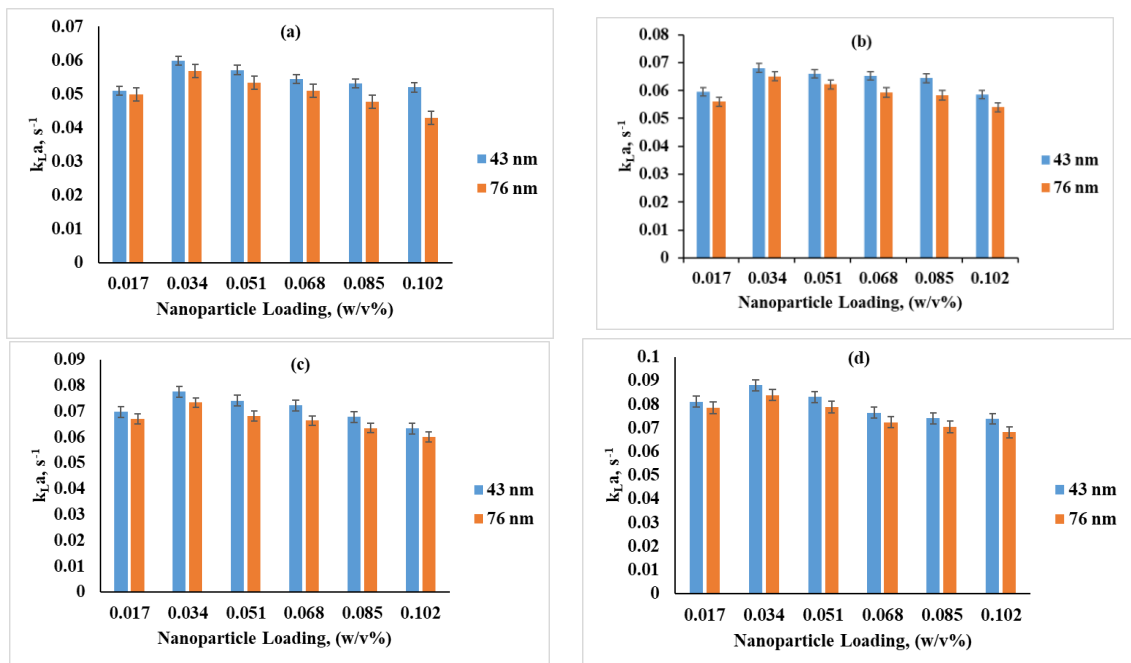


Fig. 4.34 Effect of nanoparticle size on $k_{L,a}$ at different α -Fe₂O₃ nanoparticle loading and at A=6.3 cm at different frequency of pulsation (a) 0.25 s⁻¹ (b) 0.5 s⁻¹ (c) 0.75 s⁻¹ and (d) 1 s⁻¹

As illustrated in Fig. 4.32 to 4.34 the volumetric oxygen mass transfer coefficient decreases with an increase in particle size. With increase in particle size the possibility

of agglomeration becomes more due to reduced particle -particle separation. The aggregation of particles leads to the production of larger particles of greater mass and decreased Brownian motion and micro-convection (Jama et al. 2016; Nematbakhsh and Rahbar-Kelishami 2015). The probability of sticking of gas molecules to the surface of the particle depends on the size of the nanoparticles (Levdanskii and Smolik 2008). Smaller particles have more preference for the adhesion to the g-l interface or the adhesion rates for the smaller particles are higher than those for larger particles, and therefore the larger particles are easily swept away from the gas-liquid interface (Darvanjooghi et al. 2018; Ruthiya et al. 2005). The diffusion limitation increases as the particle diameter increases which in turn decreases the enhancement of mass transfer (Wenmakers et al. 2016). The surface-to-volume ratio will be higher for smaller diameter nanoparticles which result in uniform distribution of particles and give the best enhancement (Godson et al. 2010). Smaller-size nanoparticles exhibit higher surface charge density compared to larger-size nanoparticles (Abbas et al. 2008). As a result, the electrostatic repulsion force between the nanoparticles and the liquid molecules increases which enhances the adsorption to the surface and the surface tension of nanofluids decreases with decrease in size of nanoparticles (Brown et al. 2013). Moreover, smaller particles provide larger surface area, which increases the surface free energy and consequently decreases the surface tension of the nanofluids.

Bhuiyan et al. (2015b), observed that the surface tension has decreased with decreasing nanoparticle size. (Nematbakhsh and Rahbar-Kelishami (2015), experimentally found that the tendency of clustering of nanoparticles increased with the increase in nanoparticle size as a result, the nanofluid showed the poor distribution stability, that lead to the decrease in mass transfer coefficient. The dispersion stability, viscosity, and surface tension of nanofluids show their effect on the efficiency of the transfer processes (Wu et al. 2017). Lower surface tension and viscosity favour in increasing the k_{La} (García-Ochoa and Gómez 1998; Kimweri 2001; Patwari et al. 1986). In the present study, the surface tension and viscosity increased with the increase in particle size as shown in Fig.4.1 and Fig.4.2. As observed in Table 4.6 mass transfer enhancement is higher with lower size of the nanoparticles in the nanofluid. Zhang et al. (2021), have also reported that the mass transfer enhancement increases with the decrease in the size of the nanoparticles and they attributed it to the intensification of Brownian motion, which is inversely proportional to the nanoparticle size. This

inferred that the better molecular transport occurred at the smaller size of the nanoparticles.

Table 4.6 Maximum Enhancement factor obtained at critical loading of TiO₂, SiO₂ and α -Fe₂O₃ nanoparticles with amplitude of pulsation of 3.2 cm at the lowest frequency of 0.25 s⁻¹, at air flow rate of 1.8 LPM.

Nanofluid type	Nanoparticle loading, % w/v	Average Nanoparticle size, nm	Enhancement factor
TiO ₂ -25	0.068	25	4.37
TiO ₂ - 72	(TiO ₂ -25 critical loading)	72	1.84
TiO ₂ -25	0.051	25	3.32
TiO ₂ -72	(TiO ₂ -72 critical loading)	72	2.39
SiO ₂ - 12	0.051	12	2.30
SiO ₂ - 24	(SiO ₂ critical loading)	24	2.17
α -Fe ₂ O ₃ - 43	0.034	43	1.65
α -Fe ₂ O ₃ - 76	(α -Fe ₂ O ₃ critical loading)	76	1.61

4.8 Comparison of the effect of TiO₂ SiO₂ and α -Fe₂O₃ nanofluids on volumetric oxygen mass transfer coefficient (k_{LA}) in a pulsed plate column

It is found from the results presented in earlier sections that, TiO₂, SiO₂, and α -Fe₂O₃ nanofluids could be used for the enhancement of gas-liquid mass transfer characteristics in pulsed plate columns. This section compares the TiO₂, SiO₂, and α -Fe₂O₃ nanofluids efficiency in enhancing the gas-liquid mass transfer. Fig 4.35 shows the effect of TiO₂ and SiO₂ nanofluids on k_{LA} at different nanoparticle loadings at amplitude of pulsation of 6.3 cm, frequency of pulsation of 1 s⁻¹ with similar average nanoparticle size (TiO₂ of 25 nm and SiO₂ of 24 nm). Similarly, Fig 4.36 shows the effect of TiO₂ and α -Fe₂O₃ nanofluids on k_{LA} at different nanoparticle loadings at amplitude of pulsation of 6.3 cm, frequency of pulsation of 1 s⁻¹ with similar average nanoparticle size (TiO₂ of 72 nm and α -Fe₂O₃ of 76 nm).

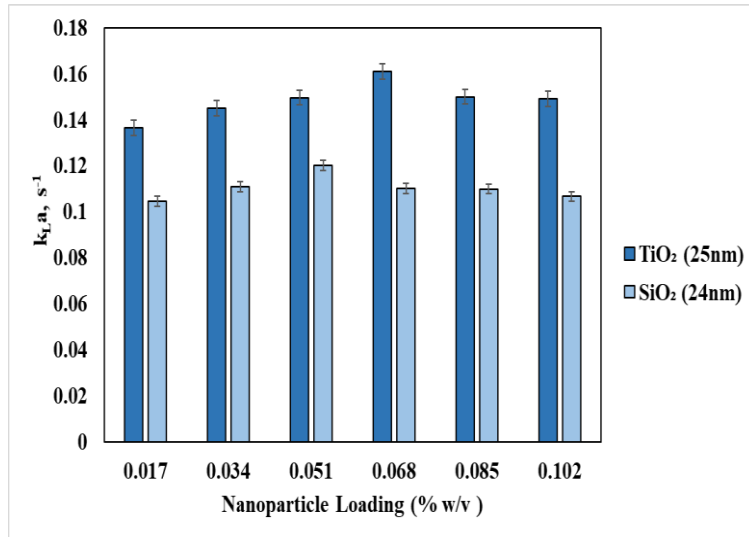


Fig.4.35. Effect of TiO₂ and SiO₂ nanofluids on $k_{L,a}$ at different nanoparticle loadings with similar average particle size (25 nm and 24 nm respectively) at $A= 6.3$ cm, $f = 1$ s⁻¹

1

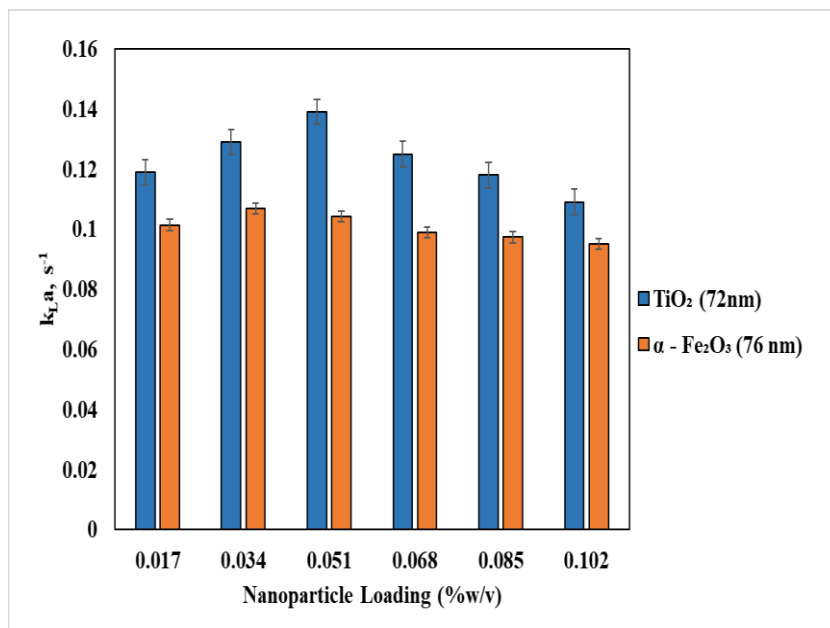


Fig.4.36. Effect of TiO₂ and α -Fe₂O₃ nanofluids on $k_{L,a}$ at different nanoparticle loadings with similar average particle size (72 nm and 76 nm respectively) at $A= 6.3$ cm, $f = 1$ s⁻¹.

Table 4.7: Enhancement factor obtained at critical loading of TiO₂, SiO₂ and α -Fe₂O₃ nanoparticles with amplitude of pulsation of 6.3 cm at the highest frequency of 1 s⁻¹, at air flow rate of 1.8 LPM.

Nanoparticle Type	Nanoparticle loading, % w/v	Average Nanoparticle size, nm	Enhancement factor
TiO ₂	0.068	25	1.87
SiO ₂	(TiO ₂ critical loading)	24	1.35
TiO ₂	0.051	25	1.81
SiO ₂	(SiO ₂ critical loading)	24	1.20
TiO ₂	0.051	72	1.31
α -Fe ₂ O ₃	(TiO ₂ critical loading)	76	1.06
TiO ₂	0.034	72	1.45
α -Fe ₂ O ₃	(α -Fe ₂ O ₃ critical loading)	76	1.12

As observed in Fig 4.35 and 4.36 the volumetric oxygen mass transfer coefficient was higher in TiO₂ nanofluid than in SiO₂ and α -Fe₂O₃ nanofluid. The enhancement factors obtained at critical loading of TiO₂, SiO₂ and α -Fe₂O₃ nanoparticles with highest amplitude 6.3 cm and frequency of 1 s⁻¹ are given in Table 4.7. The maximum enhancement factor was observed for the TiO₂ nanofluid compared with SiO₂ and Fe₂O₃ nanofluid. This is mainly because TiO₂ nanoparticles have more O₂ adsorption ability than the SiO₂ and α -Fe₂O₃ nanoparticles and the oxygen transport capacity of TiO₂ nanofluid is greater than that of SiO₂ nanofluid (Jiang et al. 2015). Due to the polarity of SiO₂ being hydrophilic, it would interact with water and form the nanofluid with a certain viscosity, so the resistance of gas through the liquid film is increased and the number of gas molecules in the liquid phase through the liquid film is reduced in the same time which leads to the decrease in the rate of gas-liquid mass transfer (Mondragon et al. 2012). The electrostatic repulsion forces exerted between the nanoparticles and the liquid molecules vary with the type of nanoparticles used leading to variation in absorbability at the interface and the surface tension of nanofluids. The surface tension and viscosity of SiO₂ and α -Fe₂O₃ nanofluids were found to be higher than that of TiO₂ nanofluids, thus leading to a lower gas-liquid mass transfer coefficient with SiO₂ and α -Fe₂O₃ nanofluids.

Therefore, it is observed that the size of nanoparticles in the nanofluid is not the only determining factor for gas-liquid mass transfer enhancement. The type of nanoparticles

also changes the characteristics of the nanofluid and thus k_{LA} enhancement is also a function of the type of nanoparticles.

Thus, it may be concluded that nanofluids containing suitable types and sizes of nanoparticles at optimum loading may be chosen corresponding to the desired column operating conditions required for the process. If flexibility in column operating conditions is available as per the process requirement, then the optimum pulsing velocity conditions to maximize the k_{LA} may be chosen. Table 4.8 presents the maximum k_{LA} and k_{LA} enhancement factors along with the optimum conditions for the operation of PPC to obtain these values. Table 4.9 presents the Comparison of Maximum k_{LA} enhancement factors at the optimum conditions of operation of various reactors with this study.

Table 4.8. Maximum k_{LA} and k_{LA} enhancement factors along with the optimum conditions for the operation of PPC

Nanofluid	Critical Loading, %w/v	Optimum conditions for Max. k_{LA}	Max. k_{LA} Values, s^{-1}	Optimum Conditions for Maximum Enhancement Factor	Max. Enhancement factor
TiO ₂ -25	0.068	A = 6.3cm f = 1s ⁻¹ U _g = 0.029m/s	0.161	A = 3.2cm f = 0.25s ⁻¹ U _g = 0.011m/s	4.37
TiO ₂ -72	0.051		0.142		2.39
SiO ₂ - 12	0.051		0.132		2.30
SiO ₂ - 24			0.121		2.17
α-Fe ₂ O ₃ - 43	0.034		0.112		1.65
α-Fe ₂ O ₃ - 76			0.109		1.61

Table 4.9. Comparison of Maximum k_{LA} enhancement factors at the optimum conditions of operation of various reactors with this study

Nanofluid	Reactors	Optimum conditions	Maximum Enhancement Factor	Reference
Magnetite (Fe ₃ O ₄)-coated with oleic acid	Agitated, sparged reactor	volume fractions below 1%	6.0	(Olle et al. 2006)
n-hexadecane droplets	Laboratory scale stirred reactor	Volume fractions below 0.01- 0.02%,	1.04–1.06	(Nagy et al. 2007)
Fe ₂ O ₃ -water	Agitated aerobic bioreactor	Volume fraction of 0.065%	1.63	(Manikandan et al. 2012)
TiO ₂ -water and SiO ₂ -water with Na ₂ SO ₃	thermostatic stirred tank	solids loading of 0.4 kg/m ³	1.82 and 1.7	(Jiang et al. 2015)
Activated carbon particles	Stirred tank bioreactor	Volume fraction of 0.006%	1.4	(Ding et al. 2023)
TiO ₂ -25 – water with Na ₂ SO ₃	Pulsed plate column	Volume fraction of 0.068 % w/v	4.37	This Study
SiO ₂ -12 – water with Na ₂ SO ₃	Pulsed plate column	Volume fraction of 0.051 % w/v	2.3	This Study
α-Fe ₂ O ₃ water with Na ₂ SO ₃	Pulsed plate column	Volume fraction of 0.034 % w/v	1.6	This Study

As observed in Table 4.9, the k_{LA} enhancement in PPC is as high as 4.37 with TiO_2 -25 nanofluid and is much higher than that which could be achieved in a thermostatic stirred tank. The enhancement obtained with $\alpha-Fe_2O_3$ nanofluid is around 1.6 which is comparable with that obtained in an agitated aerobic bioreactor. The enhancement obtained in PPC with SiO_2 nanofluid is around 2.3 and is higher than that achieved in thermostatic stirred tank. Agitated sparged reactor could give higher enhancement of 6.0 compared to PPC only with Fe_3O_4 nanoparticles coated with oleic acid. On comparison, it may be concluded that the effect of nanofluid in k_{LA} enhancement is superior in PPC than in other types of contactors.

CHAPTER 5 Theoretical Analysis and Modelling Studies

This chapter presents the results of the verification of the mechanism of mass transfer enhancement in TiO₂, SiO₂, and α -Fe₂O₃ nanofluids found using order of magnitude analysis. A theoretical model is applied and verified to predict the mass transfer enhancement in the presence of TiO₂, SiO₂, and α -Fe₂O₃ nanofluids. The dimensionless correlations using the MRA model and the ANN model relating the column operating conditions with k_{LA} are developed for the prediction of k_{LA} in the presence of TiO₂, SiO₂, and α -Fe₂O₃ nanofluids.

5.1 Order of magnitude analysis for mass transfer enhancement mechanism

Various mechanisms and models have been proposed to explain the enhanced mass transfer in nanofluids. Several researchers (Kebblinski et al. 2001; Khanolkar and Suresh 2015; Krishnamurthy et al. 2006; Olle et al. 2006) have looked into the cause of the observed improvement in mass transport using an order of magnitude analysis based on the computation of the characteristic time of the various mechanisms. As discussed in Krishnamurthy et al. (2006); Prasher et al. (2005, 2006a), there might be three important effects in the mass transport of a nanofluid. Firstly the diffusion time, as reported by Krishnamurthy et al. (2006), is the time required for the oxygen to diffuse through a distance equal to the diameter of nanoparticle t_m was calculated by Equation (5.1).

$$t_m = \frac{d^2}{2D} \quad (5.1)$$

Secondly, the translational Brownian motion, which is the time required for a Brownian particle to travel a distance equal to its diameter (t_b) was calculated by Equation (5.2).

$$t_b = \frac{3\pi\eta d^3}{2K_B T} \quad (5.2)$$

where d = diameter of the nanoparticle (m); D = diffusion coefficient of oxygen in water (m²/s) (1.97E-09 m²/s); η = viscosity of water (N.s/m²) (7.89E-04 N.s/m² at 303.15K); K_B = Boltzmann constant (J/K) (1.380649E-23), T = temperature (K) (303.15K).

and finally the convective motion of the liquid elements in the continuous liquid due to the Brownian movement of the nanoparticles. As the nanoparticles in a bulk liquid collide with the fluid molecules it might increase the velocity of the surrounding molecules. Further to investigate if the mass transfer enhancement is due to the increased nanoscale stirring of the liquid caused by the Brownian motion of the nanoparticles, it is the time required for convection currents to travel a particle diameter, t_c as calculated (Prasher et al. 2006) using Equation (5.3) was compared with t_m and t_b .

$$t_c = \frac{d^2}{\nu} \quad (5.3)$$

Where ν is the kinematic viscosity of water, m^2/s ($8.005E-7 m^2/s$)

Hence based on these effects in the present study, to investigate the reason for enhanced oxygen mass transport with TiO_2 , SiO_2 and $\alpha-Fe_2O_3$ nanofluid as compared to the base fluid in PPC, an order of magnitude analysis was performed. The calculated values of t_m , t_b and t_c in PPC for TiO_2 , SiO_2 and $\alpha-Fe_2O_3$ nanofluid are shown in table 5.1. It is observed that $t_m < t_b$ by two orders of magnitude for different nanofluids irrespective of size of nanoparticles.

Table. 5.1 The values of t_m , t_b and t_c for TiO_2 , SiO_2 and $\alpha-Fe_2O_3$ nanofluid.

Nanoparticle Type	Nanoparticle Size	t_m , (sec)	t_b , (sec)	t_c , (sec)
TiO_2	25 nm	1.59E-07	1.4E-05	7.81E-10
	72 nm	1.32E-06	3.35E-04	6.48E-09
SiO_2	12 nm	3.65E-04	1.55E-06	1.8E-10
	24 nm	1.46E-07	1.24E-05	7.2E-10
$\alpha-Fe_2O_3$	43 nm	4.69E-08	7.14E-05	2.31E-09
	76 nm	1.47E-06	3.96E-04	7.23E-09

Thus, the diffusion rate of oxygen is two orders of magnitude faster than the rate of travel of the nanoparticles by Brownian motion. Hence. the Brownian motion of the particles does not contribute directly to enhancement in oxygen mass transfer. The particles themselves do not physically push the oxygen molecules from one point to

another. It is thus concluded that the Brownian motion is not the mechanism responsible for oxygen mass transfer enhancement.

As shown in Table 5.1, t_c is three orders of magnitude smaller than t_m . It implies that the convection currents caused by Brownian motion of the particles is much faster than the mass diffusion of oxygen or the Brownian motion of the particle itself. Thus, the disturbance field created by the motion of the nanoparticles in the fluid can be the possible reason for the enhancement in mass transport.

Ataíde et al. (2013), in their studies on oxygen transport enhancement by functionalized magnetic nanoparticles in cylindrical tanks with impellers, have also found through the order of magnitude analysis that the mechanism of micro convection promoted by the nanoparticles has an impact on the oxygen mass transfer enhancement. Krishnamurthy et al. (2006), have also conducted an order of magnitude analysis for mass transfer in Al_2O_3 nanofluid and found that nanoscale convection induced by the Brownian motion of the nanoparticles causes enhanced mixing and mass transfer enhancement in nanofluids.

5.2 Pseudo-homogeneous model

At the gas-liquid interface, to interpret the mass transport across a liquid boundary layer in the presence of solid nanoparticles, a homogeneous model is applied and the mass transfer in the particles is instantaneous (Nagy 2013; Nagy et al. 2007). The pseudo-homogeneous model is explained considering the differential mass balance equation for the boundary layer at the gas-liquid interface and is given in equation (5.4). The diffusion time within nanosized particles (t_m) as it was shown in section 5.1 is a few orders of magnitude less than that through the gas-liquid boundary layer. In the case of the pseudo-homogeneous model the size of the dispersed phase (nanosized particles) is much smaller than the thickness of the laminar boundary layer. Thus, the diffusion process within the nanosized particles (internal mass transfer) can be regarded as instantaneous as compared to the diffusion in the laminar boundary layer. The differential mass balance equation can be given for the boundary layer at the gas-liquid interface is as follows (Nagy 2013; Nagy et al. 2007):

$$D_{nf} \frac{\partial^2 C_A}{\partial x^2} - \frac{\Phi}{1 - \Phi} \frac{\partial C_{Anf}}{\partial t} = \frac{\partial C_A}{\partial t} \quad (5.4)$$

The equation (6) is simplified with boundary conditions

$$(i) \ t = 0, \ x > 0; \ C_A = 0 = C_{Anf}$$

$$(ii) \ t = 0, \ x = 0; \ C_A = C_{Ai}$$

Applying the surface renewal theory, the rate of mass transfer at gas-liquid interface is given (Nagy 2013) in equation (5.5).

$$J_{nf} = \sqrt{D_{nf} s} \sqrt{\frac{1 - \Phi + \Phi H}{1 - \Phi}} \times C^* \quad (5.5)$$

Where, J_{nf} = overall mass transfer rate with nanofluids, mol/m²s,

s = Surface renewal rate, s⁻¹,

H = Henry's constant for dissolved oxygen in water at 25°C,

D_{nf} = Diffusivity of the nanofluid is calculated using Equation (3.1) as shown in section 4.1.

Enhancement factor, E is calculated using the equation (5.6),

$$E = \frac{J_{nf}}{J_{bf}} \quad (5.6)$$

Where J_{bf} is the overall mass transfer rate with base fluid.

From Eq. (5.5) and (5.6)

$$E = \sqrt{\frac{D_{nf}}{D_L}} \sqrt{\frac{1 - \Phi + \Phi H}{1 - \Phi}} \quad (5.7)$$

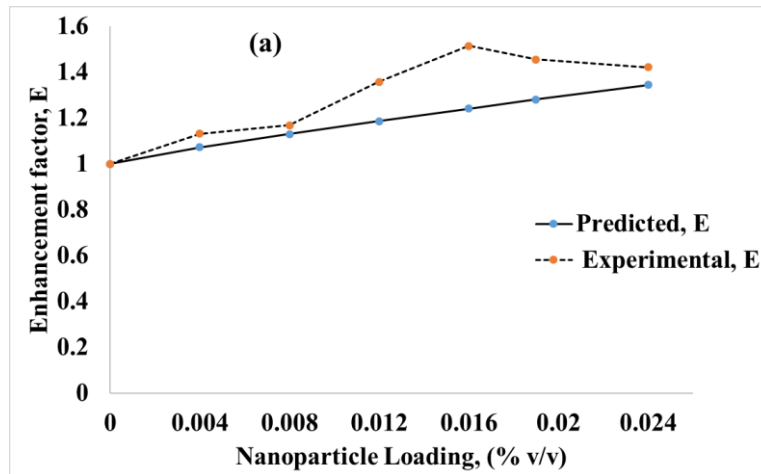


Fig 5.1. Predicted and experimental Enhancement in mass transfer rate in the presence of TiO₂ nanofluids.

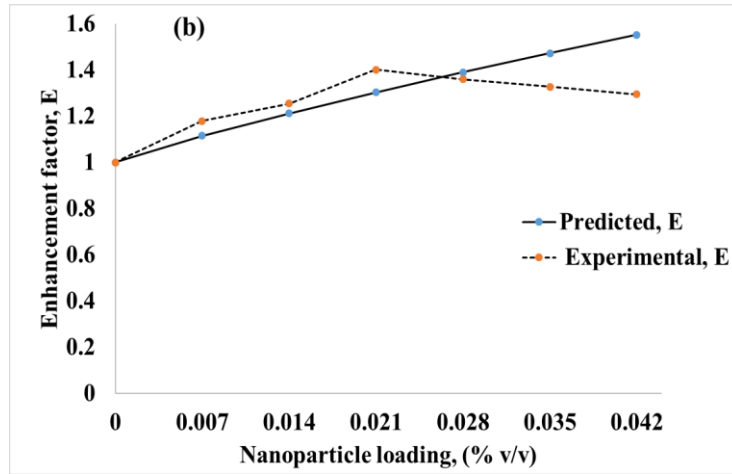


Fig 5.2. Predicted and experimental Enhancement in mass transfer rate in the presence of SiO₂ nanofluids.

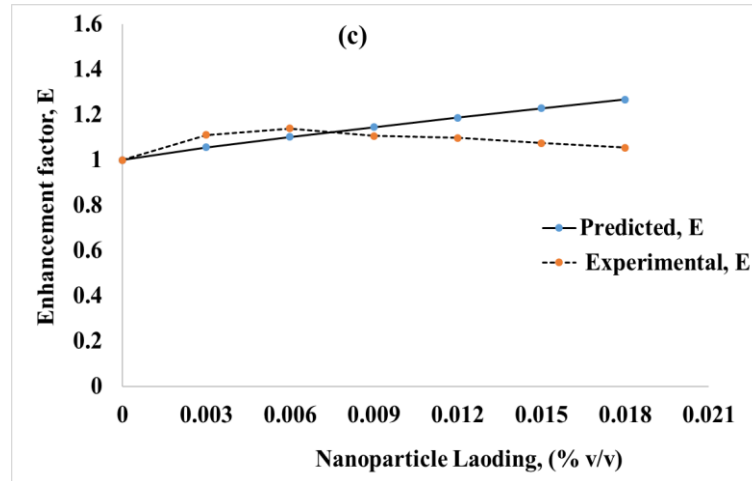


Fig 5.3. Predicted and experimental Enhancement in mass transfer rate in the presence of α -Fe₂O₃ nanofluids.

The experimental enhancement factor and predicted from the pseudo homogeneous model for TiO₂ SiO₂ and α -Fe₂O₃ nanofluid at the amplitude of pulsation of 6.3 cm, frequency of pulsation of 0.25 s⁻¹, and with an air flow rate of 4.8 LPM, are illustrated in Fig.5.1, Fig.5.2, and Fig.5.3 respectively.

The dotted line represents the experimentally found enhancement in mass transfer rate and the continuous line represents the model predicted enhancement in mass transfer rate. Though the closeness among the predicted and the experimental enhancement in mass transfer rate is good as depicted by the Coefficient of determination (R^2) and minimal Mean absolute error values shown in Table 5.3, the trend of change in the enhancement factor with increase in nanoparticle loading is found to differ for

experimental and predicted factors. There is a significant increase in the experimental enhancement of the mass transfer rate with increase in nanoparticle loading at lower loading values, reaching a maximum at a critical loading. This is mainly due to the convective currents caused by the Brownian movement of nanosized particles. Further, there is a decrease observed in the enhancement factor with increase in nanoparticle loading. As discussed by Nagy et al (2007), the colloidal movement of nanoparticles helps in generating the enhanced velocity gradients, which increases the rate of diffusion of the absorbed constituent. The rate of mass transfer varies due to the aggregation of nanoparticles (Prasher et al 2006). At the higher loading, the problem of aggregation arises easily. Hence the enhancement in mass transfer rate has decreased with increase in loading values at higher loading. However, there is an increase in predicted enhancement in the mass transfer coefficient with the increase in the loading at the entire range. This may be due to not considering the aggregation effect in the model. The enhancement equation takes into account the volume fraction of nanoparticles in the nanofluid and the diffusivity in the nanofluid. But, the model is based on the assumption which considers that the surface renewal rate is the same in the presence and absence of nanoparticles. However, the deviation of experimental enhancement from the predicted enhancement indicates that the surface renewal rate (s) gets altered in the presence of nanoparticles. The surface renewal rates were calculated using the experimental flux both with the base fluid and nanofluids under different conditions using Equation (5.5). The variation in surface renewal rate with varying pulsing intensities, and superficial gas velocities (0.011 m/s, 0.019 m/s and 0.029 m/s) are shown in Fig 5.4, 5.5 and 5.6 and the values are presented in Table 5.2. respectively. As observed in Fig 5.4 to Fig 5.6 the surface renewal rate is the lowest with base fluid and higher for nanofluids indicating enhancement of turbulence intensity and the mass transfer with nanofluids this is due to convection currents generated by Brownian movement of the particles. Further as observed from Figure 5.4 to 5.6, the surface renewal rate increases with the increase in both the pulsing velocities and superficial air velocities showing that the increase in these operating conditions lead to higher turbulent intensities causing the faster renewal of the surface attributing to mass transfer enhancement.

These results indicate that the pseudo homogeneous model can accurately predict the enhancement till the critical loading conditions, but not at loading conditions above the critical loading.

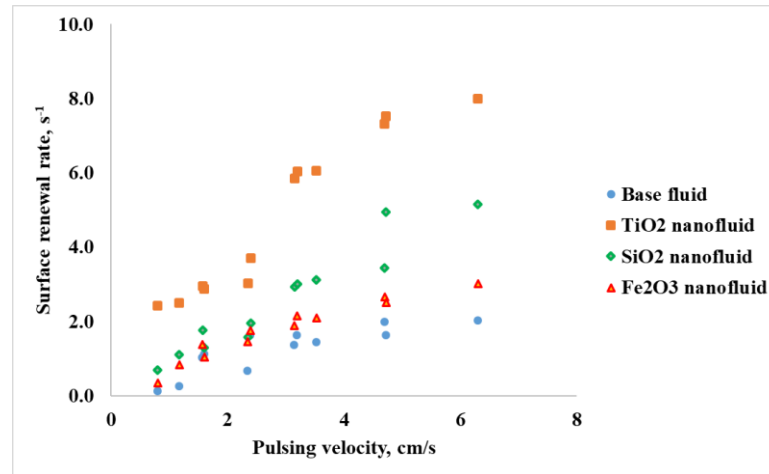


Fig 5.4 The variation in Surface renewal rate (s), at critical nanoparticle loading for TiO₂, SiO₂ and α -Fe₂O₃ nanofluid at varying pulsing velocity at an air flow rate of 0.011 m/s.

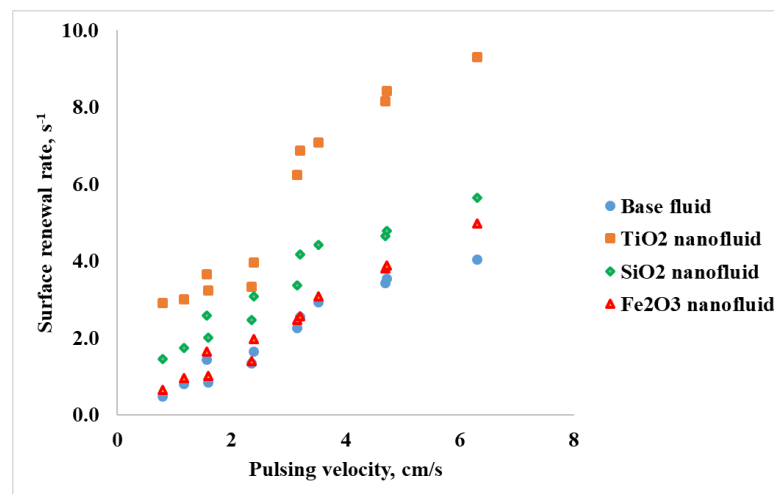


Fig 5.5 The variation in Surface renewal rate (s), at critical nanoparticle loading for TiO₂, SiO₂ and α -Fe₂O₃ nanofluid at varying pulsing velocity at an air flow rate of 0.019 m/s.

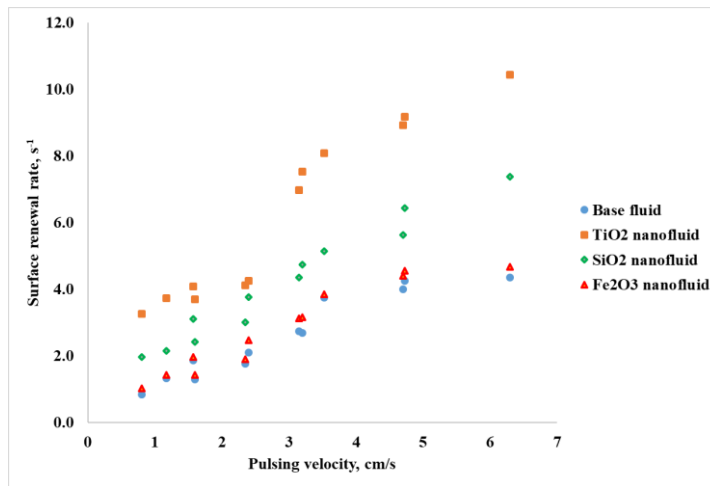


Fig 5.6 The variation in Surface renewal rate (s), at critical nanoparticle loading for TiO₂, SiO₂ and α -Fe₂O₃ nanofluid at varying pulsing velocity at an air flow rate of 0.029 m/s.

Table 5.2 Calculated surface renewal rate values using experimental flux with basefluid and nanofluids under critical loading of nanoparticles and varying pulsing velocities and superficial gas velocity.

(A×f), cm/s	Surface renewal rate (s), s ⁻¹											
	Superficial air velocity, 0.011m/s				Superficial air velocity, 0.019m/s				Superficial air velocity, 0.029m/s			
	BF	Ti O ₂	SiO ₂	α - Fe ₂ O ₃	BF	TiO ₂	SiO ₂	α -Fe ₂ O ₃	BF	TiO ₂	SiO ₂	α - Fe ₂ O ₃
0.8	0.1	2.4	0.7	0.4	0.5	2.9	1.5	0.7	0.9	3.3	2.0	1.0
1.175	0.3	2.5	1.1	0.8	0.8	3.0	1.7	1.0	1.3	3.7	2.1	1.4
1.575	1.0	2.9	1.8	1.4	1.4	3.7	2.6	1.6	1.9	4.1	3.1	2.0
1.6	1.1	2.9	1.3	1.0	0.8	3.2	2.0	1.0	1.3	3.7	2.4	1.4
2.35	0.7	3.0	1.6	1.5	1.3	3.3	2.5	1.4	1.8	4.1	3.0	1.9
2.4	1.6	3.7	1.9	1.8	1.6	4.0	3.1	2.0	2.1	4.3	3.8	2.5
3.15	1.4	5.8	2.9	1.9	2.3	6.2	3.4	2.5	2.7	7.0	4.4	3.1
3.2	1.6	6.0	3.0	2.2	2.5	6.9	4.2	2.6	2.7	7.5	4.7	3.2
3.525	1.4	6.1	3.1	2.1	2.9	7.1	4.4	3.1	3.7	8.1	5.1	3.9
4.7	2.0	7.3	3.4	2.7	3.4	8.2	4.6	3.8	4.0	8.9	5.6	4.4
4.725	1.6	7.5	5.0	2.5	3.5	8.4	4.8	3.9	4.3	9.2	6.4	4.6
6.3	2.0	8.0	5.1	3.0	4.0	9.3	5.6	5.0	4.4	10.4	7.4	5.8

Table 5.3 statistical parameters for different nanofluids of the Pseudo homogenous model

Nanoparticle	Statistical Parameters		
	R ²	MSE	MAE
TiO ₂	0.98	0.0185	0.1091
SiO ₂	0.99	0.0148	0.0323
α -Fe ₂ O ₃	0.99	0.0118	0.0575

5.3 Development of dimensional correlations for k_{LA} : Multiple Regression Analysis (MRA) model

Dimensionless correlations with MRA and Artificial neural network based models may be developed with the experimental results to better suit to predict the k_{LA} values in PPC. To facilitate the prediction of k_{LA} with TiO₂, SiO₂, and α -Fe₂O₃ nanofluids in PPC, the k_{LA} values were determined by varying the frequency (0.25 s⁻¹, 0.5 s⁻¹, 0.75 s⁻¹ and 1 s⁻¹) and amplitude (3.2 cm, 4.7 cm, and 6.3 cm) of pulsation with different superficial air velocities (0.011m/s, 0.019m/s, and 0.029 m/s) and nanoparticle loading (0.017 % w/v, 0.034 % w/v, 0.051 % w/v, 0.068 % w/v, 0.081 % w/v, and 0.102 % w/v) conditions in PPC. The experiments were conducted at the above conditions with TiO₂-25, TiO₂-72, SiO₂-12, SiO₂-24, α -Fe₂O₃-43 and α -Fe₂O₃-76 nanofluids. Totally 1296 experimental data sets covering the entire range of conditions with TiO₂-25, TiO₂-72, SiO₂-12, SiO₂-24, α -Fe₂O₃-43 and α -Fe₂O₃-76 nanofluids were used to develop the MRA models are shown in Appendix I, II and III. MRA models for TiO₂, SiO₂ and α -Fe₂O₃ nanofluid were developed. Each MRA model covered totally 432 data sets obtained with both the sizes of the nanoparticles of a particular nanofluid. A single dimensionless correlation of the form given in equation (5.8) was used to correlate the experimental data in the form of dimensionless numbers. It correlates the Sherwood number (Sh) with the Oscillating Reynolds number (Re_o)(Abbott et al. 2013), Gas flow Reynolds number (Re_g), Schmidt number (Sc), and Brownian Reynolds number (Re_B) (Bahmanyar et al. 2014).

$$\mathbf{Sh} = k \mathbf{Re}_o^a \mathbf{Re}_g^b \mathbf{Sc}^c \mathbf{Re}_B^d \quad (5.8)$$

where Sherwood number, Oscillating Reynolds number (Abbott et al. 2013) (Abbott et al. 2013), Gas flow Reynolds number, Schmidt number, and Brownian Reynolds number (\mathbf{Re}_B) (Bahmanyar et al. 2014) is defined as follows:

$$\mathbf{Sh} = \frac{k_{La} \times d^2}{D_{nf}} ; \mathbf{Re}_o = \frac{2\pi \times d \times (A \times f) \times \rho_{nf}}{\mu_{nf}} ; \mathbf{Re}_g = \frac{d_{sp} \times \rho_G \times U_g}{\mu_G} ;$$

$$\mathbf{Sc} = \frac{\mu_{nf}}{\rho_{nf} \times D_{nf}} ; \mathbf{Re}_B = \frac{1}{v_{nf}} \left(\sqrt{\frac{18K_bT}{\rho_p \pi d_p}} \right)$$

D_{nf} is the diffusivity of the nanofluid which was calculated using Equation (4.1) (Feng and Johnson 2012) as shown in section 4.1.

We consider the effect of the convection of the liquid near the particles due to their Brownian movement. At smaller particle sizes, Brownian movement-based convection may dominate, whereas, at larger particle sizes, a diffusional motion-based transfer may predominate. An increase in the nanoparticle loading above a certain value lead to a decrease in the particle-to-particle separation, and hence greater is the tendency of aggregation. Aggregation produces fewer larger particles of greater mass. Any model should be able to make a transition such that at small particle sizes or loading some mechanism dominates and at larger particle sizes other mechanism dominates. To account for the effect of these particles of larger mass and the effect of size of the particles on the shift in dominant mechanism of transport, Brownian Reynolds number (Krishnamurthy et al. 2006a; Prasher et al. 2006b) is used in the model.

The correlation was developed using non-linear multiple regression analysis to predict the k_{La} in PPC in the presence of TiO_2 , SiO_2 , and $\alpha\text{-Fe}_2\text{O}_3$ nanofluids and is shown in equation (5.9), equation (5.10) and Equation (5.11) respectively.

$$\mathbf{Sh} = 354.24 \mathbf{Re}_o^{0.42} \mathbf{Re}_g^{0.16} \mathbf{Sc}^{0.94} \mathbf{Re}_B^{0.46} \quad (5.9)$$

$$\mathbf{Sh} = 275.95 \mathbf{Re}_o^{0.39} \mathbf{Re}_g^{0.23} \mathbf{Sc}^{0.72} \mathbf{Re}_B^{0.23} \quad (5.10)$$

$$\mathbf{Sh} = 1083.14 \mathbf{Re}_o^{0.46} \mathbf{Re}_g^{0.34} \mathbf{Sc}^{0.47} \mathbf{Re}_B^{0.21} \quad (5.11)$$

Table 5.4 shows the range of validity of nanoparticle loading, dimensionless numbers, and statistical parameters. The statistical parameters such as coefficient of determination (R^2), mean squared error (MSE) and mean absolute error (MAE) (Kahani and Vatankhah 2019) were used to determine the goodness of fit and were calculated using Equation (5.12)-Equation (5.14) respectively. The values are shown in Table 5.4.

$$R^2 = 1 - \left(\frac{\sum_{i=1}^N (P_i - E_i)^2}{\sum_{i=1}^N (E_i)^2} \right) \quad (5.12)$$

$$MSE = \frac{1}{N} \sum_{i=1}^N (P_i - E_i)^2 \quad (5.13)$$

$$MAE = \frac{1}{N} \sum_{i=1}^N (P_i - E_i) \quad (5.14)$$

Where, N = total number of data points, P_i = predicted values of Sh from the model, E_i = experimental values of Sh from the experimental data. The statistical parameters shown in Table 5.4 indicate the goodness of fit and the validity of the model. The plots of experimental values of Sherwood number vs. the predicted values of Sherwood number are shown in Fig 5.7 (a), (b) and (c) for TiO_2 , SiO_2 , and $\alpha\text{-Fe}_2\text{O}_3$ nanofluids respectively.

This indicates the goodness of fit of the data into correlations, thus proving the validity and potential applicability of the correlations to predict the $k_{L,a}$ values in PPC in the presence of TiO_2 , SiO_2 , and $\alpha\text{-Fe}_2\text{O}_3$ nanofluids. The dimensionless correlation developed in the present study may be useful to the designers of pulsed plate columns used for aerobic bioprocesses such as biological wastewater treatment or production of valuable bio products or for photocatalytic processes where, oxygen transfer coefficients are one of the important parameters for the design where these nanoparticles are either intentionally added to enhance the mass transfer or are present in the reactor to serve as a catalyst, adsorbent or as biomass supports.

Table 5.4 Range of validity of dimensionless numbers and statistical parameters for different nanofluids.

Nanoparticle type and Loading (%w/v)	Nanoparticle Size	Dimensionless numbers	Statistical Parameters		
			R ²	MSE	MAE
TiO ₂ 0.017 ≤ Φ ≤ 0.102	25 and 72 nm	2000 ≤ Re _o ≤ 30000 0.135 ≤ Re _g ≤ 0.370 800 ≤ Sc ≤ 1700 0.0004 ≤ Re _B ≤ 0.001	0.99	1.08E-04	8.97E-06
SiO ₂ 0.017 ≤ Φ ≤ 0.102	12 and 24 nm	2000 ≤ Re _o ≤ 20000 0.135 ≤ Re _g ≤ 0.370 1300 ≤ Sc ≤ 2200 0.0008 ≤ Re _B ≤ 0.002	0.99	6.03E-05	5.655E-05
α-Fe ₂ O ₃ 0.017 ≤ Φ ≤ 0.102	43 and 76 nm	1200 ≤ Re _o ≤ 20000 0.135 ≤ Re _g ≤ 0.370 1300 ≤ Sc ≤ 2700 0.008 ≤ Re _B ≤ 0.023	0.993	7.12E-08	1.14E-04

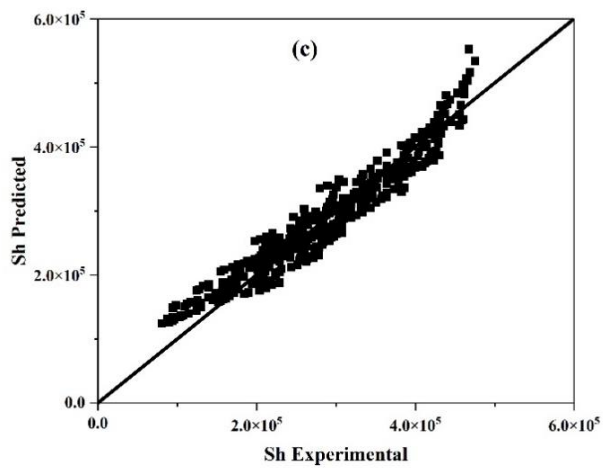
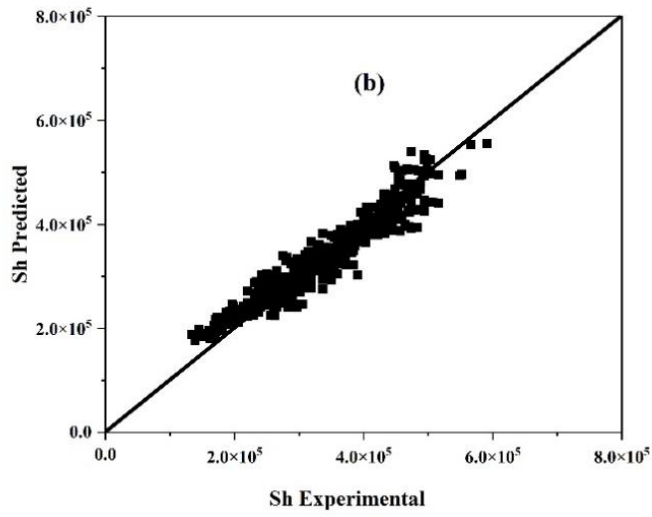
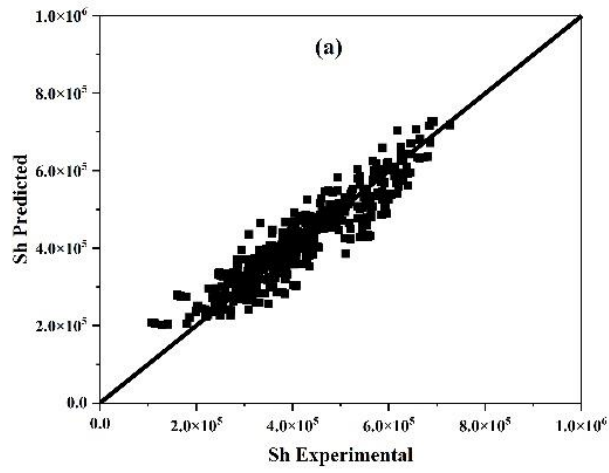


Fig.5.7 Predicted and experimental Sherwood number for (a) TiO_2 nanofluid (b) SiO_2 nanofluid (c) $\alpha\text{-Fe}_2\text{O}_3$ nanofluid

5.4 Artificial Neural Network (ANN)

The ANN model has been developed in the present study by considering all the factors in the entire range of data in a single model, to make the model more user-friendly. ANN is a powerful modeling tool, which is motivated by the human nervous system. It is composed of multiple interrelated processing elements called neurons. It has a network structure wherein neurons are arranged in different layers such as, initially an input layer that receives the input variable data, a hidden layer in which the data is processed, and finally, an output layer that sends the processed information. Each neuron of the hidden layer is interconnected to input and output layers using weights and biases (Janghorban Esfahani et al. 2012). The main advantage of an ANN is that a precise output or target can be obtained by training and regulating the determined input (Kahani and Vatankhah 2019). From the literature findings, it is reported that ANN is used in many applications such as to predict the k_{LA} , gas hold-up, and the average bubble diameter in bubble columns using column geometry and operating conditions as input parameters (Baawain et al. 2007). The ANN-based model was also developed for the prediction of biodegradation of phenol in pulsed plate bioreactor (Shetty et al. 2008). Hemmat Esfe et al. (2015), proposed the ANN model to predict the thermal conductivity ratio of SiO_2 -DWCNT/ethylene glycol nanofluid as a function of volume concentration and temperature. (Kahani and Vatankhah 2019) developed an optimized ANN model to predict the thermal performance of a Wickless heat pipe with Al_2O_3 /water nanofluid. The theoretical models cannot predict the k_{LA} accurately in the entire range of nanoparticle loading and different mechanisms govern the enhancement under different conditions. As the dependency of k_{LA} on various operating variables is highly nonlinear, ANN model was developed to predict k_{LA} in PPC with nanofluids.

In the present work, the neural network consisted of five inputs and one output variable. The input variables for the neural networks were nanoparticle loading, superficial gas velocity, the amplitude of pulsation, frequency of pulsation, and nanoparticle size. k_{LA} is the output variable. Fig. 5.8. shows the structure of a feed-forward neural network with an input layer, hidden layer, and output layer. Feed-forward neural networks are used to learn the relationship between independent variables, which serve as inputs to the network, and dependent variables which are designated as outputs of the network. Feedforward neural networks (FFNNs) can represent more complex classification

functions. An FFNN includes an input, output, and several hidden layers. The number of hidden layers represents the depth of the network. All layers include interconnected nodes. The network trains itself by computing differences between the processed output by the network and the actual target output. The network then adjusts the weights associated with each connection according to a set learning rate and the error values. After many such successive adjustments as the network loops over each time in the ANN, this way tends to produce outputs that are increasingly similar to the target output (results)(Das et al. 2021).

Totally 432 data points were used, which were obtained from batch experiments at different operating parameters and were shown in Annexures I, II, and III. Among them, 302 (70% of total data points) points were used for network training and 65 points each (15% of the total data points) for validation and testing respectively. The network was trained with the Levenberg- Marquardt backpropagation algorithm (trainlm) using the NN tool of MATLAB R2019a. It is important to find the optimal neurons in the hidden layer, to avoid overfitting, prolonged unnecessary training time, and the complex interconnection of weight structure. An insufficient number of neurons may create a problem in learning the complete relationship between the data (Patel and Mehta 2018). Hence, the number of neurons in the hidden layer was varied through the trial-and-error method and the optimal number of neurons was obtained based on the criteria of minimum MSE. Fig 5.9 represents the Mean Squared Error (MSE) versus the Number of Neurons hidden in the layer. The plots showing the predicted ANN output vs. the experimental value of k_{La} in the presence of TiO_2 , SiO_2 , and $\alpha-Fe_2O_3$ nanofluids for the training, testing, and validation data points are shown in Fig. 5.10, Fig. 5.11, and, Fig.5.12 respectively. The fit of these points onto the 45° line passing through the origin confirms that (i) the ANN network is well-trained (Fig. 5.10(a), 5.11 (a), 5.12(a) and (ii) the model is valid and predicts k_{La} accurately (Figure 5.10 (b) and (c); 5.11(b) and (c); 5.12 (b) and (c)) under the experimental range. The goodness of the ANN was tested by statistical parameters such as R^2 , MSE, and MAE(Kahani and Vatankhah 2019).

The R^2 value for the model is 0.989 shows an excellent fitting between the ANN-predicted and experimental values of k_{La} . The MSE and MAE of the network were found and shown in table 5.5. The results have shown a good agreement between the

experimental data and predicted data. Hence, it is stated that the ANN provides an efficient method for predicting the $k_{L,a}$ for the pulsed plate column in the presence of nanofluids.

Table 5.5 statistical parameters for different nanofluids

Nanoparticle	Statistical Parameters		
	R ²	MSE	MAE
TiO ₂	0.98	1.44731E-05	1.23E-04
SiO ₂	0.99	1.02734E-05	2.28517E-05
α -Fe ₂ O ₃	0.99	5.05608E-06	4.23449E-05

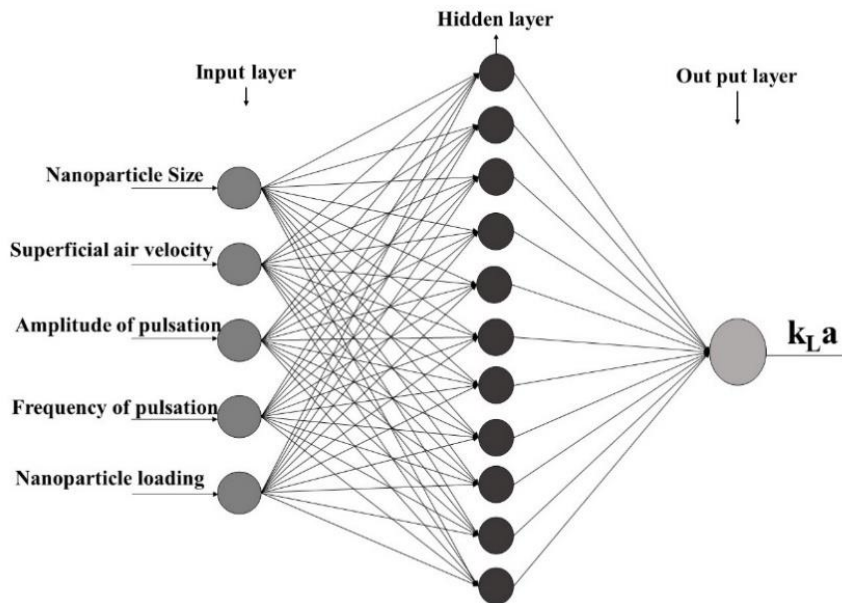


Fig. 5.8 Structure of feed-forward neural network with input, hidden, and output layer

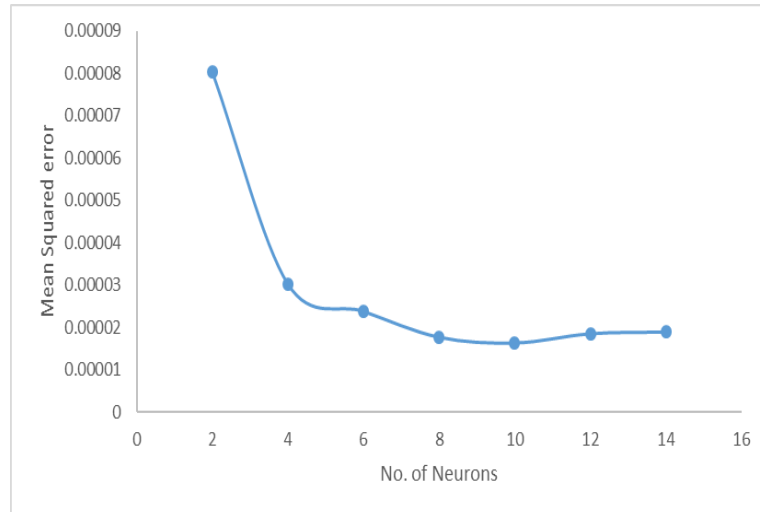


Fig.5.9 Mean Squared Error versus Number of Neurons hidden in the layer.

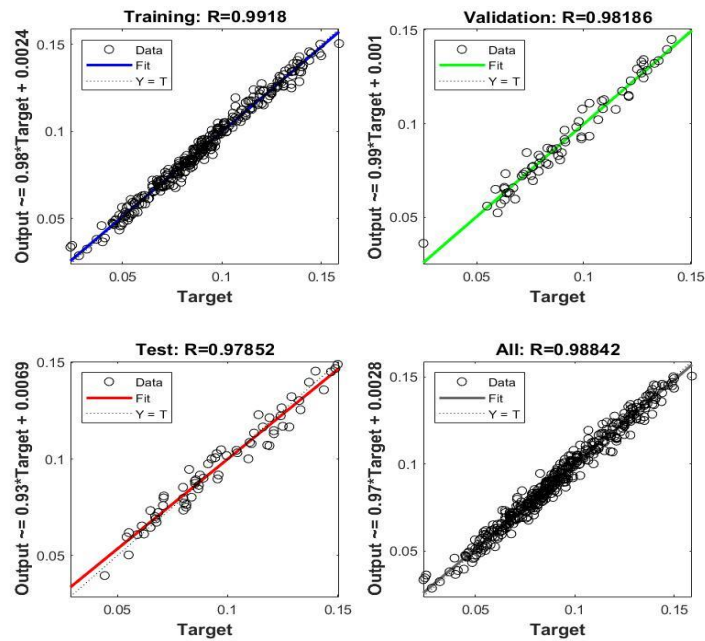


Fig. 5.10 Predicted ANN output vs. the experimental value of k_{La} in the presence of TiO_2 nanofluid for the (a) training, (b) testing, and (c) validation data points (d) overall data points.

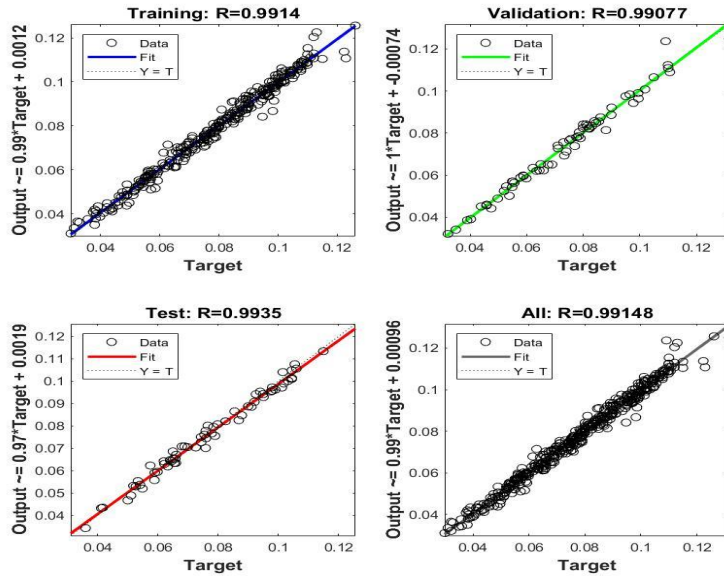


Fig. 5.11 Predicted ANN output vs. the experimental value of k_{LA} in the presence of SiO_2 nanofluids for the (a) training, (b) testing and (c) validation data points (d) overall data points.

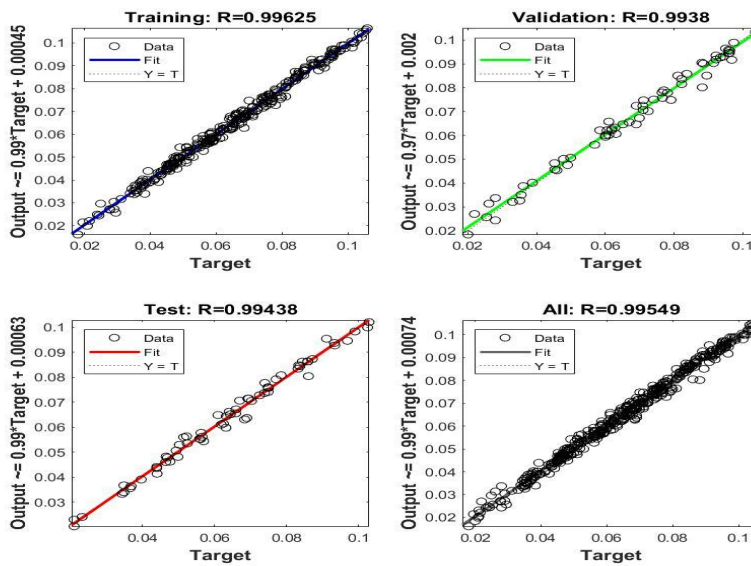


Fig. 5.12 Predicted ANN output vs. the experimental value of k_{LA} in the presence of $\alpha\text{-Fe}_2\text{O}_3$ nanofluids for the (a) training, (b) testing and (c) validation data points (d) overall data points.

Chapter 6 Summary and Conclusions

Volumetric oxygen mass transfer coefficients (k_{LA}) in PPC in the presence of TiO_2 , SiO_2 and $\alpha-Fe_2O_3$ nanofluids were determined at different experimental conditions. The effect of weight percent of nanoparticles, size of nanoparticles, frequency of pulsation of plates, amplitude of pulsation of plates and superficial air velocity on volumetric oxygen mass transfer coefficient were studied.

Based on the results of experiments conducted and interpretations thereof, the following conclusions were drawn.

- TiO_2 -25, TiO_2 -72, SiO_2 -12, SiO_2 -24, $\alpha-Fe_2O_3$ -43 and $\alpha-Fe_2O_3$ -76 nanofluids efficiently enhanced k_{LA} in PPC with reference to base fluids.
- k_{LA} was found to increase with the increase in nanoparticle loading, reached a maximum and then decreased with further increase in nanoparticle loading. The nanoparticle loading of 0.068 % w/v and 0.051% w/v have been found to be optimum for TiO_2 -25 and TiO_2 -72 nanofluid respectively. Similarly, the nanoparticle loading of 0.051 % w/v has been found to be optimum for SiO_2 -12 and SiO_2 -24 nanofluids. Also, the nanoparticle loading of 0.034 % w/v has been found to be optimum for $\alpha-Fe_2O_3$ -43 and $\alpha-Fe_2O_3$ -76 nanofluids.
- k_{LA} was found to be increased with increase in frequency of pulsation from $0.25s^{-1}$ to $1s^{-1}$ and also found that maximum k_{LA} was obtained at frequency of pulsation of $1s^{-1}$ with all the amplitude conditions studied. whereas, the maximum enhancement factor was obtained at the lowest frequency.
- k_{LA} increased with increase in amplitude of pulsation from 3.2cm to 6.3cm and maximum enhancement factor was obtained at lowest amplitude.
- k_{LA} increased with increase in superficial air velocity from 0.011m/s to 0.029m/s and maximum enhancement factor was obtained at lowest superficial air velocity.

- Nanofluids with lower size particles such as TiO₂-25, SiO₂-12, and α-Fe₂O₃-43 provided higher k_{LA} compared to those with higher size particles *viz.* TiO₂-72, SiO₂-24 and α-Fe₂O₃-76 nanofluids.
- One or more of the hydrodynamic regimes could be observed in terms of the effect of the pulsing velocity on k_{LA} and the pulsing velocity for regime transition depends on the type of nanofluids, size of nanoparticles, and nanoparticle loading.
- k_{LA} enhancement with nanofluid is better at lower pulsing conditions.
- A maximum enhancement factor of 4.37 could be achieved with TiO₂-25 nanofluid followed by that with TiO₂-72 nm which provided an enhancement factor of 2.39 under optimum conditions of A= 3.2 cm, f=0.25 s⁻¹, and U_g=0.011 m/s.
- The enhancement factor provided by SiO₂ nanofluids was in the range of 2.17 (SiO₂-24 nanofluid) and 2.30 with SiO₂-12 nanofluid, whereas the least enhancement of around 1.65 and 1.61 could be achieved with α-Fe₂O₃-43 and α-Fe₂O₃-76 nanofluid.
- TiO₂ nanofluid provides better k_{LA} enhancement factor than SiO₂ and α-Fe₂O₃ nanofluid. Therefore, it can be concluded that the size of nanoparticles in the nanofluid is not the only determining factor for gas-liquid mass transfer enhancement. The type of nanoparticles also changes the characteristics of the nanofluid and thus k_{LA} enhancement is also a function of the type of nanoparticles.
- Order of magnitude analysis implies that the convection currents caused by Brownian motion of the particles is much faster than the mass diffusion of oxygen or the Brownian motion of the particle itself. Thus, the disturbance field created by the Brownian motion of the nanoparticles in the fluid can be the possible reason for the enhancement in mass transport.
- Pseudo homogeneous model was applied to predict k_{LA} enhancement with nanofluid and these results indicate that the model can accurately predict the

enhancement till the critical loading conditions, but not at loading conditions above the critical loading.

- This model could be used to determine the surface renewal rates at critical loading conditions, which were found to increase with the pulsing velocities and superficial air velocities.
- Dimensionless MRA models involving Sherwood number, Oscillating Reynolds number, Gas flow Reynolds number, Schmidt number, and Brownian Reynolds number, were developed to predict k_{LA} with TiO_2 , SiO_2 and $\alpha-Fe_2O_3$ nanofluids in pulsed plate column using the experimental data.
- Further ANN based model was developed with 10 hidden neurons to predict k_{LA} with nanoparticle size, superficial air velocity, amplitude of pulsation, frequency of pulsation and nanoparticle loading as the input parameters, by training with the experimental input-output data. Further the ANN model was tested and validated with the experimental results.

The results of this study indicate that the pulsing conditions required to achieve the desired mass transfer characteristics can be reduced by using a nanofluid instead of the base fluid. It is concluded that the enhanced oxygen mass transfer characteristics can be achieved with the TiO_2 , SiO_2 , and $\alpha-Fe_2O_3$ nanofluids in the pulsed plate column with the tremendous saving of energy. The contribution of this study to the field of mass transfer includes the addition of new knowledge on the extent of mass transfer enhancement that could be achieved by using nanofluids in pulsed plate column. The dimensionless correlations and ANN models developed in the present study can accurately predict k_{LA} and thus may find potential applications in the design of pulsed plate column when used as gas-liquid mass transfer contactors, bioreactors, or photocatalytic reactors.

Future Scope of the Work

- Studies on the performance of the Pulsed plate column as a bioreactor in the presence of nanofluids.
- Studies on CO₂ absorption in the Pulsed plate column in the presence of nanofluids.
- Studies on mass transfer enhancement in liquid-liquid extraction system in the presence of nanofluids in pulsed plate column.
- Studies on the effect of liquid velocity on gas-liquid mass transfer coefficient in a Pulsed plate column operated under continuous mode.

References

- Abareshi, M., Sajjadi, S. H., Zebarjad, S. M., and Goharshadi, E. K. (2011). "Fabrication, characterization, and measurement of viscosity of α -Fe₂O₃-glycerol nanofluids." *J. Mol. Liq.*, 163(1), 27–32.
- Abbas, Z., Labbez, C., Nordholm, S., and Ahlberg, E. (2008). "Size-dependent surface charging of nanoparticles." *J. Phys. Chem. C*, 112(15), 5715–5723.
- Abbott, M. S. R., Harvey, A. P., Valente Perez, G., and Theodorou, M. K. (2013). "Biological processing in oscillatory baffled reactors: Operation, advantages and potential." *Interface Focus*, Royal Society.
- Abufalgha, A. (2018). "Behaviour of oxygen transfer in a simulated multiphase hydrocarbon-based bioprocess in a bubble column reactor." *Master. thesis, Univeristy of Stellenbosch*, (March).
- Aglawe, K. R., Yadav, R. K., and Thool, S. B. (2020). "Preparation, applications and challenges of nanofluids in electronic cooling: A systematic review." *Mater. Today Proc.*, 43, 366–372.
- Agnihotri, P., Tala, R., Doot, P., and Lad, V. N. (2019). "Microfluidics for selective concentration of nanofluid streams containing magnetic nanoparticles." *Sep. Sci. Technol.*, 54(2), 289–292.
- Akhgar, S., Safdari, J., Towfighi, J., Amani, P., and Mallah, M. H. (2017a). "Experimental investigation on regime transition and characteristic velocity in a horizontal–vertical pulsed sieve-plate column." *RSC Adv.*, 7(4), 2288–2300.
- Akhgar, S., Safdari, J., Towfighi, J., Amani, P., and Mallah, M. H. (2017b). "Experimental investigation on regime transition and characteristic velocity in a horizontal-vertical pulsed sieve-plate column." *RSC Adv.*, 7(4), 2288–2300.
- Akita, K., and Yoshida, F. (1973). "Gas Holdup and Volumetric Mass Transfer Coefficient in Bubble Columns. Effects of Liquid Properties." *Ind. Eng. Chem. Process Des. Dev.*, 12(1), 76–80.
- Ali, H. M., Babar, H., Shah, T. R., Sajid, M. U., Qasim, M. A., and Javed, S. (2018).

“Preparation techniques of TiO₂ nanofluids and challenges: A review.” *Appl. Sci.*, 8(4).

Ali, R., Asjad, M. I., and Akgül, A. (2021). “An analysis of a mathematical fractional model of hybrid viscous nanofluids and its application in heat and mass transfer.” *J. Comput. Appl. Math.*, 383, 113096.

Alper, E., Wichtendahl, B., and Deckwer, W. D. (1980). “Gas absorption mechanism in catalytic slurry reactors.” *Chem. Eng. Sci.*, 35(1–2), 217–222.

Amani, P., Safdari, J., Gharib, A., Badakhshan, H., and Mallah, M. H. (2017). “Mass transfer studies in a horizontal pulsed sieve-plate column for uranium extraction by tri-n-octylamine using axial dispersion model.” *Prog. Nucl. Energy*, 98, 71–84.

Amaral, A., Gillot, S., Garrido-Baserba, M., Filali, A., Karpinska, A. M., Plósz, B. G., Groot, C. de, Bellandi, G., Nopens, I., Takács, I., Lizarralde, I., Jimenez, J. A., Fiat, J., Rieger, L., Arnell, M., Andersen, M., Jeppsson, U., Rehman, U., Fayolle, Y., Amerlinck, Y., and Rosso, D. (2019). “Modelling gas–liquid mass transfer in wastewater treatment: When current knowledge needs to encounter engineering practice and vice versa.” *Water Sci. Technol.*, 80(4), 607–619.

Amaris, C., Bourouis, M., and Vallès, M. (2014). “Passive intensification of the ammonia absorption process with NH₃/LiNO₃ using carbon nanotubes and advanced surfaces in a tubular bubble absorber.” *Energy*, 68, 519–528.

An, G., Sun, B., An, Y. H., Qian, M. H., and Xu, Q. (2010). “Reaction rate of NaCO₃-CO₂-H₂O system in bubbling column with reciprocating plate.” *Guocheng Gongcheng Xuebao/The Chinese J. Process Eng.*

Anoop, K. B., Kabelac, S., Sundararajan, T., and Das, S. K. (2009). “Rheological and flow characteristics of nanofluids: influence of electroviscous effects and particle agglomeration.” *J. Appl. Phys.*, 106(3), 34909.

Ardestani, F., Ghaemi, A., Safdari, J., and Hemmati, A. (2021). “Modeling of mass transfer coefficient using response surface methodology in a horizontal-vertical pulsed sieve-plate extraction column.” *Prog. Nucl. Energy*, 139.

Armaković, S. J., Savanović, M. M., and Armaković, S. (2023). “Titanium Dioxide as

- the Most Used Photocatalyst for Water Purification: An Overview.” *Catalysts*, 13(1).
- Armou, S., Mir, R., Hammami, Y. El, Zine-Dine, K., and Hattab, M. El. (2017). “Heat and mass transfer enhancement in absorption of vapor in laminar liquid film by adding nano-particles.” *J. Appl. Fluid Mech.*, 10(6), 1711–1720.
- Ashrafmansouri, S.-S., and Esfahany, M. N. (2014). “Mass transfer in nanofluids: A review.” *Int. J. Therm. Sci.*, 82, 84–99.
- Ashrafmansouri, S. S., and Nasr Esfahany, M. (2014a). “Mass transfer in nanofluids: A review.” *Int. J. Therm. Sci.*, 82(1), 84–99.
- Ashrafmansouri, S. S., and Nasr Esfahany, M. (2014b). “Mass transfer in nanofluids: A review.” *Int. J. Therm. Sci.*, Elsevier Masson s.r.l.
- Ashrafmansouri, S. S., Willersinn, S., Esfahany, M. N., and Bart, H. J. (2016a). “Influence of silica nanoparticles on mass transfer in a membrane-based micro-contactor.” *RSC Adv.*, 6(23), 19089–19097.
- Ashrafmansouri, S. S., Willersinn, S., Esfahany, M. N., and Bart, H. J. (2016b). “Influence of silica nanoparticles on mass transfer in a membrane-based micro-contactor.” *RSC Adv.*, 6(23), 19089–19097.
- Ataíde, F. A. P., Azevedo, C. de, Lima, J. C., Leblebici, M. E., Dias, M., Lopes, J. C., and Oliveira, R. (2013). “Oxygen Transport Enhancement By Functionalized Magnetic Nanoparticles (FMP) In Bioprocesses.” *9th Eur. Congr. Chem. Eng.*
- Audet, J., Thibault, J., and LeDuy, A. (1996). “Polysaccharide concentration and molecular weight effects on the oxygen mass transfer in a reciprocating plate bioreactor.” *Biotechnol. Bioeng.*, 52(4), 507–517.
- Azimi, N., Rahimi, M., Khodaei, M. M., Roshani, M., Karami, E., Ebrahimi, E., and Mohammadi, F. (2019). “Intensification of liquid-liquid extraction in a tubular sono-extractor using 1.7 MHz ultrasound and SiO₂ nanoparticles.” *Chem. Eng. Process. Intensif.*, 137, 28–38.
- Baawain, M. S., El-Din, M. G., and Smith, D. W. (2007). “Artificial neural networks modeling of ozone bubble columns: Mass transfer coefficient, gas hold-up, and bubble

size.” *Ozone Sci. Eng.*, 29(5), 343–352.

Bahmanyar, A., Khoobi, N., Moharrer, M. M. A., and Bahmanyar, H. (2014). “Mass transfer from nanofluid drops in a pulsed liquid-liquid extraction column.” *Chem. Eng. Res. Des.*, 92(11), 2313–2323.

Bahmanyar, A., Khoobi, N., Mozdianfard, M. R., and Bahmanyar, H. (2011). “The influence of nanoparticles on hydrodynamic characteristics and mass transfer performance in a pulsed liquid-liquid extraction column.” *Chem. Eng. Process. Process Intensif.*, 50(11–12), 1198–1206.

Bairwa, D. K., Upman, K. K., and Kantak, G. (2015). “Nanofluids and its Applications.” *Int. J. Eng. Manag. Sci.*, 2(1), 14–17.

Barros, P. L., Ein-Mozaffari, F., and Lohi, A. (2022). “Gas Dispersion in Non-Newtonian Fluids with Mechanically Agitated Systems: A Review.” *Processes*, 10(2).

Baz-Rodríguez, S. A., Botello-Alvarez, J. E., Estrada-Baltazar, A., Vilchiz-Bravo, L. E., Padilla-Medina, J. A., and Miranda-López, R. (2014). “Effect of electrolytes in aqueous solutions on oxygen transfer in gas-liquid bubble columns.” *Chem. Eng. Res. Des.*, 92(11), 2352–2360.

Becher, P. (1972). “The calculation of cohesive energy density from the surface tension of liquids.” *J. Colloid Interface Sci.*, 38(2), 291–293.

Beiki, H., Esfahany, M. N., and Etesami, N. (2013a). “Turbulent mass transfer of Al₂O₃ and TiO₂ electrolyte nanofluids in circular tube.” *Microfluid. Nanofluidics*, 15(4), 501–508.

Beiki, H., Nasr Esfahany, M., and Etesami, N. (2013b). “Laminar forced convective mass transfer of γ -Al₂O₃/electrolyte nanofluid in a circular tube.” *Int. J. Therm. Sci.*, 64, 251–256.

Bhuiyan, M. H. U., Saidur, R., Amalina, M. A., Mostafizur, R. M., and Islam, A. K. M. S. (2015a). “Effect of nanoparticles concentration and their sizes on surface tension of nanofluids.” *Procedia Eng.*, Elsevier Ltd, 431–437.

Bhuiyan, M. H. U., Saidur, R., Amalina, M. A., Mostafizur, R. M., and Islam, A. K. M.

- S. (2015b). "Effect of nanoparticles concentration and their sizes on surface tension of nanofluids." *Procedia Eng.*, 105(Icte 2014), 431–437.
- Bhuiyan, M. H. U., Saidur, R., Mostafizur, R. M., Mahbubul, I. M., and Amalina, M. A. (2015c). "Experimental investigation on surface tension of metal oxide-water nanofluids." *Int. Commun. Heat Mass Transf.*, 65, 82–88.
- Bouaifi, M., Hebrard, G., Bastoul, D., Roustan, M., and 833, E. A. (2001). *A comparative study of gas hold-up, bubble size, interfacial area and mass transfer coefficients in stirred gas-liquid reactors and bubble columns. Chem. Eng. Process.*
- Boukerma, K., and Kadja, M. (2017). *Convective Heat Transfer of Al₂O₃ and CuO Nanofluids Using Various Mixtures of Water-Ethylene Glycol as Base Fluids. Technol. Appl. Sci. Res.*
- Brauer, H. (1985). "Biological waste water treatment in a reciprocating jet bioreactor, chapter 22 of Biotechnology, vol. 2." VCH Verlagsgesellschaft mbH, Weinheim.
- Brauer, H. (1990). "Growth of fungi and bacteria in the reciprocating jet bioreactor." *Bioprocess Eng.*, 6(1–2), 1–15.
- Brown, M. A., Duyckaerts, N., Redondo, A. B., Jordan, I., Nolting, F., Kleibert, A., Ammann, M., Wörner, H. J., Bokhoven, J. A. Van, and Abbas, Z. (2013). "Effect of surface charge density on the affinity of oxide nanoparticles for the vapor-water interface." *Langmuir*, 29(16), 5023–5029.
- Buongiorno, J. (2006). "Convective transport in nanofluids." *J. Heat Transfer*, 128(3), 240–250.
- Cabaleiro, D., Estellé, P., Navas, H., Desforges, A., and Vigolo, B. (2018). "Dynamic viscosity and surface tension of stable graphene oxide and reduced graphene oxide aqueous nanofluids." *J. Nanofluids*, 7(6), 1081–1088.
- Chamsa-ard, W., Brundavanam, S., Fung, C. C., Fawcett, D., and Poinern, G. (2017). *Nanofluid types, their synthesis, properties and incorporation in direct solar thermal collectors: A review. Nanomaterials.*
- Chang, H., Jwo, C. S., Lo, C. H., Su, C., Tsung, T. T., Chen, L. C., Lin, H. M., and

Kao, M. J. (2005). "Process development and photocatalytic property of nanofluid prepared by combined ASNSS." *Mater. Sci. Technol.*, 21(6), 671–677.

Chaturabul, S., Wannachod, P., Rojanasiraprapa, B., Summakasipong, S., Lothongkum, A. W., and Pancharoen, U. (2012). "Arsenic removal from natural gas condensate using a pulsed sieve plate column and mass transfer efficiency." *Sep. Sci. Technol.*, 47(3), 432–439.

Chen, H., Witharana, S., Jin, Y., Kim, C., and Ding, Y. (2009). "Predicting thermal conductivity of liquid suspensions of nanoparticles (nanofluids) based on rheology." *Particuology*, 7(2), 151–157.

Cheng, S. Y., Liu, Y. Z., and Qi, G. S. (2019). "Progress in the enhancement of gas–liquid mass transfer by porous nanoparticle nanofluids." *J. Mater. Sci.*, 54(20), 13029–13044.

Chiang, P.-C., and Pan, S.-Y. (2015). "Application of Mass Transfer Models in Environmental Engineering." *Mass Transf. - Adv. Process Model.*, InTech.

Choi, K. H., Chisti, Y., and Moo-Young, M. (1996). "Comparative evaluation of hydrodynamic and gas-liquid mass transfer characteristics in bubble column and airlift slurry reactors." *Chem. Eng. J. Biochem. Eng. J.*

Choi, S. U. S. (1995). "Enhancing thermal conductivity of fluids with nanoparticles." *Am. Soc. Mech. Eng. Fluids Eng. Div. FED*, 231(January 1995), 99–105.

Choy, V., Patel, N., and Thibault, J. (2011). "Application of image analysis in the fungal fermentation of *Trichoderma reesei* RUT-C30." *Biotechnol. Prog.*, 27(6), 1544–1553.

Daniel, S., and Brauer, H. (1994). "Continuous production of citric acid in the reciprocating-jet-bioreactor." *Bioprocess Eng.*, 11(4), 123–127.

Darvanjooghi, M. H. K., Esfahany, M. N., and Esmaeili-Faraj, S. H. (2018). "Investigation of the effects of nanoparticle size on CO₂ absorption by silica-water nanofluid." *Sep. Purif. Technol.*, 195, 208–215.

Das, A., Kumawat, P. K., and Chaturvedi, N. D. (2021). "A Study to Target Energy Consumption in Wastewater Treatment Plant using Machine Learning Algorithms."

Comput. Aided Chem. Eng., Elsevier, 1511–1516.

Das, S. K., Choi, S. U. S., and Patel, H. E. (2007). “Heat Transfer in Nanofluids — A Review Heat Transfer in Nanofluids —.” 7632(2006).

Dehghan, P., Azari, A., and Azin, R. (2020). “Measurement and correlation for CO₂ mass diffusivity in various metal oxide nanofluids.” *J. Environ. Chem. Eng.*, 8(1).

DEJAN, S., and VLADA, Veukov. (1988). “Mass Transfer Characteristics in a Gas-Liquid Reciprocating.” *Can. J. Chem. Eng.*, 66(Table 1).

Deodhar, M. S., Shirode, a R., and Kadam, V. J. (2014). “International Journal of Pharmaceutical Sciences and Drug Research Review Article CODEN (USA): IJPSPP High Performance Nanoparticle Fluid Suspensions (Nanofluids): A Future of Pharmaceutical Nanotechnology.” *Int. J. Pharm. Sci. Drug Res.*, 6(4), 263–270.

Deshmukh, G., Jose, N., Shidhav, R., Suryawanshi, A., Datir, R., and Ravindra, M. R. (2019). “Nanofluids : An Introduction to New Generation Heat Transfer Fluids.” 3(2), 41–48.

Dhanasekaran, S., and Karunanithi, T. (2010). “Mass transfer studies in a novel perforated plate bubble column.” *Int. J. Chem. React. Eng.*, 8.

Dhanasekaran, S., and Karunanithi, T. (2012a). “Bubble diameter and effective interfacial area in anovel hybrid rotating and reciprocating perforated plate bubble column.” *Int. J. Chem. React. Eng.*, 10(1).

Dhanasekaran, S., and Karunanithi, T. (2012b). “Improved gas holdup in novel bubble column.” *Can. J. Chem. Eng.*, 90(1), 126–136.

Dhinesh Kumar, D., and Valan Arasu, A. (2018). “A comprehensive review of preparation, characterization, properties and stability of hybrid nanofluids.” *Renew. Sustain. Energy Rev.*, 81(May 2017), 1669–1689.

Dhuriya, R., Dalia, V., and Sunthar, P. (2018). “Diffusiophoretic enhancement of mass transfer by nanofluids.” *Chem. Eng. Sci.*, 176, 632–640.

Ding, C., Xu, C., He, T., Liu, X., Zhu, Y., Sun, L., Ouyang, J., and Gu, X. (2023).

“Oxygen mass transfer enhancement by activated carbon particles in xylose fermentation media.” *Bioprocess Biosyst. Eng.*, 46(1), 15–23.

Dong, J., Zheng, Q., Xiong, C., Sun, E., and Chen, J. (2022). “Experimental investigation and application of stability and thermal characteristics of SiO₂-ethylene-glycol/water nanofluids.” *Int. J. Therm. Sci.*, 176(December 2021), 107533.

Duangthongsuk, W., and Wongwises, S. (2009). “Measurement of temperature-dependent thermal conductivity and viscosity of TiO₂-water nanofluids.” *Exp. Therm. Fluid Sci.*, 33(4), 706–714.

Eastman, J. A., Phillpot, S. R., Choi, S. U. S., and Keblinski, P. (2004). “Thermal transport in nanofluids.” *Annu. Rev. Mater. Res.*, 34, 219–246.

El-Naas, M. H., Mohammad, A. F., Suleiman, M. I., Musharfy, M. Al, and Al-Marzouqi, A. H. (2017). “Evaluation of a novel gas-liquid contactor/reactor system for natural gas applications.” *J. Nat. Gas Sci. Eng.*, 39, 133–142.

Elhambakhsh, A., Heidari, S., and Keshavarz, P. (2021). “Experimental study of carbon dioxide absorption by Fe₂O₃@ glutamine/NMP nanofluid.” *Environ. Sci. Pollut. Res.*, 29(1), 1060–1072.

Erzin, Y., Gumaste, S. D., Gupta, A. K., and Singh, D. N. (2009). “Artificial neural network (ANN) models for determining hydraulic conductivity of compacted fine-grained soils.” *Can. Geotech. J.*, 46(8), 955–968.

Esmaili-Faraj, S. H., and Nasr Esfahany, M. (2016). “Absorption of Hydrogen Sulfide and Carbon Dioxide in Water Based Nanofluids.” *Ind. Eng. Chem. Res.*, 55(16), 4682–4690.

Esmaili Faraj, S. H., Esfahany, M. N., Jafari-Asl, M., and Etesami, N. (2014). “Hydrogen sulfide bubble absorption enhancement in water-based nanofluids.” *Ind. Eng. Chem. Res.*, 53(43), 16851–16858.

Fang, L., Liu, H., Bian, Y., Liu, Y., and Yang, Y. (2017). “Experimental study on enhancement of bubble absorption of gaseous CO₂ with nanofluids in ammonia.” *J. Harbin Inst. Technol.*, 242, 80–86.

- Fang, X., Xuan, Y., and Li, Q. (2009a). "Experimental investigation on enhanced mass transfer in nanofluids." *Appl. Phys. Lett.*, 95(20).
- Fang, X., Xuan, Y., and Li, Q. (2009b). "Experimental investigation on enhanced mass transfer in nanofluids." *Appl. Phys. Lett.*, 95(20), 2–5.
- Feng, X., and Johnson, D. W. (2012). "Mass transfer in SiO₂ nanofluids: A case against purported nanoparticle convection effects." *Int. J. Heat Mass Transf.*, 55(13–14), 3447–3453.
- Gaganpreet, and Srivastava, S. (2015). "Viscosity of nanofluids: particle shape and fractal aggregates." *Phys. Chem. Liq.*, 53(2), 174–186.
- Gagnon, H., Lounès, M., and Thibault, J. (1998). "Power consumption and mass transfer in agitated gas-liquid columns: a comparative study." *Can. J. Chem. Eng.*, 76(3), 379–389.
- García-Ochoa, F., and Castro, E. G. (2001). "Estimation of oxygen mass transfer coefficient in stirred tank reactors using artificial neural networks." *Enzyme Microb. Technol.*, 28(6), 560–569.
- García-Ochoa, F., and Gomez, E. (2005). "Prediction of gas-liquid mass transfer coefficient in sparged stirred tank bioreactors." *Biotechnol. Bioeng.*, 92(6), 761–772.
- García-Ochoa, F., and Gomez, E. (2009). "Bioreactor scale-up and oxygen transfer rate in microbial processes: An overview." *Biotechnol. Adv.*
- García-Ochoa, F., and Gómez, E. (1998). "Mass transfer coefficient in stirred tank reactors for xanthan gum solutions." *Biochem. Eng. J.*, 1(1), 1–10.
- Ghadyanlou, F., Azari, A., and Vatani, A. (2022). "Experimental Investigation of Mass Transfer Intensification for CO₂ Capture by Environment-Friendly Water Based Nanofluid Solvents in a Rotating Packed Bed." *Sustain.*, 14(11).
- Ghani, S. A. (2012). "Experimental Study of Volumetric Mass Transfer Coefficients in Slurry Bubble Column Reactor." *J. Chem. Eng. Process Technol.*, 03(03), 10–13.
- Ghasem, N. (2019). "Modeling and simulation of CO₂ absorption enhancement in

hollow-fiber membrane contactors using CNT-water-based nanofluids.” *J. Membr. Sci. Res.*, 5(4), 295–302.

Ghazanfari, M. R., Kashefi, M., Shams, S. F., and Jaafari, M. R. (2016). “Perspective of Fe₃O₄ Nanoparticles Role in Biomedical Applications.” *Biochem. Res. Int.*, Hindawi Limited.

Ghazvehi, M., Nasiri, M., Mallah, M. H., and Safdari, J. (2021). “Influence of SiO₂ Nanoparticles and Surfactants on Extraction Efficiency: Sensitivity Analysis.” *Chem. Eng. Technol.*, 44(10), 1929–1938.

Godson, L., Raja, B., Lal, D. M., and Wongwises, S. (2010). “Experimental investigation on the thermal conductivity and viscosity of silver-deionized water nanofluid.” *Exp. Heat Transf.*, 23(4), 317–332.

Golkhar, A., Keshavarz, P., and Mowla, D. (2013). “Investigation of CO₂ removal by silica and CNT nanofluids in microporous hollow fiber membrane contactors.” *J. Memb. Sci.*, 433, 17–24.

Gomaa, H. G., and Taweel, A. M. Al. (2005). “Axial mixing in a novel pilot scale gas-liquid reciprocating plate column.” *Chem. Eng. Process. Process Intensif.*, 44(12), 1285–1295.

Gómez-Díaz, D., Gomes, N., Teixeira, J. A., and Belo, I. (2009). “Oxygen mass transfer to emulsions in a bubble column contactor.” *Chem. Eng. J.*, 152(2–3), 354–360.

Gupta, S. D., and Ibaraki, Y. (2006). *Plant tissue culture engineering*. Springer.

Gupta, S. K., Gupta, S., Gupta, T., Raghav, A., and Singh, A. (2020). “A review on recent advances and applications of nanofluids in plate heat exchanger.” *Mater. Today Proc.*

Gwiazda, A., Dziubiński, M., and Budzyński, P. (2020). “Intensification of mass transfer in the pulsed bubble column—Comparison of the efficiency of static and pulsed aerator.” *Chem. Eng. Process. - Process Intensif.*, 153.

H.G. Gomma, J. L. and A. M. A. T. (1991). “Gas Liquid Contacting.” (1986).

- Haghtalab, A., Mohammadi, M., and Fakhroueian, Z. (2015a). "Absorption and solubility measurement of CO₂ in water-based ZnO and SiO₂ nanofluids." *Fluid Phase Equilib.*, 392, 33–42.
- Haghtalab, A., Mohammadi, M., and Fakhroueian, Z. (2015b). "Absorption and solubility measurement of CO₂ in water-based ZnO and SiO₂ nanofluids." *Fluid Phase Equilib.*, 392, 33–42.
- Ham, P., Bun, S., Painmanakul, P., and Wongwailikhit, K. (2021). "Effective analysis of different gas diffusers on bubble hydrodynamics in bubble column and airlift reactors towards mass transfer enhancement." *Processes*, 9(10).
- Hamid, K. A., Azmi, W. H., Nabil, M. F., Mamat, R., and Sharma, K. V. (2018). "Experimental investigation of thermal conductivity and dynamic viscosity on nanoparticle mixture ratios of TiO₂-SiO₂ nanofluids." *Int. J. Heat Mass Transf.*, 116, 1143–1152.
- Han, Y., Huang, X., Lu, Y., Zhu, D., and Shi, X. (2021). "Study of intrinsic oxygen mass transfer characteristic and model on polypropylene hollow fiber membrane contactor." *Int. Commun. Heat Mass Transf.*, 121, 105045.
- Haque, M. E., Bakar, R. A., Kadirgama, K., Noor, M. M., and Shakaib, M. (2016). "Performance of a domestic refrigerator using nanoparticles-based polyolester oil lubricant." *J. Mech. Eng. Sci.*, 10(1), 1778–1791.
- Hasani Goodarzi, H., and Nasr Esfahany, M. (2016). "Experimental investigation of the effects of the hydrophilic silica nanoparticles on mass transfer and hydrodynamics of single drop extraction." *Sep. Purif. Technol.*, 170, 130–137.
- Hassan, Y. M., Guan, B. H., Chuan, L. K., Hamza, M. F., Adil, M., and Adam, A. A. (2022). "The synergistic effect of Fe₂O₃/SiO₂ nanoparticles concentration on rheology, wettability, and brine-oil interfacial tension." *J. Pet. Sci. Eng.*, 210(August 2021), 110059.
- Hatami, A., Bastani, D., and Najafi, F. (2017a). "Investigation the effect of super hydrophobic titania nanoparticles on the mass transfer performance of single drop liquid-liquid extraction process." *Sep. Purif. Technol.*, 176, 107–119.

Hatami, A., Bastani, D., and Najafi, F. (2017b). "Investigation the effect of super hydrophobic titania nanoparticles on the mass transfer performance of single drop liquid-liquid extraction process." *Sep. Purif. Technol.*, 176, 107–119.

He, Y., Jin, Y., Chen, H., Ding, Y., Cang, D., and Lu, H. (2007). "Heat transfer and flow behaviour of aqueous suspensions of TiO₂ nanoparticles (nanofluids) flowing upward through a vertical pipe." *Int. J. Heat Mass Transf.*, 50(11–12), 2272–2281.

He, Y., Li, H., Hu, Y., Wang, X., and Zhu, J. (2016). "Boiling heat transfer characteristics of ethylene glycol and water mixture based ZnO nanofluids in a cylindrical vessel." *Int. J. Heat Mass Transf.*, 98, 611–615.

Hemmat Esfe, M., Afrand, M., Yan, W. M., and Akbari, M. (2015a). "Applicability of artificial neural network and nonlinear regression to predict thermal conductivity modeling of Al₂O₃-water nanofluids using experimental data." *Int. Commun. Heat Mass Transf.*, 66, 246–249.

Hemmat Esfe, M., Saedodin, S., Wongwises, S., and Toghraie, D. (2015b). "An experimental study on the effect of diameter on thermal conductivity and dynamic viscosity of Fe/water nanofluids." *J. Therm. Anal. Calorim.*, 119(3), 1817–1824.

Hewgill, M. R., Mackley, M. R., Pandit, A. B., and Pannu, S. S. (1993). "Enhancement of gas-liquid mass transfer using oscillatory flow in a baffled tube." *Chem. Eng. Sci.*, 48(4), 799–809.

Ho, D., Kim, K., Earmme, T., and Kim, C. (2020). "Enhancing gas-liquid volumetric mass transfer coefficient." *J. Ind. Eng. Chem.*, 87, 1–17.

Hu, X., Yin, D., Chen, X., and Xiang, G. (2020). "Experimental investigation and mechanism analysis: Effect of nanoparticle size on viscosity of nanofluids." *J. Mol. Liq.*, 314, 113604.

Huang, M., Zhu, C., Fu, T., and Ma, Y. (2021). "Enhancement of gas-liquid mass transfer by nanofluids in a microchannel under Taylor flow regime." *Int. J. Heat Mass Transf.*, 176, 121435.

Imran, M., Chaudhary, A. A., Ahmed, S., Alam, M. M., Khan, A., Zouli, N., Hakami,

- J., Rudayni, H. A., and Khan, S. U. D. (2022). “Iron Oxide Nanoparticle-Based Ferro-Nanofluids for Advanced Technological Applications.” *Molecules*, MDPI.
- Irani, V., Maleki, A., and Tavasoli, A. (2019a). “CO₂ absorption enhancement in graphene-oxide/MDEA nanofluid.” *J. Environ. Chem. Eng.*, 7(1), 102782.
- Irani, V., Maleki, A., and Tavasoli, A. (2019b). “CO₂ absorption enhancement in graphene-oxide/MDEA nanofluid.” *J. Environ. Chem. Eng.*, 7(1), 102782.
- Jafari, F., Saien, J., and Rashidi, A. (2022). “Mass transfer intensification for carbon quantum dot nanofluid drops under pulsed electric fields.”
- Jafari Farsaani, D., and Ameri, E. (2022). “Effect of sodium dodecyl sulfate on CO₂ and H₂S absorption enhancement of functionalized multiwall carbon nanotubes in water: Experimental study and empirical model.” *Arab. J. Chem.*, 15(12), 104314.
- Jafarimoghaddam, A., and Aberoumand, S. (2017). “A Comparison between heat transfer performance of rectangular and semicircular tubes considering boundary effects on Brownian motions in the presence of Ag / water nanofluids: Applicable in the design of cooling system of photovoltaic cells.” *PLoS One*, 12(7).
- Jagannath, A., Vidya Shetty, K., and Saidutta, M. B. (2017). “Bioleaching of copper from electronic waste using *Acinetobacter* sp. Cr B2 in a pulsed plate column operated in batch and sequential batch mode.” *J. Environ. Chem. Eng.*, 5(2), 1599–1607.
- Jama, M., Singh, T., Gamaleldin, S. M., Koc, M., Samara, A., Isaifan, R. J., and Atieh, M. A. (2016). “Critical Review on Nanofluids: Preparation, Characterization, and Applications.” *J. Nanomater.*, Hindawi Limited.
- Jamialahmadi, M., and Müller-Steinhagen, H. (1993). “Effect of Superficial Gas Velocity on Bubble Size, Terminal Bubble Rise Velocity and Gas Hold-up in Bubble Columns.” *Dev. Chem. Eng. Miner. Process.*, 1(1), 16–31.
- Jang, S. P., and Choi, S. U. S. (2004). “Role of Brownian motion in the enhanced thermal conductivity of nanofluids.” *Appl. Phys. Lett.*, 84(21), 4316–4318.
- Janghorban Esfahani, I., Ataei, A., Shetty, K. V., Oh, T. S., Park, J. H., and Yoo, C. K. (2012). “Modeling and genetic algorithm-based multi-objective optimization of the

MED-TVC desalination system.” *Desalination*, 292, 87–104.

Jeelani, P. G., Mulay, P., Venkat, R., and Ramalingam, C. (2020). “Multifaceted Application of Silica Nanoparticles. A Review.” *Silicon*, 12(6), 1337–1354.

Jiang, J. Z., Zhang, S., Fu, X. L., Liu, L., and Sun, B. M. (2019a). “Review of gas–liquid mass transfer enhancement by nanoparticles from macro to microscopic.” *Heat Mass Transf. und Stoffuebertragung*, 55(8), 2061–2072.

Jiang, J. Z., Zhang, S., Fu, X. L., Liu, L., and Sun, B. M. (2019b). “Review of gas–liquid mass transfer enhancement by nanoparticles from macro to microscopic.” *Heat Mass Transf. und Stoffuebertragung*, Springer Verlag.

Jiang, J. Z., Zhang, S., Fu, X. L., Liu, L., and Sun, B. M. (2020). “Microscopic experimental study of nanoparticle motion for droplet evaporation enhancement in nanofluids.” *Int. Commun. Heat Mass Transf.*, 119(October), 104948.

Jiang, J. Z., Zhao, B., Cao, M., Zhuo, Y. Q., and Wang, S. J. (2015a). “Effect of nanoparticles on oxygen absorption enhancement during sulfite forced oxidation.” *Int. J. Heat Mass Transf.*, 90, 1098–1104.

Jiang, J. Z., Zhao, B., Cao, M., Zhuo, Y. Q., and Wang, S. J. (2015b). “Effect of nanoparticles on oxygen absorption enhancement during sulfite forced oxidation.” *Int. J. Heat Mass Transf.*, 90, 1098–1104.

Jiang, Y., Zhang, Z., Fan, J., Yu, J., Bi, D., Li, B., Zhao, Z., Jia, M., and Mu, A. (2019c). “Experimental study on comprehensive carbon capture performance of TETA-based nanofluids with surfactants.” *Int. J. Greenh. Gas Control*, 88, 311–320.

Jiao, C., Ma, S., and Song, Q. (2013a). “Mass transfer characteristics in a standard pulsed sieve-plate extraction column.” *Energy Procedia*, 39, 348–357.

Jiao, C., Ma, S., and Song, Q. (2013b). “Mass transfer characteristics in a standard pulsed sieve-plate extraction column.” *Energy Procedia*, Elsevier Ltd, 348–357.

Jokiel, M., Wagner, L. M., Mansour, M., Kaiser, N. M., Zähringer, K., Janiga, G., Nigam, K. D. P., Thévenin, D., and Sundmacher, K. (2017). “Measurement and simulation of mass transfer and backmixing behavior in a gas-liquid helically coiled

tubular reactor.” *Chem. Eng. Sci.*, 170, 410–421.

K R, S., Nair, A. S., K M, V., T R, S., and Nair, S. C. (2014). “an Overview of Recent Nanofluid Research.” *Int. Res. J. Pharm.*, 5(4), 239–243.

Kahani, M., and Vatankhah, G. (2019). “Thermal performance prediction of wickless heat pipe with Al₂O₃/water nanofluid using artificial neural network.” *Chem. Eng. Commun.*, 206(4), 509–523.

Kandelousi, M. S. (2017). *Nanofluid heat and mass transfer in engineering problems*. BoD–Books on Demand.

Karimi Darvanjooghi, M. H., Pahlevaninezhad, M., Abdollahi, A., and Davoodi, S. M. (2017). “Investigation of the effect of magnetic field on mass transfer parameters of CO₂ absorption using Fe₃O₄-water nanofluid.” *AIChE J.*, 63(6), 2176–2186.

Karr, A. E. (1959). “Performance of a reciprocating-plate extraction column.” *AIChE J.*, 5(4), 446–452.

Kebllinski, P., Eastman, J. A., and Cahill, D. G. (2005a). “Nanofluids for thermal transport.” *Mater. Today*, 8(6), 36–44.

Kebllinski, P., Eastman, J. A., and Cahill, D. G. (2005b). “Nanofluids for thermal transport.” *Mater. Today*, 8(6), 36–44.

Kebllinski, P., Phillpot, S. R., Choi, S. U. S., and Eastman, J. A. (2001a). “Mechanisms of heat flow in suspensions of nano-sized particles (nanofluids).” *Int. J. Heat Mass Transf.*, 45(4), 855–863.

Kebllinski, P., Phillpot, S. R., Choi, S. U. S., and Eastman, J. A. (2001b). “Mechanisms of heat flow in suspensions of nano-sized particles (nanofluids).” *Int. J. Heat Mass Transf.*, 45(4), 855–863.

Keshishian, N., Nasr Esfahany, M., and Etesami, N. (2013). “Experimental investigation of mass transfer of active ions in silica nanofluids.” *Int. Commun. Heat Mass Transf.*, 46, 148–153.

Khalil, M., Jan, B. M., Tong, C. W., and Berawi, M. A. (2017). “Advanced

nanomaterials in oil and gas industry: Design, application and challenges.” *Appl. Energy*, Elsevier Ltd.

Khan, I., Saeed, K., and Khan, I. (2019). “Nanoparticles: Properties, applications and toxicities.” *Arab. J. Chem.*, Elsevier B.V.

Khanna, A., and Shetty, V. K. (2014). “Solar light induced photocatalytic degradation of Reactive Blue 220 (RB-220) dye with highly efficient Ag@TiO₂ core-shell nanoparticles: A comparison with UV photocatalysis.” *Sol. Energy*, 99, 67–76.

Khanolkar, R. U., and Suresh, A. K. (2015). “Enhanced mass transfer rates in nanofluids: Experiments and modeling.” *J. Heat Transfer*, 137(9), 1–6.

Khooshechin, S., Moosavian, M. A., Safdari, J., and Mallah, M. H. (2017). “Mass transfer investigation in a horizontal-vertical pulsed packed extraction column.” *RSC Adv.*, 7(87), 55326–55335.

Kim, J.-K., Jung, J. Y., and Kang, Y. T. (2007). “Absorption performance enhancement by nano-particles and chemical surfactants in binary nanofluids.” *Int. J. Refrig.*, 30(1), 50–57.

Kim, J. H., Jung, C. W., and Kang, Y. T. (2014a). “Mass transfer enhancement during CO₂ absorption process in methanol/Al₂O₃ nanofluids.” *Int. J. Heat Mass Transf.*, 76, 484–491.

Kim, J. H., Jung, C. W., and Kang, Y. T. (2014b). “Mass transfer enhancement during CO₂ absorption process in methanol/Al₂O₃ nanofluids.” *Int. J. Heat Mass Transf.*, 76, 484–491.

Kim, J., Jung, J. Y., and Kang, Y. T. (2006a). “The effect of nano-particles on the bubble absorption performance in a binary nanofluid ` me a Effet des nanoparticules sur la performance d ` un syste ` bulles utilisant un nanofluide binaire absorption a.” 29, 22–29.

Kim, J. K., Jung, J. Y., and Kang, Y. T. (2006b). “The effect of nano-particles on the bubble absorption performance in a binary nanofluid.” *Int. J. Refrig.*, 29(1), 22–29.

Kim, S. H., Kim, W. G., Kang, H. U., and Jung, K. M. (2008a). “Synthesis of silica

nanofluid and application to CO₂ absorption.” *Sep. Sci. Technol.*, 43(11–12), 3036–3055.

Kim, S. H., Kim, W. G., Kang, H. U., and Jung, K. M. (2008b). “Synthesis of silica nanofluid and application to CO₂ absorption.” *Sep. Sci. Technol.*, 43(11–12), 3036–3055.

Kim, Y., and Oh, H. (2021). “Comparison between multiple regression analysis, polynomial regression analysis, and an artificial neural network for tensile strength prediction of BFRP and GFRP.” *Materials (Basel)*., 14(17), 1–13.

Kimweri, H. T. H. (2001). “Enhancement of gas-liquid mass transfer in hydrometallurgical leaching systems.” University of British Columbia.

Kodialbail, V. S., and Srinikethan, G. (2011a). “Mixing and solid-liquid mass transfer characteristics in a three phase pulsed plate column with packed bed of solids in interplate spaces-a novel aerobic immobilized cell bioreactor.” *J. Chem. Technol. Biotechnol.*, 86(10), 1310–1320.

Kodialbail, V. S., and Srinikethan, G. (2011b). “Mixing and solid-liquid mass transfer characteristics in a three phase pulsed plate column with packed bed of solids in interplate spaces-a novel aerobic immobilized cell bioreactor.” *J. Chem. Technol. Biotechnol.*, 86(10), 1310–1320.

Kojić, P., and Omorjan, R. (2017). “Predicting hydrodynamic parameters and volumetric gas–liquid mass transfer coefficient in an external-loop airlift reactor by support vector regression.” *Chem. Eng. Res. Des.*, 125, 398–407.

Komati, S., and Suresh, A. K. (2008). “CO₂ absorption into amine solutions: A novel strategy for intensification based on the addition of ferrofluids.” *J. Chem. Technol. Biotechnol.*, 83(8), 1094–1100.

Komati, S., and Suresh, A. K. (2010). “Anomalous enhancement of interphase transport rates by nanoparticles: Effect of magnetic iron oxide on gas-liquid mass transfer.” *Ind. Eng. Chem. Res.*, 49(1), 390–405.

Krishnamurthy, S., Bhattacharya, P., Phelan, P. E., and Prasher, R. S. (2006a).

“Enhanced mass transport in nanofluids.” *Nano Lett.*, 6(3), 419–423.

Krishnamurthy, S., Bhattacharya, P., Phelan, P. E., and Prasher, R. S. (2006b). “Enhanced mass transport in nanofluids.” *Nano Lett.*, 6(3), 419–423.

Kumar, A., and Subudhi, S. (2019). “Preparation, characterization and heat transfer analysis of nanofluids used for engine cooling.” *Appl. Therm. Eng.*, 160, 114092.

Labbeiki, G., Attar, H., Heydarinasab, A., Sorkhabadi, S., and Rashidi, A. (2014). “Enhanced oxygen transfer rate and bioprocess yield by using magnetite nanoparticles in fermentation media of erythromycin.” *DARU, J. Pharm. Sci.*, 22(1).

Lade, V. G., Pakhare, A. D., and Rathod, V. K. (2014). “Mass transfer studies in pulsed sieve plate extraction column for the removal of tributyl phosphate from aqueous nitric acid.” *Ind. Eng. Chem. Res.*, 53(12), 4812–4820.

Larson, R. G. (1999). *The structure and rheology of complex fluids*. Oxford university press New York.

Lee, J.-H., Lee, S.-H., Choi, C., Jang, S., and Choi, S. (2011). “A review of thermal conductivity data, mechanisms and models for nanofluids.” *Int. J. micro-nano scale Transp.*

Lee, J. K., Kim, H., Kim, M. H., Koo, J., and Kang, Y. T. (2009). “The effect of additives and nanoparticles on falling film absorption performance of binary nanofluids (H₂O/LiBr⁺ nanoparticles).” *J. Nanosci. Nanotechnol.*, 9(12), 7456–7460.

Lee, J. K., Koo, J., Hong, H., and Kang, Y. T. (2010). “The effects of nanoparticles on absorption heat and mass transfer performance in NH₃/H₂O binary nanofluids.” *Int. J. Refrig.*, 33(2), 269–275.

Lee, J. W., and Kang, Y. T. (2013). “CO₂ absorption enhancement by Al₂O₃ nanoparticles in NaCl aqueous solution.” *Energy*, 53, 206–211.

Lee, K., Saipolbahri, Z. A. Bin, Soleimani, H., Zaid, H. M., Guan, B. H., and Ching, D. L. C. (2016). “Effect of zinc oxide nanoparticle sizes on viscosity of nanofluid for application in enhanced oil recovery.” *J. Nano Res.*, 38, 36–39.

- Lee, W., Xu, R., Kim, S., Park, J. H., and Kang, Y. T. (2021). “Nanofluid and nanoemulsion absorbents for the enhancement of CO₂ absorption performance.” *J. Clean. Prod.*, 291.
- Lemoine, R., Fillion, B., Behkish, A., Smith, A. E., and Morsi, B. I. (2003). “Prediction of the gas-liquid volumetric mass transfer coefficients in surface-aeration and gas-inducing reactors using neural networks.” *Chem. Eng. Process. Process Intensif.*, 42(8–9), 621–643.
- Levdanskii, V. V, and Smolik, J. (2008). *INFLUENCE OF SIZE EFFECTS ON GAS ABSORPTION BY NANOPARTICLES*. *J. Eng. Phys. Thermophys.*
- Lewis, W. K., and Whitman, W. G. (1924). “Principles of Gas Absorption.” *Ind. Eng. Chem.*, 16(12), 1215–1220.
- Li, L., Abild-Pedersen, F., Greeley, J., and Nørskov, J. K. (2015). “Surface Tension Effects on the Reactivity of Metal Nanoparticles.” *J. Phys. Chem. Lett.*, 6(19), 3797–3801.
- Li, W., Zhao, X., Liu, B., and Tang, Z. (2014). “Mass transfer coefficients for CO₂ absorption into aqueous ammonia using structured packing.” *Ind. Eng. Chem. Res.*, 53(14), 6185–6196.
- Linek, V., Kordač, M., and Soni, M. (2008). “Mechanism of gas absorption enhancement in presence of fine solid particles in mechanically agitated gas-liquid dispersion. Effect of molecular diffusivity.” *Chem. Eng. Sci.*, 63(21), 5120–5128.
- Littlejohns, J. V., and Daugulis, A. J. (2007). “Oxygen transfer in a gas-liquid system containing solids of varying oxygen affinity.” *Chem. Eng. J.*, 129(1–3), 67–74.
- Liu, T., Liu, Y., Wang, D., Li, Y., and Shao, L. (2019). “Artificial neural network modeling on the prediction of mass transfer coefficient for ozone absorption in RPB.” *Chem. Eng. Res. Des.*, 152, 38–47.
- Liu, Y., Guo, S., Wang, J., and Li, C. (2022). “Fundamental development and research of cathodic compartment in microbial fuel cells: A review.” *J. Environ. Chem. Eng.*, 10(3), 107918.

Liu Yang, Jian-nan Huang, Weikai Ji, M. M. (2020). “Investigations of a new combined application of nanofluids in heat recovery and air purification.” *Powder Technol.*, 360, 956–966.

Lounes, M., and Thibault, J. (1993). “Hydrodynamics and Power Consumption.” 71.

Lounes, M., and Thibault, J. (1994). “Mass Transfer in a Reciprocating Plate Bioreactor.” *Chem. Eng. Commun.*, 127(1), 169–189.

Lu, S., Song, J., Li, Y., Xing, M., and He, Q. (2015). “Improvement of CO₂ absorption using AL₂O₃ nanofluids in a stirred thermostatic reactor.” *Can. J. Chem. Eng.*, 93(5), 935–941.

Lu, S., Xing, M., Sun, Y., and Dong, X. (2013a). “Experimental and theoretical studies of CO₂ absorption enhancement by nano-Al₂O₃ and carbon nanotube particles.” *Chinese J. Chem. Eng.*, 21(9), 983–990.

Lu, S., Xing, M., Sun, Y., and Dong, X. (2013b). “Experimental and theoretical studies of CO₂ absorption enhancement by nano-Al₂O₃ and carbon nanotube particles.” *Chinese J. Chem. Eng.*, 21(9), 983–990.

Lu, S., Zhao, Y., Song, J., and Li, Y. (2017). “Experimental studies of CO₂ absorption enhancement in water-based nanofluids of carbon nanotubes.” *Brazilian J. Chem. Eng.*, 34(2), 597–606.

Lu, S., Zhao, Y., Song, J., Li, Y., Aghel, B., Janati, S., Alobaid, F., Almoslh, A., Epple, B., Mehdipour, M., Keshavarz, P., Rahimpour, M. R., Lee, W., Xu, R., Kim, S., Park, J. H., Kang, Y. T., Vakylabad, A. B., Hashimoto, S., Nakajima, K., Kikuchi, T., Kamazawa, K., Shibata, K., Yamada, T., Has, C., Jiang, J. Z., Zhang, S., Liu, L., Sun, B. M., Zhang, H., Wang, B., Xiong, M., Gao, C., Ren, H., Ma, L., Nanadegani, F. S., and Sunden, B. (2021). “Experimental analysis on dynamics of liquid molecules adjacent to particles in nanofluids.” *J. Mol. Liq.*, 346(6), 529–539.

Ma, X., Su, F., Chen, J., and Zhang, Y. (2007). “Heat and mass transfer enhancement of the bubble absorption for a binary nanofluid.” *J. Mech. Sci. Technol.*, 21(11), 1813–1818.

- Mahbulul, I. M., Saidur, R., and Amalina, M. A. (2012). "Latest developments on the viscosity of nanofluids." *Int. J. Heat Mass Transf.*, 55(4), 874–885.
- Mahian, O., Kianifar, A., Kalogirou, S. A., Pop, I., and Wongwises, S. (2013). "A review of the applications of nanofluids in solar energy." *Int. J. Heat Mass Transf.*, 57(2), 582–594.
- Maier, B., Dietrich, C., and Büchs, J. (2001). "Correct application of the sulphite oxidation methodology of measuring the volumetric mass transfer coefficient $k_L a$ under non-pressurized and pressurized conditions." *Food Bioprod. Process. Trans. Inst. Chem. Eng. Part C*, 79(2), 107–113.
- Mamat, H., and Ramadan, M. (2022). "Nanofluids: Thermal Conductivity and Applications."
- Manikandan, S., Karthikeyan, N., Suganthi, K. S., and Rajan, K. S. (2012a). "Enhancement of volumetric mass transfer coefficient for oxygen transfer using Fe 2O₃-water nanofluids." *Asian J. Sci. Res.*, 5(4), 271–277.
- Manikandan, S., Karthikeyan, N., Suganthi, K. S., and Rajan, K. S. (2012b). "Enhancement of volumetric mass transfer coefficient for oxygen transfer using Fe 2O₃-water nanofluids." *Asian J. Sci. Res.*
- Manjrekar, O. N., Sun, Y., He, L., Tang, Y. J., and Dudukovic, M. P. (2017). "Hydrodynamics and mass transfer coefficients in a bubble column photo-bioreactor." *Chem. Eng. Sci.*, 168, 55–66.
- Masuda, H., Ebata, A., Teramae, K., and Hishinuma, N. (1993). "Alteration of Thermal Conductivity and Viscosity of Liquid by Dispersing Ultra-Fine Particles. Dispersion of Al₂O₃, SiO₂ and TiO₂ Ultra-Fine Particles." *Netsu Bussei*, 7(4), 227–233.
- Masutani, G. K., and Stenstrom, M. K. (1991). "Dynamic surface tension effects on oxygen transfer." *J. Environ. Eng.*, 117(1), 126–142.
- Mena, P., Ferreira, A., Teixeira, J. A., and Rocha, F. (2011). "Effect of some solid properties on gas-liquid mass transfer in a bubble column." *Chem. Eng. Process. Process Intensif.*, 50(2), 181–188.

Mestre, J. C., Cerri, M. O., Esperança, M. N., Pedrolli, D. B., and Badino, A. C. (2019). “Aeration step method for kLa measurement under growth conditions in pneumatic bioreactors.” *J. Chem. Technol. Biotechnol.*, 94(7), 2327–2332.

Meyer, J. P., Adio, S. A., Sharifpur, M., and Nwosu, P. N. (2016). “The Viscosity of Nanofluids: A Review of the Theoretical, Empirical, and Numerical Models.” *Heat Transf. Eng.*, 37(5), 387–421.

Miladinović, M. R., Stojković, I. J., Veličković, A. V., Stamenković, O. S., Banković-Ilić, I. B., and Veljković, V. B. (2019). “Optimization and kinetic modeling of waste lard methanolysis in a continuous reciprocating plate reactor.” *Chinese J. Chem. Eng.*, 27(10), 2481–2490.

Miloš Madić. (2012). “Comparative modeling of CO₂ laser cutting using multiple regression analysis and artificial neural network.” *Int. J. Phys. Sci.*, 7(16), 2422–2430.

Minakov, A. V., Rudyak, V. Y., and Pryazhnikov, M. I. (2021). “Systematic Experimental Study of the Viscosity of Nanofluids.” *Heat Transf. Eng.*, 42(12), 1024–1040.

Mirmohammadi, S. L., Mallah, M. H., Torkaman, R., and Safdari, J. (2019). “Prediction of the mean drop diameter, dispersed phase hold-up and slip velocity in a horizontal pulsed sieve plate column for uranium stripping from Loaded Alamine 336 by ammonium carbonate.” *Prog. Nucl. Energy*, Elsevier Ltd.

Mirzazadeh Ghanadi, A., Heydari Nasab, A., Bastani, D., and Seife Kordi, A. A. (2015a). “The Effect of Nanoparticles on the Mass Transfer in Liquid–Liquid Extraction.” *Chem. Eng. Commun.*, 202(5), 600–605.

Mirzazadeh Ghanadi, A., Heydari Nasab, A., Bastani, D., and Seife Kordi, A. A. (2015b). “The Effect of Nanoparticles on the Mass Transfer in Liquid–Liquid Extraction.” *Chem. Eng. Commun.*, 202(5), 600–605.

Mohagheghian, S., Still, A. L., Elbing, B. R., and Ghajar, A. J. (2018). “Study of bubble size, void fraction, and mass transport in a bubble column under high amplitude vibration.” *ChemEngineering*, 2(2), 1–25.

- Mondragon, R., Julia, J. E., Barba, A., and Jarque, J. C. (2012). "Characterization of silica-water nanofluids dispersed with an ultrasound probe: A study of their physical properties and stability." *Powder Technol.*, 224, 138–146.
- Monji, F., and Jabbareh, M. A. (2017). "Thermodynamic model for prediction of binary alloy nanoparticle phase diagram including size dependent surface tension effect." *Calphad Comput. Coupling Phase Diagrams Thermochem.*, 58(April), 1–5.
- Moo-Young, M., and Chisti, Y. (1994). "Biochemical engineering in biotechnology (Technical Report)." *Pure Appl. Chem.*, 66(1), 117–136.
- Moraveji, M. K., Mohsenzadeh, E., Fakhari, M. E., and Davarnejad, R. (2013). "Hydrodynamics and oxygen mass transfer characteristics of petroleum based micro-emulsions in a packed bed split-cylinder airlift reactor." *Brazilian J. Chem. Eng.*, 30(3), 541–550.
- Moraveji, M. K., Pasand, M. M., Davarnejad, R., and Chisti, Y. (2012). "Effects of surfactants on hydrodynamics and mass transfer in a split-cylinder airlift reactor." *Can. J. Chem. Eng.*, 90(1), 93–99.
- Munyalo, J. M., and Zhang, X. (2018). "Particle size effect on thermophysical properties of nanofluid and nanofluid based phase change materials: A review." *J. Mol. Liq.*, Elsevier B.V.
- Murshed, S. M. S., Leong, K. C., and Yang, C. (2005a). "Enhanced thermal conductivity of TiO₂ - Water based nanofluids." *Int. J. Therm. Sci.*, 44(4), 367–373.
- Murshed, S. M. S., Leong, K. C., and Yang, C. (2005b). "Enhanced thermal conductivity of TiO₂ - Water based nanofluids." *Int. J. Therm. Sci.*, 44(4), 367–373.
- Murshed, S. M. S., Sharifpur, M., Giwa, S., and Meyer, J. P. (2020). "Experimental research and development on the natural convection of suspensions of nanoparticles—a comprehensive review." *Nanomaterials*, MDPI AG.
- Murshed, S. M. S., Tan, S. H., and Nguyen, N. T. (2008). "Temperature dependence of interfacial properties and viscosity of nanofluids for droplet-based microfluidics." *J. Phys. D. Appl. Phys.*, 41(8).

- Naddaf, A., and Zeinali Heris, S. (2019). “Density and rheological properties of different nanofluids based on diesel oil at different mass concentrations: An experimental study.” *J. Therm. Anal. Calorim.*, 135(2), 1229–1242.
- Nagy, E. (2013). “Three-Phase Mass Transfer: Application of the Pseudo-Homogeneous and Heterogeneous Models.” *Am. J. Chem. Eng.*, 1(1), 24.
- Nagy, E., Feczko, T., and Koroknai, B. (2007a). “Enhancement of oxygen mass transfer rate in the presence of nanosized particles.” *Chem. Eng. Sci.*, 62(24), 7391–7398.
- Nagy, E., Feczko, T., and Koroknai, B. (2007b). “Enhancement of oxygen mass transfer rate in the presence of nanosized particles.” *Chem. Eng. Sci.*, 62(24), 7391–7398.
- Nagy, E., and Hadik, P. (2003). “Three-phase mass transfer: Effect of the size distribution.” *Ind. Eng. Chem. Res.*, 42(21), 5363–5372.
- Nagy, E., and Moser, A. (1995). “Three-phase mass transfer: Improved pseudo-homogeneous model.” *AIChE J.*, 41(1), 23–34.
- Najafipour, I., Bahmanyar, H., Mirdehghan Ashkezari, S. M., and Jafari Ozumchelouei, E. (2021). “Mass recovery of the wastewater of dill seeds produced in the hydro-distillation using the pulsed sieve plate column in comparison with the ultrasound-assisted extraction method.” *Sep. Sci. Technol.*, 56(5), 925–935.
- Nematbakhsh, G., and Rahbar-Kelishami, A. (2015). “The Effect of Size and Concentration of Nanoparticles on the Mass Transfer Coefficients in Irregular Packed Liquid-Liquid Extraction Columns.” *Chem. Eng. Commun.*, 202(11), 1493–1501.
- Nematbakhsh, G., and Rahbar Kelishami, A. (2016). “The Effect of Nanoparticles on Liquid Holdups in a Randomly Packed Liquid-Liquid Extraction Column.” *Synth. React. Inorganic, Met. Nano-Metal Chem.*, 46(1), 31–37.
- Nguyen, C. T., Desgranges, F., Roy, G., Galanis, N., Maré, T., Boucher, S., and Angue Mintsu, H. (2007). “Temperature and particle-size dependent viscosity data for water-based nanofluids - Hysteresis phenomenon.” *Int. J. Heat Fluid Flow*, 28(6), 1492–1506.
- Nikolić, L. B., Nikolić, V. D., Veljković, V. B., and Skala, D. U. (2005). “Gas hold-up in a three-phase reciprocating plate column.” *J. Serbian Chem. Soc.*, 70(11), 1363–

1371.

Nithiyantham, U., Zaki, A., Grosu, Y., González-Fernández, L., Igartua, J. M., and Faik, A. (2019). “SiO₂@ Al₂O₃ core-shell nanoparticles based molten salts nanofluids for thermal energy storage applications.” *J. Energy Storage*, 26, 101033.

Nurdin, I., and Satriananda, S. (2017). “The effect of particle volume fraction and temperature on the enhancement of thermal conductivity of maghemite (γ -Fe₂O₃) water-based nanofluids.” *AIP Conf. Proc.*, American Institute of Physics Inc.

Okonkwo, E. C., Wole-Osho, I., Almanassra, I. W., Abdullatif, Y. M., and Al-Ansari, T. (2021). *An updated review of nanofluids in various heat transfer devices. J. Therm. Anal. Calorim.*, Springer International Publishing.

Oliveira, M. S. N., and Ni, X. (2001). “Gas hold-up and bubble diameters in a gassed oscillatory baffled column.” *Chem. Eng. Sci.*, 56(21–22), 6143–6148.

Olle, B., Bucak, S., Holmes, T. C., Bromberg, L., Hatton, T. A., and Wang, D. I. C. (2006a). “Enhancement of oxygen mass transfer using functionalized magnetic nanoparticles.” *Ind. Eng. Chem. Res.*, 45(12), 4355–4363.

Olle, B., Bucak, S., Holmes, T. C., Bromberg, L., Hatton, T. A., and Wang, D. I. C. (2006b). “Enhancement of oxygen mass transfer using functionalized magnetic nanoparticles.” *Ind. Eng. Chem. Res.*, 45(12), 4355–4363.

Pahlevaninezhad, M., Etesami, N., and Nasr Esfahany, M. (2021a). “Improvement of CO₂ absorption by Fe₃O₄/water nanofluid falling liquid film in presence of the magnetic field.” *Can. J. Chem. Eng.*, 99(2), 519–529.

Pahlevaninezhad, M., Etesami, N., and Nasr Esfahany, M. (2021b). “Improvement of CO₂ absorption by Fe₃O₄/water nanofluid falling liquid film in presence of the magnetic field.” *Can. J. Chem. Eng.*, 99(2), 519–529.

Pak, B. C., and Cho, Y. I. (1998). “Hydrodynamic and heat transfer study of dispersed fluids with submicron metallic oxide particles.” *Exp. Heat Transf.*, 11(2), 151–170.

Panahinia, F., Ghannadi-Maragheh, M., Safdari, J., Amani, P., and Mallah, M.-H. (2017). “Experimental investigation concerning the effect of mass transfer direction on

mean drop size and holdup in a horizontal pulsed plate extraction column.” *RSC Adv.*, 7(15), 8908–8921.

Pang, C., Lee, J. W., and Kang, Y. T. (2015a). “Review on combined heat and mass transfer characteristics in nanofluids.” *Int. J. Therm. Sci.*, 87, 49–67.

Pang, C., Lee, J. W., and Kang, Y. T. (2015b). “Review on combined heat and mass transfer characteristics in nanofluids.” *Int. J. Therm. Sci.*, Elsevier Masson SAS.

Pang, C., Wu, W., Sheng, W., Zhang, H., and Kang, Y. T. (2012). “Mass transfer enhancement by binary nanofluids (NH₃/H₂O + Ag nanoparticles) for bubble absorption process.” *Int. J. Refrig.*, 2240–2247.

Park, S. W., Choi, B. S., and Lee, J. W. (2006). “Effect of elasticity of aqueous colloidal silica solution on chemical absorption of carbon dioxide with 2-amino-2-methyl-1-propanol.” *Korea Aust. Rheol. J.*, 18(3), 133–141.

Pashaei, H., Ghaemi, A., Nasiri, M., and Heydarifard, M. (2018). “Experimental Investigation of the Effect of Nano Heavy Metal Oxide Particles in Piperazine Solution on CO₂ Absorption Using a Stirrer Bubble Column.” *Energy and Fuels*, 32(2), 2037–2052.

Patel, V. M., and Mehta, H. B. (2018). “Thermal performance prediction models for a pulsating heat pipe using Artificial Neural Network (ANN) and Regression/Correlation Analysis (RCA).” *Sadhana - Acad. Proc. Eng. Sci.*, 43(11), 1–16.

Patwari, A. N., Nguyen-Tien, K., Schumpe, A., and Deckwer, W.-D. (1986). “Three-phase fluidized beds with viscous liquid: hydrodynamics and mass transfer.” *Chem. Eng. Commun.*, 40(1–6), 49–65.

Peyravi, A., Keshavarz, P., and Mowla, D. (2015). “Experimental Investigation on the Absorption Enhancement of CO₂ by Various Nanofluids in Hollow Fiber Membrane Contactors.” *Energy and Fuels*, 29(12), 8135–8142.

Phuoc, T. X., and Massoudi, M. (2009). “Experimental observations of the effects of shear rates and particle concentration on the viscosity of Fe₂O₃-deionized water nanofluids.” *Int. J. Therm. Sci.*, 48(7), 1294–1301.

- Pineda, I. T., Choi, C. K., and Kang, Y. T. (2014). "CO₂ gas absorption by CH₃OH based nanofluids in an annular contactor at low rotational speeds." *Int. J. Greenh. Gas Control*, 23, 105–112.
- Prabhu, S., Srinikethan, G., and Hegde, S. (2020a). "Efficient biosorption of Pb(II) on *Pteris vittata* L. from aqueous solution using pulsed plate column technique." *Sep. Sci. Technol.*, 55(17), 3089–3101.
- Prabhu, S., Srinikethan, G., and Hegde, S. (2020b). "Efficient biosorption of Pb(II) on *Pteris vittata* L. from aqueous solution using pulsed plate column technique." *Sep. Sci. Technol.*, 55(17), 3089–3101.
- Prasher, R., Bhattacharya, P., and Phelan, P. E. (2005). "Thermal conductivity of nanoscale colloidal solutions (nanofluids)." *Phys. Rev. Lett.*, 94(2), 3–6.
- Prasher, R., Bhattacharya, P., and Phelan, P. E. (2006a). "Brownian-motion-based convective-conductive model for the effective thermal conductivity of nanofluids." *J. Heat Transfer*, 128(6), 588–595.
- Prasher, R., Bhattacharya, P., and Phelan, P. E. (2006b). "Brownian-motion-based convective-conductive model for the effective thermal conductivity of nanofluids." *J. Heat Transfer*, 128(6), 588–595.
- Prasher, R., Phelan, P. E., and Bhattacharya, P. (2006c). "Effect of aggregation kinetics on the thermal conductivity of nanoscale colloidal solutions (nanofluid)." *Nano Lett.*, 6(7), 1529–1534.
- Prasher, R., Song, D., Wang, J., and Phelan, P. (2006d). "Measurements of nanofluid viscosity and its implications for thermal applications." *Appl. Phys. Lett.*, 89(13), 67–70.
- Purbia, D., Khandelwal, A., Kumar, A., and Sharma, A. K. (2019). "Graphene-water nanofluid in heat exchanger: Mathematical modelling, simulation and economic evaluation." *Int. Commun. Heat Mass Transf.*, 108(September), 104327.
- Quicker, G., Alper, E., and Deckwer, W. -D. (1987). "Effect of fine activated carbon particles on the rate of CO₂ absorption." *AIChE J.*, 33(5), 871–875.

Qureshi, M. Z. A., Ali, K., Iqbal, M. F., Ashraf, M., and Ahmad, S. (2017). “Heat and mass transfer enhancement of nanofluids flow in the presence of metallic/metallic-oxides spherical nanoparticles.” *Eur. Phys. J. Plus*, 132(1).

Radiom, M., Yang, C., and Chan, W. K. (2009). “Characterization of surface tension and contact angle of nanofluids.” *Fourth Int. Conf. Exp. Mech.*, 7522(January 2018), 75221D.

Raghav, S. B., and Dinesh, V. (2016). “Recent Developments on Nanotechnology In Solar Energy.” *Int. J. Eng. Comput. Sci.*

Rahbar, A., Azizi, Z., Bahmanyar, H., and Moosavian, M. A. (2011a). “Prediction of enhancement factor for mass transfer coefficient in regular packed liquid–liquid extraction columns.” *Can. J. Chem. Eng.*, 89(3), 508–519.

Rahbar, A., Azizi, Z., Bahmanyar, H., and Moosavian, M. A. (2011b). “Prediction of enhancement factor for mass transfer coefficient in regular packed liquid-liquid extraction columns.” *Can. J. Chem. Eng.*, 89(3), 508–519.

Rahmanian, A., Ahmad Zaini, M. A., and Tuan Abdullah, T. A. (2015). “Carbon dioxide capture from reforming gases using acetic acid-mixed chemical absorbents.” *Bull. Korean Chem. Soc.*, 36(7), 1940–1943.

Rama Rao, N. V., and Baird, M. H. I. (1986). “Gas—liquid pressure drop studies in a reciprocating plate column.” *Can. J. Chem. Eng.*, 64(1), 42–47.

Rama Rao, N. V., and Baird, M. H. I. (1988). “Characteristics of a countercurrent reciprocating plate bubble column. I. Holdup, pressure drop and bubble diameter.” *Can. J. Chem. Eng.*, 66(2), 211–221.

Ramos, A. V., Sousa-Gallagher, M. J., and Oliveira, J. C. (2023). “Dimensionless correlations for estimating the permeability of perforated packaging films to oxygen.” *J. Food Eng.*, 340(July 2022), 111252.

Ramprasad, T., Khanolkar, R., and Suresh, A. K. (2019). “Mass-Transfer Rate Enhancement in Nanofluids: Packed Column Studies and a Design Basis.” *Ind. Eng. Chem. Res.*, 58(18), 7670–7680.

- Rangappa, V. B., Kodialbail, V. S., and Bharthaiyengar, S. M. (2016a). "Effect of dilution rate on dynamic and steady-state biofilm characteristics during phenol biodegradation by immobilized *Pseudomonas desmolyticum* cells in a pulsed plate bioreactor." *Front. Environ. Sci. Eng.*, 10(4), 1–9.
- Rangappa, V. B., Kodialbail, V. S., and Bharthaiyengar, S. M. (2016b). "Effect of dilution rate on dynamic and steady-state biofilm characteristics during phenol biodegradation by immobilized *Pseudomonas desmolyticum* cells in a pulsed plate bioreactor." *Front. Environ. Sci. Eng.*, 10(4).
- Ranjbarzadeh, R., Moradikazerouni, A., Bakhtiari, R., Asadi, A., and Afrand, M. (2019). "An experimental study on stability and thermal conductivity of water/silica nanofluid: Eco-friendly production of nanoparticles." *J. Clean. Prod.*, 206, 1089–1100.
- Rashidi, H., and Mamivand, S. (2022). "Experimental and numerical mass transfer study of carbon dioxide absorption using Al₂O₃/water nanofluid in wetted wall column." *Energy*, 238.
- Rathilal, S. (2010). "Modelling of a Vibrating-Plate Extraction Column." (May).
- Reuss, M. (1995). "Stirred tank bioreactors." *Bioprocess Technol.*, 21, 207–255.
- Rezazakemi, M., Darabi, M., Soroush, E., and Mesbah, M. (2019). "CO₂ absorption enhancement by water-based nanofluids of CNT and SiO₂ using hollow-fiber membrane contactor." *Sep. Purif. Technol.*, 210, 920–926.
- Roobahani, M. A. G., Najafabadi, M. S., Abadi, K. N. H., and Bahmanyar, H. (2015). "Simultaneous Investigation of the Effect of Nanoparticles and Mass Transfer Direction on Static and Dynamic Holdup in Pulsed-Sieve Liquid–Liquid Extraction Columns." *Chem. Eng. Commun.*, 202(11), 1468–1477.
- Rudiyak, V. Y. (2015). "Diffusion of Nanoparticles in Gases and Liquids." *Handb. Nanoparticles*, Springer International Publishing, 1–21.
- Ruthiya, K. C., Schaaf, J. Van Der, Kuster, B. F. M., and Schouten, J. C. (2005). "Model to describe mass-transfer enhancement by catalyst particles adhering to a gas-liquid interface." *Ind. Eng. Chem. Res.*, 44(16), 6123–6140.

Saeednia, L., Hashemipour, H., and Afzali, D. (2015a). “Study on mass transfer enhancement in a gas-liquid system using nanomaterials.”

Saeednia, L., Hashemipour, H., and Afzali, D. (2015b). “Study on Mass Transfer Enhancement in a Gas-Liquid System Using Nanomaterials.” *Trans. Phenom. Nano Micro Scales*, 3(1), 46–53.

Saha, D. (2009). “Prediction of mass transfer coefficient in rotating bed contactor (Higee) using artificial neural network.” *Heat Mass Transf. und Stoffuebertragung*, 45(4), 451–457.

Said, Z., Cakmak, N. K., Sharma, P., Sundar, L. S., Inayat, A., Keklikcioglu, O., and Li, C. (2022a). “Synthesis, stability, density, viscosity of ethylene glycol-based ternary hybrid nanofluids: Experimental investigations and model -prediction using modern machine learning techniques.” *Powder Technol.*, 400, 117190.

Said, Z., Sundar, L. S., Tiwari, A. K., Ali, H. M., Sheikholeslami, M., Bellos, E., and Babar, H. (2022b). “Recent advances on the fundamental physical phenomena behind stability, dynamic motion, thermophysical properties, heat transport, applications, and challenges of nanofluids.” *Phys. Rep.*, 946, 1–94.

Saidur, R., Leong, K. Y., and Mohammed, H. A. (2011). “A review on applications and challenges of nanofluids.” *Renew. Sustain. Energy Rev.*, Elsevier Ltd.

Saien, J., and Bamdadi, H. (2012a). “Mass transfer from nanofluid single drops in liquid-liquid extraction process.” *Ind. Eng. Chem. Res.*, 51(14), 5157–5166.

Saien, J., and Bamdadi, H. (2012b). “Mass transfer from nanofluid single drops in liquid-liquid extraction process.” *Ind. Eng. Chem. Res.*, 51(14), 5157–5166.

Saien, J., and Hasani, R. (2017). “Hydrodynamics and mass transfer characteristics of circulating single drops with effect of different size nanoparticles.” *Sep. Purif. Technol.*, 175, 298–304.

Saien, J., and Zardoshti, M. (2015). “Mass transfer intensification of nanofluid single drops with effect of temperature.” *Korean J. Chem. Eng.*, 32(11), 2311–2318.

Salimi, J., Haghshenasfard, M., and Etemad, S. G. (2015). “CO₂ absorption in

nanofluids in a randomly packed column equipped with magnetic field.” *Heat Mass Transf. und Stoffuebertragung*, 51(5), 621–629.

Samadi, Z., Haghshenasfard, M., and Moheb, A. (2014). “CO₂ absorption using nanofluids in a wetted-wall column with external magnetic field.” *Chem. Eng. Technol.*, 37(3), 462–470.

Sarafraz, M. M., and Peyghambarzadeh, S. M. (2012). “Nucleate pool boiling heat transfer to Al₂O₃-water and TiO₂-water nanofluids on horizontal smooth tubes with dissimilar homogeneous materials.” *Chem. Biochem. Eng. Q.*, 26(3), 199–206.

Saravanan, R., Gracia, F., and Stephen, A. (2017). “Basic principles, mechanism, and challenges of photocatalysis.” *Nanocomposites visible Light. Photocatal.*, Springer, 19–40.

Schonhorn, H. (1965). “Theoretical relationship between surface tension and cohesive energy density.” *J. Chem. Phys.*, 43(6), 2041–2043.

Sen, N., Sarkar, S., Singh, K. K., Mukhopadhyay, S., and Shenoy, K. T. (2018). “Regime Transition and Holdup in Pulsed Sieve-Plate and Pulsed Disc-and-Doughnut Columns: A Comparative Study.” *Solvent Extr. Ion Exch.*, 36(1), 66–83.

Serna, J. (2016). “Heat and mass transfer mechanisms in nanofluids boundary layers.” *Int. J. Heat Mass Transf.*, 92, 173–183.

Shah, Y. T., Kelkar, B. G., Godbole, S. P., and Deckwer, W.-D. (1982). *Design Parameters Column Reactors Estimations for Bubble. AIChE J.*

Sheikhpour, M., Arabi, M., Kasaeian, A., Rabei, A. R., and Taherian, Z. (2020). “Role of nanofluids in drug delivery and biomedical technology: Methods and applications.” *Nanotechnol. Sci. Appl.*, 13, 47–59.

Shet, A., and Shetty, K. V. (2016). “Photocatalytic degradation of phenol using Ag core-TiO₂ shell (Ag@TiO₂) nanoparticles under UV light irradiation.” *Environ. Sci. Pollut. Res.*, 23(20), 20055–20064.

Shetty, K. V., Kalifathulla, I., and Srinikethan, G. (2007a). “Performance of pulsed plate bioreactor for biodegradation of phenol.” *J. Hazard. Mater.*, 140(1–2), 346–352.

Shetty, K. V., Kalifathulla, I., and Srinikethan, G. (2007b). "Performance of pulsed plate bioreactor for biodegradation of phenol." *J. Hazard. Mater.*, 140(1–2), 346–352.

Shetty, K. V., Nandennavar, S., and Srinikethan, G. (2008). "Artificial neural networks model for the prediction of steady state phenol biodegradation in a pulsed plate bioreactor." *J. Chem. Technol. Biotechnol.*, 83(9), 1181–1189.

Shetty, K. V., and Srinikethan, G. (2010). "Oxygen mass transfer coefficients in a three-phase pulsed plate bioreactor." *Int. J. Chem. React. Eng.*, 8.

Shetty, K. V., Verma, D. K., and Srinikethan, G. (2011). "Modelling and simulation of steady-state phenol degradation in a pulsed plate bioreactor with immobilised cells of *Nocardia hydrocarbonoxydans*." *Bioprocess Biosyst. Eng.*, 34(1), 45–56.

Shetty, K. V., Yarangali, S. B., and Srinikethan, G. (2013a). "Biodegradation of phenol using immobilized nocardia hydrocarbonoxydans in a pulsed plate bioreactor: effect of packed stages, cell carrier loading, and cell acclimatization on startup and steady-state behavior." *Bioremediat. J.*, 17(4), 252–263.

Shetty, K. V., Yarangali, S. B., and Srinikethan, G. (2013b). "Biodegradation of phenol using immobilized nocardia hydrocarbonoxydans in a pulsed plate bioreactor: Effect of packed stages, cell carrier loading, and cell acclimatization on startup and steady-state behavior." *Bioremediat. J.*, 17(4), 252–263.

Sideman, S., Hortaçsu, Ö., and Fulton, J. W. (1966). "Mass Transfer in Gas-Liquid Contacting Systems." *Ind. Eng. Chem.*, 58(7), 32–47.

Sincuba, N. D., Rathilal, S., and Carsky, M. (2017). "Effect of sieve tray hole diameter on the efficiency of a vibrating plate extractor." *South African J. Chem. Eng.*, 23, 38–41.

Sinha, N., and Singh, J. K. (2017). "Effect of nanoparticles on vapour-liquid surface tension of water: A molecular dynamics study." *J. Mol. Liq.*, 246, 244–250.

Skala, D., and Veljković, V. (1988a). "Mass transfer characteristics in a gas-liquid reciprocating plate column. I. Liquid phase volumetric mass transfer coefficient." *Can. J. Chem. Eng.*, 66(2), 192–199.

Skala, D., and Veljković, V. (1988b). “Mass transfer characteristics in a gas-liquid reciprocating plate column. I. Liquid phase volumetric mass transfer coefficient.” *Can. J. Chem. Eng.*, 66(2), 192–199.

Somkuwar, N., Kolhe, N., and Rathod, V. (2014). “Hydrodynamics of a Pulsed Sieve Plate Extraction Column.” *Indian Chem. Eng.*, 56(3), 235–257.

Souza, R. R., Gonçalves, I. M., Rodrigues, R. O., Minas, G., Miranda, J. M., Moreira, A. L. N., Lima, R., Coutinho, G., Pereira, J. E., and Moita, A. S. (2022a). “Recent advances on the thermal properties and applications of nanofluids: From nanomedicine to renewable energies.” *Appl. Therm. Eng.*, 201(November 2021).

Souza, R. R., Gonçalves, I. M., Rodrigues, R. O., Minas, G., Miranda, J. M., Moreira, A. L. N., Lima, R., Coutinho, G., Pereira, J. E., and Moita, A. S. (2022b). “Recent advances on the thermal properties and applications of nanofluids: From nanomedicine to renewable energies.” *Appl. Therm. Eng.*, 201.

Stamenković, I. S., Stamenković, O. S., Banković-Ilić, I. B., Lazić, M. L., Veljković, V. B., and Skala, D. U. (2005). “The gas holdup in a multiphase reciprocating plate column filled with carboxymethylcellulose solutions.” *J. Serbian Chem. Soc.*, 70(12), 1533–1544.

Stella, A., Mensforth, K. H., Bowser, T., Stevens, G. W., and Pratt, H. R. C. (2008). “Mass transfer performance in karr reciprocating plate extraction columns.” *Ind. Eng. Chem. Res.*, 47(11), 3996–4007.

Su, F., Deng, Y., and Ma, H. (2015). “Numerical Analysis of Ammonia Bubble Absorption in a Binary Nanofluid.” *Chem. Eng. Commun.*, 202(4), 500–507.

Sundaresan, A., and Varma, Y. B. G. (1990a). “Interfacial area and mass transfer in gas-liquid cocurrent upflow and countercurrent flow in reciprocating plate column.” *Can. J. Chem. Eng.*, 68(6), 952–958.

Sundaresan, A., and Varma, Y. B. G. (1990b). “Dispersed phase holdup and bubble size distributions in gas-liquid cocurrent upflow and countercurrent flow in reciprocating plate column.” *Can. J. Chem. Eng.*, 68(4), 560–568.

Suresh, S., Srivastava, V. C., and Mishra, I. M. (2009). “Techniques for oxygen transfer measurement in bioreactors: a review.” *J. Chem. Technol. Biotechnol. Int. Res. Process. Environ. Clean Technol.*, 84(8), 1091–1103.

Tan, J., Xie, Y., Wang, F., Jing, L., and Ma, L. (2017). “Investigation of optical properties and radiative transfer of TiO₂ nanofluids with the consideration of scattering effects.” *Int. J. Heat Mass Transf.*, 115, 1103–1112.

Tanvir, S., and Qiao, L. (2012a). “Surface tension of nanofluid-type fuels containing suspended nanomaterials.” *Nanoscale Res. Lett.*, 7(1), 1.

Tanvir, S., and Qiao, L. (2012b). “Surface tension of nanofluid-type fuels containing suspended nanomaterials.” *West. States Sect. Combust. Inst. Spring Tech. Meet. 2012*, 551–573.

Taweel, A. M. et al. (1984). “Measurement of Large Gas- Liquid Inter facial Areas.” 62(February).

Tholudur, A., and Ramirez, W. F. (1996). “Optimization of fed-batch bioreactors using neural network parameter function models.” *Biotechnol. Prog.*, 12(3), 302–309.

Thompson, M. L., and Kramer, M. A. (1994). “Modeling chemical processes using prior knowledge and neural networks.” *AIChE J.*, 40(8), 1328–1340.

Torab-Mostaedi, M., Ghaemi, A., and Asadollahzadeh, M. (2012). “Prediction of mass transfer coefficients in a pulsed disc and doughnut extraction column.” *Can. J. Chem. Eng.*, 90(6), 1570–1578.

Torab-Mostaedi, M., Safdari, J., and Ghaemi, A. (2010a). “Mass transfer coefficients in pulsed perforated-plate extraction columns.” *Brazilian J. Chem. Eng.*, 27(2), 243–251.

Torab-Mostaedi, M., Safdari, J., and Ghaemi, A. (2010b). “Mass transfer coefficients in pulsed perforated-plate extraction columns.” *Brazilian J. Chem. Eng.*, 27(2), 243–251.

Torres Pineda, I., and Kang, Y. T. (2016). “CO₂ absorption enhancement by nanoabsorbents in Taylor-Couette absorber.” *Int. J. Heat Mass Transf.*, 100, 39–47.

- Torres Pineda, I., Lee, J. W., Jung, I., and Kang, Y. T. (2012). “CO₂ absorption enhancement by methanol-based Al₂O₃ and SiO₂ nanofluids in a tray column absorber.” *Int. J. Refrig.*, 35(5), 1402–1409.
- Traciak, J., and Żyła, G. (2022a). “Effect of nanoparticles saturation on the surface tension of nanofluids.” *J. Mol. Liq.*, 363.
- Traciak, J., and Żyła, G. (2022b). “Effect of nanoparticles saturation on the surface tension of nanofluids.” *J. Mol. Liq.*, 363.
- Uddin, M. J., Kalbani, K. S. Al, Rahman, M. M., Alam, M. S., Al-Salti, N., and Eltayeb, I. A. (2016a). “Fundamentals of Nanofluids: Evolution, Applications and New Theory.” *Int. J. Biomath. Syst. Biol. Off. J. Biomath. Soc.*, 2(1).
- Uddin, M. J., Rahman, M. M., and Alam, S. (2016b). “Fundamentals of Nanofluids : Evolution , Applications and New Theory.” *Int. J. Biomath. Syst. Biol.*, 2(1), 1–31.
- Ungar, L. H., Powell, B. A., and Kamens, S. N. (1990). “Adaptive networks for fault diagnosis and process control.” *Comput. Chem. Eng.*, 14(4–5), 561–572.
- Usman, M. R., Sattar, H., Hussain, S. N., Muhammad, H., Asghar, A., and Afzal, W. (2009). “Drop size in a liquid pulsed sieve-plate extraction column.” *Brazilian J. Chem. Eng.*, 26, 677–683.
- Vafaei, S., Purkayastha, A., Jain, A., Ramanath, G., and Borca-Tasciuc, T. (2009a). “The effect of nanoparticles on the liquid-gas surface tension of Bi₂Te₃ nanofluids.” *Nanotechnology*, 20(18).
- Vafaei, S., Purkayastha, A., Jain, A., Ramanath, G., and Borca-Tasciuc, T. (2009b). “The effect of nanoparticles on the liquid–gas surface tension of Bi₂Te₃ nanofluids.” *Nanotechnology*, 20(18), 185702.
- Vakilnejad, A., Aroon, M. A., Al-Abri, M., Bahmanyar, H., Myint, M. T. Z., and Vakili-Nezhaad, G. R. (2018). “Experimental and theoretical investigation of thermal conductivity of some water-based nanofluids.” *Chem. Eng. Commun.*, 205(5), 610–623.
- Valera, V. Y., Codolo, M. C., and Martins, T. D. (2021). “Artificial neural network for prediction of SO₂ removal and volumetric mass transfer coefficient in spray tower.”

Chem. Eng. Res. Des., 170, 1–12.

Vasić, L. S., Banković-Ilić, I. B., Lazić, M. L., Veljković, V. B., and Skala, D. U. (2007a). “Oxygen mass transfer in a 16.6 cm i. d. multiphase reciprocating plate column.” *J. Serbian Chem. Soc.*, 72(5), 523–531.

Vasić, L. S., Banković-Ilić, I. B., Lazić, M. L., Veljković, V. B., and Skala, D. U. (2007b). “Oxygen mass transfer in a 16.6 cm i. d. multiphase reciprocating plate column.” *J. Serbian Chem. Soc.*, 72(5), 523–531.

Vavruca, I. (1978). “On the determination of the factor between cohesive energy density and surface tension.” *J. Colloid Interface Sci.*, 63(3), 600–601.

Veena, B. R., Shetty K, V., and Saidutta, M. B. (2016). “Shear stress effects on production of exopolymeric substances and biofilm characteristics during phenol biodegradation by immobilized *Pseudomonas desmolyticum* (NCIM2112) cells in a pulsed plate bioreactor.” *Prep. Biochem. Biotechnol.*, 46(5), 421–428.

Veilleux, J., and Coulombe, S. (2010). “A total internal reflection fluorescence microscopy study of mass diffusion enhancement in water-based alumina nanofluids.” *J. Appl. Phys.*

Veilleux, J., and Coulombe, S. (2011). “A dispersion model of enhanced mass diffusion in nanofluids.” *Chem. Eng. Sci.*, 66(11), 2377–2384.

Veljković, V., and Skala, D. (1986). “Hydrodynamic investigations of gas–liquid contacting in a reciprocating plate column.” *Can. J. Chem. Eng.*, 64(6), 906–914.

Vidya Shetty, K., Ramanjaneyulu, R., and Srinikethan, G. (2007). “Biological phenol removal using immobilized cells in a pulsed plate bioreactor: Effect of dilution rate and influent phenol concentration.” *J. Hazard. Mater.*, 149(2), 452–459.

Wang, Y., Deng, K., Wu, J. M., Su, G., and Qiu, S. (2020a). “A mechanism of heat transfer enhancement or deterioration of nanofluid flow boiling heat transfer.” *Int. J. Heat Mass Transf.*, 158, 119985.

Wang, Z., Guo, K., Liu, H., Liu, C., Geng, Y., Lu, Z., Jiao, B., and Chen, D. (2020b). “Effects of bubble size on the gas–liquid mass transfer of bubble swarms with Sauter

mean diameters of 0.38–4.88 mm in a co-current upflow bubble column.” *J. Chem. Technol. Biotechnol.*, 95(11), 2853–2867.

Wang, Z., Wang, Z., Zhang, M., Cui, J., Xie, M., and Jiang, Y. (2023). “Biological Applications of Nanofluids: Antimicrobial Activity and Drug Delivery.” *Nanotechnol. Mod. Med.*, Springer, 19–45.

Wen, D., Lin, G., Vafaei, S., and Zhang, K. (2009). “Review of nanofluids for heat transfer applications.” *Particuology*, 7(2), 141–150.

Wenmakers, P. W. A. M., Hoorn, J. A. A., Kuipers, J. A. M., and Deen, N. G. (2016). “Gas-liquid mass transfer enhancement by catalyst particles, a modelling study.” *Chem. Eng. Sci.*, 145, 233–244.

Wilke, C. R., and Chang, P. (1955). “Correlation of diffusion coefficients in dilute solutions.” *AIChE J.*, 1(2), 264–270.

Wu, W. D., Wu, J., Wang, Y., and Zhang, H. (2017). “The enhancing influence of nanoparticles on ammonia/water falling film absorption in binary nanofluids under pressure reducing conditions.” *J. Therm. Sci. Technol.*, 12(2).

Xuan, Y., and Li, Q. (2000). “Heat transfer enhancement of nanofluids.” *Int. J. Heat Fluid Flow*, 21(1), 58–64.

Xue, L., Keblinski, P., Phillpot, S. R., Choi, S. U. S., and Eastman, J. A. (2004). “Effect of liquid layering at the liquid-solid interface on thermal transport.” *Int. J. Heat Mass Transf.*, 47(19–20), 4277–4284.

Yadav, D., Nirala, A., Kumar, R., and Kumar Singh, P. (2020). “Density variation in nanofluids as a function of concentration and temperature.” *Mater. Today Proc.*, 46, 6576–6580.

Yadav, R. L., and Patwardhan, A. W. (2008). “Design aspects of pulsed sieve plate columns.” *Chem. Eng. J.*, 138(1–3), 389–415.

Yang, L., Du, K., Cheng, B., and Li, Y. (2011). “The effect of viscosity on the heat and mass transfer of NH₃/H₂O falling film absorption with Fe₂O₃ nanofluid.” *Asia-Pacific Power Energy Eng. Conf. APPEEC*, (50876020), 0–3.

Yang, N. S., Shen, Z. Q., Chen, B. H., and McMillan, A. F. (1986). "Pressure drop, gas holdup, and interfacial area for gas-liquid contact in Karr columns." *Ind. Eng. Chem. Process Des. Dev.*, 25(3), 660–664.

Yang, W.-J. (1982). "Gas-liquid mass transfer in rotating perforated-disc contactors." *Lett. Heat Mass Transf.*, 9(2), 119–129.

Yang, W., Wang, J., Wang, T., and Jin, Y. (2001). *Experimental study on gas-liquid interfacial area and mass transfer coefficient in three-phase circulating fluidized beds.* *Chem. Eng. J.*

Yapici, K., Osturk, O., and Uludag, Y. (2018). "Dependency of nanofluid rheology on particle size and concentration of various metal oxide nanoparticles." *Brazilian J. Chem. Eng.*, 35(2), 575–586.

Yılmaz Aydın, D., and Gürü, M. (2022a). *Nanofluids: preparation, stability, properties, and thermal performance in terms of thermo-hydraulic, thermodynamics and thermo-economic analysis.* *J. Therm. Anal. Calorim.*, Springer International Publishing.

Yılmaz Aydın, D., and Gürü, M. (2022b). "Nanofluids: preparation, stability, properties, and thermal performance in terms of thermo-hydraulic, thermodynamics and thermo-economic analysis." *J. Therm. Anal. Calorim.*, Springer Science and Business Media B.V.

Zander, A. K., Semmens, M. J., and Narbaitz, R. M. (1989). "Removing VOCs by membrane stripping." *Journal-American Water Work. Assoc.*, 81(11), 76–81.

Zhang, F., Wang, X., Wang, Q., Yang, C., and Qiu, T. (2021a). "Effect of nanoparticles on interfacial mass transfer characteristics and mechanisms in liquid-liquid extraction by molecular dynamics simulation." *Int. J. Heat Mass Transf.*, 173, 121236.

Zhang, H., Qing, S., Zhai, Y., Zhang, X., and Zhang, A. (2021b). "The changes induced by pH in TiO₂/water nanofluids: Stability, thermophysical properties and thermal performance." *Powder Technol.*, 377, 748–759.

Zhang, H., Wang, B., Xiong, M., Gao, C., Ren, H., and Ma, L. (2022a). "Process

intensification in gas-liquid mass transfer by nanofluids: Mechanism and current status.” *J. Mol. Liq.*, 346, 118268.

Zhang, J., Li, W., Mumford, K. A., Fei, W., Stevens, G. W., and Wang, Y. (2022b). “Mass transfer study and combined model for a Karr column.” *Chem. Eng. Sci.*, 254.

Zhang, L., Liu, Y., Wang, Y., Jin, L., Zhang, Q., and Hu, W. (2018a). “Experimental Study on the Enhancement of Mass Transfer Utilizing Fe₃O₄ Nanofluids.” *J. Heat Transfer*, 140(1).

Zhang, Q., Cheng, C., Wu, T., Xu, G., and Liu, W. (2020a). “The effect of Fe₃O₄ nanoparticles on the mass transfer of CO₂ absorption into aqueous ammonia solutions.” *Chem. Eng. Process. - Process Intensif.*, 154(July), 108002.

Zhang, Q., Cheng, C., Wu, T., Xu, G., and Liu, W. (2020b). “The effect of Fe₃O₄ nanoparticles on the mass transfer of CO₂ absorption into aqueous ammonia solutions.” *Chem. Eng. Process. - Process Intensif.*, 154.

Zhang, S., and Han, X. (2018). “Effect of different surface modified nanoparticles on viscosity of nanofluids.” *Adv. Mech. Eng.*, 10(2).

Zhang, Y., Zhao, B., Jiang, J., Zhuo, Y., and Wang, S. (2016). “The use of TiO₂ nanoparticles to enhance CO₂ absorption.” *Int. J. Greenh. Gas Control*, 50, 49–56.

Zhang, Z., Cai, J., Chen, F., Li, H., Zhang, W., and Qi, W. (2018b). “Progress in enhancement of CO₂ absorption by nanofluids: A mini review of mechanisms and current status.” *Renew. Energy*, 118, 527–535.

Zhou, M., Cai, W. F., and Xu, C. J. (2003). “A new way of enhancing transport process - The hybrid process accompanied by ultrafine particles.” *Korean J. Chem. Eng.*, 20(2), 347–353.

Zhu, H., Shanks, B. H., and Heindel, T. J. (2008). “Enhancing CO-water mass transfer by functionalized MCM41 nanoparticles.” *Ind. Eng. Chem. Res.*, 47(20), 7881–7887.

Zokaei-Kadijani, S., Safdari, J., Mousavian, M. A., and Rashidi, A. (2013). “Study of oxygen mass transfer coefficient and oxygen uptake rate in a stirred tank reactor for uranium ore bioleaching.” *Ann. Nucl. Energy*, 53, 280–287.

Żyła, G., Fal, J., and Estellé, P. (2017). “Thermophysical and dielectric profiles of ethylene glycol based titanium nitride (TiN–EG) nanofluids with various size of particles.” *Int. J. Heat Mass Transf.*, 113, 1189–1199.

Appendix I. Experimental k_{LA} data in the presence of TiO_2 nanofluid.

Volumetric oxygen mass transfer coefficient, (k_{LA} , s^{-1}) in the presence of TiO_2 nanofluid at 0.011m/s													
Nanoparticle size	25nm						72nm						
Nanoparticle Loading, (w/v%)	0.017	0.034	0.051	0.068	0.085	0.102	0.017	0.034	0.051	0.068	0.085	0.102	
A = 3.2cm	f = 0.25 s^{-1}	0.0448	0.0526	0.0581	0.0766	0.0718	0.0703	0.028	0.032	0.0399	0.0322	0.0255	0.0237
	f = 0.5 s^{-1}	0.0549	0.0613	0.0672	0.0835	0.0824	0.0812	0.0369	0.0394	0.0531	0.0516	0.0461	0.0455
	f = 0.75 s^{-1}	0.0772	0.0853	0.0882	0.0948	0.0927	0.0855	0.0597	0.0673	0.0757	0.0686	0.0653	0.0541
	f = 1 s^{-1}	0.0979	0.1049	0.1068	0.121	0.112	0.0925	0.0735	0.0762	0.0826	0.0729	0.0718	0.0709
A = 4.7cm	f = 0.25 s^{-1}	0.0497	0.0572	0.068	0.0789	0.0769	0.0743	0.0441	0.05041	0.0575	0.0483	0.0466	0.0451
	f = 0.5 s^{-1}	0.071	0.0799	0.0844	0.099	0.0879	0.0857	0.0583	0.0675	0.0802	0.0767	0.0755	0.0655
	f = 0.75 s^{-1}	0.1054	0.1108	0.1183	0.1211	0.0994	0.0925	0.0799	0.0851	0.0905	0.081	0.0798	0.0764
	f = 1 s^{-1}	0.118	0.126	0.131	0.135	0.128	0.119	0.0885	0.0911	0.1011	0.097	0.093	0.0891
A = 6.3cm	f = 0.25 s^{-1}	0.0542	0.0681	0.0788	0.0845	0.0811	0.0798	0.0511	0.055	0.0611	0.0529	0.0513	0.0499
	f = 0.5 s^{-1}	0.079	0.1027	0.1074	0.119	0.0984	0.0954	0.065	0.076	0.0814	0.08	0.0795	0.069
	f = 0.75 s^{-1}	0.112	0.1241	0.127	0.13	0.116	0.1127	0.082	0.0944	0.099	0.089	0.0865	0.0834
	f = 1 s^{-1}	0.126	0.131	0.134	0.1391	0.135	0.1245	0.099	0.1011	0.112	0.1044	0.098	0.0921
Volumetric oxygen mass transfer coefficient, (k_{LA} , s^{-1}) in the presence of TiO_2 nanofluid at 0.019m/s													
Nanoparticle size	25nm						72nm						
Nanoparticle Loading, (w/v%)	0.017	0.034	0.051	0.068	0.085	0.102	0.017	0.034	0.051	0.068	0.085	0.102	
A = 3.2cm	f = 0.25 s^{-1}	0.0551	0.059	0.065	0.0839	0.0821	0.0793	0.041	0.0487	0.0598	0.055	0.0495	0.0483
	f = 0.5 s^{-1}	0.063	0.071	0.083	0.091	0.0874	0.0843	0.053	0.063	0.071	0.068	0.0651	0.0623
	f = 0.75 s^{-1}	0.084	0.0911	0.094	0.1022	0.097	0.0943	0.0754	0.077	0.089	0.084	0.081	0.0799
	f = 1 s^{-1}	0.1049	0.1109	0.119	0.129	0.121	0.1105	0.0799	0.0851	0.099	0.095	0.0911	0.086
A = 4.7cm	f = 0.25 s^{-1}	0.061	0.068	0.079	0.089	0.0851	0.0811	0.055	0.061	0.0699	0.0671	0.0655	0.0629
	f = 0.5 s^{-1}	0.0783	0.089	0.0968	0.1054	0.1011	0.098	0.071	0.079	0.0855	0.083	0.079	0.073
	f = 0.75 s^{-1}	0.1095	0.115	0.122	0.128	0.121	0.116	0.0881	0.092	0.098	0.0899	0.0855	0.0839
	f = 1 s^{-1}	0.128	0.135	0.1395	0.1405	0.129	0.125	0.104	0.11	0.121	0.1085	0.1055	0.1025
A = 6.3cm	f = 0.25 s^{-1}	0.068	0.0718	0.0866	0.0941	0.0874	0.0855	0.062	0.067	0.078	0.0711	0.0699	0.0633
	f = 0.5 s^{-1}	0.089	0.1068	0.118	0.123	0.116	0.1105	0.078	0.0862	0.0963	0.0911	0.0869	0.0841
	f = 0.75 s^{-1}	0.119	0.129	0.136	0.141	0.128	0.126	0.092	0.1094	0.118	0.1044	0.0963	0.0911
	f = 1 s^{-1}	0.1295	0.138	0.1411	0.15	0.144	0.1437	0.1015	0.115	0.128	0.118	0.1066	0.1032
Volumetric oxygen mass transfer coefficient, (k_{LA} , s^{-1}) in the presence of TiO_2 nanofluid at 0.029m/s													
Nanoparticle size	25nm						72nm						
Nanoparticle Loading, (w/v%)	0.017	0.034	0.051	0.068	0.085	0.102	0.017	0.034	0.051	0.068	0.085	0.102	
A = 3.2cm	f = 0.25 s^{-1}	0.0649	0.0697	0.0786	0.089	0.0885	0.0869	0.052	0.0599	0.068	0.0588	0.0562	0.054
	f = 0.5 s^{-1}	0.073	0.0894	0.0859	0.1011	0.096	0.094	0.071	0.075	0.081	0.077	0.074	0.068
	f = 0.75 s^{-1}	0.089	0.0974	0.1011	0.118	0.112	0.1088	0.0836	0.0889	0.0968	0.0948	0.0931	0.089
	f = 1 s^{-1}	0.114	0.121	0.128	0.135	0.127	0.12	0.0911	0.0956	0.1044	0.1022	0.099	0.0945
A = 4.7cm	f = 0.25 s^{-1}	0.0684	0.0751	0.0797	0.095	0.0932	0.0899	0.0649	0.0696	0.078	0.072	0.0692	0.0672
	f = 0.5 s^{-1}	0.0814	0.091	0.098	0.11	0.1055	0.1022	0.0798	0.086	0.095	0.0876	0.084	0.0821
	f = 0.75 s^{-1}	0.1099	0.119	0.1255	0.1299	0.127	0.126	0.0965	0.1094	0.115	0.1081	0.1011	0.099
	f = 1 s^{-1}	0.1319	0.135	0.141	0.1476	0.139	0.1355	0.1099	0.119	0.131	0.122	0.114	0.11
A = 6.3cm	f = 0.25 s^{-1}	0.0759	0.086	0.095	0.1046	0.0977	0.0954	0.071	0.081	0.091	0.083	0.078	0.076
	f = 0.5 s^{-1}	0.099	0.112	0.125	0.133	0.127	0.125	0.089	0.0966	0.1055	0.1011	0.097	0.094
	f = 0.75 s^{-1}	0.125	0.128	0.136	0.149	0.1399	0.137	0.109	0.11	0.125	0.112	0.1055	0.1011
	f = 1 s^{-1}	0.1365	0.145	0.1496	0.16	0.15	0.1491	0.119	0.131	0.14	0.129	0.121	0.118

Appendix II. Experimental $k_L a$ data in the presence of SiO_2 nanofluid.

Volumetric oxygen mass transfer coefficient, ($k_L a$, s^{-1}) in the presence of SiO_2 nanofluid at 0.011m/s													
Nanoparticle size		12nm						24nm					
Nanoparticle Loading, (w/v%)		0.017	0.034	0.051	0.068	0.085	0.102	0.017	0.034	0.051	0.068	0.085	0.102
A = 3.2cm	$f = 0.25 \text{ s}^{-1}$	0.0328	0.0383	0.0403	0.0398	0.0357	0.0322	0.031	0.036	0.038	0.035	0.0322	0.0299
	$f = 0.5 \text{ s}^{-1}$	0.0489	0.0541	0.0551	0.0534	0.0526	0.0516	0.0429	0.0488	0.0497	0.0475	0.0441	0.0439
	$f = 0.75 \text{ s}^{-1}$	0.0593	0.0635	0.0676	0.064	0.061	0.057	0.0528	0.0559	0.0599	0.0561	0.0549	0.0533
	$f = 1 \text{ s}^{-1}$	0.0733	0.0781	0.0829	0.079	0.077	0.0749	0.0722	0.0755	0.0793	0.0761	0.0744	0.0711
A = 4.7cm	$f = 0.25 \text{ s}^{-1}$	0.039	0.0458	0.051	0.047	0.046	0.0417	0.0375	0.0412	0.0451	0.0422	0.0391	0.038
	$f = 0.5 \text{ s}^{-1}$	0.052	0.061	0.068	0.064	0.0621	0.056	0.0489	0.0529	0.0589	0.0566	0.0544	0.0514
	$f = 0.75 \text{ s}^{-1}$	0.065	0.0714	0.0788	0.0733	0.071	0.066	0.0626	0.0661	0.0699	0.0685	0.066	0.0633
	$f = 1 \text{ s}^{-1}$	0.0799	0.0844	0.0911	0.088	0.0855	0.0845	0.0756	0.0833	0.0879	0.0865	0.0849	0.0825
A = 6.3cm	$f = 0.25 \text{ s}^{-1}$	0.0569	0.067	0.078	0.074	0.068	0.066	0.0529	0.0581	0.066	0.063	0.059	0.055
	$f = 0.5 \text{ s}^{-1}$	0.0755	0.0833	0.0982	0.0933	0.087	0.0863	0.0655	0.074	0.081	0.077	0.075	0.069
	$f = 0.75 \text{ s}^{-1}$	0.094	0.099	0.1044	0.0994	0.096	0.0921	0.073	0.081	0.088	0.083	0.08	0.079
	$f = 1 \text{ s}^{-1}$	0.0986	0.1066	0.1099	0.1077	0.1049	0.1033	0.087	0.089	0.0968	0.0944	0.091	0.088
Volumetric oxygen mass transfer coefficient, ($k_L a$, s^{-1}) in the presence of SiO_2 nanofluid at 0.019m/s													
Nanoparticle size		12nm						24nm					
Nanoparticle Loading, (w/v%)		0.017	0.034	0.051	0.068	0.085	0.102	0.017	0.034	0.051	0.068	0.085	0.102
A = 3.2cm	$f = 0.25 \text{ s}^{-1}$	0.045	0.049	0.0585	0.057	0.0511	0.05	0.0385	0.0435	0.0459	0.0421	0.041	0.039
	$f = 0.5 \text{ s}^{-1}$	0.0589	0.0652	0.071	0.068	0.066	0.0595	0.055	0.058	0.0622	0.0591	0.0583	0.0544
	$f = 0.75 \text{ s}^{-1}$	0.0755	0.0799	0.0851	0.0785	0.0772	0.0744	0.069	0.0748	0.0785	0.0765	0.0759	0.0733
	$f = 1 \text{ s}^{-1}$	0.089	0.095	0.1018	0.099	0.097	0.0933	0.0799	0.0855	0.0899	0.0871	0.0865	0.0825
A = 4.7cm	$f = 0.25 \text{ s}^{-1}$	0.055	0.0612	0.0711	0.061	0.0588	0.0556	0.049	0.0535	0.057	0.0551	0.0544	0.0527
	$f = 0.5 \text{ s}^{-1}$	0.066	0.073	0.081	0.0788	0.073	0.07	0.059	0.0658	0.0685	0.0661	0.0641	0.0622
	$f = 0.75 \text{ s}^{-1}$	0.089	0.094	0.099	0.093	0.09	0.0895	0.086	0.0891	0.091	0.088	0.0863	0.0879
	$f = 1 \text{ s}^{-1}$	0.099	0.1015	0.1044	0.099	0.0985	0.097	0.0966	0.098	0.1011	0.097	0.095	0.093
A = 6.3cm	$f = 0.25 \text{ s}^{-1}$	0.0654	0.07	0.085	0.075	0.071	0.069	0.0633	0.067	0.075	0.071	0.069	0.065
	$f = 0.5 \text{ s}^{-1}$	0.08	0.085	0.1011	0.087	0.084	0.081	0.078	0.0819	0.085	0.0844	0.0819	0.0799
	$f = 0.75 \text{ s}^{-1}$	0.095	0.099	0.1098	0.1011	0.096	0.0944	0.0911	0.0966	0.1011	0.099	0.097	0.0923
	$f = 1 \text{ s}^{-1}$	0.1044	0.116	0.122	0.119	0.1088	0.1066	0.0988	0.1066	0.118	0.1088	0.1066	0.1055
Volumetric oxygen mass transfer coefficient, ($k_L a$, s^{-1}) in the presence of SiO_2 nanofluid at 0.029m/s													
Nanoparticle size		12nm						24nm					
Nanoparticle Loading, (w/v%)		0.017	0.034	0.051	0.068	0.085	0.102	0.017	0.034	0.051	0.068	0.085	0.102
A = 3.2cm	$f = 0.25 \text{ s}^{-1}$	0.0528	0.061	0.071	0.066	0.064	0.059	0.048	0.0498	0.0611	0.0574	0.0562	0.0534
	$f = 0.5 \text{ s}^{-1}$	0.071	0.0795	0.0855	0.078	0.074	0.0723	0.062	0.0655	0.0789	0.0767	0.0668	0.0649
	$f = 0.75 \text{ s}^{-1}$	0.0825	0.087	0.094	0.0911	0.09	0.0895	0.0789	0.0845	0.0881	0.0839	0.0811	0.0799
	$f = 1 \text{ s}^{-1}$	0.098	0.105	0.1099	0.1066	0.1044	0.1011	0.0889	0.0946	0.0984	0.0975	0.0951	0.0922
A = 4.7cm	$f = 0.25 \text{ s}^{-1}$	0.0683	0.0711	0.0835	0.0792	0.0766	0.0743	0.0611	0.0645	0.0673	0.0661	0.0634	0.0628
	$f = 0.5 \text{ s}^{-1}$	0.0788	0.0844	0.0983	0.0951	0.0933	0.0911	0.0744	0.0788	0.0823	0.0811	0.0791	0.0781
	$f = 0.75 \text{ s}^{-1}$	0.0986	0.1021	0.1055	0.1011	0.0986	0.096	0.0944	0.099	0.1022	0.0988	0.096	0.095
	$f = 1 \text{ s}^{-1}$	0.1088	0.1099	0.115	0.112	0.1095	0.1078	0.1045	0.1077	0.1085	0.1069	0.1045	0.1022
A = 6.3cm	$f = 0.25 \text{ s}^{-1}$	0.0766	0.0833	0.0911	0.087	0.0851	0.0844	0.0699	0.0759	0.0881	0.0844	0.0822	0.081
	$f = 0.5 \text{ s}^{-1}$	0.092	0.099	0.1088	0.1044	0.0988	0.0944	0.088	0.0933	0.0989	0.0966	0.0942	0.0911
	$f = 0.75 \text{ s}^{-1}$	0.1011	0.11	0.1229	0.12	0.1066	0.1011	0.1	0.1049	0.1079	0.1066	0.1045	0.1011
	$f = 1 \text{ s}^{-1}$	0.1091	0.1261	0.1316	0.125	0.112	0.11	0.1044	0.1109	0.121	0.116	0.1099	0.1088

Appendix III. Experimental k_{La} data in the presence of α -Fe₂O₃ nanofluid.

Volumetric oxygen mass transfer coefficient, (k_{La} , s ⁻¹) in the presence of α -Fe ₂ O ₃ nanofluid at 0.011m/s													
Nanoparticle size		43nm					76nm						
Nanoparticle Loading, (w/v%)		0.017	0.034	0.051	0.068	0.085	0.102	0.017	0.034	0.051	0.068	0.085	0.102
A = 3.2cm	f = 0.25 s ⁻¹	0.0277	0.029	0.027	0.0251	0.0236	0.0211	0.0261	0.028	0.0261	0.0243	0.0225	0.0199
	f = 0.5 s ⁻¹	0.045	0.0499	0.046	0.0399	0.0379	0.035	0.0389	0.0455	0.0433	0.0386	0.0366	0.0346
	f = 0.75 s ⁻¹	0.058	0.065	0.0579	0.0561	0.0543	0.052	0.0522	0.0599	0.0571	0.0552	0.0538	0.051
	f = 1 s ⁻¹	0.068	0.078	0.071	0.067	0.0653	0.063	0.065	0.071	0.066	0.0643	0.0621	0.058
A = 4.7cm	f = 0.25 s ⁻¹	0.039	0.045	0.0387	0.035	0.032	0.02963	0.0355	0.0393	0.0376	0.02988	0.027	0.0254
	f = 0.5 s ⁻¹	0.04863	0.061	0.0551	0.0516	0.0476	0.0442	0.0466	0.0571	0.0499	0.0442	0.0431	0.0411
	f = 0.75 s ⁻¹	0.0611	0.073	0.069	0.066	0.0644	0.0611	0.0595	0.071	0.066	0.0634	0.0599	0.0566
	f = 1 s ⁻¹	0.0758	0.0833	0.078	0.0754	0.0733	0.072	0.074	0.0781	0.0753	0.0722	0.0681	0.0661
A = 6.3cm	f = 0.25 s ⁻¹	0.051	0.0599	0.0571	0.0544	0.0531	0.052	0.0499	0.0568	0.0533	0.051	0.0477	0.0429
	f = 0.5 s ⁻¹	0.0595	0.0681	0.066	0.0653	0.0644	0.0586	0.058	0.0651	0.0622	0.0593	0.0583	0.054
	f = 0.75 s ⁻¹	0.0697	0.0775	0.0741	0.0722	0.0677	0.0633	0.067	0.0733	0.0681	0.0663	0.0644	0.0611
	f = 1 s ⁻¹	0.081	0.088	0.083	0.07644	0.074	0.0738	0.0784	0.0839	0.0787	0.0744	0.0711	0.0691
Volumetric oxygen mass transfer coefficient, (k_{La} , s ⁻¹) in the presence of α -Fe ₂ O ₃ nanofluid at 0.019m/s													
Nanoparticle size		43nm					76nm						
Nanoparticle Loading, (w/v%)		0.017	0.034	0.051	0.068	0.085	0.102	0.017	0.034	0.051	0.068	0.085	0.102
A = 3.2cm	f = 0.25 s ⁻¹	0.0377	0.0456	0.0422	0.0381	0.0368	0.0359	0.0349	0.0426	0.0411	0.0377	0.0361	0.0351
	f = 0.5 s ⁻¹	0.0496	0.0594	0.0567	0.05469	0.0511	0.0479	0.0478	0.0563	0.0534	0.0471	0.0459	0.0452
	f = 0.75 s ⁻¹	0.0681	0.073	0.0679	0.066	0.0651	0.064	0.065	0.0711	0.0654	0.0636	0.0622	0.0611
	f = 1 s ⁻¹	0.075	0.0833	0.079	0.0762	0.0754	0.073	0.074	0.0796	0.0761	0.0754	0.0743	0.0724
A = 4.7cm	f = 0.25 s ⁻¹	0.0477	0.0519	0.0488	0.0458	0.044	0.043	0.046	0.0496	0.0445	0.0439	0.0431	0.0428
	f = 0.5 s ⁻¹	0.0611	0.0693	0.066	0.0586	0.0571	0.056	0.058	0.0656	0.0611	0.059	0.0566	0.0544
	f = 0.75 s ⁻¹	0.0861	0.0882	0.0844	0.0832	0.0811	0.077	0.0831	0.0859	0.0833	0.081	0.0783	0.0756
	f = 1 s ⁻¹	0.0941	0.0991	0.0935	0.0928	0.0919	0.089	0.0921	0.0959	0.0891	0.087	0.0845	0.0811
A = 6.3cm	f = 0.25 s ⁻¹	0.0621	0.066	0.0615	0.06	0.0588	0.0575	0.0619	0.0648	0.0586	0.056	0.0543	0.0515
	f = 0.5 s ⁻¹	0.0765	0.0811	0.0759	0.0749	0.0741	0.0739	0.075	0.0781	0.0766	0.0743	0.0725	0.0711
	f = 0.75 s ⁻¹	0.0911	0.0959	0.09	0.087	0.084	0.0799	0.087	0.0911	0.087	0.0851	0.0837	0.0789
	f = 1 s ⁻¹	0.0961	0.1044	0.0953	0.0944	0.0931	0.0929	0.0969	0.1022	0.0963	0.0946	0.0922	0.0911
Volumetric oxygen mass transfer coefficient, (k_{La} , s ⁻¹) in the presence of α -Fe ₂ O ₃ nanofluid at 0.029m/s													
Nanoparticle size		43nm					76nm						
Nanoparticle Loading, (w/v%)		0.017	0.034	0.051	0.068	0.085	0.102	0.017	0.034	0.051	0.068	0.085	0.102
A = 3.2cm	f = 0.25 s ⁻¹	0.047	0.0599	0.0533	0.0455	0.0449	0.0433	0.0492	0.0538	0.047	0.044	0.0429	0.0415
	f = 0.5 s ⁻¹	0.0575	0.0711	0.0667	0.0641	0.0611	0.0571	0.0581	0.0677	0.0633	0.061	0.0576	0.0511
	f = 0.75 s ⁻¹	0.0769	0.0816	0.0761	0.0755	0.0749	0.0722	0.0743	0.0796	0.0766	0.0723	0.0718	0.0686
	f = 1 s ⁻¹	0.0866	0.0943	0.0859	0.0842	0.0839	0.0811	0.0822	0.0911	0.0861	0.0842	0.0811	0.079
A = 4.7cm	f = 0.25 s ⁻¹	0.0581	0.0677	0.0633	0.061	0.0569	0.0566	0.0572	0.0645	0.0586	0.0551	0.0543	0.0522
	f = 0.5 s ⁻¹	0.0753	0.0836	0.0811	0.076	0.074	0.0715	0.0744	0.0795	0.0766	0.0743	0.0725	0.0711
	f = 0.75 s ⁻¹	0.0944	0.0983	0.095	0.093	0.0921	0.0911	0.0931	0.0955	0.093	0.092	0.088	0.0866
	f = 1 s ⁻¹	0.1019	0.1066	0.1044	0.0966	0.0955	0.0949	0.1015	0.1022	0.099	0.095	0.0941	0.092
A = 6.3cm	f = 0.25 s ⁻¹	0.071	0.0779	0.0733	0.069	0.067	0.065	0.0693	0.0751	0.071	0.0689	0.0673	0.0669
	f = 0.5 s ⁻¹	0.0859	0.0896	0.086	0.0834	0.0822	0.0819	0.0841	0.0895	0.0832	0.0813	0.0782	0.0755
	f = 0.75 s ⁻¹	0.0981	0.1011	0.0974	0.0961	0.0959	0.0933	0.095	0.1013	0.0911	0.089	0.0881	0.0851
	f = 1 s ⁻¹	0.1044	0.11	0.1066	0.1037	0.1029	0.0988	0.1034	0.1088	0.1041	0.0988	0.0973	0.0968

Publication based on the research work

Journal articles

1. Amruta Shet, Vidya Shetty K, (2020), “TiO₂ nanofluid for oxygen mass transfer intensification in pulsed plate column”. Chemical Engineering Communications. Volume 208, (12), Pages 1653-1675. (doi.org/10.1080/00986445.2020.1808467).
2. Amruta Shet, Vidya Shetty K, (2023), “Experimental investigation, Modelling, and Order of Magnitude Analysis of Oxygen Mass Transfer in Pulsed Plate Column with α -Fe₂O₃ Nanofluid,” a revised manuscript has *submitted to* The Canadian Journal of Chemical Engineering – *Under Review*.

Conference Proceedings

1. Amruta S Shet and Vidya Shetty K, (2019), “SiO₂ nanofluid mediated enhancement in oxygen mass transfer in pulsed plate column”, 2nd International Conference on New Frontiers in Chemical, Energy and Environmental Engineering- INCEEE 2019, During 15-16 February 2019, Organised by Department of Chemical Engineering, National Institute of Technology Warangal, India, Paper id M037: Pg. No: 72.

AMRUTA S SHET

**Permanent Address: “Amruta Nilaya”, Near Dhareshwar Janata High School,
Dhareshwar Kumta – 581327.**

Ph: +918762328320; Email id: amrutasht@gmail.com

Career Objective:

Looking forward to securing a responsible and challenging position within the Organization to serve to the fullest of my ability and upliftment of the Organization.

Education:

- ❖ PhD from the National Institute of Technology Karnataka, Surathkal.
- ❖ M. Tech in Industrial Pollution Control securing 71.4% in the year 2015 from National Institute of Technology Karnataka, Surathkal Under TEQIP program.
- ❖ B.E in Chemical Engineering securing 83.1% in the year 2012 from SDM College of Engineering & Technology (Autonomous), Dharwad affiliated Under VTU, Belgaum.
- ❖ Pre-University securing 68.5 % in the year 2008 from R B Patil Rotary College, Hubli.
- ❖ SSLC securing 84% in the year 2006 from Jain Vidyaniketan, Jakkasandra, Kanakapura Taluk, Bangalore Karnataka.

Academic Achievements:

I have worked on:

- “Composting and Vermicomposting: An Eco Tool for Organic Solid Waste Management”.
- “Extraction of protein from rice bran”.
- “Comparison of Dyes using spectrophotography method”.
- “Photocatalytic Degradation of Phenol using Ag core TiO₂ shell nanoparticles”.
- “Extraction of essential oil from Vetiver roots”.
- “Synthesis of SiO₂ nanoparticles by precipitation method”.
- “Nanofluid mediated gas-liquid Mass transfer enhancement in Pulsed plate column”.

Technical skills

- Computer skills (MS Office).
- Computer Language (C-Programming).
- Software (MATLAB, ASPEN PLUS SIMULATION, ImageJ, DWSIM).
- Design Tool (CHEMCAD, E-DRAW, Solid Edge, Origin).
- Technical writing/Editing.
- Instruments Handled (UV Spectrophotometer, Centrifuge, Ultrasonicator, Stirred tank reactors, Process controllers).

Areas Of Interest:

- Nanofluids, Photocatalysis, Transfer Operations, Environmental Engineering.

Work Experience:

- Worked as Half Time Teaching Assistant at “National Institute of Technology Karnataka” under the TEQIP Programme from July 2012 to June 2015.
- Worked as Assistant Professor at M V Jayaraman College of Engineering, Bangalore from October 2021 to November 2022.
- Subjects handled Mass Transfer, Heat transfer, Process Control and Dynamics, Material Science for Chemical Engineers, and Nanotechnology.

Paper Published

- Amruta Shet, Vidya Shetty K, (2016), “Solar light mediated photocatalytic degradation of phenol using Ag core–TiO₂ shell (Ag@ TiO₂) nanoparticles in batch and fluidized bed reactor”. Solar Energy.
- Amruta Shet, Vidya Shetty K, (2016), “Photocatalytic degradation of phenol using Ag core-TiO₂ shell (Ag@TiO₂) nanoparticles under UV light irradiation”. Environmental Science and Pollution Research.
- Amruta Shet, Vidya Shetty K, (2020), “TiO₂ nanofluid for oxygen mass transfer intensification in pulsed plate column”. Chemical Engineering Communications.

Conferences/Workshop/FDPs Attended:

- Six Days Faculty Development Programme on Current Trends in Nanomaterials and its Applications (CTNA 2022) held from 22nd – 27th August 2022 Organized by SRM Institute of Science and Technology Kattankulathur - 603 203, Tamil Nadu, India
- Three days Faculty Development Program (FDP) on “Recent Advances in Wastewater Treatment and Recycle” held from 16th -19th November 2021 organized by the Department of Chemical Engineering, SDM College of Engineering and Technology, Dharwad. Karnataka. India.
- Two-Day State Level Seminar Two-Day State Level Seminar (Online) on “Teaching Learning and Assessment Process as per OBE in the Higher Education Institutions in line with NEP 2020” on 2nd - 3rd September organized by the Sahyadri College of Engineering Bangalore.
- “International Conference on New Frontiers in Chemical, Energy and Environmental Engineering- INCEEE 2019, Organized by the Department of Chemical Engineering, National Institute of Technology Warangal, India, during 15th-16th February 2019, and presented my work.
- “International Conference on New Frontiers in Chemical, Energy and Environmental Engineering” at the National Institute of Technology Warangal, Telangana state, and presented my paper at the same conference in 2015.
- A one-day workshop on “Drinking water purification and Industrial wastewater treatment”, at the National Institute of Technology Warangal, Telangana state in 2015.
- A two-day workshop on “NBA Accreditation Awareness”, at National Institute of Technology Karnataka, Surathkal 2018.
- A one-day workshop on “Energy Sustenance towards a better environment” at SDMCET 2012.

Personal Information

Date of Birth: 09-09-1990

Father's Name: S. M. Shet

Mother's Name: Shashikala Shet

Marital Status: married

Nationality: Indian

Languages: English, Kannada, Hindi, Konkani, Marathi, and Telugu

Hobbies: Singing and Listening Music, Playing Shuttle Badminton

Address: "Amruta Nilaya", Near Dhareshwar Janata High School, Dhareshwar

Kumta – 581327. Ph: +918762328320; Email id: amrutasht@gmail.com

Declaration:

I hereby declare that the above-mentioned information is correct up to my knowledge and I bear the responsibility for the correctness of the above-mentioned particulars.

Place:

Date:

(Amruta S Shet)